Formulation and Evaluation of an Implantable Polymeric Configuration for Application in AIDS Dementia Complex

Sheri-Lee Harilall

A dissertation submitted to the Faculty of Health Sciences, University of the Witwatersrand, in fulfilment of the requirements for the degree of Master of Pharmacy

Supervisor:

Professor Viness Pillay
Department of Pharmacy and Pharmacology, University of the Witwatersrand, South Africa

Co-Supervisor:

Professor Michael Paul Danckwerts
Department of Pharmacy and Pharmacology, University of the Witwatersrand, South Africa

Johannesburg, 2011

DECLARATION

I, Sheri-Lee Harilall declare that this dissertation is my own work. It is being submitted for the degree of Master of Pharmacy in the Faculty of Health Sciences in the University of the Witwatersrand, Johannesburg. It has not been submitted before for any degree or examination at this or any other University.

…….

This ..... day of April 2011

RESEARCH PRESENTATIONS

1. Conference Abstracts

Preliminary investigation into the synthesis of polymeric nanoparticles and scaffolds intended for implantation into the brain, Sheri-Lee Harilall, Viness Pillay, Yahya E. Choonara and Michael P. Danckwerts, International Conference of Pharmaceutical and Pharmacological Sciences, Vanderbijl Park, Gauteng, South Africa, September 22-26, 2006.

Formulation of Polymeric Nanoparticles Intended for Intracranial Implantation, Sheri-Lee Harilall, Samantha Pillay, Viness Pillay, Yahya E. Choonara and Michael P. Danckwerts, South African Nanotechnology Initiative NanoAfrica, University of Cape Town, Western Cape, South Africa, November 26-29, 2006.

A comparative study of crosslinked sodium carboxymethyl cellulose-polyethylene oxide-epsilon caprolactone particles before and after treatment with 1% v/v hydrochloric acid, Sheri-Lee Harilall, Viness Pillay, Yahya E. Choonara, Girish Modi, and Sunny Iyuke, Neurological Association of South Africa Annual National Congress held at the Sandton Convention Centre, Sandton, Johannesburg, South Africa, March 28-31, 2007.

A nano-implantable site-specific system for the CNS delivery of zidovudine, Sheri-lee Harilall, Viness Pillay, Yahya E. Choonara, Girish Modi, Sunny E. Iyuke and Michael P. Danckwerts, 28th Annual Conference of the Academy of Pharmaceutical Sciences of South Africa, Langebaan, Western Cape, South Africa, September 4-7, 2007.

Formulation and Evaluation of an Implantable Polymeric Configuration for Application in AIDS Dementia Complex Utilising Nanotechnology, Sheri-Lee Harilall, Viness Pillay, Yahya E. Choonara, British Pharmaceutical Conference, Manchester Convention Centre, Manchester, United Kingdom, September 10-12, 2007.

Formulation and Optimization of a Multi-Polymeric Nano-Enabled Zidovudine-Loaded Intracranial Device using a Box-Behnken Experimental Design Strategy, Sheri-Lee Harilall, Viness Pillay, Yahya E. Choonara, Girish Modi, Dinesh Naidoo, Michael P. Danckwerts, Sunny E. Iyuke and Lisa C. du Toit, Annual Meeting of the American Association of Pharmaceutical Scientists, Los Angeles Convention Center, Los Angeles, California, United States of America, November 08-12, 2009.

Design of a Biometrically Modeled Nanocomposite Neuro-Device for the Chronic Management of Aids Dementia Complex, Yahya E. Choonara, Viness Pillay, Sheri-Lee Harilall, Lisa C. du Toit, Riaz A. Khan, Girish Modi, Dinesh Naidoo, Sunny E. Iyuke and Leith Meyer, 37th CRS Annual Meeting, Portland, Oregon, United States of America, July 10-14, 2010.

2. Podium Presentations

Analysis of Polymeric Nanoparticles Formulated by means of a Controlled Gelification of Alginate Employing Dynamic Light Scattering and Electrostatic Dispersion, Sheri-Lee Harilall, Viness Pillay, Yahya E. Choonara, Girish Modi, and Sunny Iyuke, Joint Symposium for Chemical and Metallurgical Engineering, University of Pretoria , Gauteng, South Africa, August 2-3, 2007.

Formulation and Evaluation of a Zidovudine-Loaded Polymeric Nanosystem for Application in AIDS Dementia Complex, Sheri-Lee Harilall, Viness Pillay, Yahya E. Choonara, and Michael P. Danckwerts, University of Witwatersrand Therapeutics day, University of Witwatersrand, Gauteng, South Africa, August 21-22, 2007.

Nanotechnology and its explosion in pharmaceutical research applications, Valence M. K. Ndesendo, Viness Pillay, Yahya E. Choonara, Samantha Pillay, Sheri-lee Harilall and Sunny E. Iyuke, 28th Annual Conference of the Academy of Pharmaceutical Sciences of South Africa, Club Mykonos Resort, Langebaan, Cape Town, September 4-7, 2007.

Formulation and Evaluation of an Implantable Polymeric Configuration for Application in AIDS Dementia Complex Utilising Nanotechnology, Sheri-Lee Harilall, Viness Pillay, Yahya E. Choonara, British Pharmaceutical Conference, Manchester Convention Centre, Manchester, United Kingdom, September 10-12, 2007.

A Zidovudine-Loaded Nano-Enabled Device for the Intrastriatal Management of AIDS Dementia Complex, Sheri-lee Harilall, Viness Pillay, Yahya E. Choonara, Dinesh Naidoo, Lisa C. du Toit, Girish Modi, Sunny E. Iyuke and Michael P. Danckwerts, University of Witwatersrand Faculty Research Day, University of Witwatersrand, Gauteng, South Africa, August 20, 2008.

Analysis of an AZT-loaded poly(Ɛ-caprolactone) nano-enabled device for the management of AIDS dementia complex in the Sprague-Dawley rat brain model, Sheri-lee Harilall, Viness Pillay, Yahya E. Choonara, Girish Modi, Dinesh Naidoo, Sunny E. Iyuke, Lisa C. du Toit, Leith Meyer, and Michael P. Danckwerts, 29th annual conference of the Academy of Pharmaceutical Sciences of South Africa, Hunter's Rest, Magaliesberg Mountains, North West Province, South Africa, September 22-26, 2008.

3. Papers Published

Formulation and Evaluation of an Implantable Polymeric Configuration for Application in AIDS Dementia Complex Utilizing Nanotechnology, Sheri-lee Harilall, Viness Pillay and Yahya Choonara, **Journal of Pharmacy and Pharmacology**, Scientific Proceedings, supplement 1, A-56, 2007.

Patenting of Nanopharmaceuticals in Drug Delivery: No Small Issue, Lisa Claire du Toit, Viness Pillay, Yahya E. Choonara, Samantha Pillay and Sheri-Lee Harilall, **Recent Patents on Drug Delivery & Formulation**, 1(2), pp. 131-142, 2007.

4. Patent

Polymeric Configuration for Site-Specific Drug Delivery.
Viness Pillay, Sheri-lee Harilall Samantha Pillay, Yahya E. Choonara, Girish M. Modi, Sunny E. Iyuke and Dinesh Naidoo, South Africa, Patent Application Filed, *awaiting priority date*.

ABSTRACT

Drug delivery to the brain has challenged medical professionals for several decades, with 98% of small molecules and 100% of large molecules unable to cross the blood brain barrier (BBB). Biocompatible, biodegradable polymers have been extensively researched for the oral delivery of therapeutic agents, but to date has not been successfully manipulated for the formulation of an implantable device. We have therefore utilised such polymers for the formulation and design of an implantable nanoenabled multipolymeric drug delivery device (NMDDD) for the management of AIDS Dementia Complex (ADC).

ADC is a central nervous system (CNS) complication of HIV, associated with a host of debilitating cognitive, motor and behavioural symptoms. ADC remains a serious manifestation of HIV/AIDS in both developing and developed countries, affecting both adults and children, with death expected within 6 months of initial diagnosis. Zidovudine (AZT), the current gold standard for the management of ADC, has demonstrated the best penetration into the CNS. It is capable of reducing viral replication in the CNS and managing neurological abnormalities associated with ADC, with clinical efficacy evidenced by the decline in morbidity and mortality of patients treated with this drug.

Nanotechnology, an interdisciplinary field of research, involving the manipulation of matter on a submicron level, is receiving emerging interest for the formulation of novel drug delivery systems. As they can potentially be manipulated to react in a bioresponsive manner, nanopharmaceuticals have received much attention for site-specific drug delivery and were therefore employed in the formulation of an implantable NMDDD, with AZT employed as the model drug, for the management of ADC.

Nanoparticles were prepared by means of an approach utilising controlled gelation of alginate, employing cationic crosslinking of the anionic alginate to precipitate nanoparticles. A 3-factor Box-Behnken statistical design was employed for the optimisation of nanoparticle and multipolymeric scaffold formulations. Nanoparticles measuring 68.04nm (SD<0.0002) in size with a zeta potential of -13.4mV (SD<0.0005) were formulated. Nanoparticles presented with a mean dissolution time (MDT) of 46.046 hours 30 days post exposure to phosphate buffered saline (PBS), pH 7.4. In an attempt to further retard drug release and to formulate a device for implantation in the frontal lobe of the brain, nanoparticles were dispersed within a robust multipolymeric matrix. Matrix erosion was calculated at 28%$^{w}/_{w}$ (SD<0.001) for multipolymeric scaffold and a matrix resilience of 4.451%$^{w}/_{w}$ (SD<0.007) was observed 30 days post exposure to PBS, indicating slow degradation of the NMDDD. MDT was reduced to 12.570 hours (SD<0.0005) with dispersion of the nanoparticles within a polymer matrix, supporting the application of the drug-loaded MDDD in the management of ADC patients.

The optimised multipolymeric nanoparticulate scaffold was implanted into the frontal lobe of the rat brain, for investigation of drug release characteristics and tissue response to the device following in vivo administration.

ACKNOWLEDGEMENTS

I would like to thank my family for supporting me through the gruelling years it took to complete my masters. Thank you for the constant faith you had in me, even when I lost faith in myself. Thank you for pushing me beyond my limits and allowing me to realise my true potential.

Thank you Prof V. Pillay for giving me the opportunity for pursuing my passion and for the constant support and attention you bestowed onto me.

Thank you Yahya for answering my questions and for steering me in the right direction.

Thanks to Lisa, Neha, Deanne and Shirona for being great friends and for constantly motivating me and for the much needed coffee breaks we shared.

Thank you to all the staff and students of the Department of Pharmacy and Pharmacology for your help and guidance.

Roland, thank you for always being available when I need you. Your support and love is invaluable.

Most of all I would like to thank my Dad for pushing me to pursue my masters and ensuring I never gave up or lost hope. I would also like to thank my Mum for diligently asking me every day when I would complete my Masters. This inspired me to do my best and make you proud. Thank you Mummy and Daddy for supporting me always.

And lastly, I thank the Almighty for carrying me through these trying times.

DEDICATIONS

I dedicate this dissertation to the people who have supported and motivated me the most in the past years, my parents, my brothers, Remolen and Reneil, my sister Chinky and my fiancé Roland.

I also dedicate this work to my late aunt and grandmother whose faith in me has been a true inspiration.

TABLE OF CONTENTS

LIST OF FIGURES

LIST OF TABLES

CHAPTER 1

Literature Survey and Motivation for this study

1.1 Introduction

The last three decades has witnessed a rise in the number of people infected with the Human Immunodeficiency Virus (HIV), making HIV/Acquired Immunodeficiency Syndrome (AIDS) a global concern as the number of people living with the disease increases every year. HIV accounted for 33 million infections by 2007, with 25 million HIV-related deaths reported since 1981. In 2006, 4.3 million new infections were reported, with 430 000 new HIV infections occurring in infants each year, despite an increase in prevention programmes and access to antiretroviral (ARV) therapy. Approximately 2 million HIV-related deaths was reported in 2007 (UNAIDS/WHO, 2006; UNAIDS Epidemic Update, 2008; das Neves *et al.*, 2009; Varatharajan and Thomas, 2009; Akhtar *et al.,* 2010, Fowler *et al.,* 2002).

Sub-Saharan Africa remains the epicenter of HIV/AIDS infections, with 67% of the HIV-infected population living in this area. Southern Africa accounts for 32% of the global HIV/AIDS population, with the only country experiencing a decline in the incidence of new HIV infections being Zimbabwe. South Africa itself houses 5.5 million HIV/AIDS sufferers, of which 240 000 are children under 15 years of age, with HIV accounting for 8.7% of deaths as recorded in the last census performed in 2001 (Statistics South Africa, 2001; UNAIDS/WHO, 2006; Yeboah, 2007; UNAIDS Epidemic Update, 2008; das Neves *et al.*, 2009; Fowler *et al.,* 2010; Kanmogne *et al.,* 2010).

A member of the subfamily of retroviruses, HIV is known to affect most, if not all systems of the body, causing a variety of immunological and neurological diseases as a result of attack on the body's immune system, particularly by cluster of differentiation 4 (CD4) T-lymphocyte depletion, leaving the body susceptible to fatal infections and cancers (World Health Organisation, 1993; Bowers, 1996; Penedo *et al.*, 2003; Pirzada *et al.,* 2006; Samikkanu *et al.,* 2010). Viral entry into the body results in an initial flu-like symptom or viraemia due to the immune reconstitution symptom, which occurs as the body's immune system rapidly degrades. After this initial phase, the patient goes in to an asymptomatic period which can last for months or years prior to the onset of AIDS, a syndrome which results from advanced HIV infection. AIDS is diagnosed when life-threatening opportunistic infections, such as Kaposi's sarcoma and lymphoma's occur or if the CD4 or T4 lymphocyte count falls below 200 cells/mm^3 (Pirzada *et al.,* 2006).

The HIV pandemic is said to have started in Leopoldville, Cameroon in 1927, with the virus being noticed during a clinical trial of the antimalarial drug, plasmaquine (Parris, 2007). The pandemic was thought to have been due to the polio vaccine programme in Stanleyville, 1958 (Parris, 2007). However, the first official AIDS patient was identified in 1981 with AIDS developing into a global pandemic shortly after (Wu *et al.*, 2007), with the effects of HIV/AIDS was only felt in sub-Saharan Africa in the early 1990's (Yeboah, 2007).

HIV infection of the CNS is associated with a host of complications including encephalopathy, dementia and motor dysfunction, with 7-20% of patients exhibiting neurological symptoms as the initial signs of infections. Autopsy studies have found that 75-90% of HIV/AIDS patients exhibit neurohistological damage (Bodor and Buchwald, 1999; Sawchuk and Yang, 1999). AIDS Dementia Complex (ADC), a CNS condition caused by the HIV-1 strain of the retrovirus, is a serious manifestation of HIV/AIDS in both developed and developing countries (Portegies *et al.*, 1994; Kim *et al.*, 1996; Vitiello *et al.*, 1997; Saksena *et al.*, 1998; Pemberton *et al.*, 2001; Schutzer *et al.*, 2004; Giunta *et al.*, 2006). Affecting one third of adults and one half of children living with AIDS, ADC is a source of severe morbidity and limited survival, with death being expected within 6 months after diagnosis is made. Developmental delays in cognitive and motor function, as well as loss of acquired skills have been noted in children with ADC. The dementia is also responsible for declined intellectual scores in children and is the leading cause of dementia in young adults worldwide (Portegies *et al.*, 1989; Frumkin, 1992; Wong *et al.,* 1992; Bower, 1996; Gabuzda, 1996; Vitiello *et al.*, 1997; Price, 1998; Chang *et al.*, 2004; Wu *et al.*, 2007; Perry *et al.,* 2010).

The condition consists of many progressive diseases which can easily be mistaken for other problems, such as depression, drug-induced side effects and opportunistic infections of brain, like toxoplasmosis or lymphomas. Due to the variety of manifestations of the complex, ADC is poorly understood and frequently misdiagnosed (Link, 1992). With little being known of the pathogenesis of the condition, it is a source of severe morbidity, as well as being associated with limited survival (Price, 1998). ADC is responsible for a host of cognitive, motor and behavioural symptoms ranging in severity from minor cognitive symptoms, such as forgetfulness, lack of attention and disturbed sleep patterns, to severe dementia and paralysis (Portegies *et al.*, 1989; Lawrence *et al.*, 2002; Yiannoutsos *et al.*, 2004; Thompson *et al.*, 2005; Martín-García *et al.*, 2006; Cook-Easterwood *et al.*, 2007; Akhtar *et al.,* 2010).

The presentation of symptoms of ADC is associated with severe immunosuppression. At this stage the patient is susceptible to opportunistic infections, which further compromises

the immune system. Initiation of highly active antiretroviral therapy (HAART) at this stage is beneficial to the patient as HAART serves to decrease viral load and improve immune function. The incidence of ADC has declined by 50% with the introduction of antiretroviral therapy in first world countries (Avison *et al.*, 2002, Chang *et al.*, 2004; Valcour *et al.*, 2004; González-Scarano *et al.*, 2005; Cook-Easterwood *et al*, 2007; Beblo *et al.,* 2010) as HAART prevents and reverses clinically symptomatic ADC. HAART consists of the use of a triple regimen of ARV's, consisting of two nucleoside reverse transcriptase inhibitors (NRTI's) in combination with either a non-nucleoside reverse transcriptase inhibitor (NNRTI), a protease inhibitor (PI) or and integrase inhibitor (Rao *et al.*, 2008; das Neves *et al.*, 2009; Cihlar and Ray, 2010). The addition of zidovudine (AZT) into this regimen is beneficial in that AZT demonstrates the best penetration into the brain among the NRTI's (Galinsky *et al*., 1990; Gallo, 1994).

Drug incorporation into nanosystems is used to achieve site-specific drug delivery, therefore providing better control of drug release. This improves the efficacy, pharmacokinetics and pharmacodynamics, as sub-micron distribution of the drug particles improving the physicochemical properties of the encapsulated drug (Roney *et al.*, 2005). Targeted drug delivery improves the therapeutic efficacy of the drug, as well as resulting in a reduction in the quantity administered to achieve a therapeutic response and minimises side effects experienced due to drug therapy. Drug delivery devices using nanosystems can be manipulated to react in a bioresponsive manner, to provide site-specific drug delivery and to control drug degradation. Nanoparticles are capable of opening tight junctions and are therefore capable of crossing the BBB (Roney *et al.*, 2005; Jolck *et al.,* 2010; Subbia *et al.,* 2010). Nanoparticles can also be used as carriers for poorly soluble drugs, thereby improving their bioavailability (Pison *et al.*, 2006; Popovic and Brundin, 2006; Reis *et al.*, 2006; Anderson and Power, 2010).

Polymers with desirable physicochemical and physicomechanical properties can be successfully used to develop nano-enabled implantable devices, which are capable of prolonged drug release over desired time periods. Biodegradable polymers such as polycaprolactone (PCL), pectin, and alginate can be used in the design of nano-enabled implantable drug delivery systems, as byproducts of such polymers are biocompatible, nontoxic, and readily excreted from the body (Liu *et al.,* 2005; Popovic and Brundin, 2006; Rezwan *et al.*, 2006; Cameron *et al.,* 2010). These polymers are non-mutagenic, non-cytogenic and non-teratogenic and are therefore safe for implantation. Such polymers have been employed in simulating a polymer scaffold to deliver drug-loaded polymeric nanoparticles, due to their desirable mechanical properties and superior drug permeability

(Liu *et al.*, 2005; Luong-Van *et al.*, 2006; Popovic and Brundin, 2006; McKenzie *et al.*, 2003; Rezwan *et al.*, 2006). The device, comprising of a polymeric scaffold and drug-loaded nanoparticles will be implanted intracranially to achieve modulated drug release in a site-specific manner.

Intracranial implantation of the drug loaded nanoparticulate multipolymeric device into the frontal lobe of the brain yields site-specific presentation of the drug, negating the need for the drug to bypass the blood brain barrier. Direct implantation into the brain allows for lower doses of drug to be administered and prevents the occurrence of systemic adverse effects resulting from the systemic circulation of drug molecules. The frontal lobe is the preferred site of implantation as no sensory or motor functions are located at the chosen site of implantation (Figure 1.1).

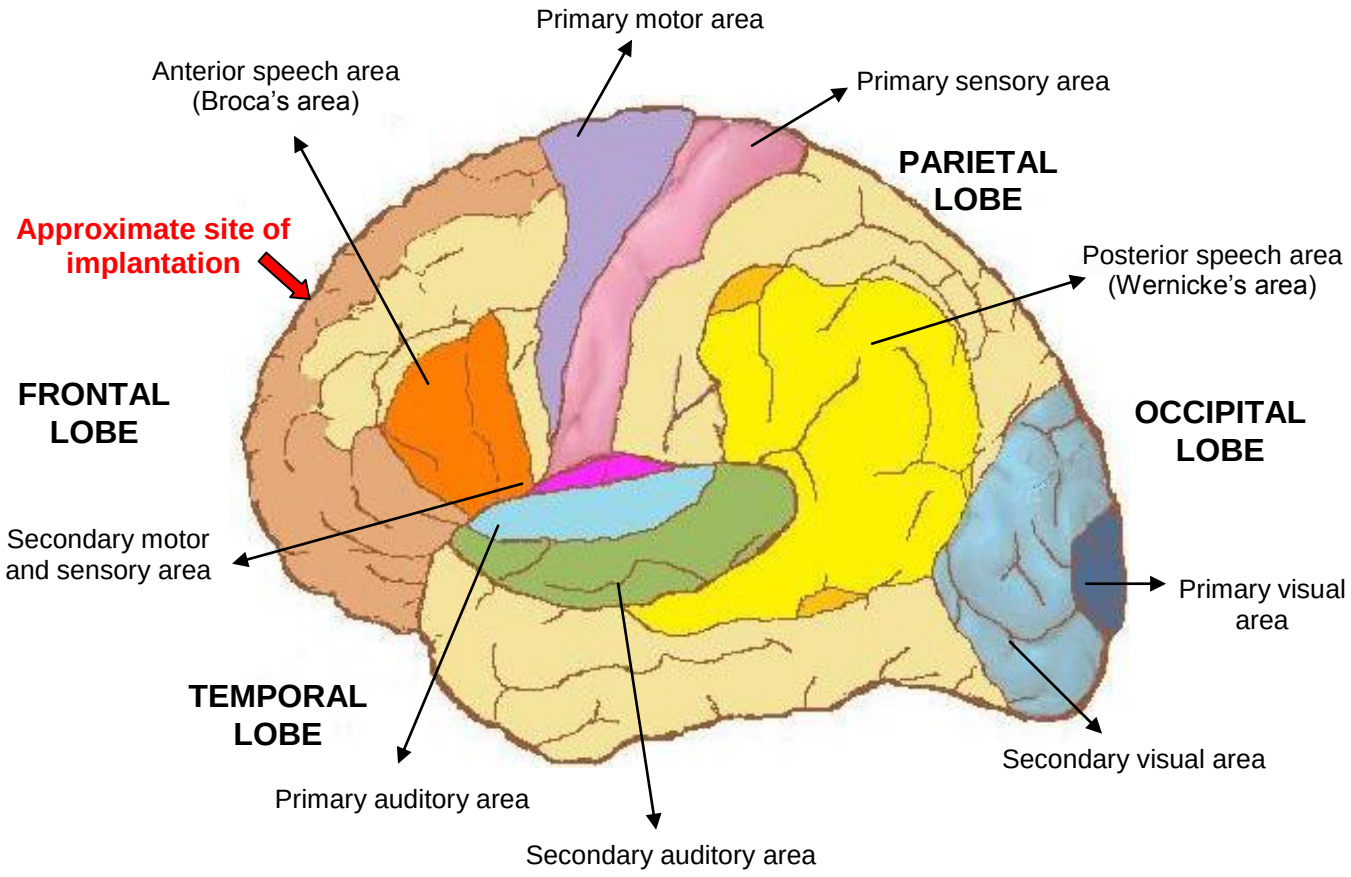

Figure 1.1: *Anatomical illustration of the brain indicating the presence of sensory and motor sites within the different lobes of the brain. The site of implantation is indicated (adapted from Bina, http://massoudbina.com/neurodisorders/BrainAnatomy.php, (24/07/2010).*

1.2. Rationale for the study

ARV medication and immune reconstitution drugs have accounted for an increase in the number of people living with chronic HIV/AIDS in the last decade, resulting from a decrease in immunosuppression and opportunistic infection, which is usually responsible for death in AIDS sufferers. This in turn led to an increase in the number of people developing ADC, as more HIV patients have progressed to old age, when neurological disorders due to aging precipitates ADC. However, milder symptoms of ADC are commonly experienced. This can be managed with adequate ARV therapy which is capable of penetrating the blood brain barrier (Lawrence *et al.*, 2002; Valcour *et al.*, 2004; Beblo *et al.,* 2010). The symptoms of ADC can be managed using psychoactive drugs, including antipsychotics, antidepressants, anxiolytics, psychostimulants, antimanics, and anticonvulsants. Neuroprotective agents may also work to retard neuronal death and therefore improve mental function (Thompson *et al.*, 2005). However, these do not treat the underlying cause of the disease, nor do they halt its progression, as they do not target the HI virus. ARV's that target the HI virus are therefore required (Link, 1992).

Existing therapies used for the management of ADC are mainly administered via the oral route, employing triple-drug therapy, with a combination of nucleoside reverse transcriptase inhibitors (NRTI's), non-nucleoside reverse transcriptase inhibitors (NNRTI's), nucleotide reverse transcriptase inhibitors (NtRTI's) or a protease inhibitors (PI's) (Ramachandran *et al.*, 2006; Varatharajan and Thomas, 2009). There are many barriers to the absorption of these drugs from the gastrointestinal tract. Acidic conditions in the stomach are responsible for the reduction in the bioavailability of didanosine, a nucleoside reverse transcriptase inhibitor (NRTI), whereas the reduced aqueous solubility is responsible for the reduction in the bioavailability of the non-nucleoside reverse transcriptase inhibitors (NNRTI's). Oral bioavailability of the protease inhibitors (PI's) is reduced due to poor solubility of the drugs in the gastrointestinal fluid, decreased intestinal permeability, as well as first-pass metabolism. Zidovudine therapy is hindered by the first pass metabolism, which reduces the bioavailability of this drug (Allan Macnab *et al.,* 1996; Carvalho *et al.,* 2010). Higher concentrations of this drug are therefore required when employed to treat ADC; however this has been shown to increase the risk of severe anaemia (Aungst, 1999; Agarwal *et al.,* 2010). The poor bioavailability as well as the associated side effects creates the need for localized drug delivery of ARV agents for the management of ADC (Alavijeh *et al.*, 2005). It is also thought that systemic ARV's are not sufficient to eradicate HIV in the CNS, creating a need for localised drug therapy (Lawrence *et al.*, 2002). In a study conducted by Pialoux *et al.* (1997), it was established that therapy with a combination of AZT, lamivudine, and indinavir

served to reduce plasma viral loads below 200copies/mL, indicating effective management of the HI virus within the body, however neurological disorders resulting from HIV still ensued. This supports the need for localised delivery of ARVs for the management of ADC as adequate distribution of ARVs following systemic administration is not achieved (Pialoux *et al.*, 1997; Sawchuk and Yang, 1999).

The BBB restricts the entry of substances into the brain depending on the size and endothelial permeability of the substance. It comprises of tight cell junctions and an ATP-dependent efflux pump, which hinders the delivery of drug into the brain, thus making therapy to the brain via the systemic route difficult. Small lipophilic molecules and peptides are able to cross the BBB, however these molecules undergo rapid systemic degradation prior to reaching the site of action (Pardridge, 1995; Varatharajan and Thomas, 2009). High dose parenteral therapy is often necessary to achieve sufficient concentrations of drug in the brain; however, this is accompanied by a host of systemic side effects.

Polymeric nanoparticles used for the controlled delivery of drug were first developed in the 1970's (Feijen *et al.*, 2005). Nanomaterials are defined as materials containing components with a minimum of one dimension in the nanometer size range (Yang *et al.*, 2008). Commercially available nanomaterials, a term which refers to a range of materials including nanotubes, nanospheres, nanomicelles and nanoliposomes, extend into many scientific fields, including electronics, cosmetics, and medicine (Liu *et al.*, 2008; Yang *et al.*, 2008). The formulation of a nano-enabled polymeric implant allows for site specific drug release within the CNS, negating concerns such as first pass metabolism, systemic side effects due to the high dosages required for therapeutic efficacy and the challenges posed by the BBB. Safe and effective drug delivery into the brain resulting from localized delivery will ensue, with subsequent improvement in patients' quality of life as the management of the ADC will be considerably enhanced (Price, 1998; Ghaderi *et al.,* 2010; Jolck *et al., 2010;* Subbia *et al.,* 2010).

Various applications exist for the nanoparticle-loaded system. It can be utilised for the prolonged drug delivery, where controlled delivery over extended periods of time is required. Other possible applications for such a device are for use as a subcutaneous implant to achieve systemic drug release which bypasses the gastrointestinal tract and the liver, or for the local treatment of skin conditions. The device is useful for drugs which are sensitive to the acidic environment of the stomach and drugs which are susceptible to a high degree of first pass metabolism. Nanosystems are capable of penetrating barriers such as the blood brain barrier, the pulmonary system and the tight junctions of the skin, which were previously

difficult to treat due to their complex anatomic make-up. Nanoparticles can act to enhance the uptake and retention of drug at these sites, thereby serving to successfully manage the numerous disease conditions by achieving superior therapeutic efficacy (Hughes, 2005; Rao *et al.*, 2008; Jolck *et al.,* 2010). The effective management of ADC and other neurological manifestations of HIV/AIDS require sustained concentration of drug in appropriate dosages delivered site specifically (Brewster *et al.* 1995). This can be acheived with nanotechnology.

1.3 Novelty of this study

- The first implantable NMDDD for application in ADC.
- Novel combination of polymers for the formulation of nanoparticles and scaffolds.
- An innovative polymeric modification technique was employed for scaffold fabrication which is proposed to emanate in a unique modulated drug release mechanism.
- The first in vivo implantation of AZT loaded NMDDD into the brain of Sprague Dawley rats.

1.4 Aim and Objectives

The aim of this study is to develop a nano-enabled multipolymeric drug delivery device for intracranial implantation into the frontal lobe of the rat brain, enabling controlled, site-specific delivery of drug, for application in ADC. AZT was employed as the model drug due to its demonstrated favorable penetration into the CNS.

To achieve this, the following objectives are outlined:

1. To formulate drug-loaded nanoparticles investigating various methods such as the salting-out approach, the emulsification-diffusion approach, or the nanoprecipitation approach.
2. To formulate robust multipolymeric scaffolds employing a crosslinking approach.
3. To evaluate the physicochemical and physicomechanical properties of the nanoparticulate and multipolymeric platform.
4. To assess the drug release behaviour from the nanoparticulate system.
5. To incorporate the drug-loaded nanoparticles into a multipolymeric scaffold device and assess the *in vitro* release, swelling, and erosion studies in simulated biological media.
6. To employ a 3-factor Box-Benhken statistical design for the synthesis of variants to explicate the effect of independent variables set during preliminary studies to establish a correlation between variables by the analysis of the physicochemical characteristics of the prepared formulations, with subsequent formulation optimisation.
7. Development and optimization of a surgical protocol for the implantation of multipolymeric devices into the rat brain employing a Sprague Dawley rat model.

8. To perform *in vivo* animal studies to determine drug release, polymer degradation and resultant histomorphological changes in the brain post implantation.

1.5 Overview of the dissertation

Chapter 1 briefly outlines the rationale for the study being carried out. The challenges faced with the management of neurological diseases, including ADC due to the restrictions imposed by the BBB are also noted. The rationale for the study being conducted as well as the aims and objectives and an overview of the chapters are summarized in Chapter 1.

Chapter 2 contains information regarding the HIV pandemic and ADC, including the severity of the condition and limitations associated with current therapeutic agents available for the management of this condition. The limitations posed by the BBB and techniques used CNS drug delivery are also highlighted. Nanotechnology, the latest revolutionary field of research in science today is discussed, including its application in medicine and the benefits of polymeric nanosystems for the management of ADC.

The pre-formulation studies carried out are highlighted in **Chapter 3**. The formulation of polymeric nanoparticles employing two preparation techniques, namely the controlled gelification of alginate and the salting out approach are explored. The formulation of multipolymeric scaffolds using a variety of hydrophilic and hydrophobic polymers employing a crosslinking approach using multivalent salt solutions is also assessed. Physicochemical characterisation and drug release parameters are ascertained for the prepared formulations, with the rationale for the chosen formulations for further studies highlighted.

The optimization of AZT-loaded alginate nanoparticles and the formulation of multipolymeric polycaprolactone/epsilon caprolactone/cellulose acetate phthalate scaffolds are presented in **Chapter 4**. A 3-factor Box-Behnken design was employed to optimise nanoparticle and polymer scaffold formulations which were then analyzed to ascertain the physicochemical and physicomechanical properties of the prepared formulations. Drug release from both the nanoparticles and multipolymeric device containing dispersed nanoparticles were also evaluated in this chapter. Evaluation of the optimized formulation then followed.

Chapter 5 highlights *in vivo* studies utilizing a male Sprague Dawley rat model. Implantation of the optimized NMDDD in the frontal lobe of the brain employing a technique analogous to that used for the insertion of an intra-cranial pressure monitor in the human subject was undertaken. This was followed by histomorphological analysis, bioerosion, and drug release

in the CNS ascertained by means of ultra performance liquid chromatographic (UPLC) analysis.

Chapter 6 includes recommendations for future work to be carried out to further improve the device for human application.

Chapter 7 outlines concluding remarks for the performed study.

CHAPTER 2

AIDS Dementia Complex: Currently Available Treatment Strategies and Limitations Posed by the Blood Brain Barrier

2.1 Literature Survey

2.1.1 AIDS Dementia Complex: The neurological manifestation of HIV

Human Immunodeficiency Virus (HIV) infection of the central nervous system (CNS) is associated with neurocognitive impairment, ranging in severity from mild cognitive disorder (MND) to AIDS dementia complex (ADC), resulting from HIV replication within the CNS. ADC is a clinical manifestation resulting from the presence of the HIV-1 strain of the retrovirus within the CNS. The condition remains a serious manifestation of HIV in both developed and developing countries (Portegies *et al.*, 1994; Kim *et al.*, 1996; Vitiello *et al.*, 1997; Saksena *et al.*, 1998; Pemberton *et al.*, 2001; Schutzer *et al.*, 2004; Giunta *et al*., 2006; Varatharajan and Thomas, 2009). ADC occurs in the late stage of infection due to severe immune suppression and has been considered an Acquired Immunodeficiency Syndrome (AIDS) defining condition since 1987 when a diagnosis is made in the absence of AIDS, however this is uncommon (Portegies *et al.*, 1989; Kim *et al.*, 1996; Sawchuk and Yang, 1999; Lawrence *et al.*, 2002). The dementia results in a host of cognitive, motor and behavioural symptoms, ranging in severity from minor cognitive symptoms, such as forgetfulness and lack of attention, to severe dementia and paralysis (Portegies *et al.*, 1989; Lawrence *et al.*, 2002; Yiannoutsos *et al.*, 2004; Thompson *et al.*, 2005; Martín-García *et al.*, 2006; Cook-Easterwood *et al.*, 2007).

Neurological dysfunction of the brain, spinal cord, meninges and neurons are observed in AIDS patients. However, of these, ADC remains the most clinically significant, affecting approximately 60% of HIV-infected individuals (Sawchuk and Yang, 1999; Robertson *et al.,* 2010).

HIV has been identified in the brain as early as 2 days after initial infection; however, this remains clinically insignificant until the onset of full blown AIDS. (Bower, 1996; Sakaie *et al.*, 1999; Enting *et al.*, 2000; Chang, *et al.*, 2004; Wu *et al.*, 2007). ADC results from HIV infection in the brain in the absence of opportunistic infections, such as cryptococcal meningitis, *Toxoplasma gondii*, Epstein Barr virus, tumours and other causes of dementia, narcotic, and alcohol abuse and drug therapy being examples of such causes (Lawrence *et*

al., 2002). The virus enters and is harboured in the CNS, resulting in a subcortical dementia affecting the subcortical regions of the brain, namely the basal ganglia and the deep white matter. This can be noted by the increased metabolism occurring in these regions of the brain (Gallo, 1994; Bower, 1996; Kim *et al.*, 1996; Sawchuk and Yang, 1999; Avison *et al.*, 2002; Chang *et al.*, 2004; Yiannoutsos *et al.*, 2004).

ADC progresses rapidly, with global mental impairment occurring within 2months of the initial symptoms in some patients. Death follows within 1 to 6months, usually as a result of systemic infection or aspiration pneumonia (Kim *et al.*, 1996; Sawchuk and Yang, 1999; Giunta *et al.*, 2006). Early identification and treatment of ADC is crucial, especially for patients in which ADC progresses rapidly (Pemberton *et al.*, 2001). Magnetic resonance imaging (MRI) of the brain identifies abnormal brain pathology with the ADC sufferers as seen in Figure 2.1

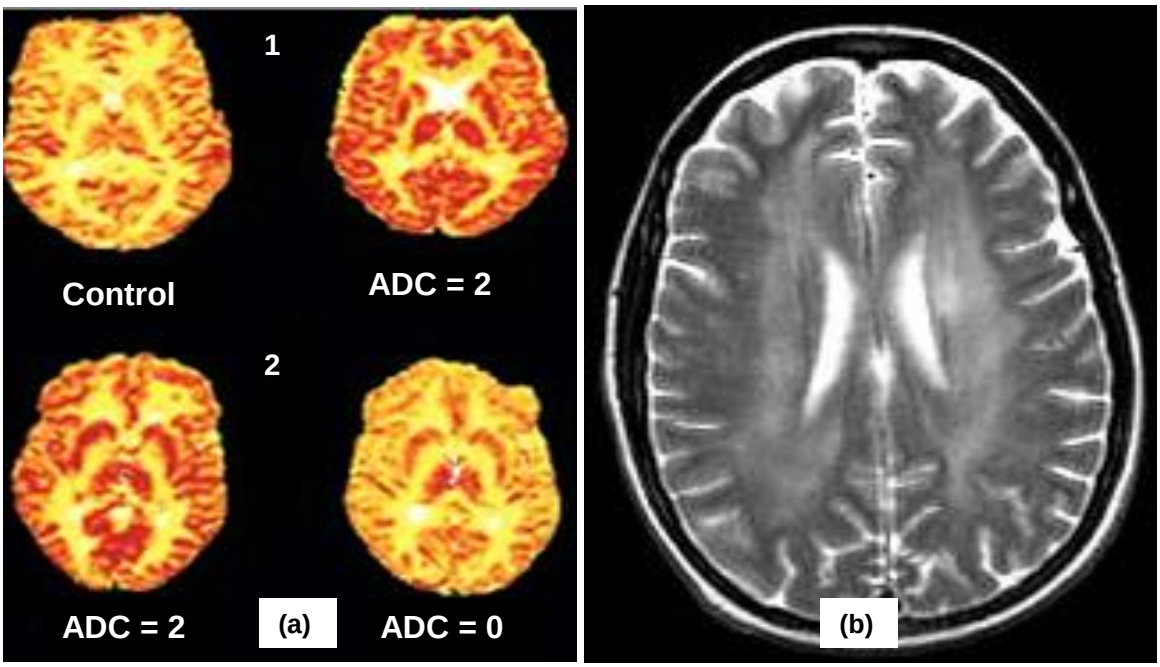

Figure 2.1: *(a) Dynamic contrast functional MRI images of normalised cerebral blood volumes at the level of the basal ganglia. (1) A healthy subject (left) and an HIV positive patient (right) with Stage 2 ADC. (2) MRI images from the same patient before treatment with AZT (left) and after 6months of treatment with AZT (right) and (b) MRI of a patient with ADC, displaying diffuse white matter abnormalities at the level of the lateral ventricle. The cortical sulci are prominent, indicating atrophy (Sakaie and Gonzalez, 1999).*

The manifestations of ADC, a name coined in 1985 by Drs. Navia and Price, have been reported since the early days of the HIV epidemic and had previously been given a variety of names and descriptions, “HIV encephalopathy or encephalitis”, “multifocal giant-cell encephalitis”, “subacute encephalitis”, “HIV associated dementia” and “progressive

dementia", being just a few. The most acceptable definition of ADC had been published in May 1991 by Dr. Janssen and colleagues. This includes only the most debilitating manifestations of ADC, being major cognitive and motor disorders, and neglects the more common, but harder to detect symptoms, such as irritability and moodiness (Link, 1992). ADC is characterised by neurocognitive deficits which impairs a person's ability to function at work and perform tasks of daily activity (Vitiello *et al.*, 1997; Robertson *et al.,* 2010).

ADC is a serious concern in developing countries due to inadequate access to ARV therapy. Poor compliance due to the complicated drug regimens has increased resistance to ARV's, compounding the ADC pandemic (Wu *et al.*, 2007).

2.1.2 HIV entry into the brain

ADC is thought to be as result of immune activation and viral replication in the brain (Pemberton *et al.*, 2001). The HIV virus is thought to enter the CNS within days to weeks after initial infection through infected immune cells, including T cells, monocytes, and trojan horse trafficking of infected macrophages across the blood brain barrier (BBB), which migrate into the brain to replenish the perivascular population in the brain (Sawchuk and Yang, 1999; Thompson *et al.*, 2005; Giunta *et al.*, 2006; Varatharajan and Thomas, 2009; Akhtar *et al.,* 2010; Valcour *et al.,* 2010; Vinogradov *et al.,* 2010). HIV entry can also be attributed to infiltration of infected cells across the choroid plexus and compromised BBB, allowing the entry of free viruses into the CNS (Avison *et al.*, 2002; Martín-García *et al.*, 2006). A viral reservoir within the brain is thus established soon after initial HIV infection, which is resistant to anti-retroviral (ARV) therapy (Melton *et al.*, 1997). However, clinically significant infection of the CNS only occurs later in the course of the disease when patients are significantly immunocompromised, with a resulting cluster of differentiation 4 (CD4) T cell depletion below 200cells/mm^3, with resultant cognitive, motor and behavioural defects associated with ADC (Giunta *et al.*, 2006; Varatharajan and Thomas, 2009). CD4 cells are glycoproteins expressed on the surface of T cells, assisting with T cell activation and subsequent activation of the immune cascade upon interacting with antigens. CD4 depletion is significant in HIV due to it being an indicator immune system function and subsequently an indicator of AIDS when the count falls below 200cells/mm^3. Healthy individuals have a circulating CD4 count of 800-1200cells/mm^3 (Rocha and Tanchot, 2004; Pirzada *et al*., 2006; Cai and Li, 2009; Wolbers *et al*., 2010).

ADC does not result from direct neuronal infection within the CNS and is instead as a result of neuronal dysfunction and death (apoptosis) caused by dendritic degeneration, due to toxin release within the CNS, specifically in the hippocampus (affecting cognition) and the basal

ganglia (affecting motor function), by viral protein release from infected mononuclear phagocytes (Avison *et al.*, 2002; Lawrence *et al.*, 2002; González-Scarano *et al.*, 2005; Thompson *et al.*, 2005; Giunta *et al.*, 2006; Martín-García *et al.*, 2006).

Perivascular macrophages (derivatives of monocytes), multinucleated giant cells (caused by HIV induced fusion of microglia and macrophages), microglia, endothelial cells (cells which line blood vessels in the brain), astrocytes (cells which fill the spaces between neurons and provide support and insulation for neurons) and T lymphocytes, are all infected by the HIV-1 virus as these cells have CD4 receptors to which the HIV-1 can bind, facilitating viral entry into the cell (Budka, 1991; Lawrence *et al.*, 2002; Avison *et al.*, 2002; Cook-Easterwood *et al.*, 2007; Akhtar *et al.,* 2010; Valcour *et al.,* 2010; Vinogradov *et al.,* 2010). Of these cells, macrophages are the primary source of indirect nerve damage, as they act as viral reservoirs within the CNS. Infected macrophages and astrocytes shed gp 120 (proteins on the outer coat of the HIV virus) and tat genes (a transactivator proteins which aids viral production). These proteins are both directly and indirectly neurotoxic (Link, 1992; Gabuzda, 1996; Xiong *et al.*, 2000; Lawrence *et al.*, 2002; Sammikkannu *et al.,* 2010). Tat genes increase intracellular Ca^{2+} which causes oxidatitive damage and apoptosis. Tat genes may also facilitate apoptosis indirectly by stimulating the secretion of matrix metalloproteinase and other such substances. These substances activates macrophages and microglia, which in turn increases the availability of nitric oxide, superoxide anions, platelet activating factor and arachidonic acid metabolites, which are not unique to ADC, but is found in most neurodegenerative diseases (Lawrence *et al.*, 2002; Sammikkannu *et al.,* 2010).

Proinflammatory cytokines such as tumour necrosis factor alpha, gamma (TNFα, TNFγ), alpha interferon (IFNα), platelet activating factor (PAF), nitric oxide (a free radical responsible for vasodilation), arachidonic acid, as well as chemokines are produced in abundance by cells infected by HIV (Avison *et al.*, 2002, Cook-Easterwood *et al.*, 2007; Ramirez *et al.,* 2010). Proliferation of astrocytes (astrogliosis), indicative of widespread astrocyte activation and damage, causes demyelination of neurons, which in turn increases the synthesis of inflammatory cytokines and arachidonic acid metabolites. Astrocyte glutamate clearance is blocked by gp 120, resulting in an exocitotoxic neurotoxic cascade, which is initiated due to activation of the arachidonic pathway (Bowers, 1996; Avison *et al.*, 2002; Wu *et al.*, 2007). In addition to this, macrophages release quinolinic acid into the brain, which binds to nerve cells and causes nerve cell death (Link, 1992). This series of events leads to inflammation, causing a general pattern of dysregulation within the CNS, associated with all cases of clinical dementia, which in turn results in apoptosis (Bowers, 1996; Avison *et al.*, 2002; Lawrence *et al.,* 2002; Ramirez *et al.,* 2010; Wang *et al.,* 2010).

Apoptosis occurs not only at the site of HIV exposure, but also at remote regions due to gap junctions, which are used by astrocytes for communication. Infected astrocytes are therefore able to communicate with other astrocytes distant in proximity to initial viral exposure, causing proliferation of HIV damage throughout the CNS (Bowers, 1996; Lawrence *et al.*, 2002; Wang *et al.,* 2010).

Histological findings indicate astrogliosis, myelin pallor and loss of myelin surrounding neuronal axons, loss of synaptic connections, and neuronal loss, which are commonly seen in brain tissue from individuals who died as a result of AIDS (Vitiello *et al.*, 1997; Lawrence *et al.*, 2002). Histopathological abnormalities predominate in the central white matter and subcortical grey matter of the brain (Kim *et al.*, 1996; Lawrence *et al.*, 2002). The extent of these neuropathological changes varies between individuals and, in a single individual, from one brain region to another. Hypertrophy is also seen in histological and imaging (computed tomography [CT] and magnetic resonance imaging [MRI]) assessments of brain tissue, which is characteristic of reactive astrocytes. Imaging studies also indicate a reduction in the basal ganglia volume and cortical hypometabolism in patients with advanced ADC. Hypermetabolism of the thalamus and basal ganglia is seen in patients with milder ADC. This leads to dysregulation of neural homeostasis, which upsets neuronal function, causing neuronal death and neurobehavioral dysfunction (Vitiello *et al.*, 1997).

The microenvironment of the CNS is sensitive to change, with minor disruptions having major impacts on cognition, behaviour and motor skills. This altered microenvironment of the CNS, as described in Figure 2.2, due to HIV results in neurotoxicity, producing the symptoms experienced by ADC sufferers (Polianova *et al.*, 2005).

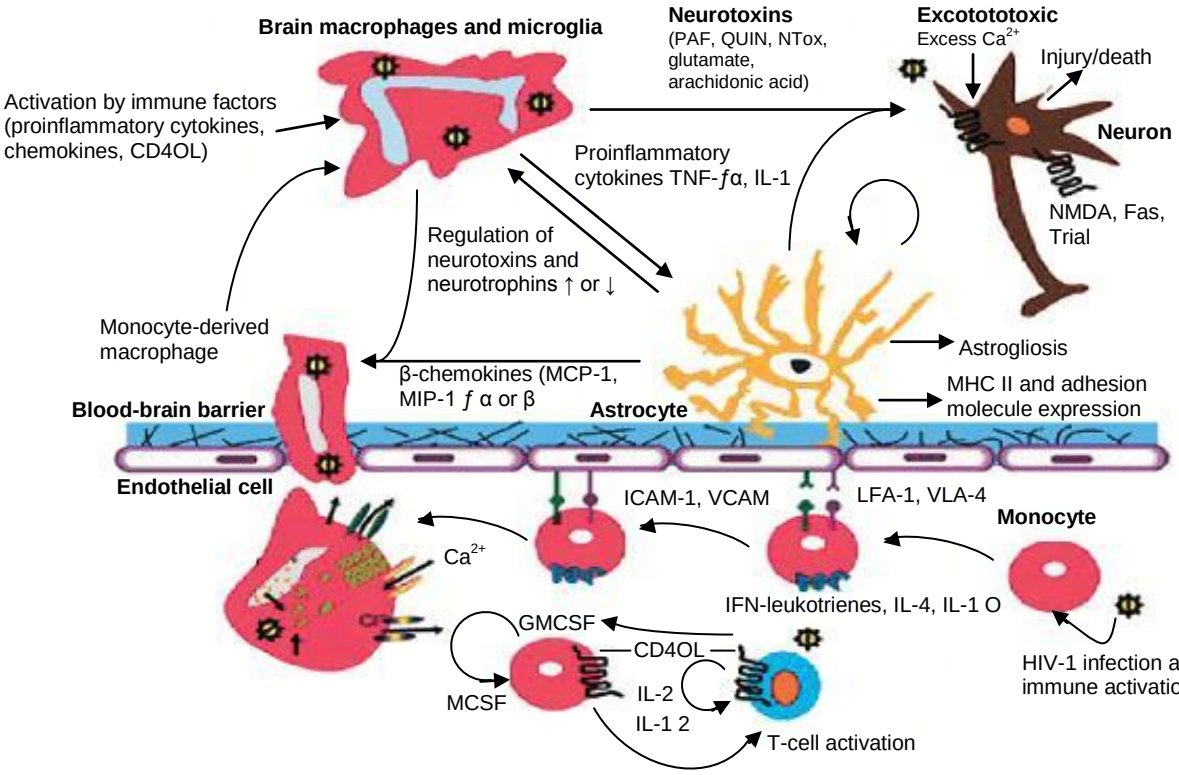

Figure 2.2: *Illustration of the entry of HIV into the central nervous system with transportation of the virus into differentiating macrophages or through lymphocyte-macrophage cell interactions (adapted from AIDS Read, 2002).*

2.1.3 Symptoms of ADC

ADC was originally identified as being an encephalitic disorder, characterised by cognitive and behavioral symptoms, as per a review of neurological disorders relating to HIV/AIDS (Wu *et al.*, 2007). Since then, it was found that ADC is responsible for a host of other neurological symptoms including disturbed sleep patterns, loss of fine motor skills, speech impairment and symptoms of affect, being apathy lethargy and social withdrawal (Link, 1992; Bower, 1996; Gabuzda, 1996; Kim *et al.*, 1996; Fernandes *et al.*, 2006; Wu *et al.*, 2007).

The term dementia describes a clinical syndrome composed of memory loss, decreased mental concentration and loss of intellectual functions due to progressive disease in the brain. Symptoms experienced by ADC suffers is in accordance with this definition, consisting of cognitive, motor and mood impairments which is progressive in nature (Bower, 1996).

The first symptoms which appear in ADC suffers are short-term memory loss and poor concentration. This is difficult to recognise and if recognised, it is rarely attributed to ADC as stress, depression and many other conditions can be implicated for such symptoms (Bower, 1996). Cognitive impairment is characterised by memory impairments, speech problems, inability to concentrate, poor judgement, impaired learning ability and speed of processing

information (Link, 1992; Bower, 1996; Kim *et al.*, 1996). Global cognitive dysfunction is found late in the course of the illness (Kim *et al.*, 1996).

Motor impairment is characterized by impaired speed of movement, loss of balance, gait ataxia, fine motor speed, and manual dexterity impairment, bladder and faecal incontinence, paralysis, poor coordination, hyper-reflexia of the lower extremities, stiff and awkward, or markedly slow movements (Link, 1992; Bower, 1996; Kim *et al.*, 1996).

Mood or affect impairments are defined as changes in emotional responses to experiences, being apathy, personality changes, irritability, lack of inhibition and loss of libido (Link, 1992; Bower, 1996; Kim *et al.*, 1996). Poor concentration, loss of short- or long-term memory, social withdrawal, slowed thinking, irritability, apathy, poor coordination, impaired judgement, and personality change are all symptoms associated with impairment of affect (Link, 1992; Vitiello *et al.*, 1997; Fernandes *et al.*, 2006; Wu *et al.*, 2007).

Behavioural changes are the least understood and often missed in a diagnosis of ADC. They are characterised as impairments in the ability to perform tasks and activities of daily living. These changes have found in 30-40% of patients in the early stages of ADC (Link, 1992). Severe mental conditions, such as depression, psychosis, and mania are also experienced by ADC sufferers, however this occurs later in the course of the condition (Link, 1992; Bower, 1996). As the condition progresses, patients develop symptoms associated with advanced dementia, as well as mutism, paraplegia, and spontaneous tremors and seizures amongst others (Gabuzda, 1996; Kim *et al.*, 1996).

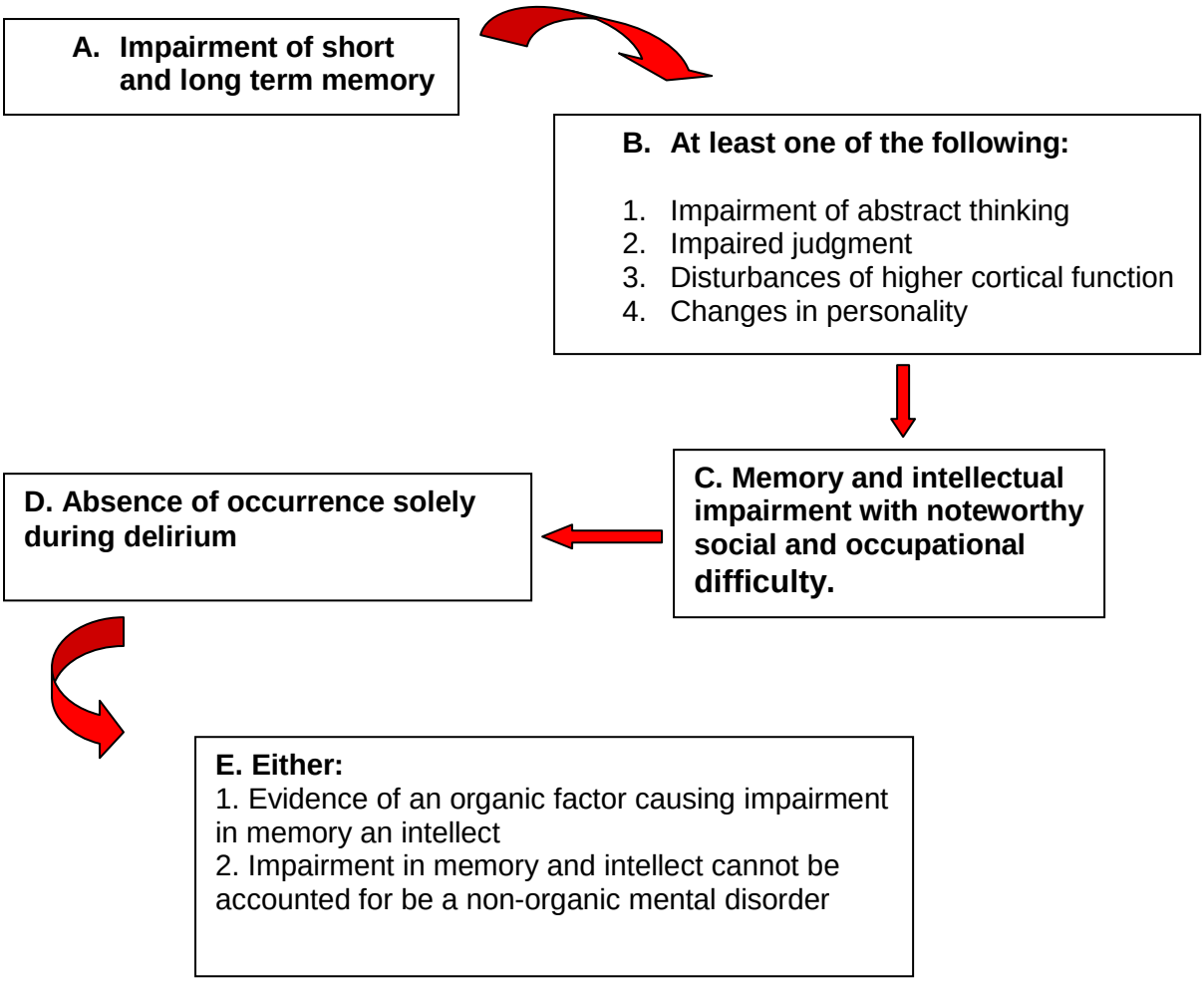

Figure 2.3: *Diagnosis of dementia (adapted from Washington, D.C: American Psychiatric Association, Diagnostic and statistical manual of mental disorders, 4th edition, 1994).*

2.1.4 Diagnosis of the condition

Many AIDS related opportunistic infections present with symptoms similar to that of ADC, toxoplasmosis, cryptococcal meningitis, and cytomegalovirus (CMV) encephalitis being a few. Direct and indirect evidence, by means of neurological, psychological and cognitive tests, are therefore required for an accurate diagnosis of ADC to be made (Bower, 1996). Assessment of cognitive function forms a crucial part in the classification of ADC, with the various stages of the condition highlighted in Table 2.1. Cognitive function is also used to differentiate ADC from other manifestations of HIV in the CNS and for appropriate therapeutic management of the condition. ADC is diagnosed primarily using a mental status test, which reveals problems such as loss of short and long term memory, orientation and concentration impairment, abstract thinking, slow verbal and motor responses, memory recall, speed of information processing, mood swings and blunted affect (Link, 1992; Kim *et al.*, 1996; Lawrence *et al.*, 2002).

Cerebrospinal fluid (CSF) examinations are also conducted, with CSF obtained from a spinal tap or a lumbar puncture, in which CSF is tested for the presence of active HIV infection. Information regarding levels of HIV DNA and RNA can also be obtained from the CSF (Bower, 1996). It has also been found that that the viral load in the CSF correlates to progressive dementia in children. Non-specific abnormalities with CSF, including mild elevations of proteins and white blood cells are observed in the CSF of patients with ADC (Epstein *et al.*, 1987; Link, 1992; Bower, 1996; Sawchuk and Yang, 1999). CSF examination is therefore used to exclude infectious and neoplastic conditions manifesting as dementia (Sawchuk and Yang, 1999).

CT scans are used to detect atrophy of brain tissue, occurring mainly in the cerebral ventricular and subarachnoid regions, which is diagnostic of ADC. These scans are also used to rule out other causes of dementia and symptoms experienced, such as subcortical lesions and toxoplasmosis (Bower, 1996; Sawchuk and Yang, 1999). MRIs, a scan far more sensitive than CT scans, which are capable of supplying a quantitative measure of metabolite concentrations, is used when CT scans are inconclusive due to the high costs incurred with the use of MRI. MRIs are capable of detecting neurochemical abnormalities in the CNS early in the course of infection, however, the cost of the scan precludes this from being carried out (Link, 1992; Sakaie *et al.*, 1999; Cysique, 2006). Single Photon Emission Computed Tomograms (SPECTs) scans employs radioactive material to measure blood flow in the brain and is used to detect early dementia due to HIV. SPECTs scans are also used to observe responses to ARV therapy by monitoring whether ARV's improves blood flow to the brain (Link, 1992; Cysique, 2006). Photon emission tomography (PET) scans are used to detect patterns in glucose metabolism. Hypermetabolism of glucose is associated with early stage ADC and hypometabolism of glucose is characteristic of late stage ADC (Bower, 1996).

Subcortical regions of the brain are most affected, being the deep white matter and the basal ganglia. However, neuronal loss can also be seen in the cortex as well, and damage to the synaptic dendritic tree also occurs. These findings can be viewed in histological analysis of ADC affected brain tissue. Onset of cognitive impairment and severity can be correlated to the extent of pathology in the subcortical brain regions (Chang *et al.*, 2004). Altered metabolic activity at various regions in the brain as well as a decrease in brain volumes and augmented water content is observed with an increase in disease severity (Sawchuk and Yang, 1999).

2.1.5 Management of ADC utilising drug therapy

With the introduction of ARV's, 2 million lives have been spared since 2002 in low and middle income countries, with a dramatic improvement observed in the quality of life of individuals living with HIV/AIDS. There has been a conspicuous increase in the number of people with access to ARV's in sub-Saharan Africa, with over 1 million people receiving treatment by June 2006. However, due to volumes of infected individuals, this accounts for less than one quarter of the population being treated in this region (UNAIDS, 2006; das Neves, 2009).

ARV's work to manage ADC indirectly by interfering with systemic viral production. Systemic viral load is decreased, resulting in a decrease in the number of viral cells available for entry into the CNS with a subsequent decline in the incidence of dementia. ARV's also serve to protect the neurons by minimising damage caused by elevated levels of cytokine and nitric oxide in the brain (Bower, 1996; Lawrence *et al.*, 2002).

2.1.5.1 Highly Active Antiretroviral Therapy

Highly Active antiretroviral therapy (HAART) has been shown to prolong life expectancy and slow the progress of HIV in infected adults and children, with a major improvement in patient quality of life (Puthanakit, 2007). The incidence of life threatening opportunistic infections, Kaposi's sarcoma, *Mycobacterium avium* complex related disease, cryptococcal menigitis and *Pneumocystis jirovicii* pneumonia, associated with high morbidity and mortality, has dramatically declined with the introduction of HAART in 1995, resulting in HIV becoming a chronic disease rather than an acute rapidly progressing condition (Sacktor, 2002; Thompson *et al.*, 2005; Cook-Easterwood *et al.*, 2007; Puthanakit, 2007; das Neves, 2009; Varatharajan and Thomas, 2009). HAART is found to be effective in suppressing systemic viral replication and subsequently decreasing viral load to nearly undetectable levels within weeks of initiating treatment. Lymphocyte function is restored, thereby decreasing mortality and the incidence of systemic opportunistic infections due to AIDS. The frequency of HIV dementia has decreased by 50% with the introduction of HAART (Lawrence *et al.*, 2002; Sacktor, 2002). HAART regimens are often complicated and require strict adherence to therapy, more than 95%, in order for therapeutic benefits to be achieved and viral mutation and drug resistance to be prevented. Such stringent drug criteria and drug toxicity, resulting in poor patient compliance, as well as drug interactions, have resulted in an increase in resistance to ARV's and subsequent declines in CD4 cell counts. It is therefore thought that neurological diseases associated with HIV may begin to rise once again (Lawrence *et al.*, 2002; Sacktor, 2002; Penedo *et al.*, 2003; Smit *et al.*, 2004; Beblo *et al.,* 2010).

Table 2.1: *ADC has been classified according to stages, ranging in severity from normal, as in early infection, to end-stage dementia, associated with severe immune depletion and death (adapted from Link 1992; Worley and Price, 1992).*

Early Stage **Stage I**	**Middle Stage** **Stage II**	**Late Stage** **Stage III**	
Stage 0: Normal neurological activity in the presence of HIV infection in the brain	Symptoms of motor dysfunction	Incontinence	
Stage 0.5: Sub-clinical stage	Poor memory and concentration	Spastic gait	
Minimal or ambiguous neurological symptoms	Slowed response to stimuli	Loss of initiative	
No impairments of daily activity	Frequently dropping objects	Withdrawal	
Stage 1: Explicit intellectual or motor impairment	marked slowness of activities	Psychosis or mania	
All but the most demanding activities of daily living can be performed	Reversing of words and numbers	Confinement to bed	
Difficulty concentrating	Ambulatory but requires assistance	**Severe Dementia**	**End Stage**
Slowed thinking	Capable of self care	Major intellectual disability	Near vegetative state
Memory loss	Incapable of performing demanding task of daily activities	Cannot walk unassisted	Rudimentary cognition
Poor coordination			Para- or quadraplegia
Change in handwriting			
Patients rely on lists to keep track of daily activities			
Mental status test remains normal			

Prior to HAART, therapy utilising single or dual nucleoside reverse transcriptase inhibitors (NRTI) were widely implemented (1992-1995). This rapidly led to ARV resistance and subsequent lack of efficacy. However, a combination of at least three ARV's from different classes proved to be more effective in managing HIV and is now the standard care for patients (Ves *et al.*, 2001; Lawrence *et al.*, 2002; das Neves, 2009; Varatharajan and Thomas, 2009). In 2003, approximately 370 000 AIDS related deaths were reported. It was estimated that the mortality rate would rise to approximately 4 to 7 million people by 2010 if no medicinal intervention was made (Badri *et al.*, 2006). With the introduction of HAART into the South African public health centres in 2002, the incidence of public hospital admission due to AIDS-related conditions has declined significantly (Badri *et al.*, 2006). HAART works to combat immunosuppression, thereby reducing disease progression and patient mortality (Thompson *et al.*, 2005). The rationale behind HAART was the use of multiple ARV's which would act synergistically at different stages of the virus's life cycle to reduce viral replication (Orsega, 2006). It was also thought that combined therapy would reduce the incidence of drug toxicity and drug resistance (Bean, 1992).

HAART helps alleviate dementia in 2 ways: (1) drugs enter the CNS to treat HIV infection, and/or (2) systemic viral load reduction and reconstitution of body-wide immunity has a positive influence on neurological function. In a study conducted by Cook-Easterwood *et al.*(2007) it was found that HAART reduced astrogliosis and TNFα production in a mouse model, supporting the use of HAART for managing ADC (Cook-Easterwood *et al.*, 2007). The problem that remains, however, is that few drugs are capable of penetrating the BBB and reaching optimal drug concentrations in the CNS. This results in suboptimal drug concentrations in the brain, which augments ARV resistance. The use of systemic treatment for the management of ADC is therefore ineffective in yielding significant declines in viral replication and viral load within the CNS (Bower, 1996; Smit *et al.*, 2004; Wu *et al.*, 2007).

Table 2.2.1: *Adult HAART regimens implemented in the South African public sector of health care (adapted from the South African National Department of Health, National Antiretroviral Treatment Guidelines, 2004).*

Regimen 1a	Regimen 1b[1]	Regimen 2
•Stavudine (40mg 12hourly, or 30mg if weight is < 60kg) •Lamivudine (150mg 12hourly) •Efavirenz (600mg at night, or 400mg if weight is < 40kg)	•Stavudine (40mg 12hourly, or 30mg if weight is < 60kg) •Lamivudine (150mg 12 hourly) •Nevirapine (200mg daily for the first 2 weeks of therapy, increased to 200mg 12hourly thereafter	•Zidovudine (300mg 12hourly •Didanosine (400mg daily, or 250mg if weight is < 60kg, taken alone, dissolved in water, unless enteric coated, on an empty stomach) •Lopinavir/Ritonavir (400/100mg 12hourly, to be kept in a cool, <25°C, dry place)

[1] ***Administered if female patient is unable to guarantee reliable contraception whilst on ARV therapy***

Table 2.2.2: *Paediatric HAART regimens implemented in the South African public sector of health care (Adapted from the South African National Department of Health, National antiretroviral treatment guidelines, 2004).*

Regimen 1	< 6 months	> 6 months, < 3 years	> 3 years
	•Stavudine (substituted with Zidovudine if no refridgerator is available at the patients home) •Lamivudine •Ritonavir or Nevirapine if no previous exposure has occurred	•Stavudine (substituted with Zidovudine if no refridgerator is available at the patients home) •Lamivudine •Ritonavir or Nevirapine if no previous exposure to nevirapine occurred	•Stavudine (substituted with Zidovudine if no refridgerator is available at the patients home) •Lamivudine •Efavirenz

Regimen 2	< 3 years or < 10kg	> 3 years or > 10kg
	•Didanosine (to be taken alone, dissolved in water, on an empty stomach) •Zidovudine (substituted to Abacavir if no refridgerator is available at the patients home) •Lopinavir/Ritonavir or Nevirapine if no previous exposure has occurred	•Didanosine (to be taken alone, dissolved in water, on an empty stomach) •Zidovudine (substituted to Abacavir if no refridgerator is available at the patients home) •Lopinavir/Ritonavir

All paediatric doses are calculated according to the paediatric dosing schedule with body surface area (BSA) used to calculate patient dose, refer to Equation 2.1.

$$BSA = \sqrt{\frac{Height(cm) \times Weight(kg)}{3600}} m^2 \qquad \textbf{(Equation 2.1)}$$

2.1.5.2 Zidovudine therpary for the management of ADC

Prior to the introduction of zidovudine (AZT) in May 1987, the incidence of ADC in AIDS suffers was as high as 53%, as seen in the first half of 1987. After the introduction of AZT the incidence of ADC decreased to 10% in the second half of 1987 and to 3% in 1988 (Portegies *et al.*, 1989; Foudraine *et al.*, 1998; Parris, 2007). A British study conducted between 1982 and 1988 found that only 2% of AIDS patients taking AZT developed ADC, whereas 20% of patients not receiving the drug developed ADC. AZT, (3'-azido-3'-deoxythymidine), formerly known as azidothymidine, is a nucleoside analogue which has a similar structure to that of thymidine, a pyrimidine deoxyribonucleoside which is naturally present in the brain (Bean, 1992; Danesi *et al.*, 1998; Uslu *et al.*, 2002; Brown *et al.*, 2003, Dunge *et al.*, 2005; Thomas and Segal, 2009; Varatharajan and Thomas, 2009). AZT was the first ARV to be developed and marketed for the treatment of HIV/AIDS (Dallas *et al*., 2000). However, the drug was first developed as an antitumor agent, with inhibition of HIV replication been discovered in 1985. The drug is active in its phosphate form, with the triphosphate form being the competitive inhibitor of reverse transcriptase (Bean, 1992; Danesi *et al.*, 1998; Sawchuk and Yang, 1999; Dallas *et al.*, 2000). Figure 2.4 illustrates the target site of ARV's on the HI virus with Figure 2.4b highlighting the mechanism of action of AZT.

As a class, the NRTI's display poor penetration into the brain, due to poor BBB permeability (Gallo, 1994). However, certain NRTI's are capable of crossing the BBB, didanosine and zalcitabine being examples of such, and are used to manage ADC. In a study conducted by Foudraine et al, it was found that Stavudine and lamivudine are also capable of penetrating the BBB, however, not as well as AZT. Of the ARV's currently approved for utilization in HAART, (refer to Table 2.3), AZT therefore remains the current gold standard for the management of ADC (Bean, 1992; Foudraine *et al.*, 1998; Dallas *et al.*, 2000).

AZT is rapidly absorbed from the gastro-intestinal tract and peak plasma concentration is reached within 0.6-2hours.It has a plasma half life ($t^1/_2$) of approximately 1.5hour. Rapid elimination of the drug occurs by the liver, necessitating frequent administration (Lotterer *et al.*, 1991; Bean, 1992; Moore *et al.*, 1995; Uslu *et al.*, 2002). However, toxicity is a major

concern with AZT therapy, especially with the high doses used to treat ADC. Doses as high as 1000mg to 2000mg, as compared to the 600mg used in HAART therapy, are required to achieve optimal therapeutic levels in the CNS (Aungst, 1999; Bean, 1992; Link, 1992; Moore *et al.*, 1995; Bower, 1996; Brown *et al.,* 2010). This can be attributed to the low bioavailability of the drug due to first pass metabolism in the liver, with only 60 to 70% of the drug present in blood plasma, of which only 25% enters the CSF circulation (Routy *et al.*, 1990; Link, 1992; Aungst, 1999; Carvalho *et al.,* 2010). However, such high doses have been revealed to increase the risk of severe aplastic anemia due to suppression of circulating erythrocytes and neutrophils (Agarwal *et al.,* 2010; Anderson and Power, 2010; Kiragga *et al.,* 2010). Pre-existing cytopenias and low CD4 counts predisposes individuals to this condition. This in turn increases the risk of opportunistic infections (Bean, 1992; Hewitt *et al.*, 1993; Moore *et al.*, 1995; Bower, 1996; Aungst, 1999). Aplastic anemia is a major limitation to AZT therapy and usually necessitates blood transfusions of recombinant human erythropoietin to replenish erythrocyte levels, dose reduction and discontinuation of AZT therapy in severe cases (Bean, 1992; Hewitt *et al.*, 1993; Dallas *et al.*, 2000). Also, patients, especially those who are severely immunocompromised, are incapable of tolerating such high doses (Link, 1992), leading to non-compliance. The poor bioavailability as well as the associated side effects, the more common ones being headaches and nausea, experience commonly with higher doses, creates the need for localized drug delivery. Localized delivery would bypass the BBB and systemic circulation, which are responsible for poor bioavailability and many of the side effects experienced with current therapies (Bean, 1992; Alavijeh *et al.*, 2005; Agarwal *et al.,* 2010; Anderson and Power, 2010; Carvalho *et al.,* 2010).

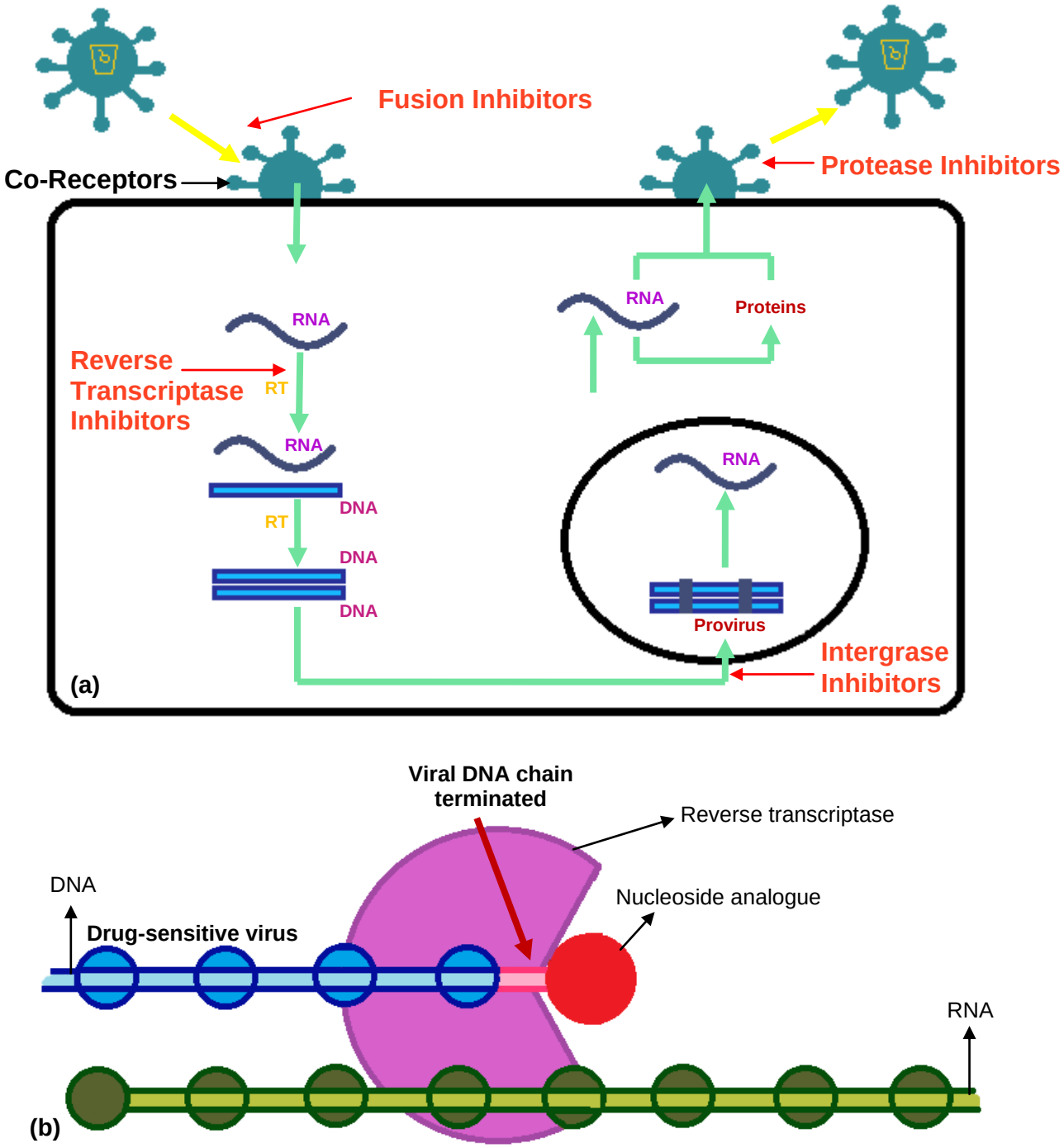

Figure 2.4: *(a) Target sites of currently available ARV drugs (adapted from http://www.oyageninc.com/drugs, (14/092010). (b) Mechanism of action of NRTI's (adapted from http://depts.washington.edu/hivaids/arvres/case3/discussion.html, (14/09/2010).*

Table 2.3: *ARV's currently approved for utilisation in HAART (adapted from Warnke et al., 2007; Ramautarsing and Ananworanich, 2010; cme.medscape.com/viewarticle/418820 (21/06/2010); www.avert.org/aids-drugs-table.htm (21/06/2010); http://www.natap.org/2003/march/031703_2.htm (21/06/2010).*

Antiretroviral agent	Trade name	Class	Manufacturer	FDA approval
Zidovudine (AZT)	Retrovir	NRTI	GlaxoSmith Kline	March 1987
Lamivudine	3TC	NRTI	GlaxoSmith Kline	November 1995
Zalcitabine (ddC)	Hivid	NRTI	Roche	June 1992
Didanosine (ddI)	Videx	NRTI	Bristol-Myers Squibb	October 1991
Stavudine (d4T)	Zerit	NRTI	Bristol-Myers Squibb	June 1994
Abacavir	Ziagen	NRTI	GlaxoSmith Kline	December 1998
Emtricitabine (FTC)	Emtriva	NRTI	Gilead Sciences	July 2003
Efavirenz	Stocrin	NNRTI	MSD	September 1998
Nevirapine	Viramune	NNRTI	Boehringer Ingelheim	June 1996
Delaviridine	Rescriptor	NNRTI	Pfizer	April 1997
Saquinavir	Forto-vase	PI	Roche	December 1995
Ritonavir	Norvir	PI	Abbott Laboratories	March 1996
Lopinavir	Aluvia	PI	Abbott Laboratories	September 2000
Amprenavir	Agenerase	PI	GlaxoSmith Kline	April 1999
Indinavir	Crixivan	PI	MSD	March 1996
Nelfinavir	Viracept	PI	Roche	March 1997
Atazanavir	Reyataz	PI	Bristol-Myers Squibb	June 2003
Fosamprenavir	Lexiva	PI	GlaxoSmith Kline	October 2003
Tipranavir	Aptivus	PI	Boehringer Ingelheim	June 2005
Darunavir	Prezista	PI	Tibotec Inc.	June 2006
Raltegravir	Isentress	Intergrase inhibitor	Merck and Co., Inc	September 2007
Enfuvirtide	Fuzeon	Entry inhibitor	Roche and Trimeris	March 2003
Maraviroc	Selzentry	Entry inhibitor	Pfizer	June 2007
Tenofovir (PMPA)	Viread	NtRTI	Aspen	August 2008

Direct injection of AZT into the spinal canal and by intracerebroventricular infusion has been shown to improve neurological function in patients with ADC (Link, 1992; Wang and Sawchu, 1995). In a pilot study conducted by Routy *et al.*, in 1989 and 1990, the effects of AZT was tested when administered orally and intrathecally. Patients were administered with 800mg of oral AZT daily, which was seen to have improved neurological function. However, therapy needed to be ceased due to haematological toxicity. With the end of AZT therapy, neurological function declined within months, necessitating AZT to be reinstated. The intrathecal route was used, resulting in an improvement in ADC symptoms, with doses as low as 50mg administered 12 hourly via a catheter implanted into the intrathecal sac of the spinal cord, in the absence of haematological side effects (Routy *et al.*, 1990). This serves to support the need for localised therapy to manage AZT, however direct implantation of a drug

delivery device into the brain, capable of releasing drug over extended periods is anticipated to be preferable to twice daily injections into the spinal cord. AZT was originally thought to cross the BBB by means of active transport using a deoxynucleoside transport system, due to the structural similarity exhibited by AZT to the endogenous nucleoside, thymidine. Thymidine actively transported into the CNS at the choroid plexus by means of the deoxynucleoside transport system (Sawchuk and Yang, 1999). Later studies have however revealed that thymidine does not cross the BBB. Research has now suggested that AZT is transported across the BBB and blood-CSF-interface by passive diffusion across transcellular pathways (Sawchuk and Yang, 1999).

The accumulation of AZT within the CNS is hindered, however, by the presence of active efflux transports, such as P-gp, present on the luminal interface of the BBB and blood-CSF-interface, which are responsible for the active transportation of AZT out of the CNS (Sawchuk and Yang, 1999; Gelperina *et al.*, 2006; Varatharajan and Thomas, 2009). This is supported by the AZT steady-state brain extracellular fluid (ECF) or CSF:plasma ratio, described as per Equation 2.2 (Sawchuk and Yang, 1999).

$$\frac{Cbr,ss}{Cp,ss} = \frac{CLin}{CLout} \qquad \textbf{(Equation 2.2)}$$

Where $C_{br,ss}$ is the steady-state drug concentration in the brain ECF or CSF; $C_{p,ss}$ is the steady-state drug concentration in plasma; CL_{in} is the influx clearance of drug and CL_{out} is the efflux clearance of drug. Bulk flow rate of CSF and exchange between the CSF and brain ECF is assumed to be negligible when compared to efflux clearance.

If passive diffusion is the only process governing AZT transport into and out of the CNS, a ratio of 1 is expected at steady-state. As this is not the case, the ratio at steady-state is less than 1, supporting the presence of active efflux transporters at the BBB and blood-CSF-interface which are responsible for removing AZT out of the CNS faster than its entry. As AZT is minimally metabolised in the CNS, no other elimination mechanism is responsible for the ratio obtained (Wong *et al.,* 1993; Sawchuk and Yang, 1999; Fox *et al.*, 2002).

Further supporting this theory of efflux is the coadministration of probenecid, a drug commonly used for the management of gout, acting as a competitive inhibitor of the efflux transporters governing AZT removal from the CNS. In a study conducted by Hedaya and Sawchuk, concomitant administration of probenecid in a rabbit model demonstrated a fourfold increase in the CNS:Plasma ratio (Hedaya and Sawchuk, 1989; Wong *et al*., 1993;

Sawchuk and Yang, 1999). Coadministration of probenecid has also been identified in a reduction in the hepatic glucuronidation of AZT, with a resultant increase in serum levels and $t^1/_2$ of AZT present in the body (McDermott *et al.*, 1992).

2.2 Nanotechnology: The Way Forward

With mans' constant quest for superiority, emerges nanotechnology, a new multidisciplinary area of research and a rapidly growing area of science dedicated to the design, preparation and use of structures in the nanometer size range, being 1000nm and smaller (Sahoo *et al.*, 2003; Pison *et al.*, 2006; du Toit *et al.*, 2007; Park *et al.*, 2007; Liu *et al.*, 2008; Yang *et al.*, 2008; Singh *et al.*, 2009; Suh *et al.*, 2009; Silva, 2010). Nanotechnology enables the control and manipulation of basic characteristics of a material without changing the chemical composition. This is due to nano-sized materials possessing novel properties and functions that are markedly different from those of the identical bulk material (Park *et al.*, 2007; Yang *et al.*, 2008; Singh *et al.*, 2009). The small size, customized surface, improved solubility and multi-functionality of nanomaterials makes nanotechnology a field applicable to all areas of science (Singh *et al.*, 2009).

The term nanotechnology was coined by K. Eric Drexler in the mid 1980's. Since then, the hype of nanotechnology has escaped no field, offering unique advantages to multiple disciplines with progress in drug delivery, sensing, imaging, cosmetics and electronics. $4 million has been injected by the defense bill into research and development associated with nanomanufacturing. The National Nanotechnology Initiative (NNI), the leaders in nanotechnology research and development, was implemented in 2001 to control Federal nanotechnology research and development. The aim of the NNI is expedite the responsible discovery and development of nanotechnology with the ultimate goal being to improve national economy and quality of life of citizens in the United States of America (USA). The 2010 USA budget supplied $1.6 billion to the NNI, serving to further fire the hype associated with nanotechnology (du Toit *et al.*, 2007; Zhan and Liu, 2010).

Michael Faraday first prepared colloidal gold particles in the nanometer size range more than 150 years ago (Park, 2007). Polymeric nanoparticles used for the controlled delivery of drug were first developed in the 1970's (Feijen *et al.*, 2005). Nanotechnology was being used long before it was recognized as being a science, with popularity growing approximately 20-30years ago (Suh *et al.*, 2009). It is estimated that in 2014, approximately 16% of revenue related to healthcare products will incorporate nanotechnological interventions, with nanoenabled drug delivery systems generating approximately $ 4.8 billion

in 2012, making nanotechnology one of the fastest growing industries to date (du Toit *et al.*, 2007).

2.2.1 Application in drug delivery

Nanomedicine is a multidisciplinary medical application of nanotechnology that according to the National Institute of Health (NIH) Nanomedicine Roadmap Initiative refers to specialized medical intervention at the nanometer scale for the diagnosis, prevention and treatment of diseases (Park, 2007; Bennewitz and Saltzmann, 2009; Wang *et al.*, 2009; Subbia *et al.,* 2010). Nanomedicine allows for the creation and manipulation of materials and devices with high therapeutic selectivity, promising to significantly improve healthcare and potentially revolutionalise the practice of medicine (Bennewitz and Saltzmann, 2009; Modi *et al.*, 2009; Singh *et al.*, 2009; Wang *et al.*, 2009). Recent advancements in the area of nanopharmaceuticals, nanoscaled drug delivery systems and biological compounds, promises to enhance patient care due to the progress made with the diagnosis and treatment of disease states with the implementation of research conducted on nanomedicine (du Toit *et al.*, 2007).

Cancer remains the current market leader with regards to nanopharmaceuticals, attributed to the funding of $144 million infused into cancer research in the USA. Nanoenabled drug delivery systems allow for rapid drug absorption, controlled release of therapeutics, enhanced bioavailability, targeted delivery or therapeutics and a subsequent decline in systemic side effects, a considerable improvement to existing products (Reis *et al.*, 2006; du Toit *et al.*, 2007; Modi *et al.*, 2009; Jolck *et al.,* 2010; Zhang and Liu, 2010). This is of particular significance with chemotherapeutic agents due to the high concentrations of toxic substances utilized in chemotherapy.

Drug incorporation into nanosystems is used to achieve site-specific drug delivery, therefore providing better control of drug release as observed in Figure 2.5. This improves the efficacy, pharmacokinetics and pharmacodynamics of the drug. Targeted drug delivery improves the therapeutic efficacy of the drug, as well as resulting in a possible reduction in the quantity administered to achieve a therapeutic response and minimises side effects experienced due to drug therapy. Drug delivery devices using nanosystems can be manipulated to react in a bioresponsive manner, to provide site-specific drug delivery and to control drug degradation. Due to their small size and large surface area, nanoparticles are capable of opening tight junctions and are therefore capable of crossing the BBB (Roney *et al.*, 2005; Rahman *et al.*, 2009; Ghaderi *et al.,* 2010; Jolck *et al.,* 2010; Silva, 2010). Nanoenabled drug delivery systems are capable of interacting with biological systems at a

molecular level, enhancing bioavailability and therapeutic efficacy of the administered drug (Modi *et al.*, 2009). Furthermore, the bioavailabilty of poorly soluble drugs is enhanced as nanoparticles can also be used as carriers for these drugs, with the small size and large surface area afforded by nanoparticles acting to solubilise the drug molecules (Pison *et al.*, 2006; Popovic and Brundin, 2006; Reis *et al.*, 2006; Majuru and Oyewumi, 2009).

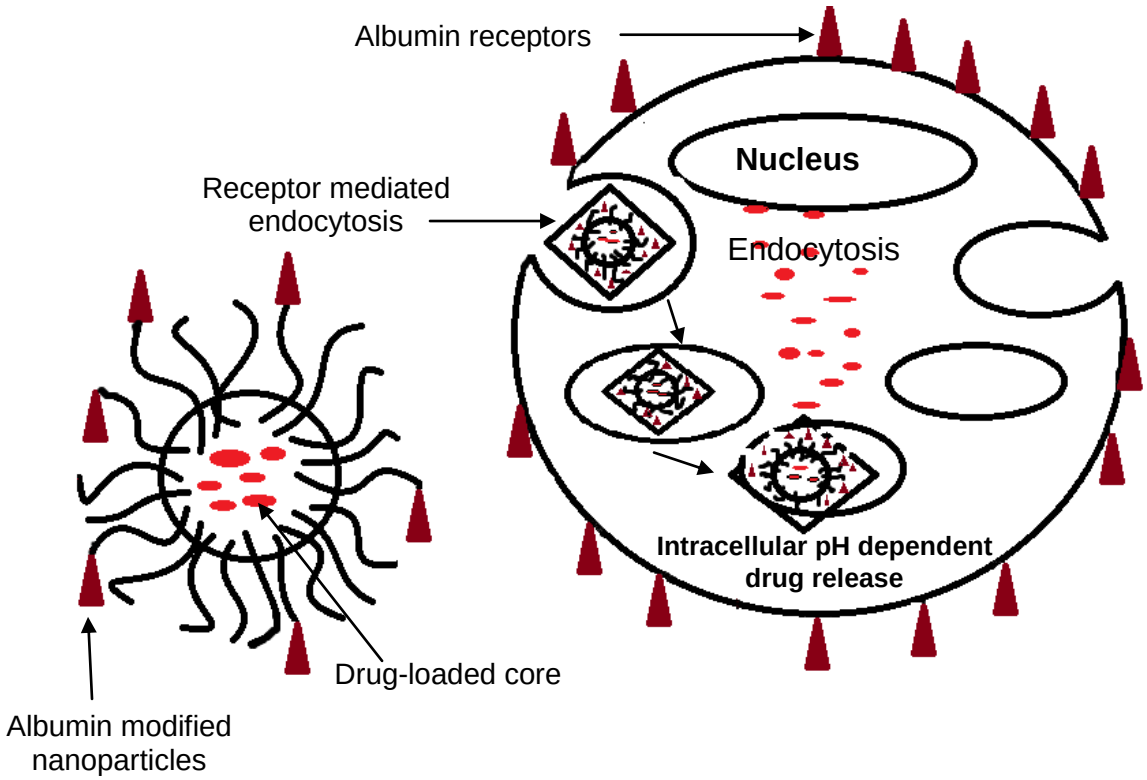

Figure 2.5: *Active drug targeting of surface modified nanoparticles depicting site specific release of drug molecules (adapted from Ganta et al., 2008).*

Nanotechnology enables the reformulation of existing pharmaceutical products with an improved pharmacokinetic and safety profile of the nanopharmaceutical, serving to decrease competition and increase revenue for pharmaceutical industries. New innovative pharmaceuticals can be developed and patented with the aid of nanotechnology, with the potential to manage complex disease states which previously challenged scientists such as cancer and neurological disorders. This also serves to increase profitability by pharmaceutical industries. The last decade has witnessed the development and release of several pharmaceutical products, highlighted in Table 2.4 (Reis *et al.*, 2006; Du Toit *et al.*, 2007; Ganta *et al.*, 2008; das Neves *et al.*, 2009; Majuru and Oyewumi, 2009; Subbia *et al.,* 2010). Abraxane^{TM} (produced and marketed by American Pharmaceutical Partners and American Bioscience Inc.) was the first polymeric, protein-conjugated nanoenabled product approved by the FDA and available on the market in January 2005. Composed of the

albumin-based chemotherapeutic, paclitaxel, with application as an injectable drug delivery system for the treatment of metastatic breast, Abraxane™ was a milestone for nanomedicine and pharmaceutical scientists. Previous paclitaxel formulations required toxic solvents such as cremophor-EL, implicated in life-threatening allergic reactions, to solubilise the drug. Abraxane™ is superior to Taxol®, the original paclitaxel injectable formulation, due to the exclusion of toxic solvents decreasing the incidence adverse effects experienced with paclitaxel therapy as well as negating the need for premedication with cortisone and antihistamines which were required to prevent and manage allergic reactions associated with Taxol® administration. Targeted delivery of the chemotherapeutic agent to the cancer cells also accounted for the decline in the incidence of systemic side effects occurring with Abraxane™ use, despite a 50% increase in the administer paclitaxel dose. Greater retention of Abraxane™ within the cancer cells and passive diffusion of the nanoparticles within the cells accounts for superior efficacy observed with Abraxane™ as compared to Taxol® (Koo *et al.*, 2005; du Toit *et al.*, 2007).

Nanoparticles utilized for medical interventions range between 10-1000nm, with drug molecules entrapped, surface adsorbed or chemically bound to the solid nanoparticulate (du Toit *et al.*, 2007; Benewitz and Saltzmann, 2009; Modi *et al.*, 2009). Numerous methodologies have been implemented for the preparation of nanoparticulates including:

- Polymerisation reaction
- Emulsion polymerization (employing single and double emulsion techniques)
- Polymer dispersion
- Supercritical fluid technology
- Emulsification solvent evaporation
- Ion induced crosslinking
- Desolvation or solvent deposition
- Electrospinning
- Salting out
- Denaturation of solvent droplets
- Foam droplet separation
- Microfluidic synthesis

Table 2.4: *Available nanoenabled formulations on the market for application in drug delivery (adapted from Harris et al., 2004; Roumeliotis, 2006, www.in-pharmatechnologist.com/Materials-Formulation/Abbott-ordains-Elan-to-marry-Tricor-and-Crestor Ahmed 2007 (21/06/2010); Hawkins et al., 2008; Gardner et al., 2008; Kratz, 2008; www.nanotechproject.org/inventories/medicine/apps (21/06/2010)*

Product	Manufacturer	Nanosystem	Product information
Abraxane™	American Pharmaceutical Partners, Inc (USA)	Erlan's Nanocrystals *•Drug delivery systems employing Erlan's nanocrystal technology, developed and patented in 1992, exhibit superior rate of dissolution and bioavailability* *•Nanocrystals are small drug particles produce by milling the drug utilising a proprietary wet-milling technique* *•The surface adsorption of stabilisers prevents agglomeration of the nanocrystals.* *A nancrystal aqueous colloidal dispersion of drug results which is applicable for all routes of administration (du Toit et al., 2007; Majura and Oyewumi 2009)*	•An injectable dosage form of the chemotherapeutic agent paclitaxel •Particles present with a mean particle size of approximately 130nm •FDA approval: January 2005
Megace®	Par Pharmaceuticals Companies, Inc (USA)	Erlan's Nanocrystals	•Appetite stimulant •Used for weight loss in patients with AIDS •Demonstrates superior rate of dissolution and bioavailability to the original oral suspension •FDA approval: July 2004
Doxil®	ALZA Corporation (USA)	Liposome	•Chemotherapeutic agent used for the treatment of refactory ovarian cancer and AIDS related kaposi's sarcoma •First marketed product to incorporate STEALTH® technology •FDA approval: February 2005
Emend®	Merck &Co., Inc (USA)	Nanocrystals	•Anti-nausea drug intended for use in patients receiving chemotherapy •FDA approval: March 2003 •Launched: April 2003
Tricor®	Abbott Laboratories (USA)	Erlan's Nanocrystals	•Cholesterol lowering agent used to reduce elevated plasma triglyceride concentrations •FDA approval: February 1998 •Launched: December 2004

Estrasorb™	Novavax Inc (USA)	Micelles	•Topical lotion containing estrogen •Used for the management of moderate to severe vasomotor symptoms associated with menopause •FDA approval: October 2003
Rapamune®	Wyeth (USA)	Erlan's Nanocrystals	•Immunosuppressant •Employed as a prophylactic anti-rejection drug following renal transplants in patients aged 13 and older •FDA approval: August 2000
Triglide	SkyePharma and Sciele Pharma Inc (USA)	Nanoparticles *•Obtained by high pressure homogenisation*	•Oral fibrate capable of reducing elevated plasma concentrations of circulating triglycerides •FDA approval: May 2005 • Launched: July 2005
VivaGel	Starpharma (Australia)	Dendrimers	•Vaginal microbicide for the prevention of sexually transmitted infections, including genital herpes and HIV •US-based NIH awarded Starpharma $20.3 million for the continued development and testing of VivaGel against HIV •FDA approval: January 2006
Ambisome	Astellas Pharma US, Inc and Gilead Sciences, Inc (USA)	Liposomes	•Broad spectrum injectable antifungal agent •Approved for the treatment of cryptococcal meningitis, aspergillosis and candida in patients refractory or intolerant to conventional Amphotericin B •FDA approval: August 1997
Amphotec	Three Rivers Pharmaceuticals (USA)	Liposomes	•Amphotericin B complex for injection •Indicated for the treatment of invasive aspergillosis, a systemic fungal infection •FDA approval: November 1996
Abelcet	Enzon Pharmaceuticals, Inc (USA)	Liposomes	•Injectable broad spectrum antifungal agent •Approved for the treatment of invasive fungal infection in immunocompromised patients refractory or intolerant to conventional Amphotericin B •FDA approval: November 1995

2.2.2 Benefits of nanoscale drug carriers

- Superior drug stability at the desired site of action.
- Biocompatibility and biodegradability of the device are ensured.
- Site-specific drug targeting can be achieved.
- Entrapped drug molecules are protected from premature degradation in body fluids.
- Controlled release of drug molecules can be achieved through manipulation of the polymeric structure.
- Nanotechnology enables safe and effective administration of therapeutic agents which were previously difficult to administer due to toxic systemic effects.
- Nanoenabled drug carriers demonstrate superior bioavailability and rapid onset of action.
- Lower drug doses can be administer resulting from an increased therapeutic index of the administered drug and reduced clearance from the body.
- Nanoparticles are capable of targeted delivery of drug due to the preferential accumulation of drug at the desired site of action, thereby reducing systemic toxicity. Targeted drug delivery also allows for treatment of the source of the disease instead of management of the symptoms of the disease, as drug accumulation in healthy tissue is minimised.
- Nanoparticles can penetrate the tiniest capillary vessels attributed to their nanoscale size.
- Prolonged residence time in the blood stream and at the site of action due to reduced uptake by the reticular-endothelial system.
- They are capable of controlled release of drug, depending on the materials used to prepare the nanoparticles.
- Nanoparticles are capable of high drug loading due to small size and large surface area.
- Nanoparticles allows for the delivery of water-insoluble drugs as the large surface area afforded to the drug molecules enhances drug solubility and dissolution.
- Nanoenabled drug delivery systems enables the extension of expiring patents with the potential to capitalize on the benefits afforded to the nanoenabled system.

2.3 The Blood Brain Barrier: The Ultimate Hurdle to CNS Drug Delivery

The BBB is a membranous homeostatic defence mechanism formed by tight endothelial cell junctions, perivascular astrocytes and blood capillaries in the brain separating the brain from systemic blood circulation. The BBB physically and metabolically protects brain tissue enforcing barrier selectivity for the movement of substances into and out of the brain parenchyma, depending on size and endothelial permeation of the molecules, providing a stable environment for neuronal activity and protecting the brain from exogenous toxicants, pathogens and immunogens. However the BBB provides a challenge to drug delivery scientists as clinically significant drug concentrations within the brain is difficult to achieve with limited pathways allowing drug access into the brain (Pardridge, 1995; Sawchuk and Yang, 1999; Fox *et al.*, 2002; Misra *et al.*, 2003; Lemaire and Desrayaud, 2005; Popovic and Brundin, 2006; Hu *et al.*, 2009; Modi *et al.*, 2009; Wang *et al.*, 2009; Georgieva *et al.,* 2010).

Blood capillaries make up 95% of the total surface area of the BBB. However, the blood capillaries present in the brain are structurally different to capillaries present in other tissue. Capillaries have a smaller diameter and thinner walls, with a higher mitochondrial density then other capillaries. The lack of small pores and intracellular fenestrations and more than 99% of brain capillaries contains high resistance tight junctions between endothelial cells, paucity of endocytic vesicles and active transport systems restricting the movement of exogenous water soluble molecules into the CNS. The movement of solutes must therefore pass directly through the endothelial membrane, transcellular and intracellular movement, to gain access into the brain (Pardridge, 1995; Bodor and Buchwald, 1999; Sawchuk and Yang, 1999; Prokai *et al*., 2000; Misra *et al.*, 2003; Varatharajan and Thomas, 2009).

As the BBB is a bilayered lipid structure, 98% of small drug molecules and almost 100% of large drug molecules cannot cross the BBB, with only small lipophilic molecules with a molecular mass less than 400Da, capable of freely diffusing through the endothelial capillaries by means of passive diffusion (Pardridge, 1995; Misra *et al.*, 2003; Lemaire and Desrayaud, 2005; Hu *et al.*, 2009; Modi *et al.*, 2009). Exogenous hydrophilic substances are allowed entry into capillary cells by various mechanisms. Paracellular movement of molecules between endothelial cells, facilitated or passive diffusion across cells, endocytosis and active transport directly across cells all enable the entry of drug molecules into the cells outside the CNS as highlighted in Figure 2.6. Active influx transporters present on the endothelium of blood vessels were first discover in 1946 by Krogh, who recognised that glucose entered the brain despite being a highly water soluble molecule. However, active efflux transporters are also present at the BBB, functioning to prevent or remove drug

molecules such as AZT, which is removed from the brain by MRPs, an ATP-driven efflux transporter. Substances that cross into the brain are also exposed to enzymatic degradation by the large mitochondria density within the endothelial cells as mentioned above (Bodor and Buchwald, 1999; Sawchuk and Yang, 1999; Lemaire and Desrayaud, 2005; Varatharajan and Thomas, 2009).

Novel drug delivery systems are therefore required to circumvent the restrictions of the BBB, thereby enhancing the delivery of therapeutics to the brain to effectively manage neurological diseases.

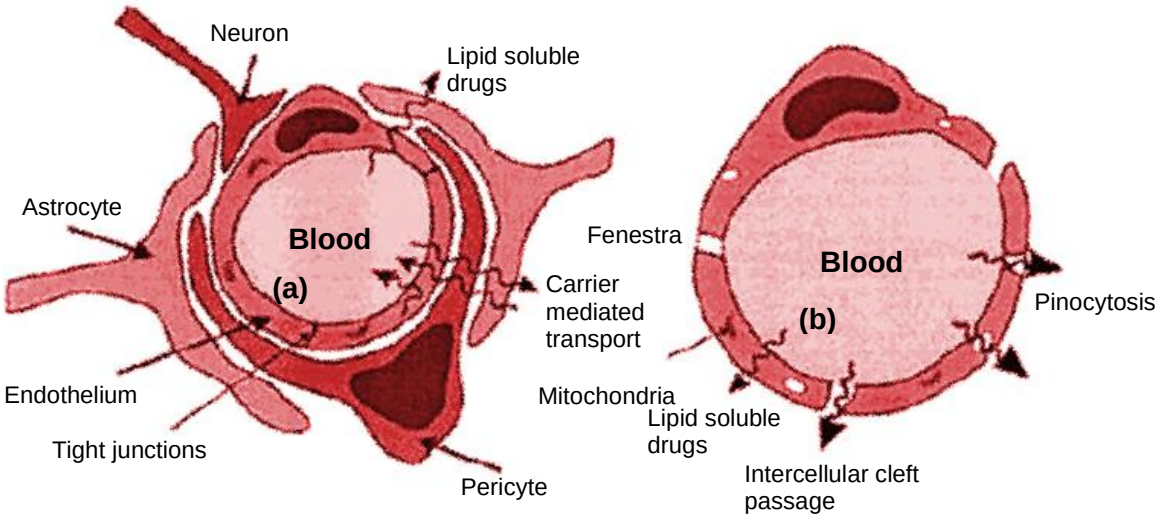

Figure 2.6: *Schematic of (a) a normal capillary as compared to (b) a brain capillary, illustrating the mechanisms of drug entry into the capillaries (adapted from Misra et al, 2003).*

2.4 Drug Delivery for the CNS

Over 1 billion people are plagued by CNS disorders worldwide. Several new approaches are currently being explored in an attempt to enhance drug delivery to the CNS. Lipophillic prodrugs, efflux pump inhibitors, transient hyperosmolar BBB “opening” by intracarotid arterial administration of a hypertonic solution, intranasal brain-targeting, circumvention of the BBB through direct drug delivery into the ventricles or cortex of the brain by direct injection or implantation and immune liposome drug delivery systems are but a few examples of such methods (Misra *et al.*, 2003; Gelperina *et al.*, 2006; Fiandaca *et al.*, 2008; Benewitz and Saltzman, 2009; Varatharajan and Thomas, 2009; Hartz and Bauer, 2010). However, of these methods, drug encapsulation within non-toxic polymeric nanomaterials is the most popular means of enhancing drug delivery to the CNS (Bennewitz and Saltzman, 2009; Modi *et al.*, 2009; Varatharajan and Thomas, 2009; Wang *et al.*, 2009).

The BBB is the most important constraint to the design and development of neurotherapeutic agents, due to the limited penetration of pharmaceuticals presented by the BBB creating an obstacle to CNS drug delivery (Lemaire and Desrayaud, 2005; Pardridge, 2005; Modi *et al.*, 2009). CNS conditions, including brain tumors, HIV encephalopathy, neurodegenerative diseases, epilepsy and cerebrovascular disease, remains the leading cause of disability and hospitalizations in the world, with more people are living with CNS disorders than with cardiac disorders, however, the global CNS market for therapeutic agents require a growth of approximately 500% to equal the global cardiac market (Misra *et al.*, 2003; Pardridge, 2005). Innovative solutions for the delivery of neurotherapeutics into the CNS are therefore required, with nanotechnology offering potential solutions to some of these constraints. The entry of systemical administered drugs is inhibited by the BBB, rendering existing therapeutic agents ineffective for the management of CNS conditions as therapeutically viable drug concentrations cannot be sustained with the CNS. Nanotechnology allows for the development of nanoenabled drug delivery systems capable of managing CNS disorders as the size limitations posed by both the BBB and neural tissue is accounted for (Misra *et al.*, 2003; Saito *et al.*, 2005; Modi *et al.*, 2009).

Polymeric nanoparticles are capable of opening tight junctions in the BBB. Modification of particle size to 50nm and less as well as manipulation of surface charge of nanosystems enables penetration of drug molecule through BBB and distribution within the brain. The long blood circulation exhibited by nanoparticles potentially increases drug uptake into the CNS due to larger concentrations of drug-loaded nanoparticles present at the BBB (Modi *et al.*, 2009; Muthu *et al.*, 2009; Suh *et al.*, 2009). Nanoparticles are currently being extensively researched for the diagnosis and treatment of CNS conditions including neurodegenerative diseases such as Parkinson's disease, Alzheimer's disease and ADC. Nanoparticles need to be sufficiently small, approximately 50nm, to cross the brain interstitial space, and require a surface charge which is either neutral or negative to attain a large volume of distribution within the brain (Thorne *et al.*, 2006; Bennewitz and Saltzman, 2009; Modi *et al*., 2009). Due to their small size, enhanced stability, large surface area and surface charge, which can be manipulated to evade recognition by the reticuloendothelial system (RES), nanoparticles translocate to the CNS and cross the BBB (Rahman *et al.*, 2009). They are also capable of controlled, targeted drug delivery and are ideal for the delivery of ARV's, such as AZT, into the brain (Pardridge, 2005).

Poly(butylcyanoacrylate) (PBCA) nanoparticles coated with polysorbate 80, approximately 250nm in diameter, is currently the only successful drug-loaded nanoparticulate system utilized for *in vivo* delivery of drug into the brain. PBCA nanoparticles adsorbed plasma

apolipoproteins post intravenous administration and is confused for low density lipoproteins, therefore crossing the BBB by receptor-mediated endocytosis (Modi *et al.*, 2009). Polyethylene glycol-coated liposomes were prepared for the delivery of chemotherapeutics into the brain (Varatharajan and Thomas, 2009). Carbon nanofibres has shown promise as nerve regenerative agents attributed to the high conductivity observed which enhances nerve function and regeneration using electrical stimulation. The small size and mechanical strength of the fibres enables good conductivity which has been implicated in decrease foreign body reaction in response to the presence of these fibres in the body (McKenzie *et al.*, 2004). Brain imaging techniques employing solid lipid nanoparticles has displayed potential to enhance MRI images obtained of the brain. Insoluble iron oxide molecules complexed with nanoparticlesto enable entry into the CNS allowing iron oxide use as super-paramagnetic MRI contrast agents, revolutionalising brain imaging (Modi *et al.*, 2009).

Polymers such as polyglycolic acid, polyethylene glycol and polylactic acid, are commonly used to prepare intracranial implants. Chemotherapeutic agents are commonly delivered using polymeric intracranial implants, with polyethylene-co-vinyl acetate, a nonbiodegradable polymer, used previously for such a purpose. Limitations to nonbiodegradable implants are that they are permanent fixtures in the brain which are capable of eliciting a foreign body response, requiring further surgery for their removal (Bennewitz and Saltzman, 2009). However, biodegradable, biocompatible polymers have been chosen for the of the drug delivery device developed in this study, negating the need for further surgery after implantation of the device. Implantation of an AZT-loaded device into the brain alleviates problems associated with systemic drug delivery, such as systemic toxicity, drug metabolism in the systemic circulation and opsonisation by blood protein (Bennewitz and Saltzman, 2009; Narishetty and Panchagnula, 2004).

Polymeric nanoparticles are easy to scale up and are cost effective making them suitable drug carriers for CNS therapeutic agents (Wang *et al.*, 2009; Modi *et al.*, 2009). Nanoparticles dispersed within an implantable multipolymeric scaffold is therefore being explored in this research for intracranial implantation to manage ADC as localised delivery has been proven to enhance therapeutic efficacy of the administered drug a reduction in the incidence of system adverse effects.

2.5 Concluding Remarks

The wide-spread use of HAART has shifted the focus of HIV from and acute condition to a chronic disease. This inturn has increased the prevelance of ADC among HIV sufferers. A neurological condition affecting both adults and children, ADC has been responsible for severe dementia and paralysis of individuals not adequately treated.

Current therapeutic regimens have demonstrated poor management of the neurological manifestations of HIV due to the restrictions posed by the BBB. As the BBB poses as a resevior for the HI virus, drug penetration into the brain is imperative for the effective management of ADC.

The era of nanotechnology is upon us. The implementation of this novel technology for the development of a localised nanoenabled drug delivery system for the management of ADC could herald revolutionary advances for the future treatment and management of HIV/AIDS and ADC.

CHAPTER 3

Preparation and Evaluation of a Multipolymeric Nano-Enabled Configuration

3.1. Introduction

The National Science Foundation in the United States of America (USA) estimates that by 2015, the annual global market for nanotechnological-related goods and services will reach $1 trillion. It has also been estimated that by 2014, 16% of healthcare and life sciences related commodities will incorporate nanotechnology, making it one of the fastest growing industries in history, and an exceptionally large economic force (du Toit *et al.*, 2007).

Nanotechnology offers much promise for the enhancement of disease diagnosis, management and prevention (Ganta *et al.*, 2008; Subbia *et al.,* 2010). Nanocarriers include a range of products, with biodegradable polymeric nanoparticles, lipid liposomes, micelles and nanocrystals being just a few. Organic and inorganic materials are used for the preparation of these products, illustrated in Table 3.1 below (Sahoo and Labhasetwar, 2003; du Toit *et al.*, 2007; Ganta *et al.*, 2008).

Biocompatible and biodegradable polymers have been researched extensively for the formulation of novel drug delivery systems, as illustrated in Table 3.4 (Hughes, 2005, Rezwan *et al.*, 2006). This study therefore employed degradable, biocompatible, non-mutagenic, non-cytogenic, and non-teratogenic for the preparation of nanoparticles and multipolymeric scaffolds. The byproducts of these polymers are nontoxic and readily excreted from the body (Liu *et al.,* 2005; Popovic and Brundin, 2006; Rezwan *et al.*, 2006). They possess desirable mechanical properties and superior drug permeability and are therefore safe for use in the human body (McKenzie *et al.*, 2003; Liu *et al.*, 2005; Luong-Van *et al.*, 2006; Popovic and Brundin, 2006; Rezwan *et al.*, 2006).

Nanoparticles were prepared using two methods, the salting out approach and the controlled gelification of alginate approach. Nanoparticles were dispersed within a multipolymeric scaffold, prepared by means of polymer crosslinking, to obtain a drug delivery device capable of sustained drug release over prolonged periods. The antiviral agent, AZT was employed as the test drug.

Table 3.1: *Nanoparticulates currently under investigation for in vivo drug delivery, diagnostics and imaging*

Nanosystem	Description of nanosystem	Method of drug entrapment	Illustration of nanosystem	References
Polymeric Nanoparticles	•Formulated from biodegradable polymers in an attempt to increase circulating the half life of the entrapped drug and to evade uptake by the reticuloendothelial system •Superior stability in biological fluids and under storage conditions •Easy preparation methodology •Sustained and controlled drug release	•Protects drug from premature degradation and prevents drug toxicity	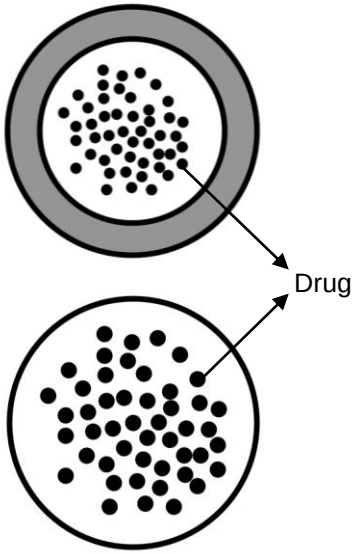	•Sahoo and Labhasetwar, 2003 •Reis *et al.*, 2006 •Benewitz and Saltzman, 2009
Nanoparticles	•Colloidal particles	•Drug entrapment within the polymer matrix. Drug can be dissolved/dispersed within the nanoparticles or attached to the surface		
Nanocapsules	•Vesicular systems	•Drug entrapment within a cavity surrounded by a polymer membrane		
Nanospheres	•Matrix systems	•Uniform dispersion of drug within the matrix		

Table 3.1: *continued*

Polymeric Micelles	•Self-association of amiphillic copolymers to form spherical supramolecular core-shell structures in aqueous systems, with hydrophobic interactions driving the assembly of the amiphiles •Narrow size distribution (20-100nm), allowing for prolonged circulation in the blood as RES uptake and renal excretion is avoided •Thermodynamic stability in physiological environments due to low critical micelle concentrations •Distinctive core-shell architecture (hydrophobic inner with an aqueous exterior) •Unique properties including high solubility, high drug loading capacity and low toxicity	•Hydrophobic drugs are partitioned in the inner hydrophobic core •Outer hydrophilic surface serves to stabilise the micelle in aqueous environments	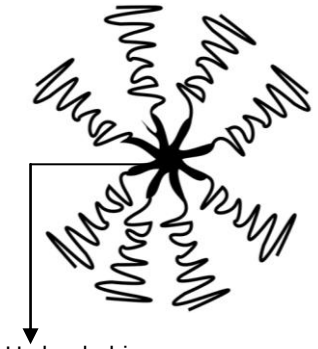	•Sahoo and Labhasetwar, 2003 •Koo *et al.*, 2005 •Du toit *et al*., 2007 •Ganta *et al*., 2008 •Benewitz and Saltzman, 2009
Liposomes	•Spherical bilayered phospholipid vesicles formulated from natural non-toxic phospholipids and cholesterol, with an inner aqueous core •Properties similar to plasma membranes •Range in diameter between 50nm-1µm •Contains hydrophilic and hydrophobic properties	•Hydrophobic and amiphillic drug are incorporated into the lipid bilayer and hydrophilic drugs are incorporated into the aqueous core •Drug encapsulation within the liposome protects against premature degradation and avoids drug toxicity	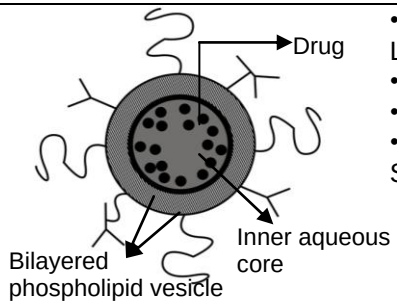	•Sahoo and Labhasetwar, 2003 •Koo *et al.*, 2005 •Ganta *et al.*, 2008 •Benewitz and Saltzman, 2009

Table 3.1: *continued*

Dendrimers	•Synthetic macromolecules of nanometer dimension with well defined architecture •Polymeric monomers which form spherical branched tree-like structures with an inner core (1-10nm in diameter) •Application as a coating agent for targeted rug delivery •Good control of polydispersity and the ability to display high surface functionality •Good aqueous solubility	•Drug encapsulation within the inner core by inubation •Drug attachment to the outer surface branches by the formation of covalent or noncovalent bonds •Dendrimer-drug networks can form	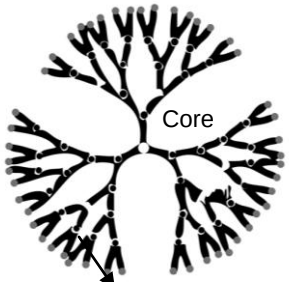	•Sahoo and Labhasetwar, 2003 •Koo *et al.*, 2005 •du toit *et al.*, 2007 •Ganta *et al.*, 2008 •Benewitz and Saltzman, 2009
Quantum Dots	•Semi-conductor nano-sized crystals with unique photochemical and photophysical properties •2-10nm in diameter, with fluorescence emission achieved between 400-2000nm •Photostability of quantum dot probes enables continuos real-time tracking of molecules over extended periods, with researchers having observed quantum dots in the lymph nodes of mice over 4months	•Ekiove and Elros first proposed the concept of quantum confinement of charge within a nanometer size range in 1982 •In 1998, Alivisatos and Nie conjugation of quantum dots with biological molecules as well as water solubility of quantum dots, enabling application for optical imaging •Enhanced stability and brightness as compared to organic dyes and fluorescent proteins	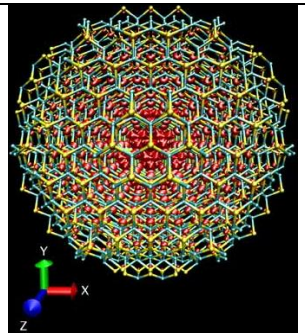 *http://www.networlddirectory.com/blogs/permalinks/5-2008/pressure-effects-on-nanomaterials.html, 14/09/2010)*	•Murray *et al.*, 2000 •Dahan *et al.*, 2003 •Bailey *et al.*, 2004 •Ballou *et al.*, 2004 •du toit *et al.*, 2007 •Ghaderi *et al.,* 2010 •Kato *et al.,* 2010
Carbon Nanotubes	•Benzene rings assembled in a tubular structure, exhibiting chemical and mechanical stability and low cytotoxicity •Outer walls can be chemically modified to for targeted drug delivery •Single-walled CNT's range in diameter between2-5nm, with their aggregates matching the conditions to achieve enhanced permeability and retention effects	•Drug attachment to the sides of the nanotubes or within the lumen of the tube •Capable of slow drug release	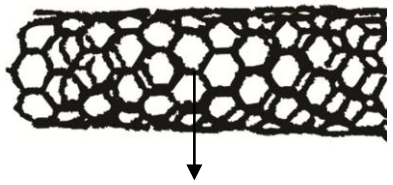	•Ajima *et al.*, 2005 •Benewitz and Saltzman, 2009

3.2 Materials and Methods

3.2.1 Materials

Alginate, pectin, polyethylene oxide (PEO), polyvinyl alcohol (PVA) and sodium carboxymethyl cellulose (NaCMC), were purchased from Sigma (St Louis, USA), epsilon caprolactone (ECL) and polycaprolactone (PCL) were purchased from Sigma-Aldrich (St Louise, MO, USA), and utilised to synthesize nanoparticles and the polymer scaffold. Calcium chloride, aluminum chloride and sodium thiosulphate salts (Sigma, St Louis, USA) were used as crosslinking agents in the synthesis of nanoparticles and the polymer scaffold.

3.2.2 Preparation of Nanoparticles

3.2.2.1 The salting out approach

The first attempt to prepare nanoparticles employed a salting out approach, whereby a polymeric dispersion was formed by agitating a 0.8% pectin solution (50mL) with a 24%$^{w}/_{v}$ zinc sulphate solution ($ZnSO_4$) containing 0.6g polyvinyl alcohol (PVA) (75mL), which was used as the salting-out reagent. The rapid addition of deionised water to the polymeric dispersion induced the formation of nanoparticles, after which nanoparticles were lyophilised for 24 hours. For AZT-loaded nanoparticles, the drug was dissolved in the pectin solution prior to addition of the crosslinking solution.

3.2.2.2 The controlled gelification of alginate approach

Calcium (Ca^{2+})-alginate gel is frequently used as a drug delivery vehicle (Liu *et al.*, 2008; Sriamornsak *et al.*, 2007). Rajaonarivony *et al.* (1993) developed a method for the preparation of alginate nanoparticles using a novel cation induced pre-gelation of alginate approach in 1993. This method has been adapted by many scientists since, with chitosan being used instead of poly-L-lysine, a cationic natural polymer which is toxic and immunogenic if injected, to prepare alginate nanoparticles. These nanoparticles were used as carrier of a variety of drugs, including insulin, chemotherapeutics, as well as the hydrophobic antihypertensive agent, Nifedipine (Zahoor *et al.*, 2005; Douglas *et al.*, 2006; Zahoor *et al.*, 2006; Li *et al.*, 2007; Sarmento *et al.*, 2007; Li *et al.*, 2008; Liu *et al.*, 2008).

Nanoparticles were prepared by the ionotropic gelification of anionic sodium alginate (0.6%$^{w}/_{v}$) (200mL) with cationic calcium chloride ($CaCl_2$) (10mL), after which a 0.5%$^{w}/_{v}$ pectin solution (40mL) was added to the Ca^{2+}-alginate gel, to form a stable nanoparticle colloidal system. The crosslinked solution was then rapidly stirred for 1hour, centrifuged (Optima® LE-80K, Beckman, USA) at 20 000rpm for 15minutes. The supernatant was then removed and freeze dried for 24hours at 25mtorrs (Virtis, Gardiner, NY, USA) to obtain a free flowing

powder, after having refrigerated the sample at -70°C (name of freezer, city, country). AZT-loaded nanoparticles were prepared similarly, with 0.3g of AZT dissolved in the alginate solution prior to $CaCl_2$ addition to enable encapsulation of the drug within a polymeric core.

In an attempt to explore the effects of formulation variables on the size and stability of the prepared nanoparticles, preliminary modifications to the above mentioned method were investigated. Barium chloride ($BaCl_2$) was used as the cationic crosslinking agent in one formulation and the other was prepared employing $CaCl_2$ as the crosslinking agent, with the exclusion of pectin. A decreased rate of addition of $CaCl_2$ and pectin was also explored in an attempt to decrease particle size, as illustrated in Table 3.2 below.

Table 3.2: *Independent variables investigated for the influence on particle size and zeta stability*

Formulation	Independent Variable
1	Crosslinking agent: $CaCl_2$
2	Decreased rate of pectin and $CaCl_2$ addition
3	Exclusion of pectin from the formulation
4	Crosslinking agent: $BaCl_2$

3.2.3 Preparation of Polymeric Scaffolds

3.2.3.1 Multipolymeric scaffolds prepared employing hydrophilic polymers

Polymer scaffolds were prepared by mixing NaCMC (3%$^{w}/_{v}$, 100mL), PEO (1%$^{w}/_{v}$, 100mL) and ECL (5%$^{w}/_{v}$, 100mL) solutions until a homogenous mixture was obtained, after which 7.265g of alginate nanoparticles loaded with zidovudine (AZT) were dispersed within the multipolymeric solution. The polymeric mixture, in 5mL increments, were then placed into Teflon moulds (measuring 15mm in diameter and 20mm in height) lubricated with liquid paraffin, containing 2mL of a 10%$^{w}/_{v}$ aluminium chloride ($AlCl_3$), calcium chloride and sodium thiosulphate ($Na_2S_2O_3$) crosslinking solution. The mixture was left to crosslink for 30minutes, after which the resultant scaffolds were removed and left to dry at ambient temperature (25°C).

NaCMC-PEO-ECL crosslinked scaffolds were then agitated in a 1%$^{v}/_{v}$ hydrochloric acid (HCl) solution for 15minutes. This was done in an attempt to reduce the swelling behavior of the scaffold, thereby improving erosion and drug release.

3.2.3.2 Aliphatic polyester multipolymeric scaffolds

Polymeric scaffolds were prepared by dissolving 20g of PCL in 100mL of acetone, followed by dissolution of 0.5g of AZT in the polymeric solution, after which the solution was poured into moulds lubricated with liquid paraffin and left to dry at ambient temperature for 48hours, with the scaffold forming upon evaporation of the acetone.

Multipolymeric scaffolds were prepared by individually dissolving aliphatic polyesters PCL (20g) and ECL (20g) in 100mL of acetone. These solutions were then agitated until a homogenous mixture was obtained, in which AZT was dissolved.

A second set of formulations were prepared with varying concentrations of PCL and ECL dissolved in acetone and crosslinked with a variety of $CaCl_2$ solutions as per Table 3.3.

Table 3.3: *Formulation variables employed for the preparation of multipolymeric aliphatic polyester scaffolds.*

Formulation variables	Lower limits	Upper limits
PCL ($\%^{w}/_{v}$)	2.5	40
ECL ($\%^{w}/_{v}$)	5	50
$CaCl_2$ ($\%^{w}/_{v}$)	0	10

3.2.4 Determination of polymeric structural variations incurred during nanoparticle and scaffold formation employing Infrared spectroscopy

Fourier Transform Infrared (FTIR) spectroscopy was utilized to assess possible structural transitions which had occurred during the preparation process by comparing the functional groups of the parent compounds with that of the formulations produced. Polymer, nanoparticle and scaffold samples were analysed using a Perkin Elmer FTIR Spectrometer (Spectrum 100, Beaconsfield, United Kingdom). Spectra are recorded over the range 4000-625cm^{-1}, with a resolution of 4cm^{-1} and 32 accumulations.

Table 3.4: *Source and background of polymer used for the preparation of nanoparticle and scaffold formulation*

Polymer	Source	Background	Chemical Structure	Reference
Alginate	•Natural polysaccharide •Algal origin	•Forms insoluble gels in the presence of bivalent calcium (Ca^{2+}) ions and other multivalent metals by binding to the carboxylic groups of adjacent G units in the polymer	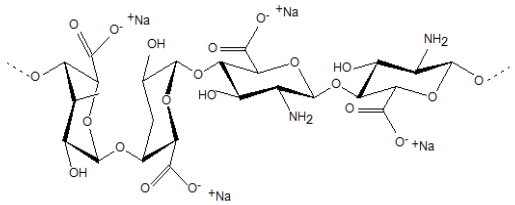	•Bajpai *et al.*, 2004 •Douglas *et al.*, 2006 •Liu *et al.*, 2008 •Sriamornsak *et al.*, 2007
Pectin	•Natural polysaccharide •Plant origin •Derived from the aqueous extraction of edible plants	•α-(1→4)-D-galacturonic acid residues in a linear arrangement, •Like alginaite, pectin forms gels in the presence of Ca^{2+} ions, sugars and acids	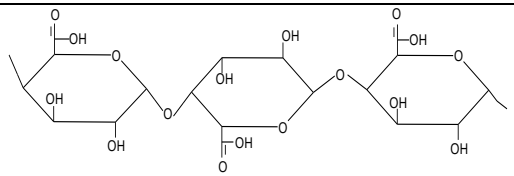	•Guo *et al.*, 1998 •Liu *et al.*, 2003 •Liu *et al.*, 2008 •Lee *et al.*, 2009 •Song *et al.*, 2009
NaCMC	•Plant polysaccharide •A carboxymethyl ether of cellulose •Present in the fibrous tissue of all plants	•A highly water soluble polymer •Attributed to the introduction of sodium carboxymethyl groups into the cellulose molecule •This is achieved by the etherification of the hydroxyl groups of the glucopyranose unit	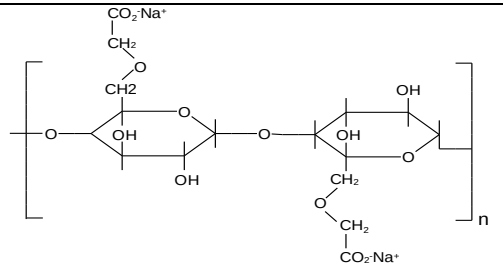	•Guo *et al.*, 1998 •Biswal *et al.*, 2004 •Pushpamalar *et al.*, 2006 •Rokhade *et al.*, 2006 •Yuan *et al.*, 2009
PEO	•A semi-crystalline polymer	• Hydrophillic hydroxyl (OH) groups present in the molecule, allowing for bioadhesivity and mucoadhesivity of the polymer • Swells and form a gel layer upon exposure to water •Controlled drug release is achieved due to this propensity of PEO to swell attributed to retarded erosion of the formulation		•Crowley *et al.*, 2002 •Maggi *et al.*, 2002

Table 3.4: *continued*

PVA	•Synthetic, hydrophilic polymer	•Demonstrates good emulsification and adhesive properties •Poor stability in water, requiring copolymerisation to reduce its solubility in aqueous systems	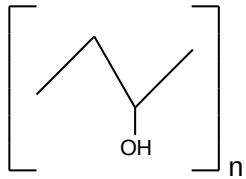	•Sudhamani *et al.*, 2003 •Sanli *et al.*, 2007
ECL & PCL	•Synthetic, semi-crystalline, aliphatic polyester •PCL is prepared by the ring-opening polymerisation of ECL	•PCL is water insoluble, however ECL demonstrates aqueous solubility •Commonly employed for the preparation of bone implants, sustained drug delivery devices and tissue-engineering scaffolds •Demonstrates slow *in vivo* degradation (more than a year) post implantation in the absence of an acidic environment •Superior drug permeability, with various catergories of drug having been encapsulated within PCl/ECL drug delivery devices •Degradation products naturally present in the human body with excretion occurring through the natural metabolic pathways		•Tarvainen *et al.*, 2002 •Jeong *et al.*, 2003 •Huang *et al.*, 2004 •Sinha *et al.*, 2004 •Liu *et al.*, 2005 •Luong-Van *et al.*, 2006 •Rezwan *et al.*, 2006 •Uto *et al.*, 2008 •Abbah *et al.*, 2009 •Chang *et al.*, 2009 •Cameron *et al.,* 2010

3.2.5 Morphological characterisation of nanoparticle and scaffold formulations

3.2.5.1 Transmission electron microscopy

Nanoparticles were dispersed in methanol and sonicated to deflocculate the particles. The samples were placed on carbon grids and analysed using transmission electron microscopy (TEM) (JEOL 1200 EX, 120keV) and photomicrographs were obtained to study the size and morphology of individual particles produced.

3.2.5.2 Scanning electron microscopy

Scanning electron microscopy (SEM), (JEOL, Tokyo, Japan) was employed for observation of the surface morphology of the multipolymeric scaffolds. Samples were coated with carbon and gold-palladium for 10minutes, after which they were visualized between 5-9keV under different magnifications. Photomicrographs were obtained at various magnifications and analyzed for description of the surface morphology. The degree of polymer entanglement, network density and porosity of the scaffolds was qualitatively determined using the photomicrographs obtained.

3.2.6 Assessment of nanoparticle size and zeta potential

A ZetaSizer Nano ZS (Malvern Instruments Ltd, UK) was utilized to determine the average sizes and size distribution of the nanoparticles, employing non-invasive back scatter (NIBS) technology with particle size distribution determined using dynamic light scattering. Brownian motion was measured and related to particle size. The Stokes-Einstein equation (Equation 3.1) was used to determine the translational diffusion coefficient (D), which defines the velocity of Brownian motion. D depends on size of the particle core and the surface structures on the particle and the concentration and type of ions in the medium. Particle size is calculated using the translational diffusion coefficient (Malvern Instruments Ltd).

$$d(H) = k / 3\pi\eta D \qquad \textbf{(Equation 3.1)}$$

Where: d(H)=hydrodynamic diameter

D=translational diffusion coefficient

k=Boltzmann's constant

T=absolute temperature

η=viscosity

The advantages of NIBS technology are:

• The laser does not have to travel through the entire sample, reducing the effect of multiple scattering, whereby the light from one particle is scattered by another particle.

• The effects of dust present in the sample are greatly reduced as dust scatters light in the forward direction.

Mean size (Z-average) and the width of the distribution, also known as the polydispersity index (PDI), is obtained from the correlation function. The correlation function determines the time it takes for the signal to decay (www.malvern.com).

Zeta potential (ZP) studies were performed to determine overall surface charge distribution and stability of the nanoparticle systems. Laser Doppler velocimetry and phase analysis light scanning (PALS) technology was employed to determine zeta potential. ZP is a physical property which is exhibited by any particle in a colloidal system. ZP is used to assess the stability of the system and is calculated from the electrophoretic mobility. This is produced by fluctuations of light intensity when an electric field is applied to the sample (www.malvern.com).

The DVLO theory developed in the late 1940's by Derjaguin, Verwey, Landau and Overbeek, suggests that the stability of a colloidal system is determined by the sum of the van der Waals attractive forces and the repulsive forces present in the electrical double layer, existing between particles as they approach each other due to Brownian motion. Repulsion between particles prevents particles from adhering together due to the existence of energy barriers between the particles. However collisions which occur with sufficient energy to overcome this barrier will be pulled together by attractive forces and will resultantly irreversibly adhere to each other. These colloidal systems therefore present with low zeta potential values. However, particles with sufficiently high repulsive forces will overcome flocculation due to adhesion, with a stable colloidal system prevailing.

3.2.7 Textural profiling to determine the physicochemical behavior of crosslinked scaffolds

Textural profiling of the 3D core of the crosslinked scaffolds enables characterisation of the physicomechanical properties of the prepared scaffolds. A TA.XTp*lus* Texture Analyzer (Stable Micro Systems, Surrey, UK) was employed to establish various stress-strain parameters of the polymeric scaffolds. Samples in both the hydrated and unhydrated states were assessed. Force-distance and force-time profiles were obtained and matrix resilience

and hardness were calculated employing the parameters outlined in Table 3.5.

Table 3.5: *Textural Analysis settings to determine matrix resilience.*

Parameters	Settings
Pre-test speed	1mm/sec
Test speed	0.5mm/sec
Post-test speed	10mm/sec
Compression force	-
Trigger type	Auto
Trigger force	0.5N
Load cell	5kg
Compression strain	50%

3.2.8 In vitro determination of Matrix Erosion of crosslinked multipolymeric scaffolds

NaCMC-PEO-ECL scaffold samples were immersed in 100mL of phosphate buffered saline (PBS) (pH 7.4, 37˚C) and placed into an orbital shaker incubator set to rotate at 20rpm at 37°C, (LASEC, Model LM-530, South Africa). Samples were removed from the PBS solution at specified time intervals, convection dried at 25˚C for 48hours and weighed to gravimetrically determine degree of matrix erosion (ME) employing Equation 3.2.

$$ME\% = \frac{M_o - M_t}{M_o} x100 \qquad \textbf{(Equation 3.2)}$$

Where, *ME%* is the extent of matrix erosion of the scaffold, M_o is the initial mass of the scaffold and M_t is the mass of the scaffold and time *t*. Studies were conducted in triplicate, (n=3).

3.2.9 *In vitro* determination of matrix swelling following hydration of the multipolymeric scaffolds

A second set of samples were tested for change in volume after exposure to 100mL of PBS at predetermined intervals to assess degree of swelling of the polymer scaffold. Samples were removed from the PBS, blotted on filter paper, after which the mean of three perpendicular diameters was calculated following measurement using calipers and volume (V) was calculated employing Equation 3.3.

$$V = \frac{4\pi r^3}{3}$$ **(Equation 3.3)**

Where, *r* is the radius (mm).

Studies were conducted in triplicate to ensure accuracy of the results obtained.

3.2.10 Drug entrapment efficiency of the prepared nanoparticles

Drug entrapment efficiency (DEE) was performed by homogenising 100mg of AZT-loaded nanoparticles in 100mL of PBS, pH7.4 (Polytron PT2000, Kinematika AG, Switzerland), to completely release all entrapped AZT. Free drug molecules were removed from the nanoparticle formulation prior to homoginisation by washing the nanoparticles in distilled water. The total content of entrapped AZT was established in triplicate by means of ultraviolet (UV) spectroscopy, (Specord 40, Analytik Jena, AG, Germany) at a wavelength of 267nm. Due to possible interference of the polymer and excipients used to prepare the samples, a solution of 100mg of drug-free nanoparticles dissolved in PBS was used as a reference. Equation 3.4 was employed to calculate DEE:

$$\%DEE = \frac{D_a}{D_t} x100$$ **(Equation 3.4)**

Where D_a is the actual amount of drug (mg/100mL) entrapped with the formulation and D_t is the theoretical amount of drug (mg/100mL) entrapped within the formulation.

The study was performed on 5 samples, (n = 5).

3.2.11 Drug Release Studies

Drug release studies were performed on nanoparticle formulations and scaffolds containing drug-loaded alginate nanoparticles in an orbital shaker incubator, after being immersed in 100mL PBS. Samples were taken at predetermined intervals, which were analysed using UV spectroscopy.

3.3. Results and Discussion

3.3.1 Infrared spectroscopy

FTIR studies indicated that the basic polymeric structures of the parent compounds was maintained, however surface interactions occurred in the formation of both the nanoparticles

and the scaffold, which is represented by the shifting of the transmittance peaks in the nanoparticle and the multipolymeric scaffold preparations.

The FTIR spectra in Figures 3.1.1.1 and 3.1.1.2 illustrates the nanoparticle preparation compared with the parent polymeric compounds and AZT. A characteristic band between 3600 and 3200cm^{-1} was observed in the spectra of alginate due to the hydroxyl groups as seen in the alginate molecule and bands at 1592 and 1406cm^{-1} are attributed to asymmetric and symmetric –COO^{-} stretching. From the FTIR spectra of pectin, the presence of hydroxyl groups was also observed between 3600 and 3200cm^{-1} and -COO^{-} stretching occurred at 1590cm^{-1}. The peak at 3458cm^{-1} in the AZT spectra is indicative of hydroxyl substituents and the bands between 3200 and 3000cm^{-1} are due to amine groups. Bands between 2100 and 1900cm^{-1} are attributed to multiple bonded N_2 molecules. The -C=O moieties present in the AZT, molecule was observed at 2813 and 1671cm^{-1}. Characteristic bands were present in the spectra of PVA at 3274 and 2907cm^{-1} indicating the presence of hydroxyl groups and –C-H stretching vibrations respectively. The bands present between 1300 and 1000cm^{-1} are due to the bending vibrations of alcohol moieties present in PVA molecule or to –C-O stretching vibrations (refer to Table 3.4).

The alginate nanoparticle formulation presented with bands between 3600 and 3200cm^{-1} indicating the presence of possible hydroxyl or amino substituents. The band at 3332cm^{-1} is more defined than that of alginate, indicating possible interactions of the polymers with AZT, as AZT has an amino substituent present at 3458cm^{-1} as seen on the FTIR spectra. Polymer interactions with AZT are further supported by the presence of a band at 2110cm^{-1} which can be attributed to N_2 substitution or bonding (e.g. ionic bonds). Shifting of the –COO^{-} stretch to 1642cm^{-1} on the nanoparticle spectra indicates possible interaction of the polymers with AZT or $CaCl_2$.

The FTIR spectra of pectin nanoparticles (Figure 3.1.1.2) displayed a broad band between 3600 and 3200cm^{-1} indicating the presence of hydroxyls groups, consistent with the spectra of the parent polymers, PVA and pectin. Interaction of PVA and pectin is supported by the peak at 2944cm^{-1}, attributed to –C-H stretching vibrations observed on the spectra of PVA as well. Multiple peaks observed between 1200 and 700cm^{-1} indicate possible interactions between $ZnSO_4$ and the hydroxyl or methyl groups present in AZT during nanoparticle preparation as these peaks are absent in the spectra of pectin and PVA.

The FTIR spectra in Figure 3.1.2 illustrate the parent polymer compounds compared with the prepared multipolymeric scaffold treated and untreated with HCl. From the FTIR spectra of

NaCMC, a broad band at 3216cm^{-1} can be observed due to hydroxyl stretch vibrations and bands at 2894 and 1321cm^{-1} are due to -C-H groups. The peak at 1588cm^{-1} is typical of the carboxymethyl ether, (-CH_2-COOH), and that at 1412cm^{-1} is due to symmetric stretching of the carboxylate group. Bands present at 1018cm^{-1} are representative of >CH–O–CH_2 stretching. Bands present in the FTIR spectra of PEO at 960cm^{-1} and between 900 and 1250cm^{-1} are due to –C-O group vibrations and –C-O-C stretching respectively. The C-O groups present in the polymer structure allows for complexation of PEO with other polymers and salts (Crowley *et al.*, 2004; Neto *et al.*, 2005). Those at 2877cm^{-1} and between 1400 and 1300cm^{-1} are due to –C-H stretching and the band` at 840cm^{-1} is due to –C-H bending vibrations. Bands between 1060 and 1150cm^{-1} can be attributed to the aliphatic ether moieties in the structure of PEO. The ECL spectra displays characteristic peaks between 1050 and 1300cm^{-1}, indicative of the cyclic ester present in the structure of ECL (refer to Table 3.4) and the carbonyl –C=O stretching was observed at 1652cm^{-1} and between 3400 and 3150cm^{-1}. Bands between 2800 and 3000cm^{-1} are due to –C-H stretching.

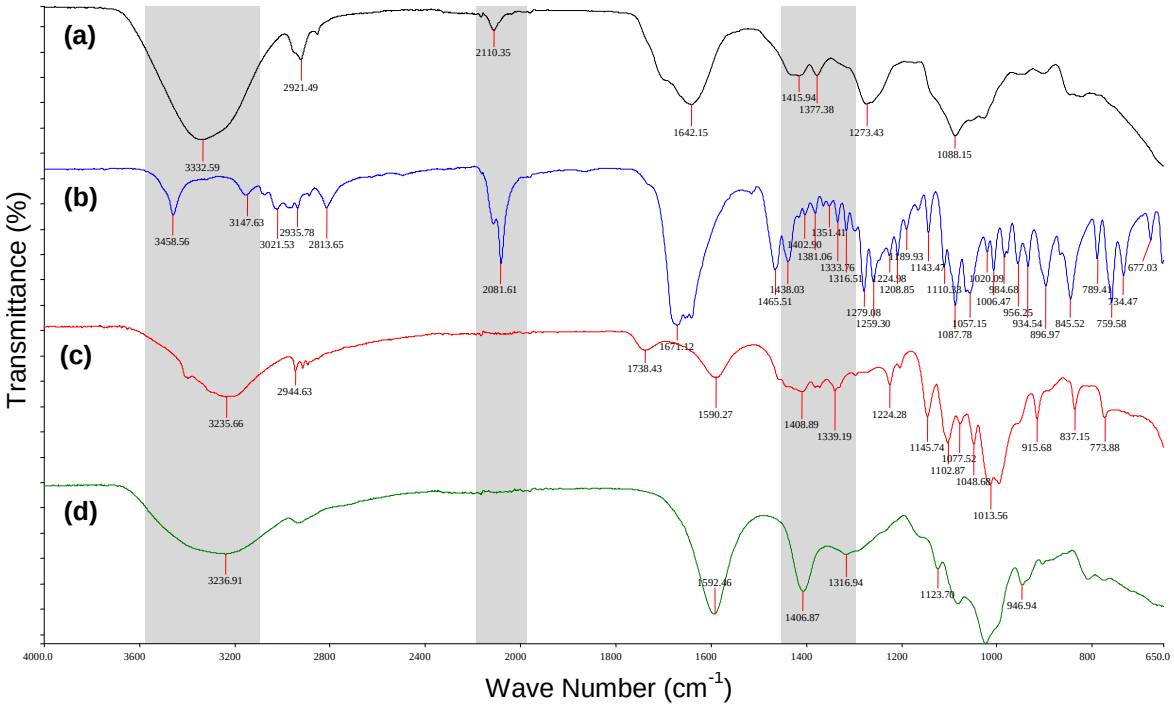

Figure 3.1.1.1: *FTIR spectra comparing the nanoparticle formulations to the native compounds of nanoparticles prepared by means of a controlled gelification of alginate. (a) Alginate nanoparticles, (b) AZT, (c) pectin, (d) alginate.*

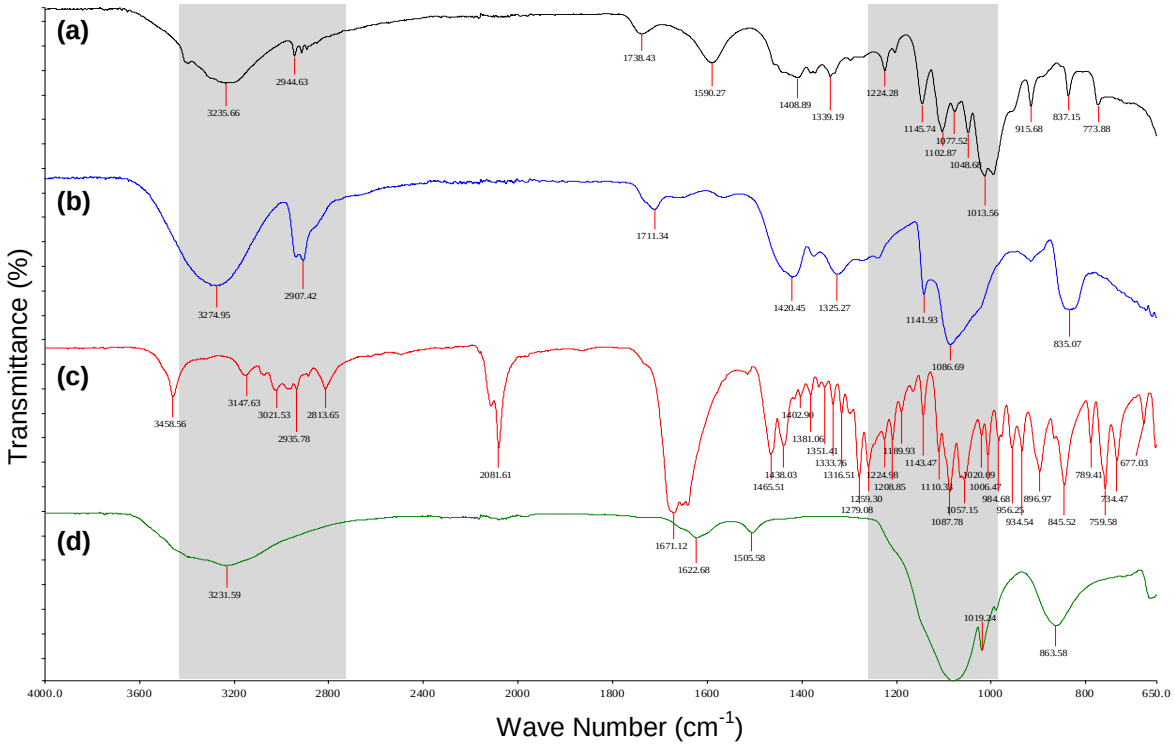

Figure 3.1.1.2: *FTIR spectra comparing the nanoparticle formulations to the native compounds of nanoparticles prepared using the salting out approach. (a) Pectin, (b) PVA, (c) AZT, (d) pectin nanoparticles.*

The carboxymethyl ether groups can be observed in both the multipolymeric scaffolds exposed and unexposed to HCl at 1606 and 1610cm^{-1}, respectively and bands present between 3450 and 3200cm^{-1} are due to hydroxyl groups. Bands present in the spectra of HCl treated and untreated scaffolds at 1610 and 1606cm^{-1} respectively indicate possible ester moieties, attributed to multipolymeric interactions. A shift in the occurrence of the hydroxyl groups can be seen from 3306 to 3224cm^{-1} in the untreated and HCl treated scaffolds respectively, indicating possible interactions of the hydroxyl groups in NaCMC with H^+ ions upon exposure to HCl. This is further supported by fewer bands present in the FTIR spectra of HCl treated multipolymeric scaffolds as compared to untreated scaffolds.

Strong carbonyl bands were observed on the spectra of PCL at 172.02cm^{-1}, indicative of an aliphatic ester. –C-O groups were observed at 1163 and 1233cm^{-1} and –$(CH_2)_4$ moieties were seen between 1290-1420cm^{-1}. No changes were seen when PCL was dissolved in acetone. Interaction of ECL with acetone was observed a reduction of bonds in the spectra as well as the presence of an additional bond present between 1700-1750cm^{-1}, (refer to Figure 3.1.3). Crosslinking of ECL with $CaCl_2$ served to alter the spectra of ECL, whereas few chemical changes were observed when PCL was crosslinked with $CaCl_2$. This will potentially impact on matrix erosion and drug release of scaffolds prepared using PCL and ECL.

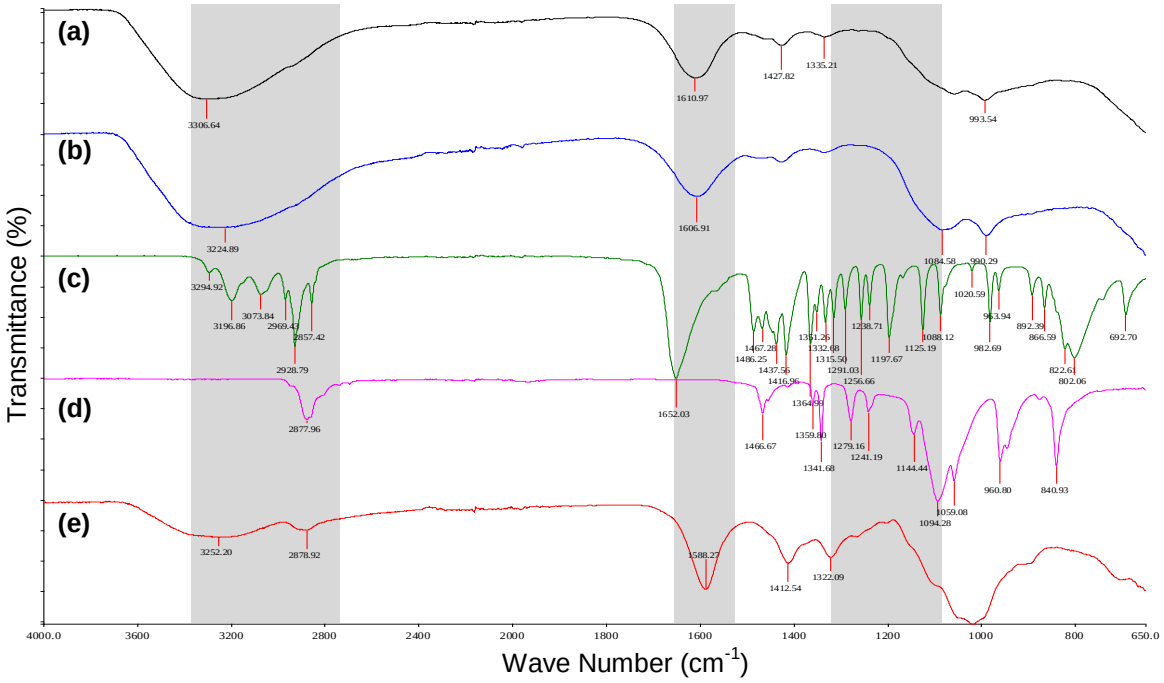

Figure 3.1.2: *FTIR of the HCl treated and untreated multipolymeric scaffold produced, compared to the parent polymer compounds. (a) HCL untreated multipolymeric scaffolds, (b) HCl treated scaffolds, (c) ECL, (d) PEO, (e)NaCMC.*

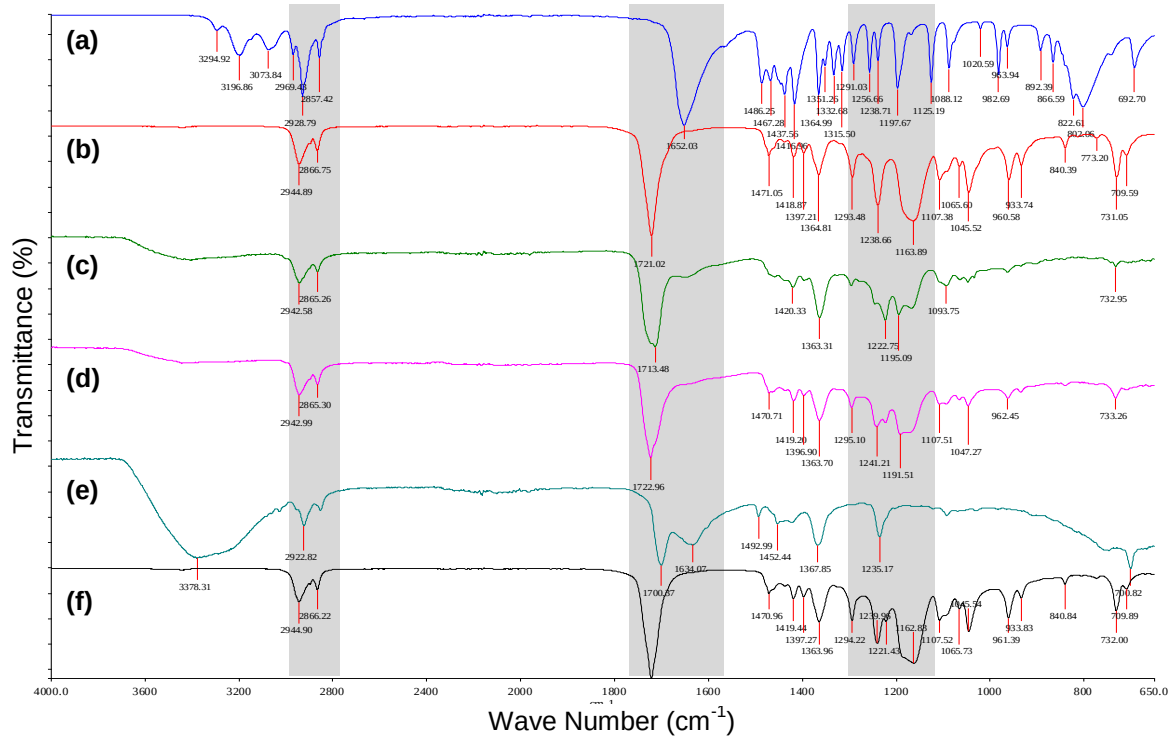

Figure 3.1.3: *FTIR spectra of ECL and PCL blends indicating changes in the chemical structure of the polymers when crosslinked with $CaCl_2$ and when dissolved in acetone. (a) ECL, (b) PCL, (c) ECL and PCL crosslinked with $CaCl_2$, (d) PCL crosslinked with $CaCl_2$, (e) ECL crosslinked with $CaCl_2$, (f) ECL and PCL combined.*

3.3.2 Microscopy Studies

3.3.2.1 Morphological analysis of the nanoparticles employing Transmission electron microscopy

TEM conducted on the drug-loaded alginate nanoparticles, prepared by means of the controlled gelification of alginate approach, revealed the presence of spherical particles ranging between 200-700nm, whereas drug-free nanoparticles displayed a tendency to agglomerate, as seen in Figure 3.2.1. Micrographs obtained from drug-loaded nanoparticles indicated the formation of nanotubes ranging between 500-900nm. Particles were present within the tubes ranging between 50-200nm. These particles are thought to be entrapped drug particles, as seen in Figures 3.2.2 and 3.2.3.

Spherical nanoparticles were observed on the TEM images of nanoparticles crosslinked with $BaCl_2$. A large variation in particle size, ranging between 50-600nm was observed with minimal agglomeration present, attributed to the large radius of Ba^{2+} ions imparting electrostatic charge repulsion to the nanoparticles (Bajpai *et al.*, 2004; Malvern Instruments Ltd). Microparticles were also present on these micrographs. Nanoparticles prepared excluding pectin from the formulation displayed notable agglomeration with an even distribution of particle size, measuring 100nm. As no AZT was loaded into these formulations, nanotube formation was absent in the TEM images obtained.

Figure 3.2: *TEM images of nanoparticles prepared using the controlled gelification of alginate approach.*

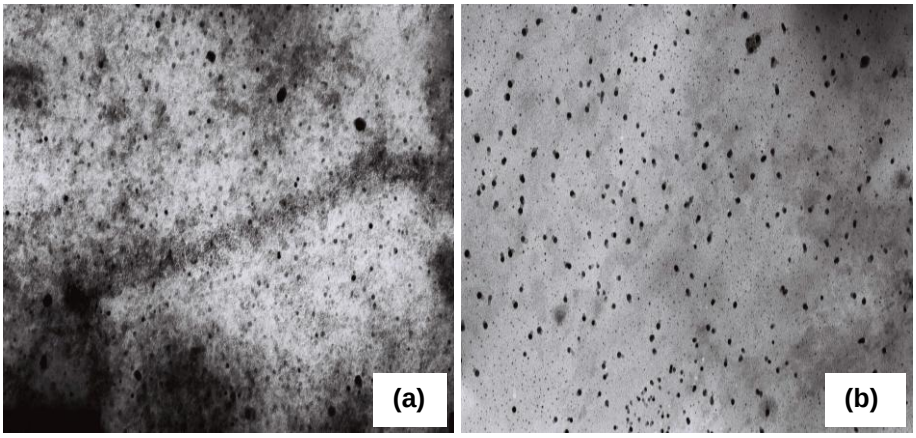

Figure 3.2.1: *(a) Drug-free nanoparticles and (b) AZT-loaded nanoparticles displaying the presence of spherically shaped particles in the nanometer size range. AZT-loaded nanoparticles show lack of agglomeration, (1mm=20nm).*

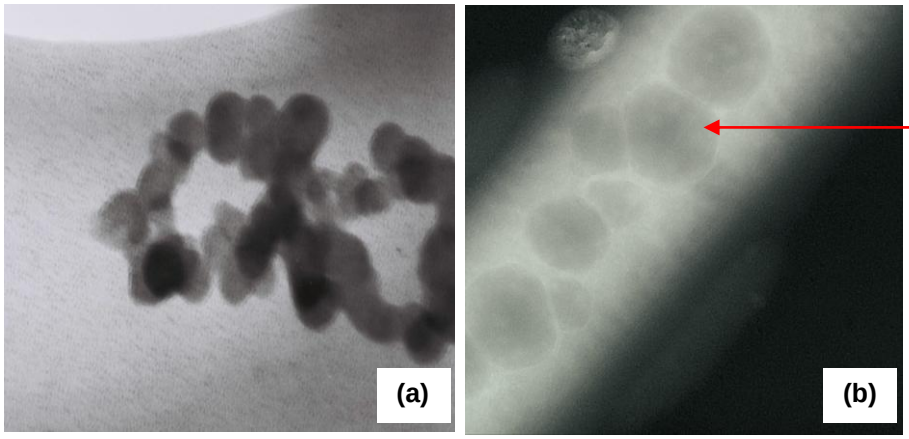

Figure 3.2.2: *(a) AZT-loaded nanoparticles illustrating association between the particles, ranging 50-100nm in size, indicating the potential formation of nanotubes, (1mm=10 nm) and (b) an AZT-loaded nanorod measuring 275nm in diameter, (1mm=11nm).*

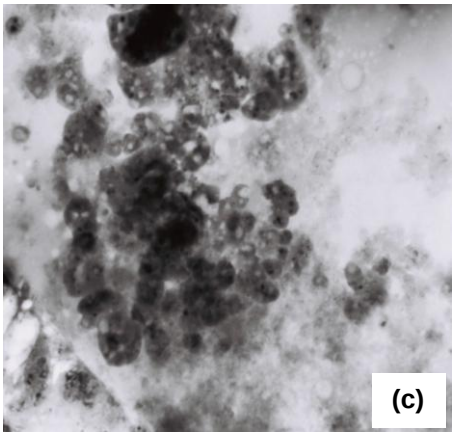

Figure 3.2.2c: *A large variation in particle size observed with nanoparticles crosslinked with $BaCl_2$. Agglomeration is present on the micrograph, however, it is minimal, (1mm=20nm).*

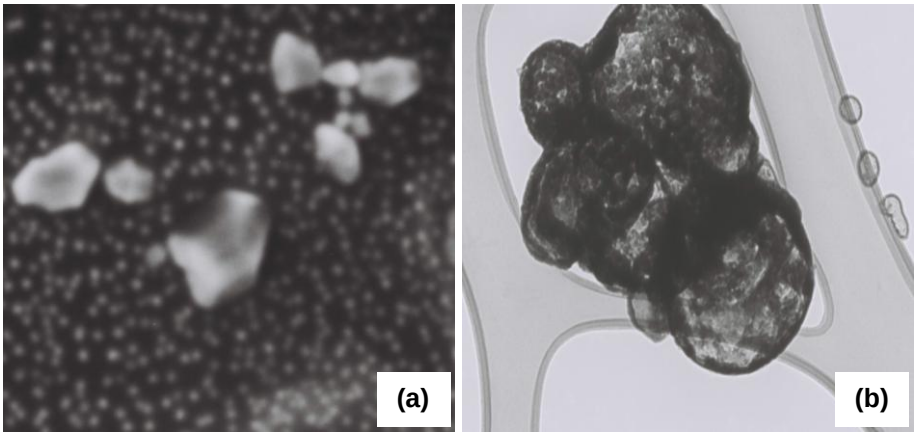

Figure 3.2.3: *(a) TEM of nanoparticles prepared excluding pectin from the formulation indicating a uniform distribution of particle size and shape, with the agglomeration seen on the TEM image (1mm=25nm). (b) Notable agglomeration of AZT-loaded nanoparticles can be seen, measuring 175-700nm in diameter, prepared with pectin excluded from the formulation (1mm=11nm).*

Micrographs obtained of drug-free Zn-pectin nanoparticles, prepared using the salting out approach, revealed agglomeration, as well as individual spherical particles with a sheath surrounding the particles, ranging in size between 10-350nm. Microparticles, due to nanoparticle agglomeration and poor crosslinking of pectin with $ZnSO_4$, can also be seen on the micrographs of drug-free Zn-pectin nanoparticles.

Agglomeration of drug-free and AZT-loaded nanoparticles prepared using both the salting out and the controlled gelification of alginate approach can be attributed to a low charge distribution within the colloidal systems. Addition of AZT to the formulation served to further reduce charge distribution within the formulations. Although AZT is an uncharged molecule, interaction of AZT with alginate, supported by FTIR analysis, would serve to modify charge distribution within the colloidal system (Oh *et al.*, 1998), causing agglomeration of the nanoparticle formulation.

Drug-loaded nanoparticles ranged between 20-200nm. Nanotube formation can also be observed with the salting-out approach. Nanotube formation is possibly due to the N_2 group present in the structure of AZT which interact with pectin and alginate to form tubular structures (refer to Figure 3.2.2)

Figure 3.3: *TEM images of Zn-pectin nanoparticles prepared using the salting out approach.*

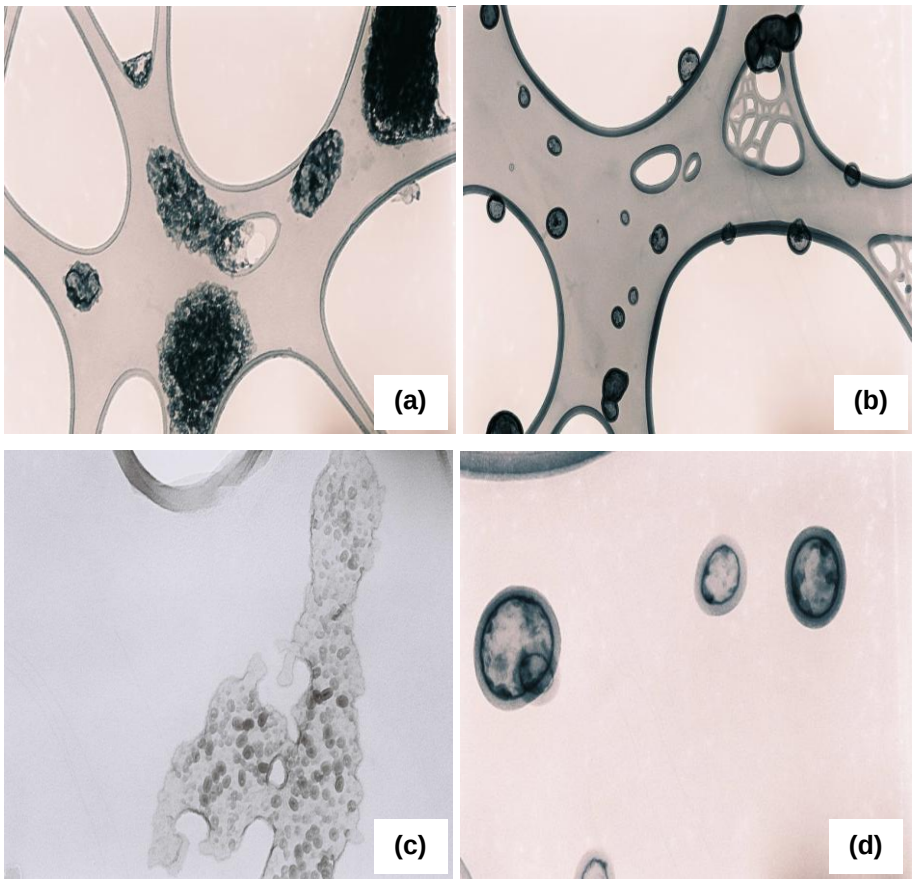

Figure 3.3.1: *Drug-free Zn-pectin nanoparticles prepared using the salting out approach. (a) Displays agglomeration of, and (b) displays individual particles displaying a large range of particle sizes, between 40-320nm. (c)Spherical nanoparticles in the absence of agglomeration, interdispersed within tubular nanostructures, (1mm=10nm). (d) A sheath can be seen surrounding the particles, (1mm=25nm).*

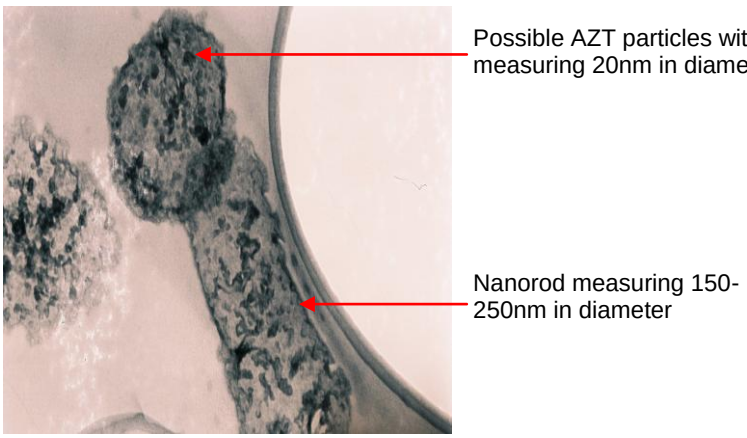

Figure 3.3.2: *AZT-loaded nanoparticles with particles within which could possibly be drug particles. A nanorod can be seen, also possibly containing AZT particles within, (1mm=10nm).*

3.3.2.2 Scanning electron microscopic analysis of the multipolymeric scaffolds

SEM conducted on the NaCMC-PEO-ECL multipolymeric scaffolds revealed a porous polymer matrix, as observed in Figure 3.4.1b. Scaffolds exposed to 1%$^{v}/_{v}$ HCl exhibited smaller, more uniform pores than scaffolds untreated with HCl. HCl treated scaffolds contained large areas of densely packed polymer matrices, interspersed by porous regions, whereas HCl untreated scaffolds contained immense craters within the matrix and densely packed polymer regions were rarely noted on the photomicrographs. Two of the polymers used for the preparation of the multipolymeric scaffold are hydrogels, namely CMC and PEO. Hydrogels are three-dimensional crosslinked polymer capable of extreme swelling due to absorption and retention of water. Hydrogels therefore have a loosely crosslinked structure due to their hydrophilic nature, resulting in the presence of air bubbles in the scaffolds unexposed to HCl (Don *et al.*, 2008). Exposure of the scaffolds to HCl causes the COONa group in CMC to change to the acidic COOH which displays a more compact polymeric matrix (Liu *et al.*, 2002). The craters were attributed to entrapped air bubbles within the polymer matrix.

The distinct bright white areas on the surface of multipolymeric scaffolds are due to a high electric charge on the scaffold surface accredited to the presence of multivalent ions, present on the surface of the polymer matrix (Parolis *et al.*, 2008), as well as free H^{+} and Cl^{+} ions on scaffolds exposed to 1%$^{v}/_{v}$ HCl.

A porous polymer matrix is ideal for the dispersion of drug-loaded nanoparticles (Yuan *et al.*, 2009). Drug release is anticipated be enhanced as the nanoparticles will be released as the polymer matrix swells or erodes, allowing for the prolonged delivery of drug. Premature drug degradation will be prevented and drug toxicity will be reduced as controlled drug release will be achieved (Hughs, 2005; Zahoor *et al.*, 2005).

SEM was also conducted on multipolymeric scaffolds crosslinked once only. Photomicrographs obtained from these samples contained larger pores and more craters within the polymer matrix. Higher concentrations of Ca^{2+} and Al^{3+} ions form intramolecular complexes within CMC, resulting in a tightly coiled polymer matrix, causing smaller pores to be present in multi-crosslinked scaffolds (Don *et al.*, 2008; Liu *et al.*, 2002; Parolis *et al.*, 2008). Air pockets are clearly visible in the scaffold matrix as seen in Figure 3.2.2a. This formulation is not idyllic for nanoparticle dispersion, supporting the need for multiple crosslinking to achieve an optimum formulation.

A densely packed polymer matrix was observed with PCL scaffolds. Upon exposure to PBS, pH 7.4, an increase in porosity was not observed as water was unable to permeate into the polymer matrix due to the high degree of crystallinity observed with polyester polymers (Rezwan *et al.*, 2006). However surface erosion of the polymer scaffold was observed. When PCL was blended with ECL, a more porous polymer matrix was produced, ideal for the dispersion of nanoparticles. Upon prolonged exposure to PBS, pH 7.4, the porosity of the scaffold matrix was observed to increase due to permeation of water into the matrix and an increase in crystalline regions was noted. This is due to PCL and ECL degrading by hydrolytic desterification (Rezwan *et al.*, 2006; Tarvainen *et al.*, 2002) occurring primarily in the amorphous regions of the polymer as these regions are less stable than the crystalline regions (Rezwan *et al.*, 2006; Luong-Van *et al.*, 2006).

Figure 3.4: *Scanning Electron Micrograph of crosslinked polymeric scaffolds, revealed surface morphology of the prepared scaffolds.*

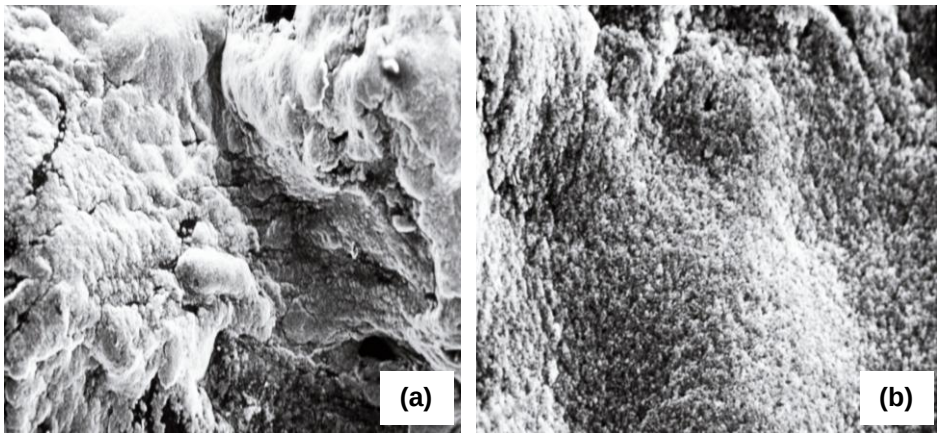

Figure 3.4.1: *(a) Densely packed polymer matrix due to efficient crosslinking of the multipolymeric scaffold, (1mm=50µm). (b)Uniform pores are present within the polymer matrix of scaffolds exposed to 1%$^{v}/_{v}$ HCl, which can efficiently entrap drug-loaded nanoparticles, thereby serving to modulate drug release (1mm=125µm). Brighter white areas are attributed to multivalent ions present on the surface of the scaffolds.*

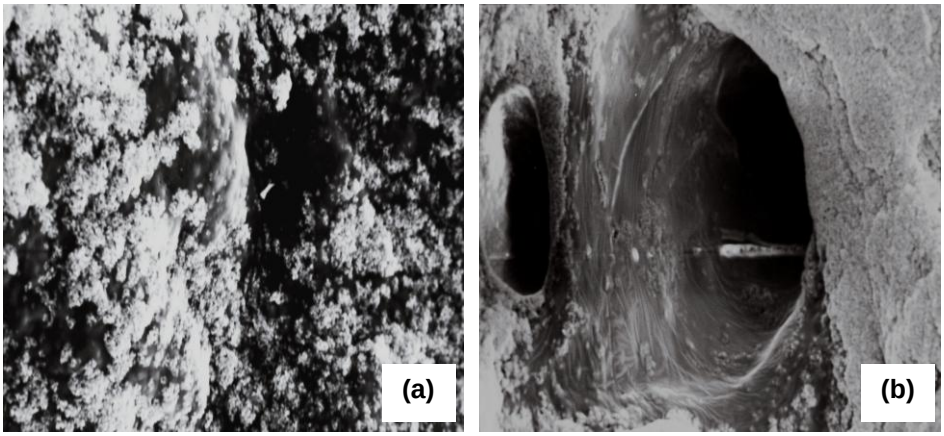

Figure 3.4.2: *(a) Craters can be seen between the pores in the matrix due to air bubbles in the polymer solution during scaffold preparation (1mm=50µm). (b) Upon closer magnification, densely packed polymer regions and porous areas can be observed surrounding the craters (1mm=250µm).*

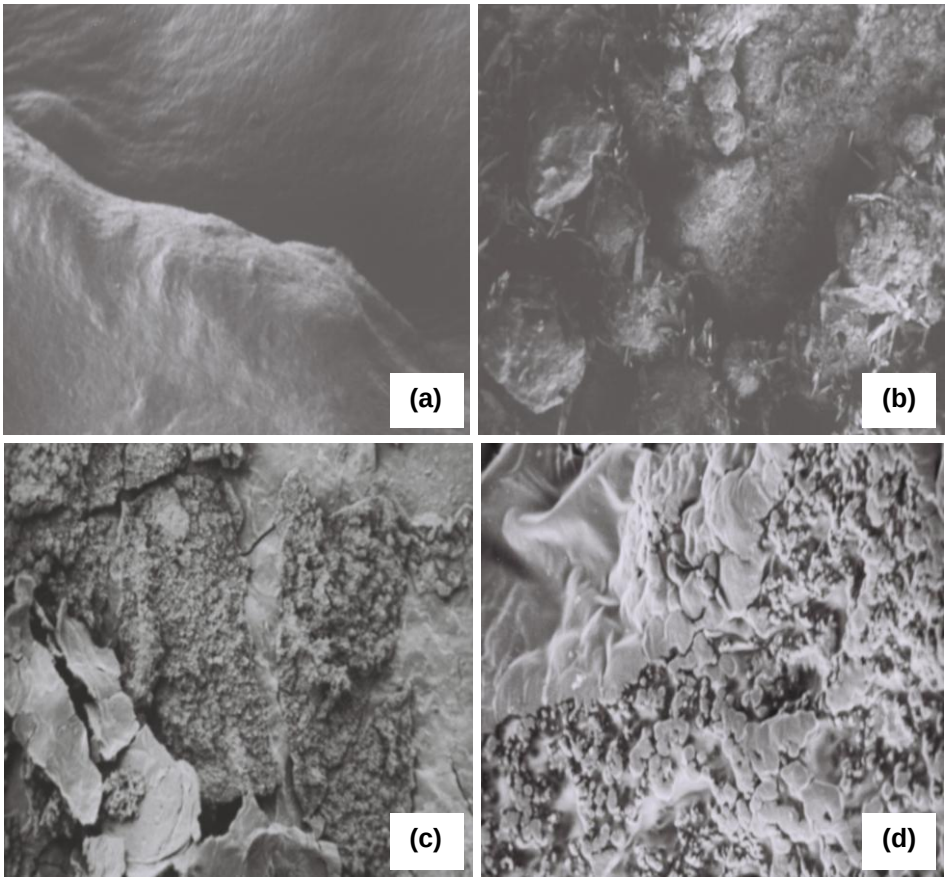

Figure 3.4.3: *SEM images of (a) PCL scaffolds indicating a densely packed polymer matrix (1mm=125µm). (b) Multipolymeric PCL-ECL scaffolds demonstrating porosity of the scaffold matrix with crystalline areas observed (1mm=100µm). (c) PCL-ECL scaffolds crosslinked with $CaCl_2$ with larger pores observed in the polymer matrix as compared to (d) non-crosslinked PCL-ECL scaffolds (1mm=250µm).*

Crosslinking PCL-ECL solutions with $CaCl_2$ served to further increase porosity of the scaffolds, (refer to Figure 3.4.3). As PCL and ECL demonstrate sow degradation in the body (Abbah *et al.*, 2009; Luong-Van *et al.*, 2006; Sinha *et al.*, 2004), an increase in matrix porosity is required for release of nanoparticles and drug at the desired site of action. Porous regions are surrounded by regions of densely packed polymer matrices which would serve to sustain drug release over prolonged periods.

3.3.6 Zeta Analysis

Zeta potential and particle size distribution was determined in deionised water. Non-invasive back scatter (NIBS) technology was employed to determine particle size distribution using Dynamic Light Scattering (DLS), whereby Brownian motion was measured, which was then related to particle size.

Zn-Pectin nanoparticles displayed an average size distribution of 1323nm (SD<0.008), with a polydispersity index (PDI) of 0.816 for AZT-loaded nanoparticles and 119.6nm (SD<0.005), PDI 0.676, for drug-free nanoparticles. Multiple wide peaks were obtained, indicating the tendency of the colloidal system to agglomerate, (refer to Figure 3.5.1). Microparticles were observed with AZT-loaded nanoparticles as agglomerates were formed which could not be redispersed upon sonication of the nanoparticles prior to analysis. This was confirmed with zeta potential analysis, whereby AZT-loaded nanoparticles displayed an average zeta potential of -0.012mV (SD<0.001), indicating an instable colloidal system, whereas drug-free nanoparticles displayed an average zeta potential of -0.419mV (SD<0.004), indicating a more stable colloidal system. This system is less likely to agglomerate.

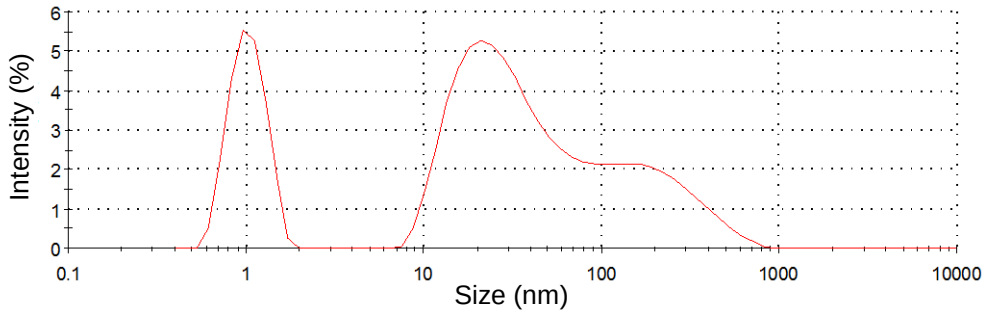

Figure 3.5.1: *Size distribution profile of drug-free Zn-Pectin nanoparticles, indicating the presence of particles ranging from 1 to 1000nm. Multiple wide peaks indicate the tendency of the nanoparticles to agglomerate (n=3; SD<0.002 in all cases).*

The use of DLS for the analysis of a sample containing a mixture of extremely large and small particles yields large Z-averages as the contribution to the total light scattered by the small particles will be extremely small, as seen in Figure 3.5.1 (Malvern Instruments Ltd).

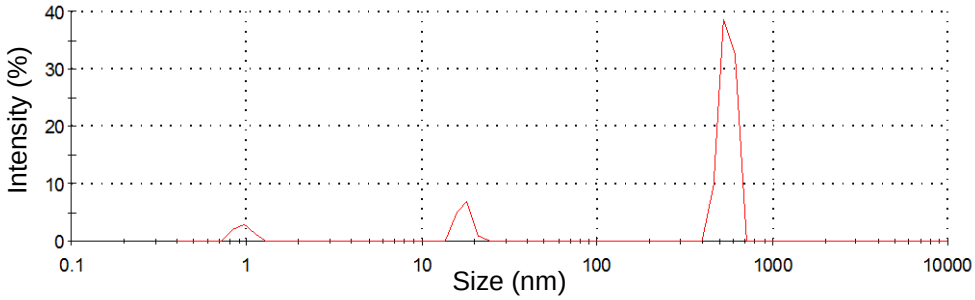

Figure 3.5.2: *Size distribution profiles of AZT-loaded Zn-Pectin nanoparticles indicate the presence of particle in the 600nm size range. A single narrow peak was obtained indicating flocculation of the nanoparticles prior to analysis (n=3; SD<0.002 in all cases).*

Particle size distribution studies conducted on nanoparticles prepared using the controlled gelification of alginate approach revealed an average size distribution of 576.1nm (SD<0.005), PDI 0.464, for AZT-loaded nanoparticles, and 752.1nm (SD<0.005), PDI 0.547, for drug-free nanoparticles. Wider peaks were obtained as seen in Figure 3.5.1. This is due to the tendency of nanoparticles to agglomerate, which can be noted by the peak in the 900nm range in Figure 3.5.4. Agglomeration of the nanoparticles can be reduced by the addition of a surface active agent to the formulation, which will be explored in further studies.

Nanoparticles crosslinked using $BaCl_2$ presented with an average size distribution of 880.8nm (SD<0.002) with a PDI of 0.215. This indicated a large particle size variation of the colloidal system as the PDI is utilised to estimate the width of particle distribution (Malvern Instruments Ltd). Ba^{2+} ions have a larger radius (1.74A°) than Ca^{2+} ions (1.14A°) with Ba^{2+} crosslinking with alginate having been found to yield smaller beads than Ca^{2+} crosslinking attributed to Ba^{2+} capable of filling a larger space between alginate molecules with a more tightly packed matrix obtained (Bajpai *et al.*, 2004). However, size distribution of nanoparticles formulated using $BaCl_2$ as the crosslinking agent yielded larger particles. This is possibly due to the high concentrations of $BaCl_2$ used, with resultant poor crosslinking of alginate due to the premature gelation of the solution occurring with the introduction of $BaCl_2$.

The absence of pectin from the formulation resulted in smaller nanoparticles being formed, 161.9nm (SD<0.004), PDI 0.400. This was expected as pectin would add bulk of the crosslinked alginate nanoparticles, thereby increasing the size of the nanoparticles.

However, pectin served to add stability to the colloidal system as pectin is an anionic polymer (Liu *et al.*, 2003). The absence of pectin in the nanoparticle formulation resulted in preparation of an unstable colloidal system due to a reduction in the repulsive forces present in the colloidal system. The zeta potential of 0.305mV (SD<0.007) obtained with this formulation confirmed this. The positive charge distribution present within this colloidal system can be attributed to free Ca^{2+} ions.

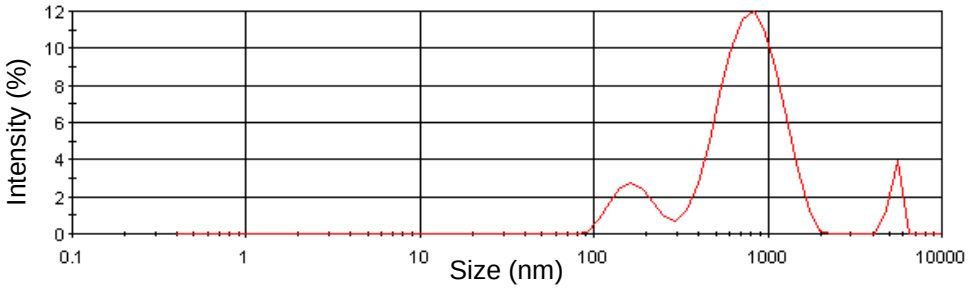

Figure 3.5.3: *Size distribution profile of drug-free nanoparticles prepared using the controlled gelification of alginate approach. The profile indicated the presence of particles ranging from 100nm to 1000nm (n=3; SD<0.002 in all cases).*

Wide peaks and peaks close to the 1000 nm range are due to agglomeration of the colloidal system.

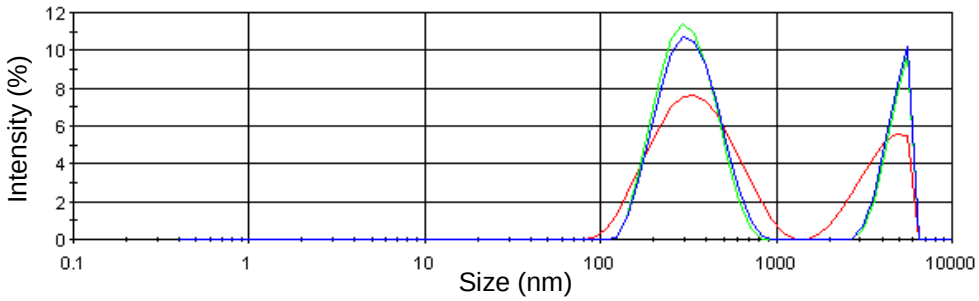

Figure 3.5.4: *Size distribution profile of AZT-loaded nanoparticles indicated a uniform size distribution of particles, as seen by all three peaks appearing in the 400-600d.nm size range (n=3; SD<0.002 in all cases).*

The average zeta potential of AZT-loaded alginate nanoparticles was -3.53mV (SD<0.003) and that of drug-free nanoparticles was -6.39mV (SD<0.002). The poor zeta potential obtained can be attributed to the high degree of crosslinking between the cationic Ca^{2+} salt and the anionic alginate. A strong positive surface charge from the Ca^{2+} ions is prevented due to ionotropic crosslinking of the Ca^{2+} ions with the carboxyl groups of the guluronic acid residues, which makes up alginate, in which Ca^{2+} is held in the centre of the 3-dimensional structure. Alginate is an anionic polymer, resulting in the negative zeta potential obtained.

(Bajpai and Sharma, 2004; Li *et al.*, 2008; Zactiti and Kieckbusch, 2006). Although AZT in an uncharged molecule (Oh *et al.*, 1998), there is a possible interaction of AZT with the polymers, as observed from the FTIR spectra, with resultant inferior crosslinking of Ca^{2+} with alginate. Free Ca^{2+} ions are therefore present in the colloidal system, causing instability of the nanoparticle formulation.

$BaCl_2$ is more capable of donating negative ions to the colloidal system than $CaCl_2$, indicated by the zeta potential of -7.54mV (SD<0.006) obtained with the nanoparticle formulation crosslinked with $BaCl_2$, (refer to Firgure 5.5.5b) This can be explained due to the larger radius exhibited by Ba^{2+} ions allowing enhanced electrostatic charge distribution of the colloidal system (Bajpai *et al.*, 2004; Malvern Instruments Ltd).

However, alginate nanoparticles prepared by crosslinking with $CaCl_2$ with pectin included in the formulation exhibited superior size distribution and formulation stability and were therefore chosen for further studies.

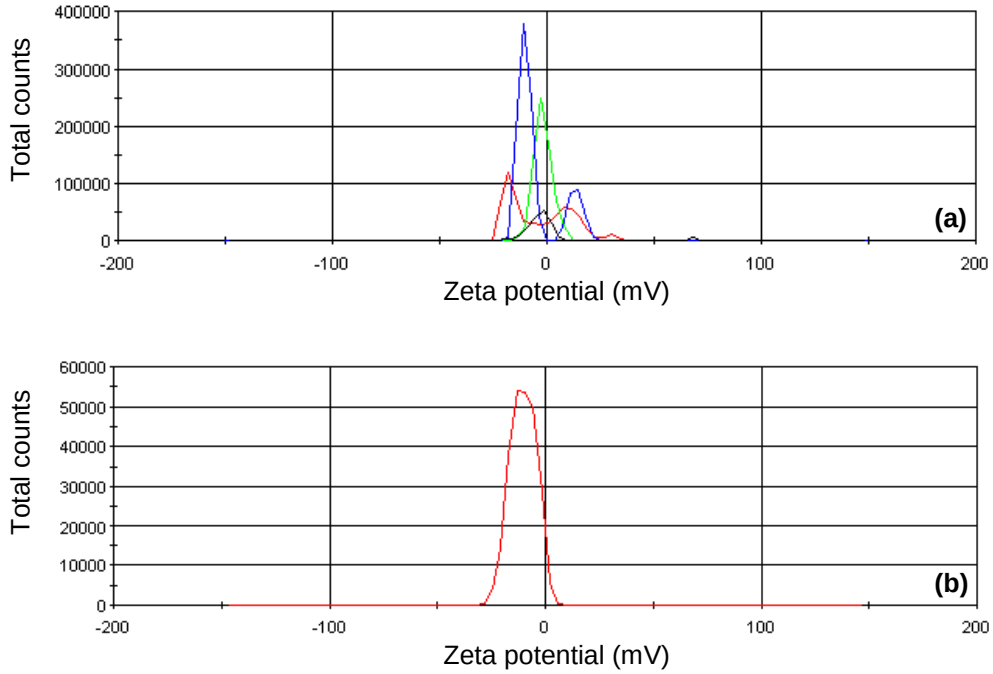

Figure 3.5.5: *(a) Multiple peaks obtained in the Zeta potential profile of AZT-loaded nanoparticles prepared by means of a controlled gelification of alginate approach indicates particles with an inconsistent distribution of potential. A Z-average of -3.53mV was obtained, indicating a degree of instability of the nanoparticles produced. (b) Enhanced stability was observed with nanoparticles crosslinked with $BaCl_2$. This can be attributed to $BaCl_2$ being capable of donating negative ion to the formulation for efficiently than $CaCl_2$, leading to electrostatic/charge stabilization of the colloidal system (n=3; SD<0.002 in all cases).*

Zeta potential results from either steric repulsion or electrostatic stabilisation of particles as per Figure 3.6. Steric repulsion involves polymer adsorption onto the particle surface, preventing the particles from coming into close contact with each other. Electrostatic charge stabilisation involves the distribution of charged species within the colloidal system, serving to enhance particle repulsion (Malvern Instruments). Electrostatic charge stabilisation accounts for the zeta potential obtained for colloidal systems prepared using both the salting out approach and the cation induced gelification of alginate approach attributed to the use of high concentration of salt solutions for the preparation of the nanoparticles.

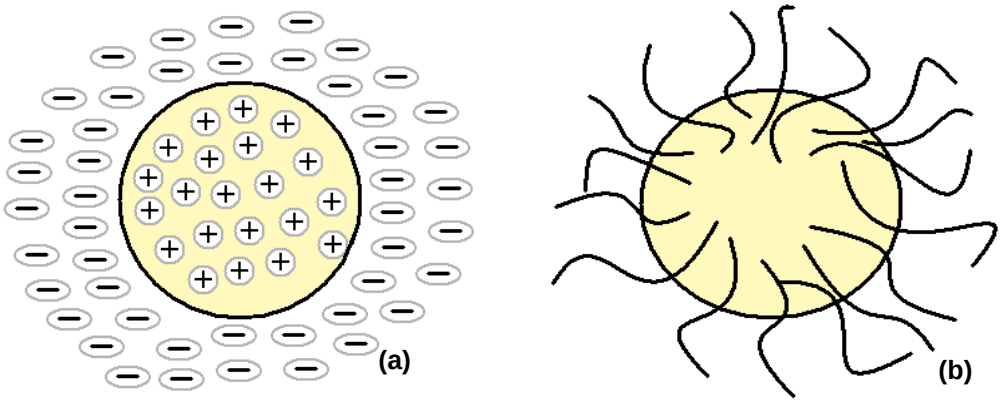

Figure 3.6: *Schematic of (a) electrostatic stabilisation and (b) steric repulsion of nanoparticles in a colloidal system.*

3.3.8 Textural Analysis of multipolymeric scaffolf matrices

Assessment of matrix resilience (MR) provides information regarding *in vitro* degradation and drug release behaviour of the multipolymeric scaffold device. MR also has implications for device storage. It is therefore imperative to have a rigid polymeric scaffold which can withstand fracture during storage and handling of the device. Textural analysis performed on unhydrated samples revealed a decrease in the resilience of HCl treated particles compared to untreated systems with a MR of 12.83% (SD<0.004) as compared 18.12% (SD<0.004) obtained with untreated particles. This was expected as scaffolds exposed to HCl presented with less porous matrices as observed in Figure 3.7.1a due to acid transition of the COONa groups in CMC to COOH. This could possibly result in a brittle scaffold, accounting for the low MR obtained. Less water will therefore permeate into the polymer matrix leading to reduced disentaglement of the polymer matrix, allowing for prolonged drug release. However, hardness of both treated and untreated particles was similar, with treated particles having a mean value of 3.45nm (SD<0.001) and untreated particles having a mean value of 3.712nm (SD<0.006).

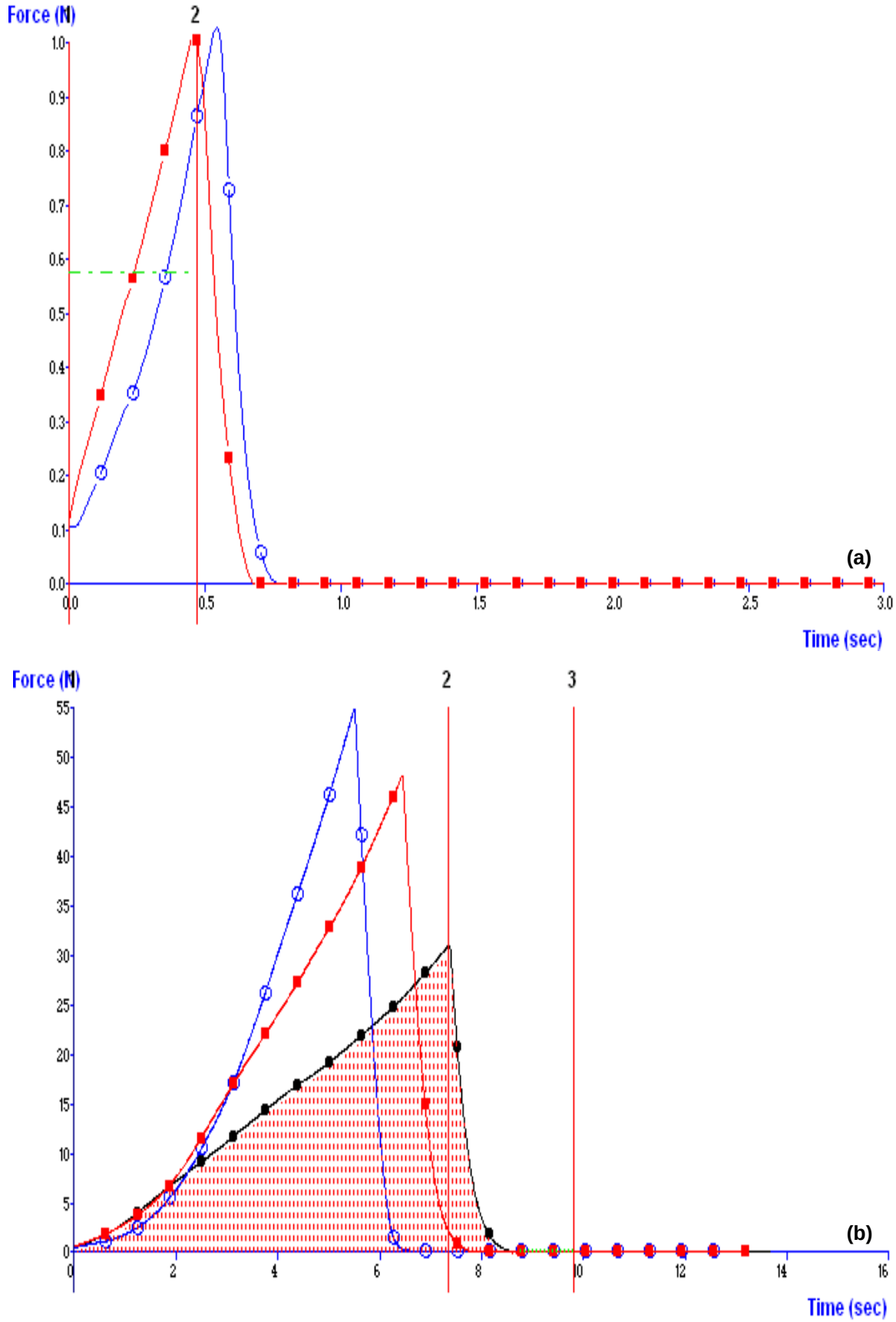

Figure 3.7.1: *Typical (a) hardness and (b) resilience profiles of untreated particles (n=3; SD<0.001 in all cases).*

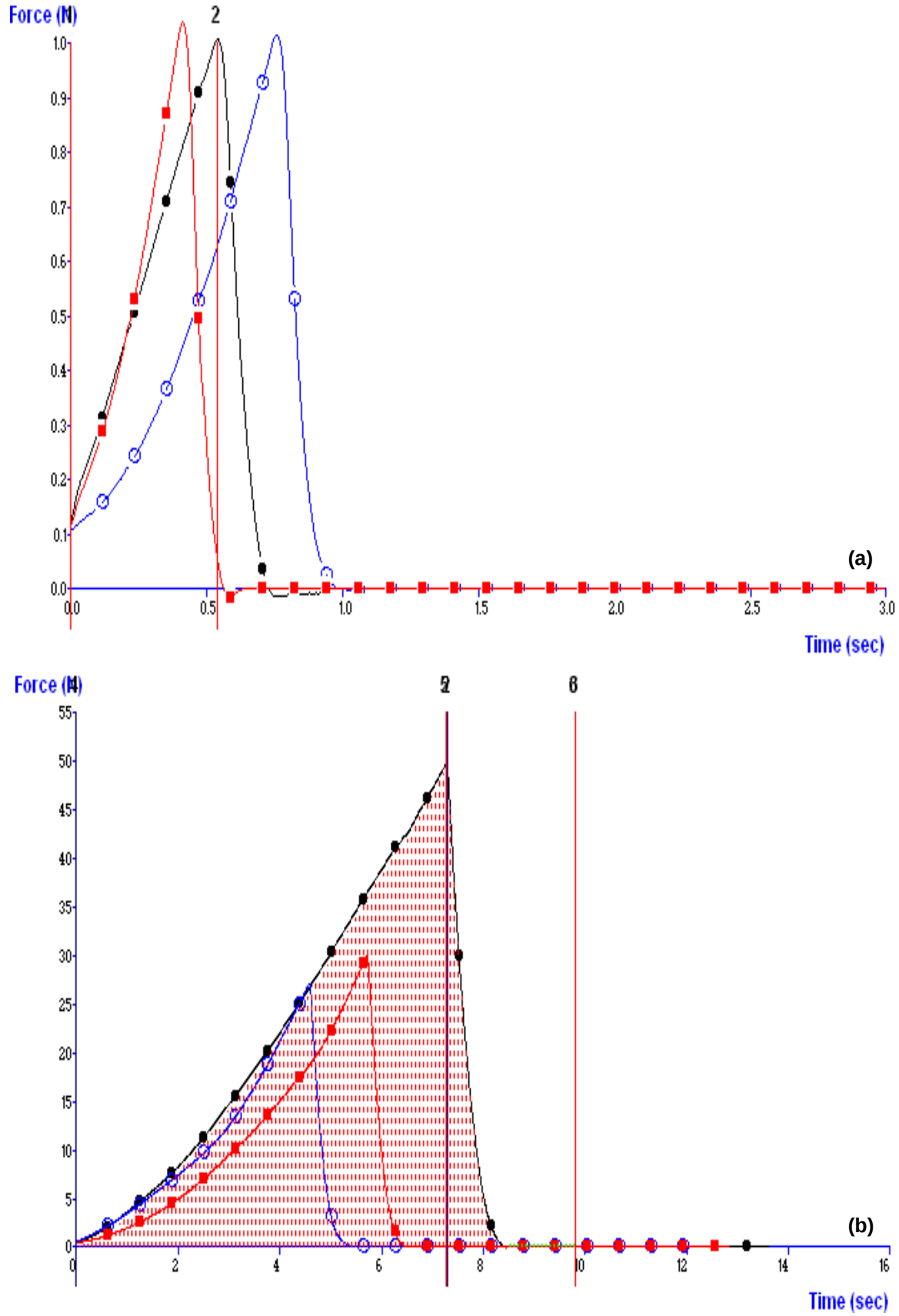

Figure 3.7.2: *Typical (a) hardness and (b) resilience profiles of HCl treated particles (n=3; SD<0.001 in all cases).*

Upon hydration, matrix resilience declined with HCl treated and untreated samples, with scaffolds unexposed to HCl displaying a MR of 8.043% (SD<0.004) and scaffolds exposed to HCl displaying a MR of 6.361% (SD<0.004). MR of both sets of samples declines with further exposure to PBS, (refer to Figure 3.8), due to swelling and chain relaxation of the polymer matrix. The viscoelastic property of the scaffold resultantly increases and MR declines.

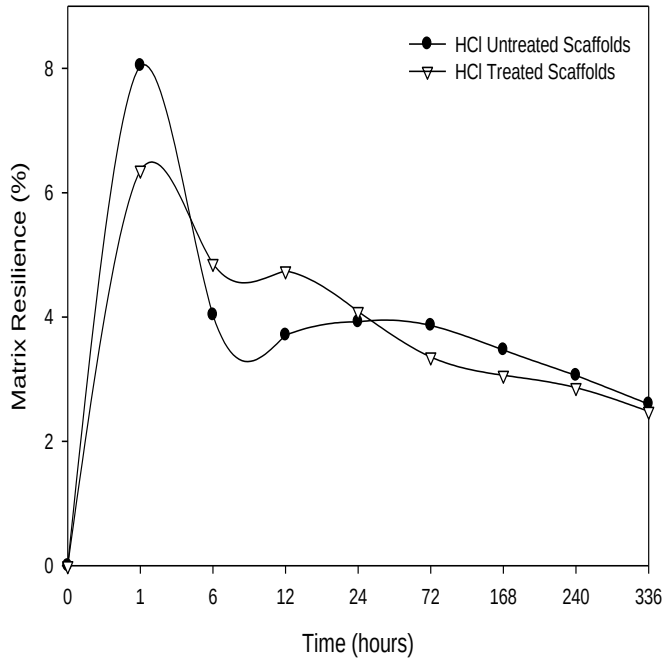

Figure 3.8: *Percentage resilience of HCl treated and untreated scaffolds, indicating a decline in porosity with increased exposure to PBS, pH 7.4 (n=3; SD<0.004 in all cases).*

3.3.9 Matrix erosion and Swelling

Upon treatment with 1%$^{v}/_{v}$ HCl, the carboxylate COONa groups in NaCMC are converted to to the acidic COOH form. This COOH form is less susceptible to ionisation in PBS, as the COO^- group has a greater affinity for the H^+ ion resulting in a lower degree of ion exchange of the Na^+ and H^+ to reform COONa. The polymeric matrix resultantly imbibes less water, reducing the swelling behaviour of HCl treated particles. Exposure to HCl also leads to a more densely crosslinked polymer matrix which is less prone to swelling than the loosely packed untreated scaffolds (Liu *et al.*, 2002; Rokhade *et al.*, 2006). However, both sets of scaffolds still exhibit extensive swelling behaviour as seen in Figure 3.9 below. This is attributed to the highly hydrophilic nature of the polymers which enhances the rate and water uptake capacity (Rokhade *et al.*, 2006).

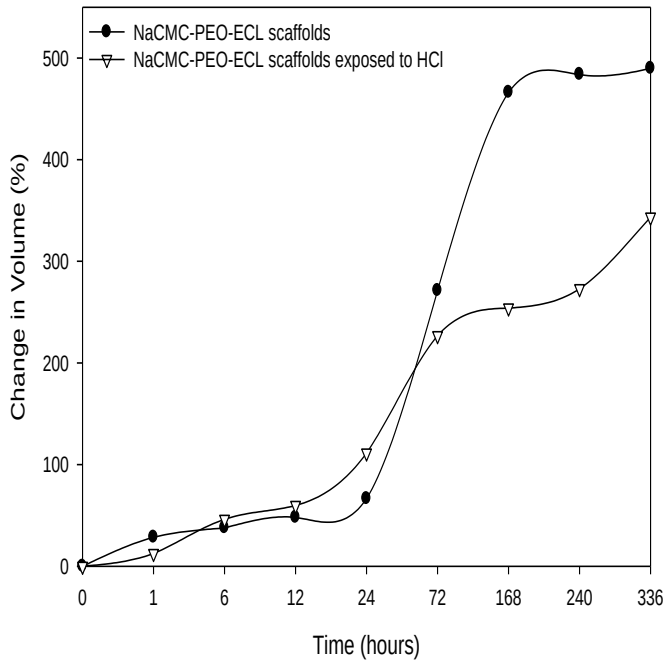

Figure 3.9: *Swelling behavior of HCl treated and untreated multipolymeric scaffolds (n=3; SD<0.001 in all cases).*

A decrease in the amount of water penetrating into the scaffold reduces the disentanglement of the polymeric matrix, leading to reduced erosion of the multipolymeric scaffolds treated with HCl, noticed in the first 24hours as compared to untreated scaffolds (refer to Figure 3.10a) (Parolis *et al.*, 2008; Baijpai *et al.*, 2004). However, upon prolonged exposure to PBS, pH 7.4, NaCMC-PEO-ECL multipolymeric scaffolds, treated and untreated with HCl, displayed weight gain, thought to be due to sequestration of phosphate and Na^+ ions within the polymer matrix and resultant decrease of the entanglement of the polymer chains (Liu *et al.*, 2002). Multipolymeric scaffolds exposed to HCl displayed a larger percentage weight gain than those unexposed to HCl.

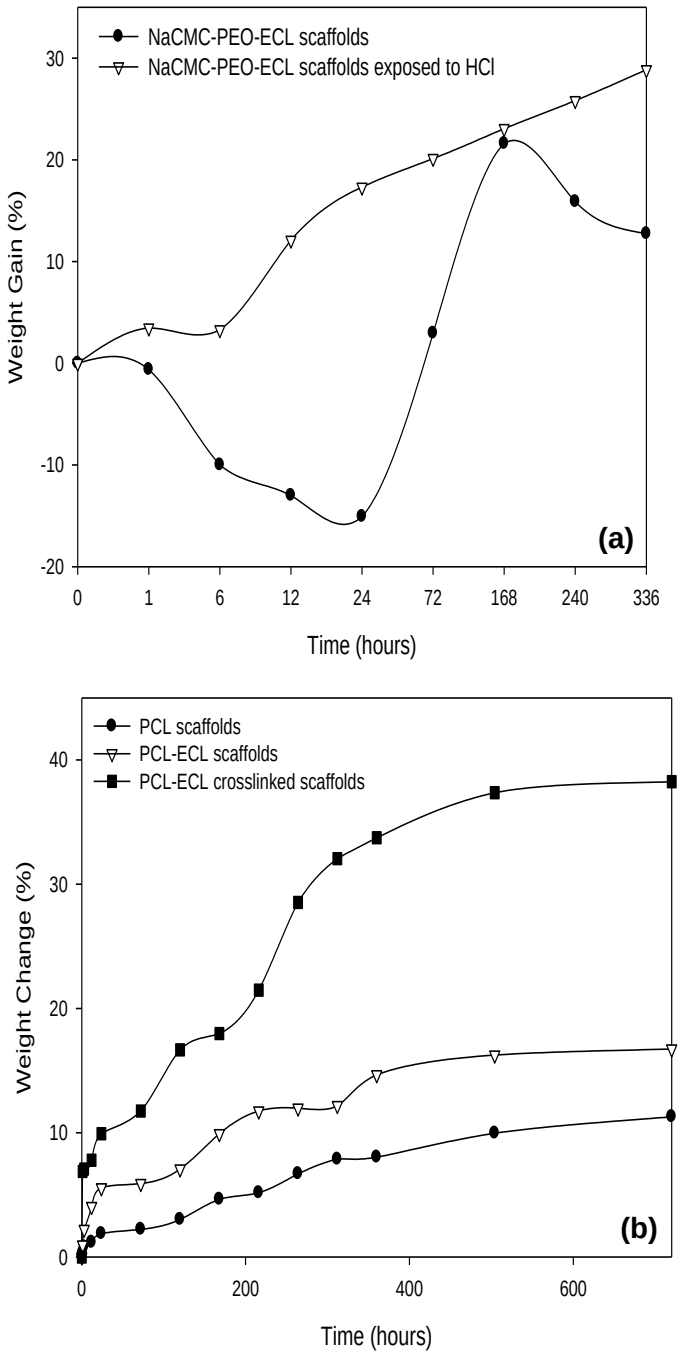

Figure 3.10: *(a) Percentage weight change of HCl treated and untreated NaCMC-PEO-ECL crosslinked scaffolds, indicating the degree of entrapped moisture and ions within the polymer matrix accounting for the gain in weight of the scaffolds (b) Matrix erosion of scaffolds prepared using polyester polymers, crosslinked and not crosslinked with $CaCl_2$ determined over 30 days (n=3; SD<0.001 in all cases).*

Scaffolds prepared using a combination of PCL and ECL displayed a higher percentage weight loss, 16.737% (SD<0.002), than scaffolds prepared with PCL alone, 11.279% (SD<0.005) 30 days post exposure to PBS, pH 7.4 (refer to Figure 3.10b). PCL is a hydrophobic polymer which has been utilized extensively for the sustained delivery of pharmaceuticals in the past (Tarvainen *et al.*, 2002; Sinha *et al.*, 2004; Chang *et al.*, 2009). It

was therefore expected that scaffolds prepared using PCL would display slow erosion of the polymer matrix. Although ECL is also a synthetic aliphatic polyester from which PCL is prepared (Chang *et al.*, 2009; Tarvainen *et al.*, 2002; Uto *et al.*, 2008), it is not a hydrophobic polymer. Combining the two polymers to prepare a multipolymeric scaffold therefore served to increase the rate of scaffold erosion.

Crosslinking PCL-ECL solutions with $CaCl_2$ served to increase the porosity of the resultant scaffold, hence increasing matrix erosion to 38.253% (SD<0.002) 30 days post exposure to PBS, pH 7.4. Increased porosity of the crosslinked scaffold caused an increase in water penetration into the polymer matrix, causing disentanglement of the polymer chains, resulting in erosion of the scaffolds.

Swelling was not observed with scaffolds prepared using PCL and ECL. This was expected due to the crystalline nature of the polymers which does not accommodate water uptake into the polymer matrix (Luong-Van *et al.*, 2006; Sinha *et al.*, 2004; Uto *et al.*, 2008).

3.3.10 Drug Entrapment Efficiency and Drug Release

A calibration curve, as per Figure 3.11 was generated for AZT using PBS, pH 7.4 at 25°C, employing a UV spectrophotometry at the wavelength of maximum absorption, 267nm.

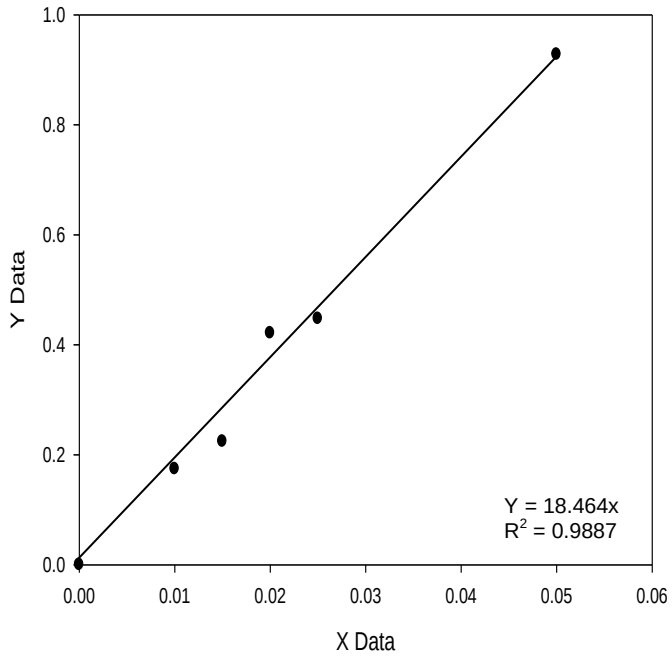

Figure 3.11: *Calibration plot for zidovudine in PBS, pH 7.4 at λ_{267nm} (n=3; SD<0.0002 in all cases).*

Alginate nanoparticles exhibited superior DEE, 91.1%, as compared to 76.53% obtained with Zn-pectin nanoparticles. The unusually high DEE of the alginate nanoparticle formulation is accredited to the ability of alginate to form a gel in the presence of an aqueous medium, with the hydrophilic AZT entrapped within this gel structure with nanoparticle precipitation upon crosslinking of the alginate-AZT solution with $CaCl_2$ (Muthu *et al.*, 2009; Zahoor *et al.*, 2005; 2006).

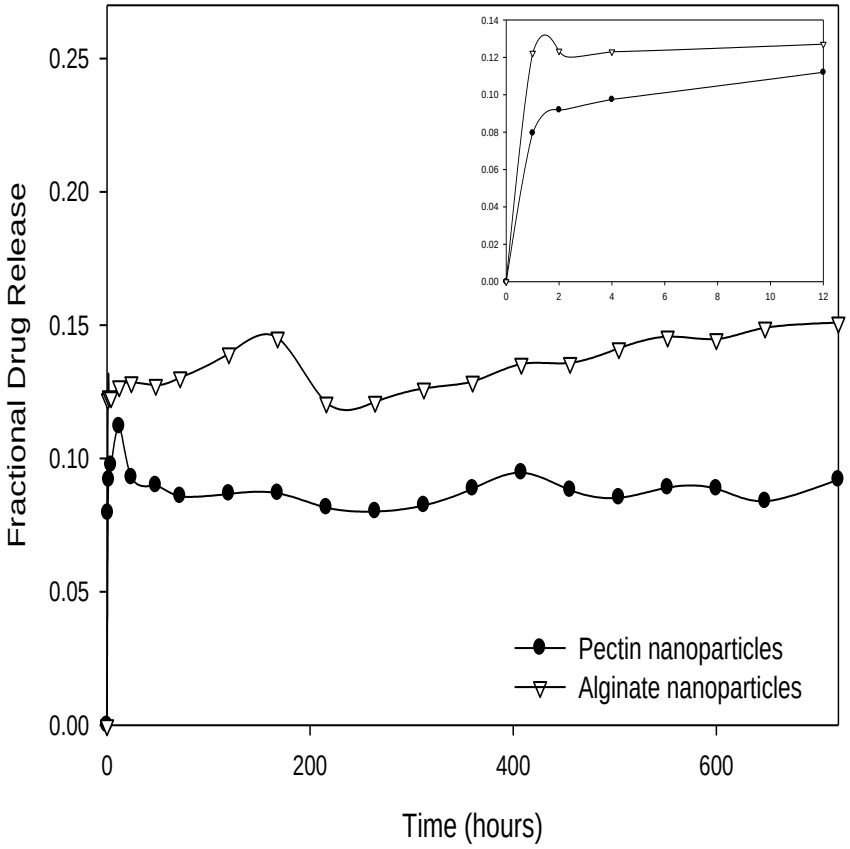

Figure 3.12.1a: *Drug release profile of Zn-pectin and alginate nanoparticles under cerebrospinal fluid simulated conditions (20rpm, 37ºC, 0.1M PBS, pH7.4) (n=3; SD<0.005 in all cases).*

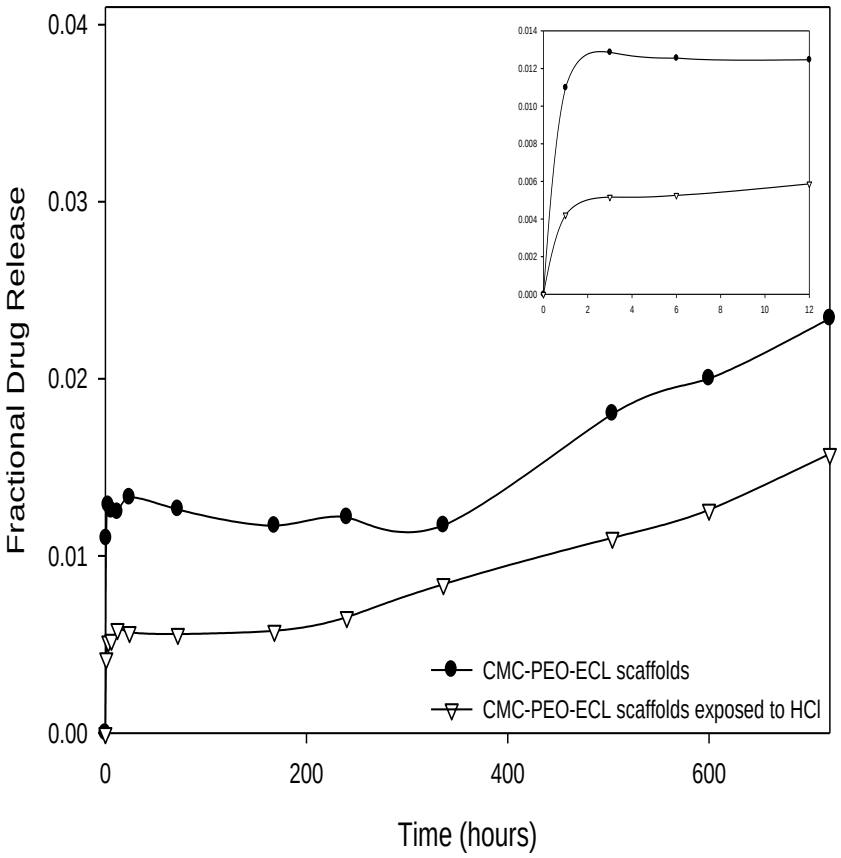

Figure 3.12.1b: *Drug release profile of alginate nanoparticles dispersed within HCl treated and untreated polymeric scaffolds, under cerebrospinal fluid simulated conditions (20rpm, 37ºC, 0.1M PBS, pH7.4) (n=3; SD<0.005 in all cases).*

Biphasic release was observed with both nanoparticle formulations, consisting of an initial burst release of drug within hours of exposure to PBS, followed a constant release rate of AZT over the remaining 30days of nanoparticle analysis (refer to Figure 3.12a). Zn-pectin nanoparticles displayed a burst release within 48hours of 7.9% of drug and alginate nanoparticles displayed a burst of 14.9% of the entrapped drug after 1 hour post exposure to PBS. Burst release was attributed to association of the AZT onto the surface of the polymers by weak interactive forces, which was reversed upon exposure to PBS (Li *et al.*, 2008).

Incorporation of alginate nanoparticles, chosen due to its superior DEE, into the polymeric scaffold significantly retarded drug release, 2.341% (SD<0.005) obtained with NaCMC-PEO-ECL scaffolds untreated with HCl and 1.576% (SD<0.005) obtained with NaCMC-PEO-ECL scaffolds treated with HCl, 30days post exposure to PBS, pH 7.4.

Erosion of the scaffold is due to weakening of the crosslinked bonds with exposure to phosphate buffered saline (PBS), pH 7.4. ECL degrades by means of hydrolysis of the ester bonds, without creating a localised acidic environment upon degradation. When exposed to

the $CaCl_2$ salt solution, $CaCl_2$ either forms bonds with the ester groups on the lactone ring or the Ca^{2+} surrounds the ester group and protects it from degradation (Huang *et al.*, 2004; Luong-Van *et al.*, 2006; Rezwan *et al.*, 2006). PEO degrades by means of hydrolysis of the ester bonds. CMC and PEO imbibes large quantities of water due to its hydrophilic nature, resulting in rapid degradation of PEO, subsequently causing break down of the polymer scaffold (Rokhade *et al.*, 2006; Zweers *et al.*, 2004). The degree of swelling and subsequent drug release is determined by the availability of hydrogen bond in the polymer matrix for water molecules to attach to. For scaffolds treated with $1\%^{v}/_{v}$ HCl, the availability of such bonds is decreased, thereby resulting in reduced drug release (Rokhade *et al.*, 2006). The PBS penetrated the scaffold matrix, which has small uniform pores as well as air pockets, causing it to erode, allowing for nanoparticles to diffuse out.

Nanoparticles released drug by a similar method with swelling of the nanoparticles upon exposure to PBS playing a major role in drug release. This is consistent with the polymers used to prepare the nanoparticles, being alginate and pectin, which are hygroscopic in nature and prone to swelling in the presence of water. This swelling behaviour would allow for weakening of the crosslinked bonds between the polymers and the $CaCl_2$, and release of drug from the nanoparticles. Swelling of the nanoparticles will also facilitate surface erosion and subsequent release of drug (Bajpai *et al.*, 2004, Zactiti *et al.*, 2006).

PCL, a hydrophobic polymer, has been extensively investigated for the long term delivery of drug molecules (Jeong *et al.*, 2003; Sinha *et al.*, 2004; Tarvainen *et al.*, 2002). Drug molecules are integrated into the amorphous regions of PCL (Luong-Van *et al.*, 2006). The slow degradation of PCL (Luong-Van *et al.*, 2006; Sinha *et al.*, 2004; Tarvainen *et al.*, 2002), which occurs primarily from the amorphous regions of PCL (Rezwan *et al*, 2006), accounts for the drug release of 4.144% obtained 30days post exposure to PBS, pH 7.4 (refer to Figure 3.13.2). Copolymerisation of PCL with ECL served to enhance drug release to 9.001%. This was due to ECL imparting hydrophillicity to the prepared scaffold, thereby enhancing water penetration into the polymer matrix, enhancing release of the hydrophilic AZT (Thomas and Panchagnula 2003; Prakash *et al*., 2008). AZT-loaded alginate nanoparticles where therefore dispersed within PCL-ECL scaffolds and drug release was assessed, which amounted to 2.1% (SD<0.001) 30 days post exposure to PBS, pH 7.4.

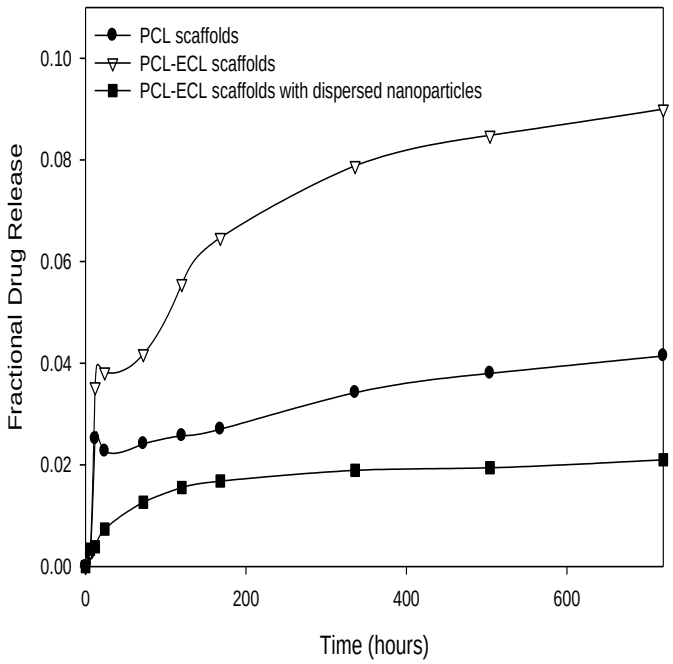

Figure 3.12.2: *Release of AZT from polymer scaffolds prepared using aliphatic polyesters with AZT and AZT-loaded nanoparticles dispersed within (n=3; SD<0.001 in all cases).*

3.4. Concluding Remarks

Nanotechnology is a rapidly evolving interdisciplinary field. It is based on the manipulation of matter on a submicron scale, with nanomedicine allowing for the development of drug delivery devices with superior drug absorption, controlled release of drugs and an enhanced side effect profile (du Toit *et al.*, 2007; Park 2006; Park *et al.*, 2007).

From the studies conducted, the controlled gelification of alginate method of producing nanoparticles was chosen for further analysis as alginate nanoparticles exhibited a more stable formulation, as determined by zeta potential analysis and smaller particles are formed using this approach. Drug release obtained with alginate nanoparticles was more suitable than that of pectin nanoparticles for dispersion of within a multipolymeric scaffold matrix for possible application as an implantable drug delivery device. Alginate nanoparticles prepared in the absence of pectin and those crosslinked with $BaCl_2$ was excluded from further studies due to the unsatisfactory zeta potential and average particle size distribution results obtained with these formulations respectively.

Pectin nanoparticles demonstrated suitable size and drug release properties for application as a drug carrier in the absence of a scaffold matrix. However, further investigations are required to enhance the stability of the formulation and to decrease agglomeration.

Dispersing the polymeric nanoparticles with a multipolymeric scaffold served to noticeably decrease drug release. Exposing the multipolymeric scaffolds prepared to 1 $\%^{v}/_{v}$ HCl served to enhance the swelling behaviour of the scaffolds, thereby enhancing drug release and creating a suitable device for the prolonged release of drug over a period of one month.

PCL-ECL multipolymeric scaffolds displayed higher suitability for further analysis. Although these scaffolds exhibited a higher drug release than NaCMC-PEO-ECL scaffolds exposed to 1$\%^{v}/_{v}$ HCl, when AZT-loaded alginate nanoparticle were dispersed within the scaffold matrix, the lack of swelling detected with these scaffolds renders them more attractive for implantation into the brain.

CHAPTER 4

Fabrication and Optimization of a Multipolymeric Scaffold Incorporating AZT-Loaded Nanoparticles for the Management of ADC Applying a Design of Experiments Approach

4.1 Introduction

Controlled release drug delivery systems have been creating waves in the pharmaceutical industry in recent years. Many biodegradable and biocompatible polymers such as polycaprolactone (PCL), epsilon caprolactone (ECL), cellulose and polysaccharide derivatives have been extensively researched for the design and formulation of controlled release drug delivery devices (Jeong *et al.*, 2003).

Due to the selectivity of the blood brain barrier (BBB), delivery of therapeutic agents into the central nervous system (CNS) has previously challenged pharmaceutical scientists (Vergoni *et al.*, 2009; Kato *et al.,* 2010; Lin *et al.,* 2010; Semreen *et al.,* 2010). Many approaches have been investigated to enhance the permeability of the BBB, osmotic pumps, silicone reservoirs and prodrugs being just a few (Ciofani *et al.*, 2008; Bennewits *et al.*, 2009) Implantation of drug delivery devices into the brain has been utilized in the past. However, this procedure requires subsequent removal of the device at a later stage, due to lack of biodegradability of the device, and is therefore unacceptable to patients due to its invasive nature. Infection, inflammation and device failure add to the unsuitability of such devices (Ciofani *et al.*, 2008). Polymeric drug delivery devices (DDDs) are capable of overcoming such challenges faced with the use of biodegradable, biocompatible devices capable of delivering and sustaining drug concentration over predetermined time periods. This is particularly useful for drugs with short half lives ($t^1/_2$) as sustained drug delivery negates the need for frequent dosage intervals (Ciofani *et al.*, 2008).

Nanotechnology has received significant attention in recent years for the treatment and management of CNS conditions (Sahoo *et al.*, 2003; Rao *et al.*, 2008; Yang *et al.*, 2008; Lin *et al.,* 2010). This can be attributed to their small size and biocompatibility (Park *et al.*, 2007). However restricting nanotechnology to the 100nm and smaller size scale is impractical when it comes to drug delivery, as efficiency of a drug delivery device is independent of size (Park, 2007).

Combining polymer technology and nanotechnology is a revolutionary means of overcoming many current challenges of drug delivery to the CNS. Polymeric nanomaterials offer superior biodistribution and targeted delivery of drug, reducing systemic side effects and drug resistance (Park *et al.*, 2007). Targeting drug molecules to the desired site of action is imperative for the treatment and management of CNS conditions due to the high concentrations of toxic drug required. Exposure of the therapeutic agents to unaffected tissue is minimal with site-specific drug targeting, reducing systemic toxicity resulting from drug therapy (Kidane *et al.*, 2005; Husseini *et al.*, 2008). Site specific drug delivery is also cost effective as lower concentrations of drug are required for therapeutic efficacy (Husseini *et al.*, 2008).

The management of AIDS dementia complex (ADC) requires therapeutically effective drug concentrations, which is sustained at these concentrations over extended time periods. The BBB poses an obstacle for the transport of drugs into the brain. This impedes effective antiretroviral (ARV) therapy and promotes drug resistance as optimum drug concentrations are not attained. Clinically useful drug delivery systems which are capable of bypassing the BBB and achieving and sustaining therapeutic levels of drug in the brain are therefore required (Rao *et al.*, 2008).

Preliminary studies carried out in Chapter 3 yielded sufficient information from which a prototype formulation can be established and evaluated. A statistical design of experiments (DOE), defined as the strategy used to implement experiments such that information is obtained in an efficient and precise manner, was employed to determine critical limits for formulation processing of variables (Altekar *et al*., 2006). DOE have been employed since 1967 in the optimisation of drug formulations and have found application in numerous industries after having first been discussed by Sir Ronald Fisher in 'The Design of Experiments'. Since then, this systematic technique is applicable to all conventional dosage forms and can be used for the optimisation of all modern drug delivery systems. DOE is used to improve the efficiency of experimentation as it allows access to precise and detailed information regarding the system under investigation with the minimum number of experiments having to be carried out, as the designed experiments are generated based on statistical theory (Singh *et al*., 2005; Altekar *et al*., 2006).

The Box-Behnken design, developed by George Box and Donald Behnken in 1960, is an experimental design used to obtain the responses of the prepared device with regards to surface methodology. The design aims to achieve the following goals:

- Each independent variable is placed at three equally spaced values, requiring a minimum of three levels.
- The design should fit a quadratic model.
- The ratio of the number of experimental points to the number of coefficients in the quadratic model should be maintained in the range of 1.5 to 2.6.
- The estimation variance should be based on the distance from the centre, and should vary minimally inside the smallest hypercube containing the experimental points.

The 3 factor Box–Behnken design involves the use of three blocks, in which 23 factors are varied through the 3 possible high, low and midpoint combinations (Box and Behnken, 1960; Annadurai and Sheeja, 1998).

4.2 Materials

Materials employed were described in Chapter 3. Cellulose acetate phlalate (CAP) purchased from Sigma-Aldrich (St. Louise, MO, USA) was included in the preparation of multipolymeric scaffold devices. All other reagents were of analytical grade and were used as received in accordance with standard operating protocols.

4.3 Methods

4.3.1 Formulation preparation using the Box-Behnken design

Various concentrations of polymer and salt solutions were prepared for preparation of nanoparticle and multipolymeric scaffold formulations. Temperature, crosslinking time (CT) and stirring speed was also assessed to ascertain the impact of these parameters on formulation size and potential for nanoparticles and matrix erosion and resilience for scaffolds formulations. From these studies, upper and lower parameters were chosen which were statistically analysed using a 3 Factor Box-Behnken design template, using MINITABS® V15 software (Minitab Inc, Pennsylvania, USA), for the preparation of the nanoparticle and scaffold formulations in an attempt to optimize the responses highlighted in Table 4.1. The Box-Behnken experimental design was used to optimise the formulations as it can efficiently determine quadratic terms in a regression model. The design was used to ascertain the effects of the formulation variables on the physicochemical and physicomechanical properties of the prepared device.

4.3.1.1 Preparation of Nanoparticles

Nanoparticle formulations were prepared using a controlled gelification of alginate approach (Zahoor *et al.*, 2005; Zahoor *et al.*, 2006; Sarmento *et al.*, 2007), whereby sodium alginate and zidovudine (AZT) solution was prepared in distilled water. Calcium chloride ($CaCl_2$) was added to the solution in a drop wise manner to facilitate crosslinking highlighted in Figure 4.1.1. A 0.05%$^w/_v$ pectin solution and a 10%$^w/_v$ polyvinyl alcohol (PVA) solution were then added to the crosslinked suspension to ensure optimum formulation stability. Upper and lower parameters and response factors were determined, as highlighted in Table 4.1, and were utilized to to generate a Box-Behnken template. Thirteen formulations were prepared in accordance with the 3 Factor Box-Behnken design template, established using Minitab® V15 software, as outlined in Table 4.2. The nanoparticle solutions were then centrifuged to enable precipitation and collection of the nanoparticles, dried at ambient temperature (25°C) and lyophilized (Virtis®, Gardiner, NY, USA) for 24 hours to obtain a free flowing powder.

Table 4.1: *Upper and lower limits of parameters and response factors used for the formulation of nanoparticle and multipolymeric scaffold formulations.*

Independent Factors	**Lower Levels**		**Upper Levels**
AZT-loaded Nanoparticles			
Alginate concentration (%$^w/_v$)	0.06		0.5
$CaCl_2$ Concentration (%$^w/_v$)	2		10
Crosslinking time (min)	15		180
Responses	**Lower**	**Upper**	**Objectives**
Average size distribution (d.nm)	33.31	912.5	Minimise
Zeta potential (mV)	-0.659	-14.6	Maximise
Multipolymeric Scaffolds			
CAP concentration (%$^w/_v$)	5		20
ECL concentration (%$^w/_v$)	10		50
$CaCl_2$ concentration (%$^w/_v$)	0		15
Responses	**Lower**	**Upper**	**Objectives**
Matrix erosion (%)	7.413	63.269	Minimise
Matrix resilience (%)	1.113	11.71	Maximise

Table 4.2: *A 3 Factor Box-Behnken template with randomly generated alginate nanoparticle formulations.*

Formulations	[Alginate] ($\%^{w}/_{v}$)	[$CaCl_2$] ($\%^{w}/_{v}$)	Crosslinking time (min)
1	0.06	10	97.5
2	0.5	6	180
3	0.06	6	180
5	0.28	10	15
6	0.5	10	97.5
7	0.06	6	15
9	0.28	2	15
10	0.5	2	97.5
11	0.28	2	180
12	0.28	6	97.5
13	0.28	10	180
14	0.06	2	97.5
15	0.5	6	15

4.3.1.2 Preparation of Polymeric Scaffolds

Thirteen crosslinked PCL/ECL/CAP scaffold-like devices were prepared in accordance with the 3 Factor Box-Behnken design template as illustrated in Table 4.3. The polymers, in varying concentrations, were individually dissolved in acetone, after which they were mixed together and crosslinked with $CaCl_2$. Nanoparticles were dispersed within the crosslinked multipolymeric solution to enable controlled drug delivery over a predetermined time interval. The crosslinked polymeric mixture was then poured into glass moulds (6mm in diameter and 2mm in depth) and pre-lubricated with liquid paraffin and allowed to dry at ambient temperature (refer to Figure 4.1.2).

Table 4.3: *A 3 Factor Box-Behnken template with randomly generated PCL-ECL-CAP scaffold formulations.*

Formulations	[ECL] ($\%^{w}/_{v}$)	[$CaCl_2$] ($\%^{w}/_{v}$)	[CAP] ($\%^{w}/_{v}$)
1	10	15	12.5
2	50	7.5	20
3	10	7.5	20
4	30	7.5	12.5
5	30	15	5
6	50	15	12.5
7	10	7.5	5
9	30	0	5
10	50	0	12.5
11	30	0	20
13	30	15	20
14	10	0	12.5
15	50	7.5	5

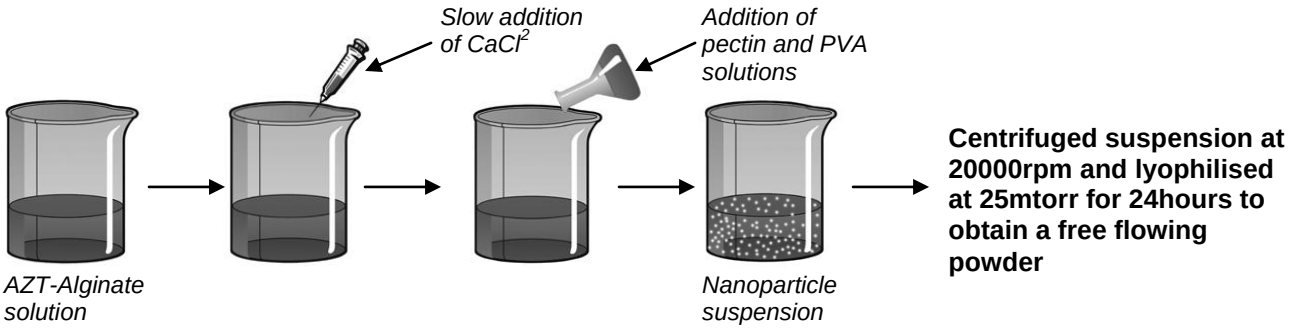

Figure 4.1.1: *Schematic representation of nanoparticle preparation employing the controlled gelification of alginate approach.*

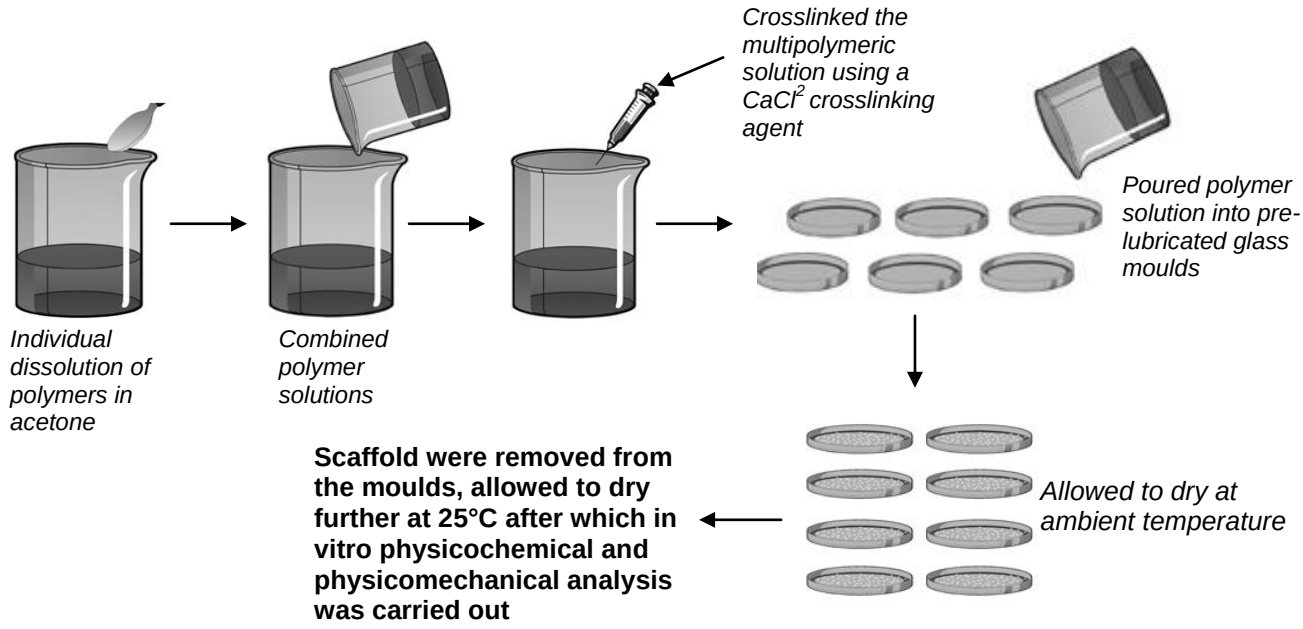

Figure 4.1.2: *Schematic representation of PCL/ECl/CAP multipolymeric scaffold preparation.*

4.3.2 Fourier Transform Infrared analysis for the description of the molecular transitions of scaffold and nanoparticle formulations

Fourier Transform Infrared (FTIR) spectroscopy was utilized to assess possible structural transitions which had occurred during the preparation process by comparing the functional groups of the parent compounds with that of the formulations produced. Polymer, nanoparticle and scaffold samples were analysed using a Perkin Elmer FTIR Spectrometer (Spectrum 100, Beaconsfield, United Kingdom).

4.3.3 Microscopic analysis of surface morphology

Scanning electron microscopy (SEM) and transmission electron microscopy (TEM) images the surface of solid specimens using high-energy beams of electrons. The electrons interact with the atoms in the sample producing signals containing information regarding the sample's surface topography, chemical composition, crystalline structure, orientation of materials making up the sample, as well as electrical conductivity (Suzuki, 2002). Particle size can also be obtained from TEM images.

4.3.3.1 Transmission electron microscopy

Nanoparticle samples were dispersed in methanol and sonicated, after which they were placed on carbon grids and analysed using TEM (JEOL 1200 EX, 120keV). Photomicrographs were obtained to study the size and morphology of individual particles produced.

4.3.3.2 Scanning electron microscopy

SEM, conducted using a thermal emission electron microscope (JEOL JSM, Tokyo, Japan), was employed on the multipolymeric scaffolds. Samples were mounted on aluminum stubs, coated with carbon and gold-palladium for 10minutes, after which they were visualized at acceleration voltages ranging between 5-9keV under different magnifications. Photomicrographs were obtained and analysed to study surface morphology. The degree of polymer entanglement, network density and porosity of the scaffolds were qualitatively determined using the photomicrographs obtained.

4.3.4 Zeta analysis

Zeta potential and particle size distribution were determined in deionised water using a ZetaSizer Nano ZS (Malvern Instruments Ltd, UK). 1mL samples were diluted with deionised water, filtered (0.22µm filter Millipore Co., Massachusetts, USA) to maintain the number of counts per second in the region of 600 (Layre *et al*., 2006) and analysed using disposal cuvettes, to assess particle size, or capillary cells, to assess zeta potential. The viscosity and refractive index of the continuous phase were set to those specific to deionized water (Malvern Instruments Ltd, Malvern, Worcestershire, UK). Measurements were taken in triplicate, with size intensity and zeta potential distribution profiles used to assess average nanoparticle size and stability.

4.3.5 Textural Analysis

A TA.XT.Plus Texture Analyzer (Stable Micro Systems, Surrey, UK) was used to establish various stress-strain parameters of the multipolymeric scaffolds in both the hydrated and unhydrated states to determine textural transitions occurring during different degrees of matrix hydration. A flat-tipped cylindrical steel probe measuring 50mm in diameter was attached to the force transducer and matrix resilience (MR) was obtained using the parameter setting listed in Table 3.5 in Chapter 3, Section 3.2.7. Force-time profiles were generated by means of Texture Exponent Software (Version 3.2) at a rate of 200 points per second and used to calculate matrix resilience.

4.3.6 Matrix Erosion and Swelling Studies

Pre-weighed samples was immersed in 100mL of PBS (pH 7.4, 37˚C) and placed into an orbital shaker incubator set to rotate at 20rpm at 37°C, (LASEC, Model LM-530, South Africa). Samples were removed from the PBS solution at specified time intervals, convection dried at 25˚C for 48hours and weighed to gravimetrically determine degree of matrix erosion.

A second set of samples were tested for change in volume after exposure to buffer at predetermined intervals to assess degree of swelling of the multipolymeric scaffolds.

4.3.7 Drug Entrapment Efficiency and Drug Release

Drug entrapment efficiency (DEE) was calculated as per Equation 3.4, as described in Chapter 3, Section 3.2.10

Drug release studies were performed on nanoparticles as well as on multipolymeric scaffolds incorporating nanoparticles within the matrix. AZT-loaded samples were immersed into 100mL of PBS (pH7.4) after which they were placed into an orbital shaker incubator set to rotate at 20rpm at 37°C. Samples were taken at predetermined intervals, which were then analysed using UV spectroscopy. The time-point approach, a model independent analysis, was then used to analyse the dissolution data, whereby the mean dissolution time (MDT) was established at 30days for each formulation (Pillay and Fassihi, 1999). MDT, calculated using Equation 4, provides a more accurate analysis of drug release as well as a precise comparison of numerous data sets.

$$MDT = \sum_{i=1}^{n} ti \frac{M_t}{M_\infty} \qquad \textbf{(Equation 4.1)}$$

Where Mt is the fraction of dose released in time ti = (ti + ti-1)/2 and M_∞ corresponds to the loading dose (Pillay and Fassihi, 1999).

4.3.9 Optimisation of the nanoparticles and multipolymeric scaffold formulations employing a Box-Behnken design of parameters

Physicochemical and physicomechanical analysis were conducted on both scaffold and nanoparticle formulations using a range of polymer and salt concentrations as described in Table 4.4, to optimize formulation parameters employing a Box-Behnken statistical design. Nanoparticles were prepared incorporating PVA into the formulation to facilitate an improvement in the stability of the nanoparticle colloidal system. Of the PVA concentrations tested, 10%$^{w}/_{v}$ solutions demonstrated the most favorable surfactant properties as observed with the zeta potential and the smaller average nanoparticle size obtained, refer to Table 4.5. Larger particles were observed with PVA concentrations above 10%, attributed to the highly viscous nature of the polymer solution which facilitated agglomeration of the nanoparticles. Nanoparticles prepared with PVA concentrations less than 10% presented with larger particles, with instability observed within the colloidal system as demonstrated by the ZP

obtained as seen in Table 4.5. This can be attributed to insufficient surfactant properties instilled to the colloidal systems when prepared with 0.5-2.5%$^{w}/_{v}$ PVA solutions.

Multipolymeric scaffolds were prepared using ethyl cellulose and CAP as plasticiser agents. CAP was favored over ethyl cellulose and chosen for further studies, attributed to scaffolds prepared with CAP presenting with extended drug release behavior due to slow matrix erosion. SEM studies conducted revealed a more porous scaffold prepared with formulations containing low PCL concentrations. PCL concentration was fixed at 37.5%$^{w}/_{v}$ as scaffolds prepared with higher concentrations of PCL presented with 11.83% to 7.26% drug being released over 30 days. The viscous nature of PCL solutions above 37.5%$^{w}/_{v}$ retarded mixing of PCL, ECL and CAP solutions and resultantly impeded crosslinking of the multipolymeric solution with $CaCl_2$.

A quadratic response was generated using a Box-Behnken design from which a second order polynomial model was constructed for the prediction of device behaviour using the independent variables previously investigated. This facilitated a mechanistic evaluation of correlations between pertinent processing factors such as the polymer type and $CaCl_2$ concentrations and cross-linking time utilised for the preparation of nanoparticle and scaffold formulations. Nanoparticle formulations were characterized according to the average particle size, zeta potential and drug release behaviour. Multipolymeric scaffolds were exemplified in terms of their matrix erosion, resilience and drug release characteristics. Nanoparticle and multipolymeric scaffolds were then optimized in terms of the responses obtained formulated for implantation into the rat brain.

Table 4.4: *Variable levels employed in the optimisation of nanoparticle and multipolymeric scaffold formulations.*

Input Variables	Lower Levels	Upper Levels
AZT-loaded Nanoparticles		
Alginate concentration ($\%^{w}/_{v}$)	0.06	1
Pectin concentration ($\%^{w}/_{v}$)	0	1
PVA concentration ($\%^{w}/_{v}$)	0	15
$CaCl_2$ Concentration ($\%^{w}/_{v}$)	2	15
Crosslinking time (min)	5	180
Stirring speed (where 1 = 100rpm and 5 = 500rpm)	1	5
Multipolymeric Scaffolds		
CAP concentration ($\%^{w}/_{v}$)	5	30
Ethyl cellulose concentration ($\%^{w}/_{v}$)	5	15
ECL concentration ($\%^{w}/_{v}$)	10	70
PCL concentration ($\%^{w}/_{v}$)	10	50
$CaCl_2$ concentration ($\%^{w}/_{v}$)	0	1
Crosslinking time (mins)	5	60
Evaporation time (days)	1	14

Table 4.5: *PVA concentrations employed for the preparations of nanoparticles and responses obtained.*

PVA concentration ($\%^{w}/_{v}$)	Ave Size distribution (nm)	Zeta potential (mV)
0	752.1	-3.53
0.5	455.90	-4.13
1	203.27	-4.99
2.5	170.65	-6.53
5	101.95	-6.85
10	93.21	-8.42
15	462.8	-8.53

4.3.10 Termal analysis of native polymer and prepared nanoparticle and scaffold formulations employing advanced Differential Scanning Calorimetry (aDSC)

Thermal analysis is on the oldest analytical methods employed, with the first thermometric experiment performed in 1887 by a French sciencetist Henri Louis Le Chatelier (Le Chatelier, 1887).

Differential Scanning Calorimetry (DSC) is a thermoanalytical technique used to quantify the change in the amount of heat required to increase the temperature of a sample measured as a function of temperature, with the behaviour of the sample determined by comparison to an inert substance, a reference, with the sample and reference maintained at the similar temperatures throughout the experiment. DSC, developed by E.S Watson and M.J O'Neil in 1960, is frequently used in the pharmaceutical and polymer industry to study curing processes, polymer degradation, melting point (T_m) as well as to evaluate polymer and drug purity. Polymer crosslinking can be assessed using thermograms, as crosslinking is an exothermic process, with a peak occurring soon after the glass transition temperature (Dean, 1995; Pungor, 1995; Skoog *et al.*, 1998).

Thermal analysis was undertaken on the AZT-loaded nanoparticles, multipolymeric scaffold and the optimised nanoparticle-loaded scaffold formulation to ascertain thermal behaviour using DSC (Mettler Toledo DSC1, STARe System, Switzerland). 15-20mg samples were accurately weighed using a calibrated scale and were evenly distributed on perforated 40µL aluminum pans. The powder was then pressed to the crucible base using a Teflon rod. A pin-point hole, measuring 20µm in diameter was punched into the crucible lid, after which the crucible was sealed and placed on the heat-flux plate and exposed to temperature gradients as per Table 4.6.1 under a constant pressure of N_2 atmosphere in order to minimise oxidation. The reference crucible was prepared in a similar manner, however, the crucible was left empty and two holes were punched into the crucible lid so as to differentiate the two crucibles.

Thermal transitions were assessed in terms of the glass transition temperature (T_g), which was measured as the reversible heat flow due to variation in the magnitude of the C_p-complex (C_p), T_m and the temperature of crystallization (T_c). The temperature calibration was accomplished with a melting transition of 6.7mg indium. The thermal transitions of the native polymers were compared to the prepared nanoparticle and scaffold formulations.

Table 4.6.1: *Initial and final temperatures employed for DSC analysis*

Sample	Start temperature (°C)	End temperature (°C)
Alginate	-15	265
Pectin	-10	230
PVA	-30	218
AZT	-20	172
PCL	-30	85
ECL	-25	280
CAP	-20	250
Nanoparticles	-15	355
Scaffolds	30	250
Implants	-20	160

Table 4.6.2: *Instrument parameters employed to perform assess thermal transitions.*

Sine Segment	Loop Segment
Initial temperature: as per Table 4.6.1 Heating rate: 1°C/min Amplitude: 0.8°C	Increments: 0.8°C End temperature: as per Table 4.6.1

4.4. Results and Discussion

4.4.1 Fourier transform infrared analysis of the native polymer compounds and the prepared nanoparticle and multipolymeric scaffold formulations

Infrared (IR) spectroscopy is the qualitative measurement of spectra in the IR region (0.7-500 μm) of the electromagnetic spectrum, providing information concerning the chemical bonds and structure of molecules based on the manner in which IR radiation is absorbed by the chemical bonds in the compound (Mckelvy *et al.*, 1998; Yuen *et al.*, 2008; Roonasi *et al.*, 2009). Fourier transform infrared (FTIR) spectroscopy is a measurement technique, based on the dipole moment of molecules, by which to collect IR spectra (Yuen *et al.*, 2008). Vibrational FTIR spectroscopic techniques are non-destructive to the applied sample and can potentially provide rapid, convenient solution to analytical problems, providing information regarding molecular structures of complex mixtures using a simple sample preparation technique (Gillie *et al.*, 2000; Islam *et al.*, 2004).

The nanoparticle formulation, (Figure 4.21e), presented with bands between 3600 and 3200cm^{-1} indicating the presence of possible hydroxyl and amino substituents, such as the amino group of AZT evidence at 3458cm^{-1} consistent with the presence of AZT and the polysaccharide polymers employed for the formulation of nanoparticles. The band at

3332cm^{-1} is more defined than that of alginate, indicating possible interactions of the polymers with the amino moieties present in AZT. Polymer interactions with AZT are further supported by the presence of a band at 2110cm^{-1} which can be attributed to N_2 substitution. Shifting of the –COO^- stretch to 1642cm^{-1} indicated possible polymer interaction with drug or $CaCl_2$. Chemical modifications which occurred during nanoparticle formulation were independent of PVA, as seen in Figure 4.2.1. As PVA was incorporated into the formulation to merely impart surfactant properties to the nanoparticles, this was expected.

Characteristic peaks between 1050 and 1300cm^{-1}, were observed in the spectra of ECL, indicative of the cyclic ester present in the structure of ECL (refer to Figure 4.2.2b) and the carbonyl (-C=O) stretching was observed at 1652cm^{-1} and between 3400 and 3150cm^{-1}. Bands between 2800 and 3000cm^{-1} are due to -C-H stretching. A strong carbonyl band was observed with PCL at 1721.02 cm^{-1}, indicating the presence of an aliphatic ester. This band was also observed in the multipolymeric scaffold at 1721.40cm^{-1}, consistent with PCL being the dominant polymeric entity in the multipolymeric scaffold. Bands at 1163 and 1233cm^{-1} are due to -C-O groups and those between 1290-1420cm^{-1} are attributed to -$(CH_2)_4$ groups.

The multipolymeric scaffold presented with a band at 1721.40cm^{-1}, consistent with PCL and CAP. The band at 1656cm^{-1} can be attributed to the presence of a -C=O as observed in the spectra of ECL. The band at 3313cm^{-1} is due to -C=O stretching and those between 3000 and 2800cm^{-1} are due to -C-H stretching. This can be observed in the spectra of all polymers. Bands between 1500 and 650cm^{-1} are similar to those observed in the spectra of PCL and ECL, with shifting of the bands due to polymer interactions and interaction of the polymers with $CaCl_2$. Hydrogen interactions between the hydroxyl groups of CAP and the carbonyl groups of PCL also accounts for the band shifting observed (Ruseckaite and Jimenez, 2003).

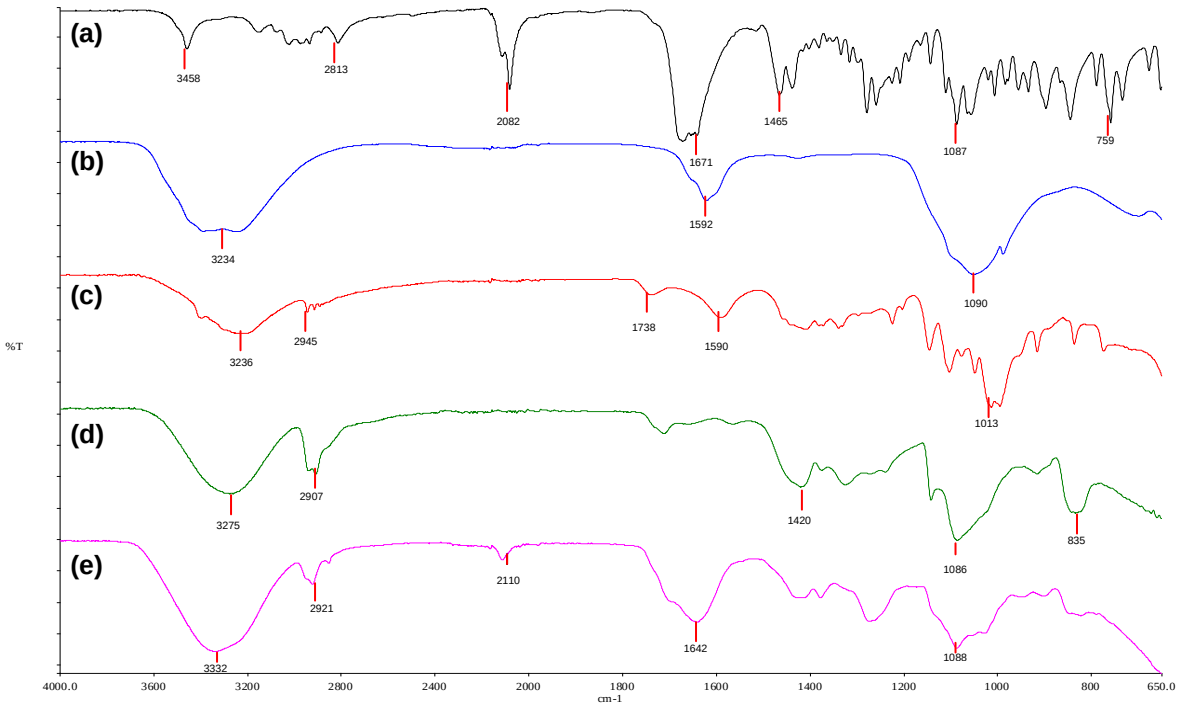

Figure 4.2.1: *FTIR images of AZT-loaded nanoparticles and their formulatory components depicting vibrational transitions occurring during nanoparticle preparation, with some peak designations indicated. (a) AZT, (b) alginate, (c) pectin, (d) PVA, (e) nanoparticle formulation.*

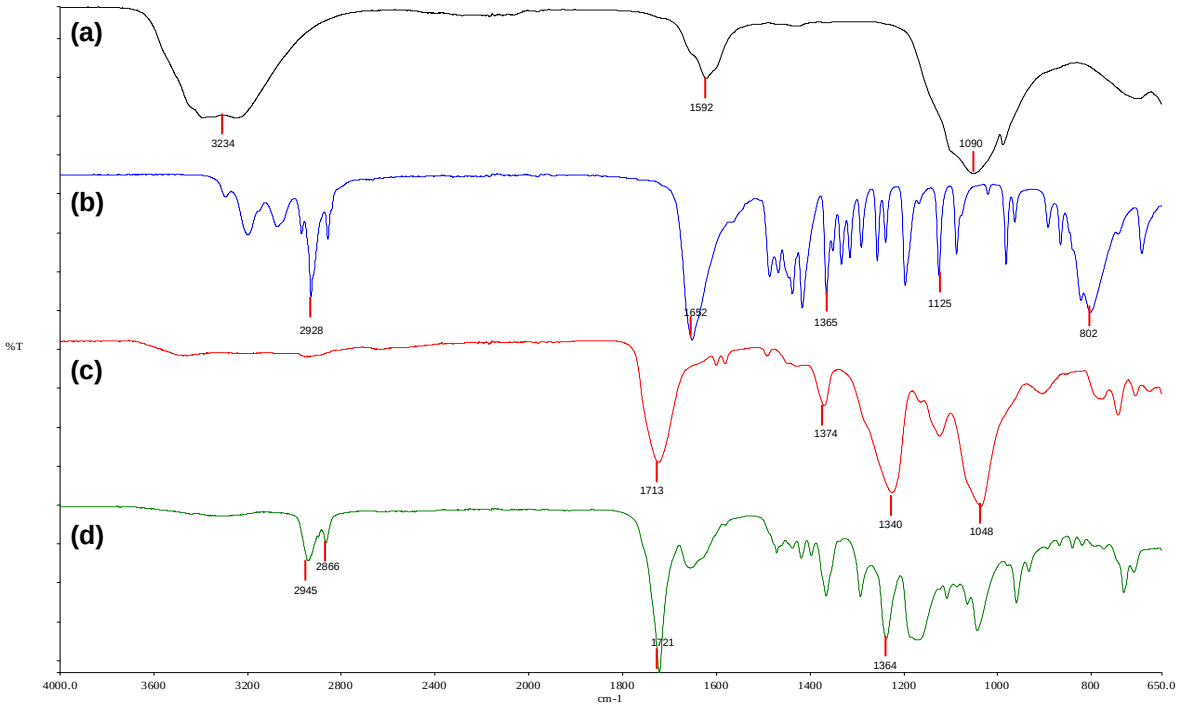

Figure 4.2.2: *FTIR images depicting multipolymeric scaffolds illustrating interactions and alterations in the scaffold as compared to the parent polymer compounds. (a) PCL, (b) ECL, (c) CAP, (d) multipolymeric scaffolds.*

4.4.2 Microscopic evaluation of the prepared formulations

4.4.2.1 Transmission Electron Microscopic analysis of the nanoparticles

Spherical particles in the nanometre size range were observed on TEM images obtained as observed in Figure 4.3. Nanoparticles prepared with 0.28mg/100mL alginate and crosslinked with 10mg/10mL $CaCl_2$ presented with particles ranging between 45-120nm with little agglomeration. This was attributed to superior crosslinking of these formulations, yielding more stable colloidal systems containing smaller nanoparticles.

Notable agglomeration and larger particles, 300-475nm, were observed with formulations containing high alginate and low $CaCl_2$ concentrations. Inadequate crosslinking of Ca^{2+} with the viscous alginate solution with resultant large particles with a low surface charge distribution accounted for this tendency of the nanoparticles to agglomerate. This was consistent with zeta analysis findings described in Chapter 3. However, agglomeration was less pronounced than that observed with nanoparticles prepared in Chapter 3 due to the presence of PVA in the nanoparticle formulations which imparted surfactant properties to the prepared colloidal systems (Sanli *et al.*, 2007; Bennewitz and Saltzman, 2009).

Nanotubes were observed with all AZT-loaded nanoparticle formulations. Nanotube formation was due to the presence of N_2 molecules in the AZT structure which interacts with the polymer chains in the nanoparticles. AZT interaction with alginate and pectin was observed in the FTIR spectrum of the nanoparticle formulation, with shifting and alterations in the bands observed with the nanoparticle formulation, supporting interaction of the N_2 moieties with the –CH groups in alginate and pectin.

Particles were observed within the nanotubes which is thought to be dispersed and entrapped AZT. These entrapped particles are also present in micrographs of spherical nanoparticles which were analysed at higher magnifications. AZT-loaded nanoparticles were prepared by crosslinking a solution containing both alginate and AZT. It is therefore possible for incompletely solubilised AZT to be entrapped within an alginate matrix in the observed manner. This would allow for prolonged controlled release of AZT as drug release was obtained with swelling and erosion of the alginate core (Bajpai *et al.*, 2004; Moebus *et al.*, 2009), accounting for the low fractional release obtained with all prepared nanoparticle formulations. This observation was not made for AZT-free nanoparticles.

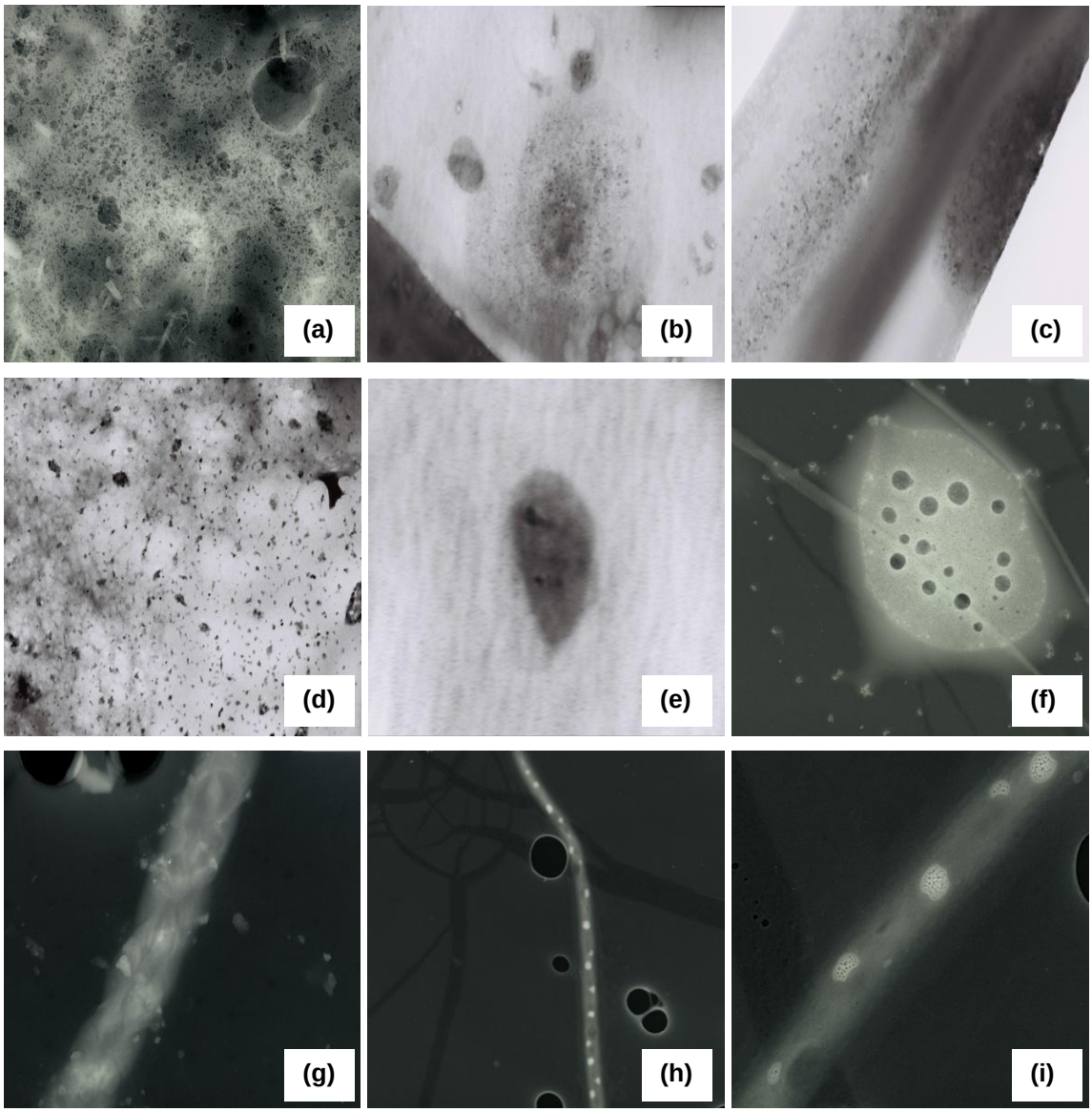

Figure 4.3: *TEM images of nanoparticle formulations prepared using the Box Benhken parameters. (a) F6 presented with a dispersion of large and small spherical particles, (1mm=67nm). (b) and (c) F12 presented with evenly distributed spherical particles, ranging between 33-60nm, (1mm=33nm and 20nm respectively). (d) Agglomeration was observed with F7, indicated by the darker areas on the micrograph, (1mm=33nm). (e) Drug-free F1 indicating a single nanoparticle imaged at a magnification of 100, measuring 50nm by 80nm in diameter, (1mm=10nm). (f) AZT-loaded F1 analysed under high magnifications showing a single nanoparticle with entrapped particles, thought to be dispersed AZT (1mm=10nm). (g) Nanotube formation, measuring 115nm in diameter, was observed with AZT-loaded nanoparticle formulations, (1mm=50nm). (h) and (i) Upon closer magnification, particles were seen entrapped within the nanotube structures measuring 55-60nm, proposed to be dispersed AZT molecules, (1mm=40nm and 20nm respectively).*

4.4.2.2 Scanning Electron Microscopic Analysis of the Multipolymeric Scaffolds

From the photomicrographs in Figure 4.4, it was observed that scaffolds prepared with higher polymer concentrations in the absence of a crosslinking agent displayed a more densely packed matrix than those containing low polymer concentrations. Small, uniformly dispersed pores were present within the polymer matrices, serving as an ideal location for the entrapment of nanoparticles (Yuan *et al.*, 2009).

Multipolymeric scaffolds crosslinked with $CaCl_2$ presented with higher porous matrices, with a random dispersion of large and small pores observed on the micrographs. Larger pores are surrounded by regions of densely packed polymer. This would serve to retard PBS penetration into the polymer matrices, allowing for slow degradation of the multipolymeric scaffolds. Cracks and fissures observed within the multipolymer matrices can be attributed to the brittle nature of the prepared scaffolds.

CAP is used often as a coating agent (Bechard *et al.*, 1995). For the formulation of PCL-ECL-CAP multipolymeric scaffolds, CAP has applicability with reference to its coating properties and as a plasticiser. This accounts for the coating observed around the scaffold in Figure 4.4i with a more porous matrix observed below. Larger areas of densely packed polymer matrices can be observed with scaffolds prepared with higher CAP concentrations, supporting the use of CAP as a plasticiser. CAP has been reported to coalesce upon exposure to heat and moisture, with hydrolytic degradation with elevated temperatures (Liu *et al.*, 2002). At body temperature, 37°C, coalescence is anticipated to occur allowing for slower erosion of the multipolymeric matrix as PBS penetration into the polymer matrices is impeded and hence slow release of AZT-loaded nanoparticles from the multipolymeric scaffolds results.

Upon erosion of the multipolymeric scaffolds, highly crystalline regions were observed within the polymer matrices (refer to Figures 4.4h and i). This is consistent with the high ECL and PCL concentrations used to prepare the scaffolds. PCL and ECL are semi-crystalline polymers which undergo hydrolytic degradation of the esters bonds primarily within the amorphous regions, with the crystalline regions degrading at a much slower rate (Rezwan *et al.*, 2006). However matrix porosity was more pronounced with these scaffolds owing to the presence of the crosslinking agent due to high PCL and ECL content. Porosity is ideal for the dispersion of nanoparticles. Scaffold erosion and subsequent drug release is augmented with an increase in matrix porosity. With exposure to PBS, porosity was observed in the scaffold matrix due to erosion of the matrix as water penetrated the multipolymeric structure.

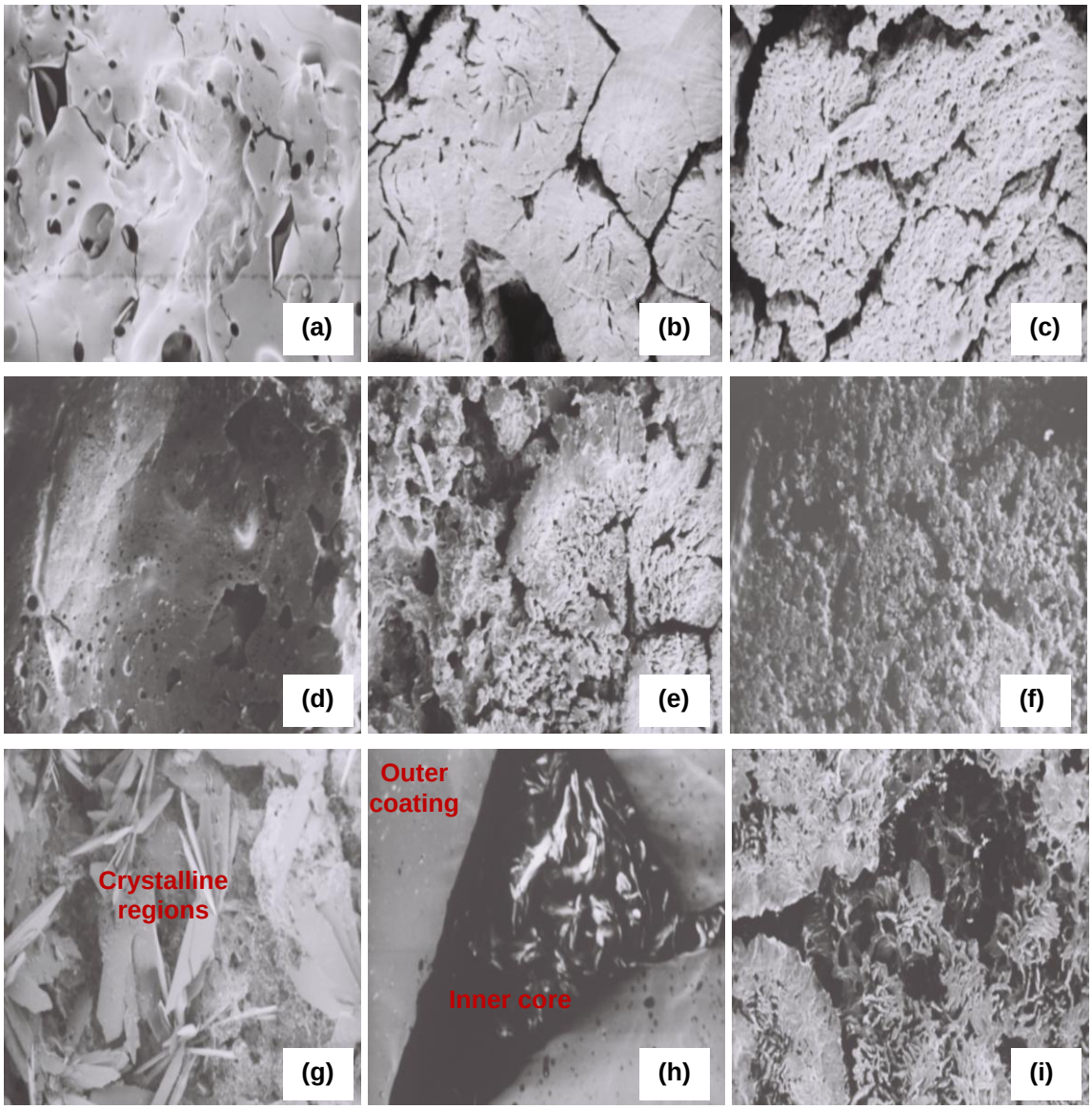

Figure 4.4: *SEM images of the prepared PCL/ECL/CAP scaffolds analysed under various magnifications and keV of 5mV. (a) F10, prepared in the absence of $CaCl_2$, presented with a tightly packed matrix, (1mm=100µm). (b) 7 days post exposure to PBS, (1mm=33µm) and (c) 21 days post exposure to PBS, (1mm=25µm). (d) Formulation 2, crosslinked with a 7.5%$^{w}/_{v}$ $CaCl_2$ solution presented with similar trends to formulation 10, (e) 7 days post exposure to PBS, and (f) 30 days post exposure to PBS (1mm=200µm, 250µm and 250µm respectively). (g) Crystallinity was observed with formulation 6, (1mm=333 µm). (h) CAP coating can be seen, indicated by the lighter areas, with the inner multipolymeric core exposed as the CAP erodes, (1mm=33µm). (i) Larger pores were observed with scaffolds, F1, crosslinked with a 15%$^{w}/_{v}$ $CaCl_2$ solution, (1mm=250µm).*

4.4.3 Size and Zeta Potential Analysis of Nanoparticle Formulation

Formulations prepared using high alginate and low $CaCl_2$ concentrations presented with a large average size distribution, which can be attributed to poor crosslinking occurring, especially formulations prepared using a shorter CT (15minutes). Penetration of Ca^{2+} ions into the viscous alginate solution is poor, yielding a loosely crosslinked polymer gel and resultant larger particles. These formulations presented with a ZP ranging between -2.41 and -3.79mV indicating comparatively moderate stability of the colloidal system. As alginate is a negatively charged polymer (Bajpai and Sharma, 2004; Zactiti and Kieckbusch, 2006; Li *et al.*, 2008), this was expected. However, formulations prepared with high alginate concentrations (0.5mg/200mL) and short CT (15minutes), presented with instability, as seen with formulation 15, due to the formation of loose aggregates rather than individual insoluble nanoparticles. The ZP of -1.87mV observed with formulation 15 can be attributed to poor penetration of Ca^{2+} into the viscous alginate solution due to insufficient agitation of the formulation. As with formulation 10, the presence of free Ca^{2+} ions served to destabilise the colloidal system. Charge stabilisation can be achieved by altering the concentration of ions in the solution with a resultant decrease in flocculation of the colloidal system leading to the formulation of smaller particles (www.malvern.com). This is due to potentially reversible adhesion/cohesion occurring between particles.

The DVLO theory, developed by Deraguin, Verwey, Landau and Overbeek in the 1940's, suggests that the stability of a particle is dependent upon its total potential energy function V_T, as per the equation below:

$$V_T = V_A + V_R + V_S \qquad \textbf{(Equation 4.2)}$$

Where V_S is the potential energy due to the solvent, and V_A and V_R are the van der Waals attractive forces and electrical double layer repulsive forces contributing towards formulation stability as the particles approach each other (www.malvern.com).

Formulations prepared with lower alginate concentrations presented with average size distributions ranging between 102.6 and 38.93nm with PDI's above 0.4, indicating an even size distribution with the colloidal systems as observed in Figure 4.6.1. The smaller particles produced can be attributed to adequate penetration of Ca^{2+} ions into the less viscous alginate solutions, resulting in more effective crosslinking. The peak present in the micrometer size range in Figure 4.6.1 can be attributed to agglomeration of nanoparticles due to sedimentation upon analysis. Formulations prepared with a longer CT presented with smaller particles than those crosslinked for 15 minutes. An average particle size distribution

of 88.38nm with a PDI of 0.836 was observed with formulation 1, resulting from the high $CaCl_2$ concentration and long CT used in the preparation of this formulation.

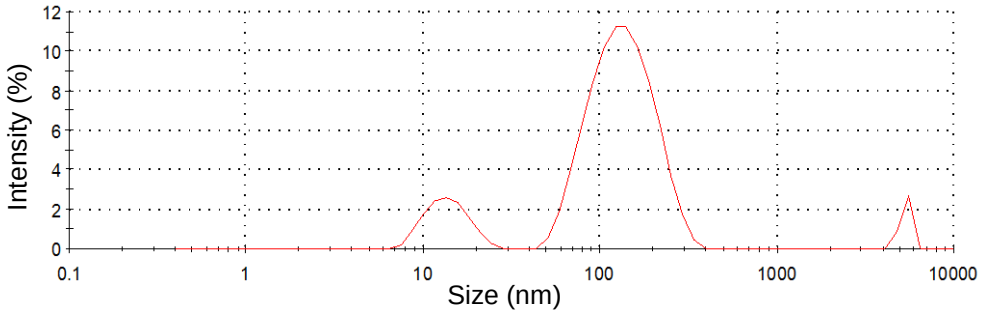

Figure 4.6.1: *Formulation 9 presents with a Z-average of 102.6nm and a PDI of 0.692. The single sharp peak indicates uniformity of the nanoparticles, supported by the PDI of 0.692 obtained (n=3, SD<0.005 in all cases).*

A positive ZP was observed with formulations 7, 9, and 14. This can be attributed to the low alginate concentrations used to prepare these formulations. Alginate is a negatively charged polymer (Bajpai and Sharma, 2004; Zactiti and Kieckbusch, 2006; Li *et al.*, 2008). Lower alginate concentrations would yield a colloidal system containing a lower distribution of negatively charged species than formulations prepared with higher alginate concentrations. The ZP of 2.52mV observed with formulation 9 can be attributed to the short CT (15minutes) used to prepare this formulation, with resultant free Ca^{2+} ions present in the colloidal system due to inadequate crosslinking of Ca^{2+} ions with alginate.

Formulation 10 was prepared with a high alginate concentration, however the low $CaCl_2$ concentration employed to crosslink this formulation yielded a ZP of -0.831mV indicating formulation instability. This was due to inadequate penetration of Ca^{2+} ions into the viscous alginate solution, with resultant free Ca^{2+} ions in the colloidal system, counteracting the negative charge distribution imparted to the colloidal system by the high alginate concentration.

Formulation stability was observed for formulations 12 and 13 due to the higher $CaCl_2$ concentrations and longer CTs employed for the preparation of these formulations. Formulations 12 and 13 also presented with suitable average particle size distributions of 38.93nm and 46.15nm respectively, indicating adequate Ca^{2+} crosslinking.

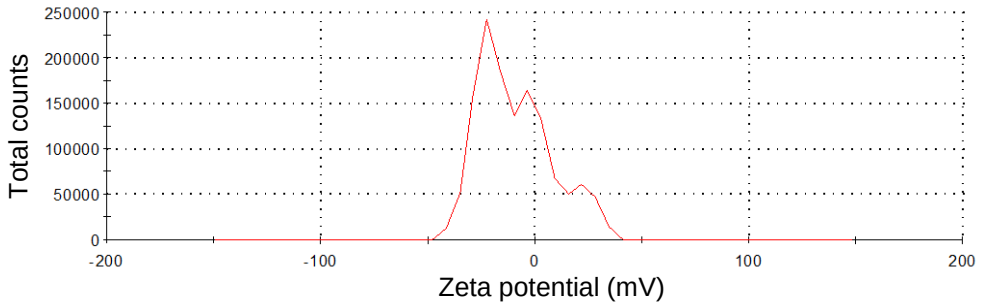

Figure 4.6.2: *Stability was demonstrated with formulation 13, indicated by the average ZP of -20.5mV obtained (n=3, SD<0.0002).*

Electron transfer within the formulation was sufficient enough to allow for repulsion between the particles. Additional peaks observed closer to 0mV indicates possible agglomeration of particles.

Table 4.6: *Zeta analysis results obtained from the 15 formulations generated using the Box Benhken design.*

Formulation	Alginate (mg/mL)	$CaCl_2$ (mg/mL)	CT (min)	Z-average (nm)	PDI	ZP (mV)
1	0.06	10	97.5	88.38	0.836	-2.47
2	0.5	6	180	637.7	0.559	-3.79
3	0.06	6	180	239.7	0.628	-2.59
5	0.28	10	15	230.8	0.646	-1.66
6	0.5	10	97.5	552.9	0.368	-2.41
7	0.06	6	15	284.5	0.836	0.164
9	0.28	2	15	102.6	0.692	2.52
10	0.5	2	97.5	388.8	0.498	-0.831
11	0.28	2	180	155.9	0.533	-3.31
12	0.28	6	97.5	38.93	0.686	-14.5
13	0.28	10	180	46.15	0.723	-20.5
14	0.06	2	97.5	41.97	0.436	0.5
15	0.5	6	15	399.6	0.381	-1.87

4.4.4 Analysis of Polymer Matrix Resilience Using Textural Profiling

An increase in MR was observed with formulations 1, 4, 5 and 7 after 30 days of exposure to PBS (pH 7.4). This was attributed to low ECL (10-30%$^{w}/_{v}$), and CAP (5-12.5%$^{w}/_{v}$) concentrations present in these scaffolds. Crosslinking with $CaCl_2$ served to increase the porosity of the scaffolds, allowing for increased PBS permeation into the multipolymeric scaffolds. This increases solubility of the unionised CAP which occurs at pH's above 6 as the phthalic acid groups become ionised, allowing for hydrolysis of CAP (Bechard *et al.*, 1995).

Formulation 7, prepared using 10%$^{w}/_{v}$ ECL and 5%$^{w}/_{v}$ CAP displayed the highest MR at 11.7% (SD<0.007) 30 days post exposure to PBS, pH 7.4.

Little variation MR was observed with scaffolds uncrosslinked with $CaCl_2$ and an initial MR of 2.8% (SD<0.007) was observed with formulation 10, which increased to 3.1% (SD<0.007) after 30 days of exposure to PBS, pH 7.4. These scaffolds contained small evenly distributed pores in the absence of craters. ECL and PCL are known for its slow degradation resulting from hydrolytic de-esterification (Tarvainen *et al.*, 2002; Sinha *et al.*, 2004; Rezwan *et al.*, 2006; Abbah *et al.*, 2009). Smaller evenly distributed pores present in the matrix reduced water permeation into the polymer matrix with resultant reduced polymer disentanglement and thus matrix erosion.

Scaffolds prepared with high polymer concentrations displayed a decrease in matrix resilience upon exposure to PBS. This is possibly due to the degradation of the acetyl and phthalic acid groups of CAP, yielding the insoluble cellulose acetate (Bechard *et al.*, 1995), which would serve to decrease matrix resilience. The crystalline segments of ECL are more stable than the amorphous regions thus contributing to reduced matrix resilience due to reduced water permeation into the multipolymeric matrix (Rezwan *et al.*, 2006).

4.4.5 Matrix Erosion and Swelling Studies

An average weight loss between 20-40% (SD<0.001) was observed 30 days post exposure to PBS with scaffolds containing greater concentrations of $CaCl_2$ and CAP displaying higher weight loss. The acetyl and phthalyl acid groups in CAP are reported to degrade at pH's greater than 6 (Bechard *et al.*, 1995). Matrix erosion was assessed in PBS (pH 7.4). Penetration of PBS into the matrices of crosslinked scaffolds would therefore serve to hydrolyse CAP, resulting in erosion of the multipolymeric matrix. However, matrix erosion is expected to decline upon prolonged exposure to PBS due to hydrolysis of CAP to form the insoluble cellulose acetate (Bechard *et al.*, 1995).

Scaffolds prepared with 20%$^{w}/_{v}$ CAP displayed slower erosion due to the higher concentrations of cellulose acetate present in the multipolymeric scaffolds after hydrolysis of CAP, consistent with the decrease in matrix resilience observed with these scaffold formulations. Scaffolds prepared in the absence of $CaCl_2$, displayed lower erosion of the multipolymeric matrices. This can be attributed to a more tightly packed polymeric matrix, with decreased water penetration.

Formulation 13, prepared using 20%$^{w}/_{v}$ CAP and 15%$^{w}/_{v}$ $CaCl_2$, displayed unexpected high weight loss, at 59.28% after 30 days of exposure to PBS. Disintegration was observed 0.5 days after exposure to PBS, pH 7.4. This could be due to possible leaching of Ca^{2+} ions out of the polymer matrix, with a resultant increase in water permeation into the scaffold matrix and increased erosion of the scaffold matrix.

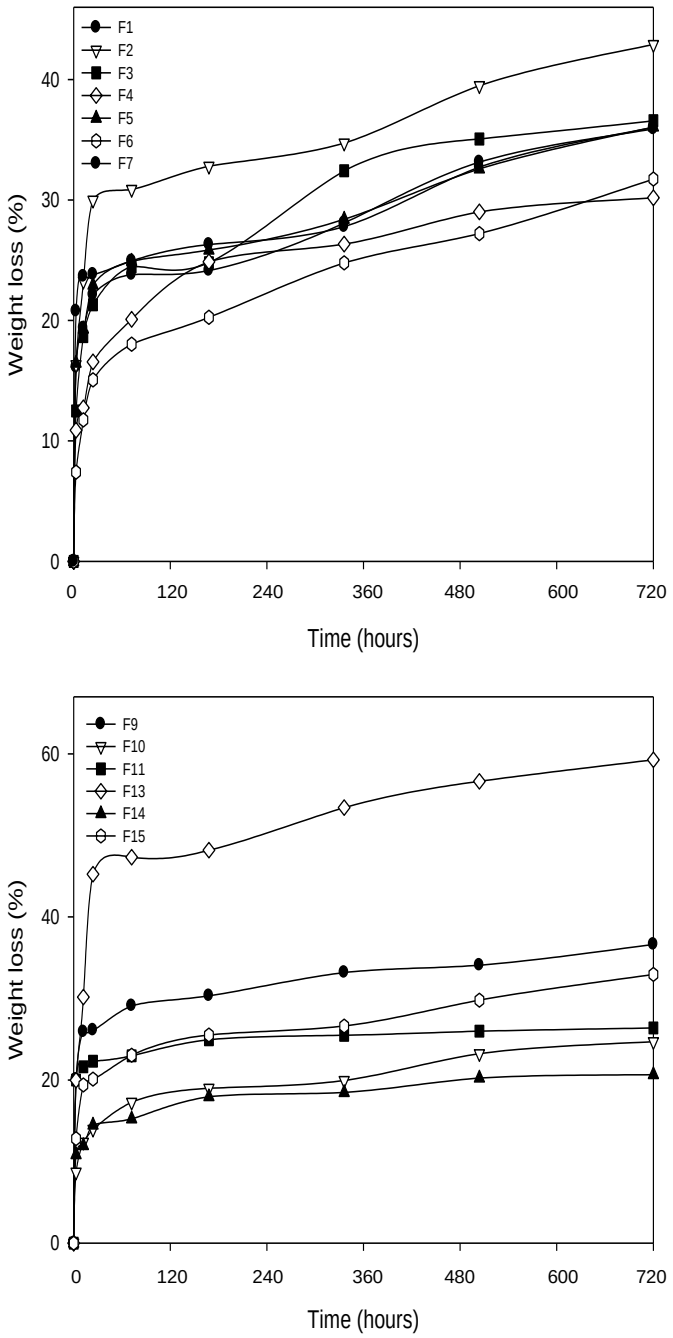

Figure 4.7: *Weight loss observed with the multipolymeric scaffolds prepared using the Box-Benhken design parameters (n=3, SD<0.001).*

Scaffolds prepared with higher ECL concentrations demonstrated lower weight loss of the multipolymeric matrices. ECL is semi-crystalline polyester which degrades by slow hydrolysis of the ester bonds, with the crystalline segments in the polymer more stable than the amorphous regions (Tarvainen *et al.*, 2002; Sinha *et al.*, 2004; Luong-Van *et al.*, 2006; Rezwan *et al.*, 2006). Enhanced crystallinity of the multipolymeric scaffolds is responsible for the low weight loss observed.

No swelling was observed with the multipolymeric scaffolds.

4.4.6 Drug entrapment efficiency of the nanoparticles

An average DEE of 91.1% was calculated for AZT-loaded nanoparticles. The high DEE obtained is accredited to the high drug:polymer ratio and the ability of alginate to form a gel in the presence of an aqueous medium, with the hydrophilic AZT encapsulated within this gel structure (Zahoor *et al.*, 2005; 2006). Alginate gelation occurs under mild conditions in an aqueous environment, enabling the entrapment of a variety of drug molecules into this gel structure (Bajpai *et al.*, 2004). As AZT is a hydrophilic drug, a high degree of AZT entrapment within the Ca^{2+}-alginate gel structure was expected (Thomas and Panchagnula, 2003; Prakash *et al.*, 2008).

4.4.7.1 Drug release from the nanoparticles and multipolymeric systems

Drug release from the nanoparticle formulations not confined within the polymeric scaffold displayed burst release of AZT within the first 24-48hours. Burst release of AZT is due to association of AZT onto the surface of alginate by weak interactive forces, which is reversed upon exposure to PBS (Li *et al.*, 2008). Burst release of drug is not uncommon in monolith drug delivery systems, which although dangerous due to potential toxicity resulting from dose dumping, can be utilised advantageously for conditions requiring an initial high dose of therapeutic agents followed by lower sustained maintenance doses of the drug, such as inflammatory conditions and conditions of infectious origin. However, this is not required for the treatment of ADC. Dispersion of the nanoparticles within the multipolymeric matrix served to alleviate this burst release as nanoparticles were released gradually precluding dose dumping as the multipolymeric scaffold eroded allowing for controlled release of AZT (Ciofani *et al.*, 2008).

Nanoparticle formulations prepared demonstrated average drug release of between 7-18% 30 days post exposure to PBS with formulation 6 demonstrating the lowest release at 7.75% and formulation 11 displaying with the highest release at 17.31%. Formulation 6 was crosslinked with a high concentration of $CaCl_2$, ($10\%^{w}/_{v}$) resulting in a tightly crosslinked

polymer matrix with AZT entrapped within. Drug release was therefore retarded. Formulation 11 was crosslinked with a lower $CaCl_2$ concentration. Swelling of the loosely packed alginate matrix promoted AZT release from the nanoparticles.

An overall low release of AZT from all nanoparticle formulations can be attributed efficient crosslinking of the alginate with $CaCl_2$, entrapping AZT within the nanoparticles. Alginate and pectin are hygroscopic polymers with a propensity to swell and gel when exposed to water (Liu *et al.*, 2003; Sriamornsak *et al.*, 2007; Moebus *et al.*, 2009) with resultant controlled release of AZT as the nanoparticles imbibe fluid. Swelling increases the diffusion path length for AZT to travel in order to be released into the dissolution media, thereby acting to reduce the amount of drug released (Sriamornsak *et al.*, 2007). Addition of pectin to the nanoparticle formulation served to extend drug release from the nanoparticles over prolonged periods as pectin displays an increased propensity to gel when crosslinked with Ca^{2+} and when blended with alginate. This gel layer poses a barrier to the release of hydrophilic AZT as water penetration through this layer was hindered (Liu *et al.*, 2003; Sriamornal *et al.*, 2007; Glavas *et al.*, 2009).

Loosening of the polymer network occurs as Ca^{2+} ions diffuse out of the nanoparticles due to ion exchange occurring between Na^{+} ions present in PBS which facilitated release of AZT. (Bajpai *et al*., 2004; Gao *et al.*, 2009; Moebus *et al.*, 2009). A study conducted by Bajpai *et al*., in 2004 suggested that Ca-alginate swelling occurs as a result of PBS due to ion exchange with resultant Ca^{2+} disassociation from the COO^{-} groups present on the mannuronic acid residues. Ca^{2+} forms calcium phosphate with an increase in the turbidity of the PBS as observed by Bajpai *et al*. (2004). Swelling and turbity was absent when a Tris-HCl buffer, pH 7.4 was used. Electrostatic repulsion of the negatively charged COO^{-} groups with resultant polymer chain relaxation and an increase in the water uptake into the polymer matrix account for AZT release from the nanoparticles (Bajpai *et al.*, 2004).

Pectinolysis resulting from enzymatic breakdown by enzymes naturally occurring in the body also accounts for polymer chain loosening and drug release (Li *et al.*, 2003). Alginate degradation is slow, with hydrolysis resulting from water penetration into the crosslinked alginate Ca^{2+} complex accounting for alginate degradaton (Gao *et al.*, 2009).

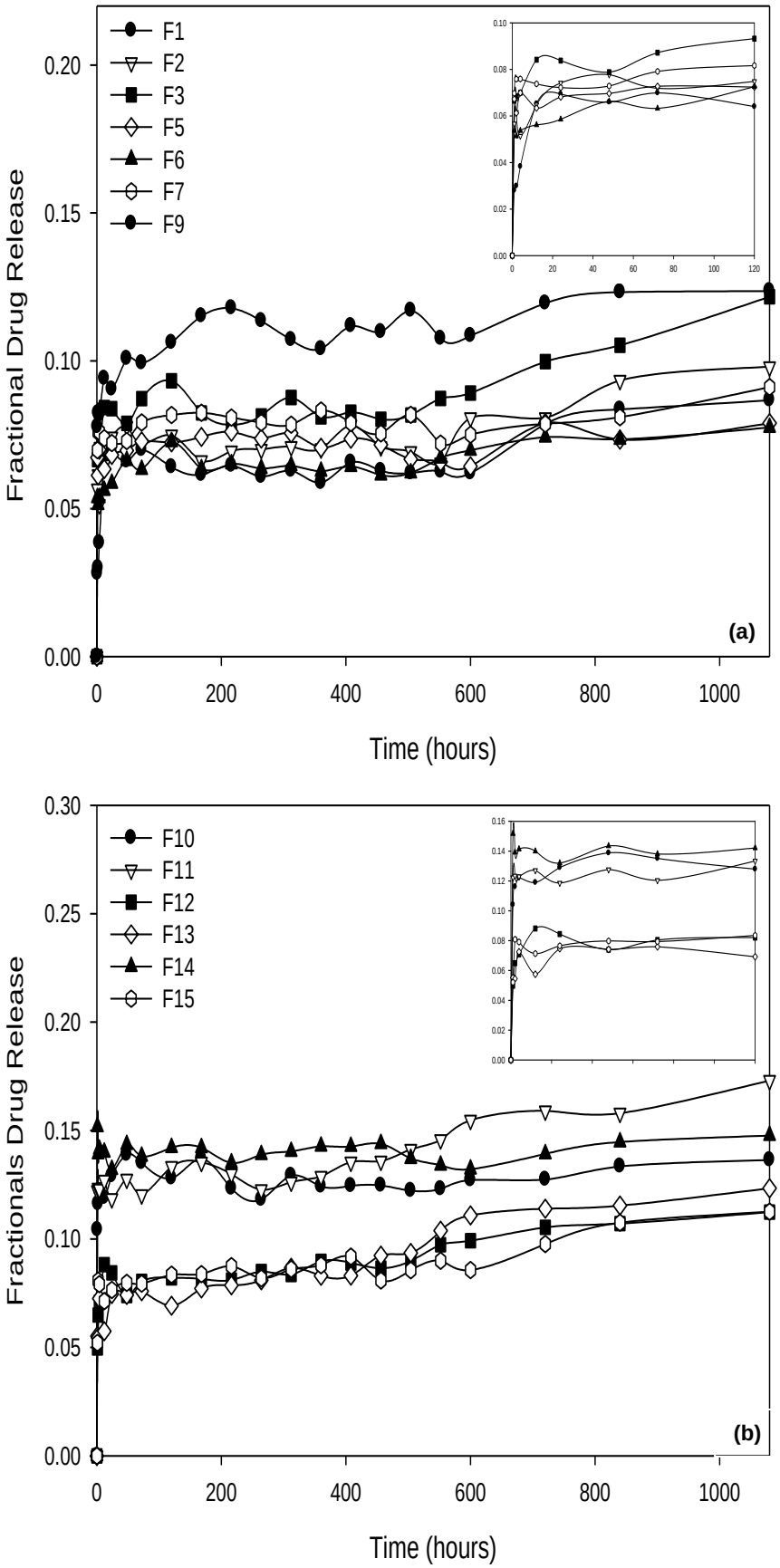

Figure 4.8: *Drug release profiles of (a) nanoparticle formulations 1-9, (b) nanoparticle formulations 10-15 prepared using the Box Benhken design template (n=3, SD<0.0005).*

4.4.7.2 Mean Dissolution Time

In vitro dissolution is used to establish bioequivalence by relating pharmacokinetic performance of the drug delivery device to drug release (Ginski *et al.*, 1999). *In vitro* dissolution is used to establish quality of the prepared formulation and is particularly important when analysing controlled release devices (Costa *et al.*, 2003). MDT, a model independent approach, was used to compute drug release, with the individual characteristics of each curve translated into a single value (Ginski *et al.*, 1999; Costa *et al.*, 2003). MDT is used to ascertain equivalence between different drug release profiles or to statistically compare profiles (Podczeck, 1993).

Table 4.7: *MDT values of nanoparticle and scaffold formulations, indicating a decline in the rate of AZT release with the dispersion of nanoparticles within a multipolymeric scaffolds.*

Nanoparticle Formulations	MDT	Scaffold Formulations	MDT
1	18.315	1	11.231
2	20.64	2	16.662
3	24.422	3	10.364
5	18.855	4	1.714
6	17.862	5	-8.27
7	20.844	6	-11.59
9	29.753	7	-10.212
10	33.239	9	-9.816
11	38.375	10	7.127
12	25.169	11	11.358
13	26.398	13	11.085
14	36.484	14	11.073
15	24.39	15	-13.38

4.4.8 Analysis of the Box-Benhken design generated for nanoparticles and multipolymeric scaffolds

4.4.8.1 Zeta size and potential study

From Figure 4.9.1 it can be concluded that low alginate and $CaCl_2$ concentrations produced formulations with optimal size distributions, between 40-250nm (SD<0.0002). Stirring time had no influence on the average diameter obtained. However, discrepancies were noted, as with formulation 13, which comprised of a 0.28mg/100mL alginate solution crosslinked with 10mg/10mL $CaCl_2$ solution over 180minutes, yielding nanoparticles with an average size distribution of 46.15nm (SD<0.0002) and a PDI of 0.489. Smaller quantities of $CaCl_2$ are introduced into the pre-gelation stage over extended periods allowing for more efficient crosslinking of alginate with resultant smaller particles being produced.

Instability was noted at the upper and lower limits of alginate and $CaCl_2$ concentrations as well as with CT, as seen in Figure 4.9.1b. Alginate is an anionic polymer which upon crosslinking with the cationic $CaCl_2$ produces nanoparticles with negative zeta potential values as seen in Table 4.6 (Bajpai and Sharma, 2004; Zactiti and Kieckbusch, 2006; Li *et al.*, 2008). When alginate concentrations are low, an inadequate charge distribution results due to the presence of the cationic Ca^{2+}. This would yield a colloidal system with reduced negativity, as seen with Formulation 7, which has an average zeta potential of 0.164mV (SD<0.00025). A more concentrated alginate solution would consequently yield a thick gel upon crosslinking. This would resultantly retard Ca^{2+} crosslinking, with a larger free Ca^{2+} ion concentration being present in the colloidal system, which would once again instil positivity to the system, consequently destabilising it.

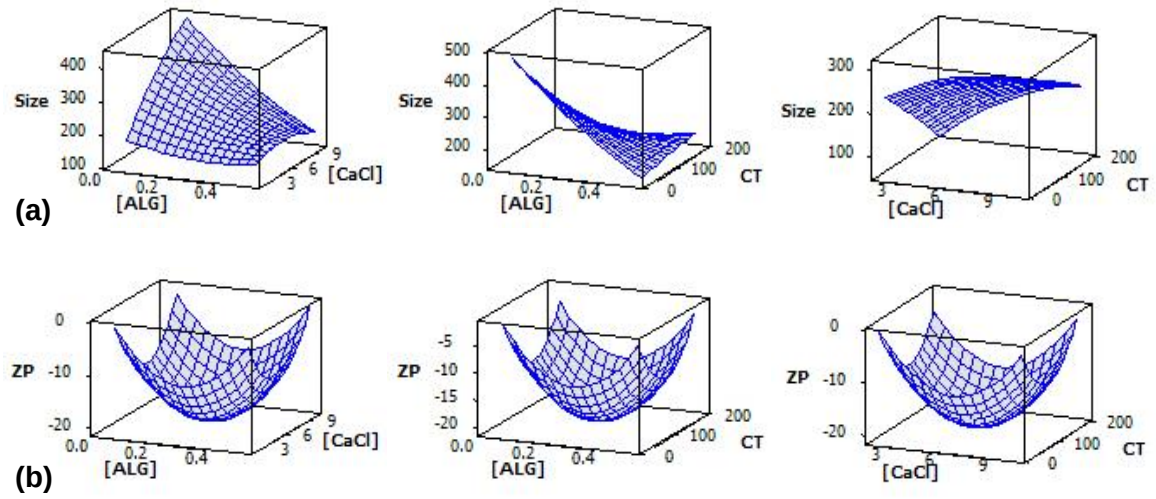

Figure 4.9.1: *Surface plots of (a) average size distribution and (b) zeta potential attained for nanoparticles prepared as per the parameters obtained from the Box-Benhken design.*

4.4.8.2 Textural Analysis of the multipolymeric scaffold device

The average MR of the prepared formulations was plotted as a function of time, as per Figure 4.9.2.1, from which the correlation co-efficient (R^2) and gradient of the curve was calculated. A positive gradient indicated an increase in the ave resilience of the formulation ove time and a negative gradient indicated a decrease in the average MR of the formulation over time as observed in Table 4.8. The R^2 value represented the variation in MR observed with the formulations, with a higher R^2 indicating a larger variation in the MR of a formulation.

Figure 4.9.2.2a indicates that the R^2 approached 1 for formulations prepared with low ECL and CAP concentrations and a high concentration of $CaCl^2$. This is consistent with the higher concentration of crosslinking agent increasing the porosity of the prepared scaffolds, resulting in greater variability being oberserved with the MR of the formulations. Low polymer

concentrations used for the preparation of the multipolymeric scaffolds would also serve to increase the porosity of the scaffold matrices.

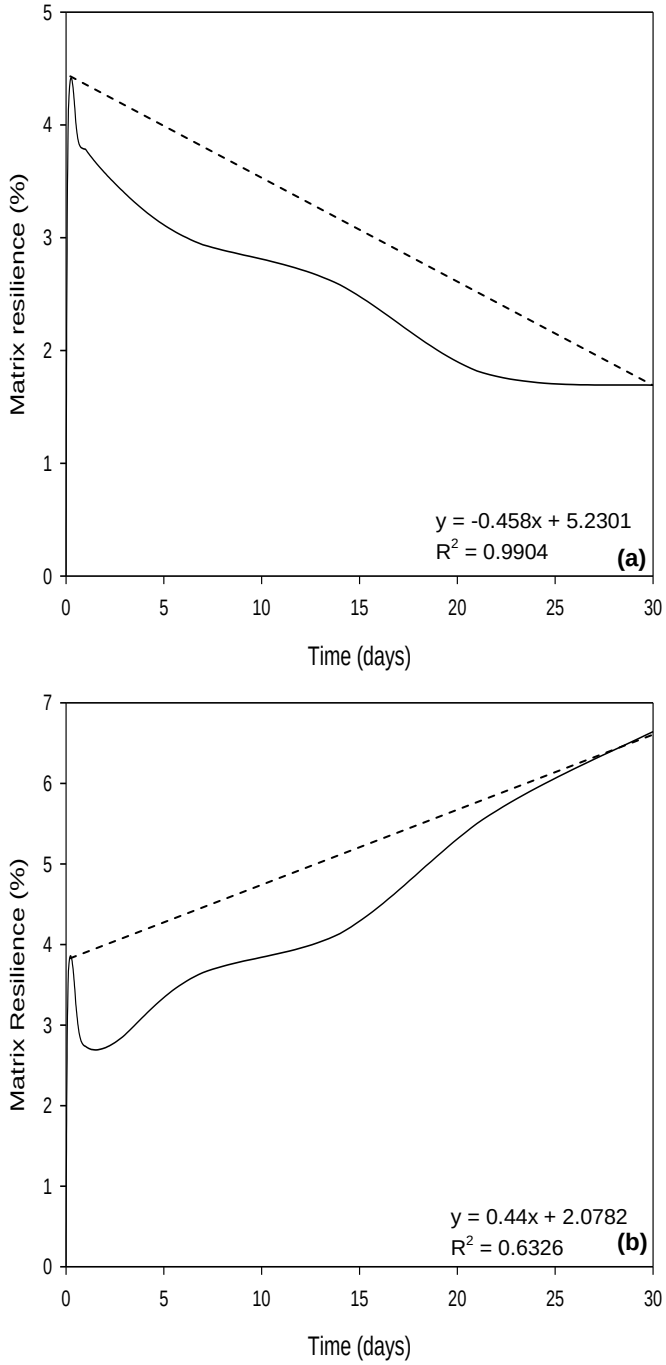

Figure 4.9.2.1: *MR plots used for the calculation of R^2 and gradients used for the optimisation of the multipolymeric scaffolds, with (a) indicating a formulation with a high R^2 value and a negative gradient and (b) indicating a formulation presenting with a low R^2 value and a positive gradient.*

As per Figure 4.9.2.2b, the gradient was affected most signicantly with the concentration of ECL utilised for the preparation of the multipolymeric scaffolds, with a high concentration of ECL producing a negative gradient and hence a formulation displaying a decrease in MR

over time. As the concentration of ECL affects the overall crystallinity of the formulation, this is expected, with an increase in the crystallinity of the formulation decreasing MR a less porous scaffold matrix, less susceptible to erosion will result.

Table 4.8: *Textural profiling of multipolymeric formulations prepared using the Box-Behnken parameters.*

Formulations	R^2	Gradient
1	0.9904	-0.458
2	0.042	-0.1845
3	0.6392	0.517
4	0.6326	0.44
5	0.6598	0.6934
6	0.8352	-0.4043
7	0.8971	1.238
9	0.8266	0.1855
10	0.0004	-0.0022
11	0.9334	-0.3189
13	**No Results**	
14	0.6932	-0.3238
15	0.9236	-0.2924

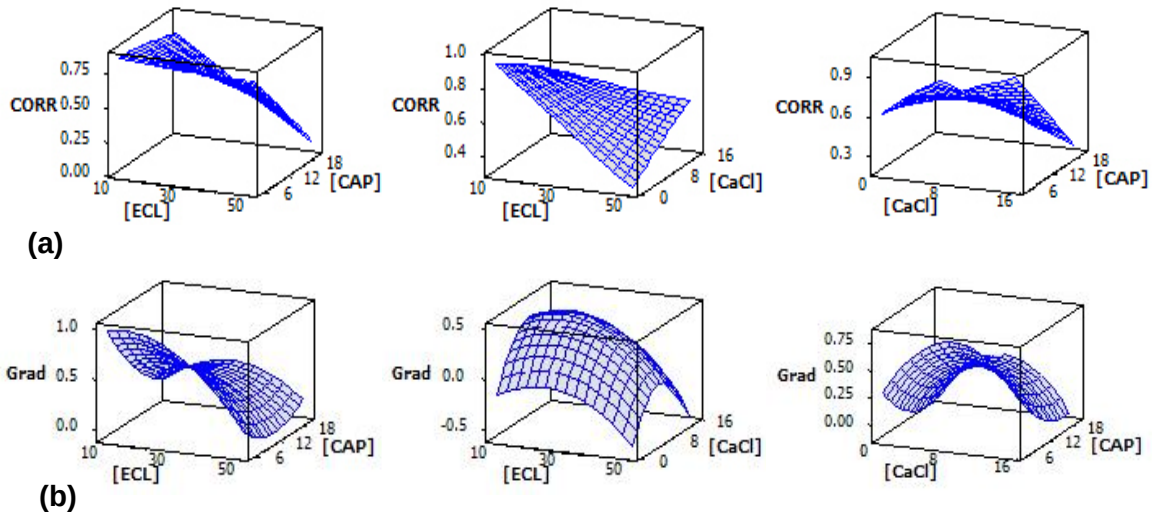

Figure 4.9.2.2: *Surface plots generated using the Box-Benhken design of parameters indicating (a) the correlation and (b) the gradient obtained with change in the concentrations of ECL, CAP and crosslinking agent used for the preparation of multipolymeric scaffolds.*

4.4.8.3 Drug Release from the nanoparticles and multipolymeric scaffolds

The surface plots generated for the nanoparticle formulations illustrated MDT to be optimum when $CaCl_2$ concentrations are low, 30%$^{w}/_{v}$ and below. This was expected as Ca^{2+} reacts with the guluronic acid residues on alginate to form a crosslinked interpolymeric network capable of entrapping drug molecules within (Li *et al.*, 2008, Moebus *et al.*, 2009). At lower $CaCl_2$ concentrations, a more loosely associated polymeric network would form, into which

larger quantities of drug would be entrapped and subsequently release with exposure to PBS.

MDT was relatively impervious to the effects of alginate concentration and ST, however minor increases in MDT were observed at the upper and lower limit of alginate concentration and when ST was kept at 100minutes. This could be attributed to possible leaching of the hydrophilic AZT upon prolonged exposure to the aqueous crosslinking solution. Lower concentrations of drug would therefore be entrapped within the nanoparticles with ensuing lower drug release upon prolonged exposure to PBS. Alginate displays an affinity for amino groups (Zahoor *et al.*, 2005), which are present on the AZT molecule (Figure 3.6b). Association of AZT to the alginate molecules is therefore independent of polymer concentration. This also accounts for the sustained release behaviour of AZT as seen in Figures 4.8a and b. However, with high alginate concentrations and low CT, as per Figure 4.9.3a, a higher MDT is expected. This can be attributed to instability of the colloidal system observed with these parameters leading to agglomeration of the nanoparticles. Larger nanoparticles are capable of imbibing more water due to the hydrophilic nature of alginate, with a resultant increase in drug release due to bulk erosion and swelling of the nanoparticles.

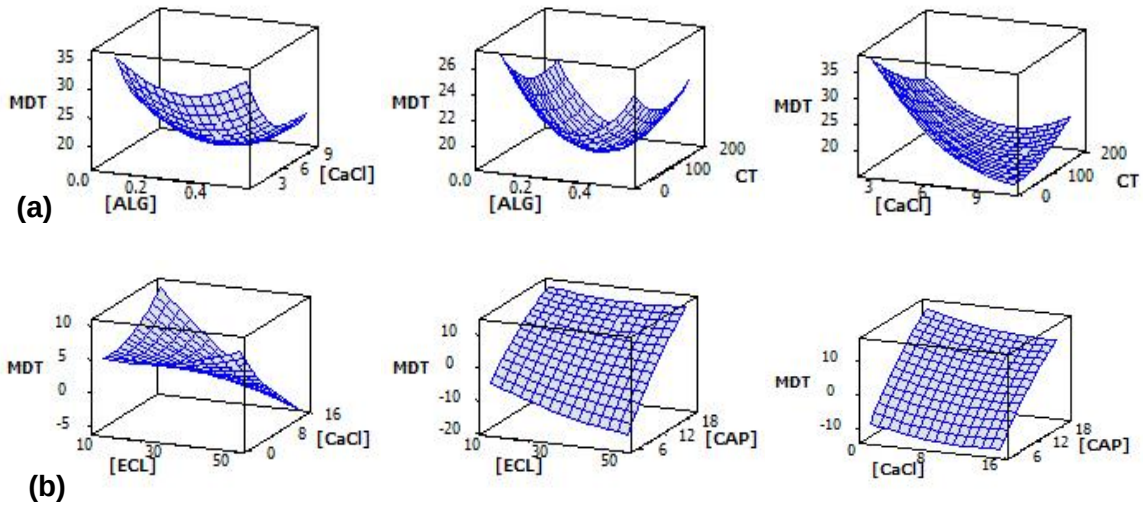

Figure 4.9.3: *Surface plots of MDT values obtained with (a) nanoparticle formulations and (b) nanoparticles dispersed within multipolymeric scaffolds.*

MDT is optimum when CAP concentrations are high. CAP was used as a hydrophobic binding agent in the preparation of the multipolymeric scaffolds. The scaffolds are therefore less prone to erosion in an aqueous dissolution medium at higher CAP concentrations, retarding nanoparticle and therefore AZT release. Marginal increases in MDT were observed as visualised on the surface plots in Figure 4.9.3. At higher ECL concentrations, the

multipolyermic scaffold would undergo degradation in the presence of PBS by hydrolysis of its ester bonds (Huang *et al.*, 2004; Luong-Van *et al.*, 2006; Rezwan *et al.*, 2006). Resultantly, higher concentrations of nanoparticles are released into the dissolution media thereby increasing AZT release. Suboptimal crosslinking of the multipolymeric polymer solution occurs at low $CaCl_2$ concentrations with increased water permeation, resulting in polymer degradation and subsequent nanoparticle release.

4.4.9 Preparation of the optimised drug delivery device using the Box-Benhken design

Optimised nanoparticle and multipolymeric scaffold formulations were computed using the Box Behnken design. Nanoparticles and multipolymeric scaffolds were prepared using the method stated in Section 4.3.1.1 and 4.3.1.2 respectively using the parameters stated in Table 4.9.

Table 4.9: *Parameters generated via the Box-Behnken template utilised for the formulation of the optimised nanoparticle and scaffold formulations.*

	Nanoparticle formulation			**Scaffold Formulation**		
Parameter	**Alginate**	**$CaCl_2$**	**CT**	**CAP**	**ECL**	**$CaCl_2$**
Upper	0.5	10	180	50	15	20
Optimised	0.3294	2	88.1896	12.285	0.2484	20
Lower	0.06	2	15	10	0	5
	MDT	**Size**	**ZP**	**MDT**	**Correlation**	**Gradient**
Objective	maximise	minimise	-10	maximise	0.99	-0.3
Target	30.9968	155.5005	-10.0013	12.3814	0.99	-0.3
Deviation factor	0,83987	0.98778	0.99987	0.82543	1.00	1.00

4.4.10 Analysis of Optimised Nanoparticles and Multipolymeric Scaffold Formulation

4.4.10.1 Zeta size and potential analysis of the nanoparticle formulation

Drug-free nanoparticles presented with an average particle size distribution of 42.54nm (SD<0.0002), with a PDI of 0.604, whereas drug-loaded nanoparticles presented with an average particle size distribution of 68.04nm (SD<0.0002), with a PDI of 0.584. Single narrow peaks were observed for both formulations, indicating uniform dispersion of the nanoparticle colloidal systems. ZPs of -13.4 and -10.61mV (SD<0.0005) were obtained for drug-loaded and drug-free nanoparticles respectively, indicating stability of the colloidal systems. This can be attributed to the presence of PVA which imparted surfactant properties

to the colloidal system, serving to reduce agglomeration and enhance formulation stability due to steric hindrance (Bennewitz and Saltzman, 2009). The lower alginate concentration used to prepare the optimised nanoparticle formulation served to enhance formulation stability due to optimum crosslinking with Ca^{2+}. Alginate concentrations of 0.329mg/100mL were used to prepare drug-loaded and drug-free optimised nanoparticle formulations, with a CT of 88.19 minutes, allowing for adequate penetration of Ca^{2+} ions into the alginate solutions with optimum crosslinking of Ca^{2+} with the guluronic units in alginate (Douglas *et al.*, 2006; Liu *et al.*, 2008; Sriamornsak *et al.*, 2008; Moebus *et al.*, 2009). Minimal free Ca^{2+} ions were therefore present in the colloidal system resulting in a stable system with a negative charge distribution, attributed to the anionic polymers used for the preparation of the optimised nanoparticle formulation (Bajpai and Sharma, 2004; Zactiti and Kieckbusch, 2006; Li *et al.*, 2008). Possible AZT interaction with alginate and pectin allowed for more efficient transfer of electrons to the colloidal system, stabilising the drug-loaded optimised nanoparticle formulation by enhancing the repulsive forces that exists between the particles as they approach each other due to Brownian motion (www.malvern.com).

Drug-loaded nanoparticles presented were larger than nanoparticles prepared without AZT due to nanotube formation and AZT encapsulation within the nanoparticles as observed in TEM images in Chapter 3, Section 3.3.2.1. The controlled gelification of alginate approach allows for the preparation of nanoparticles capable of circulating drug within the CNS due to the small size (68.04nm) as particles in the size range of 20-50nm have been found to bypass the BBB and circulate within the brain. The negative potential (-13.4mV) obtained abets sustained drug delivery throughout the CNS as neutral or negatively charges molecules presents with a greater volume of distribution within the CNS (Thorne *et al.*, 2006; Yang *et al.*, 2008; Benewitz and Saltzman, 2009; Rahman *et al.*, 2009).

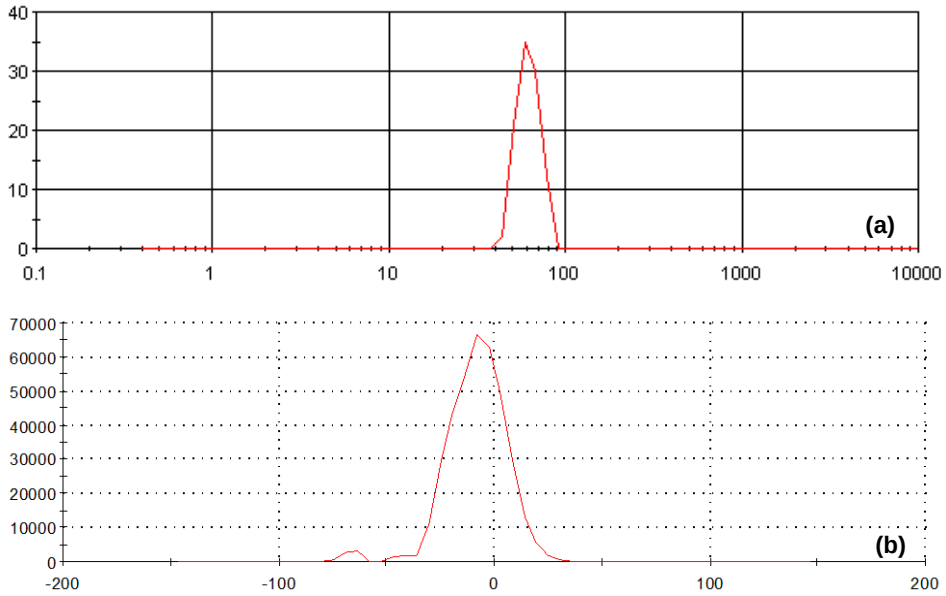

Figure 4.10: *(a) An average size distribution of 68.04nm was obtained for optimised AZT-loaded nanoparticles. (b) Stability of the formulation as implied by the ZP of -13.4mV obtained owing to electrostatic charge stabilisation of the colloidal system.*

4.4.10.2 Matrix resilience studies of the multipolymeric scaffolds

An average MR of 1.862% (SD<0.007) was obtained 1 hour post exposure to PBS, pH 7.4, indicating low porosity of the prepared scaffold. MR increased to 4.451% (SD<0.007) 30 days post exposure to PBS. Porosity increased with increased exposure to PBS consistent with erosion of the scaffold matrix due to CAP degradation. Due to slow degradation of aliphatic polyesters, ECL and PCL, MR remained low with prolonged exposure to PBS. Water permeation into the polymer matrix was resultantly low, with reduced disentanglement of the polymer matrix, ideal for the prolonged release of AZT-loaded nanoparticles from the polymer scaffold. Entrapped phosphate ions present within the pores of the scaffold matrix, attributed to diffusion of PBS into the multipolymeric matrix, could also be responsible for the low matrix resilience obtained. The mechanical strength demonstrated by the prepared multipolymeric device is reflected by the ability of the device to remain intact during dissolution testing, handling and storage (Liu and Williams, 2002).

4.4.10.3 Thermal transitions between prepared formulations and parent compounds

DSC thermograms were used to illustrate thermal transitions which occurred in terms of T_g, and T_m in the formulation of nanoparticle and multipolymeric scaffold formulations.

Analysis of the thermograms revealed endothermic transitions at the temperatures as listed in Table 4.10, corresponding to the meting point of the samples. Changes in the thermodynamic behaviour of the nanoparticle and scaffold samples were attributed to polymer chain rotation occurring during the preparation of nanoparticle and scaffold

formulations. Interaction of PCL with ECL and CAP yielded a decrease in the T_m observed with the multipolymeric scaffold formulation, 50°C as compared to that of PCL which was observed at 60°C as depicted in Figures 4.11.2b and 4.11.1b respectively.

Table 4.10: *Thermal events observed with native polymer and prepared nanoparticle and multipolymeric scaffold samples analysed employing DSC.*

	Temperature transition points (°C)	
Formulation component	T_g	T_m
PCL	-60	60
ECL	-18	-15
CAP	175	192
Alginate	125	280
Pectin	-5	152
PVA	119	198
AZT	-	40
AZT-loaded nanoparticles	155	240
Multipolymeric scaffold	-	50

T_g of PCL and ECL was obtained from literature (Kweon et al., 2003; Lee and Yang, 2002).

T_g, observed as a discontinuity of the baseline, is a second order transition involving a discontinuous change in a second thermodynamic quantity, specifically heat. T_g occurs when crystallisation is impossible under the given conditions being assessed, with T_g being a more subtle transition than crystallisation, melting, evaporation or chemical reactions as T_g has neither enthalpy or entropy, with changes occurring only in heat capacity (C_p). The specific heat capacity change (ΔC_p) is the change observed between the onset and end of the transition. T_g is generally taken as the intersection of the midpoint of the ΔC_p with a straight line joining the onset and the end of the transition (Aulton *et al.,* 1995). Vertically dashed lines are representative of the glass transition and horizontally dashed lines represent shifting of the baseline resulting from ΔC_p where β represents the heating rate ($\Delta T/t$), at the glass transition, as depicted in Figure 4.11.1a.

The optimised nanoparticle formulation demonstrated typical changes in its structure at the T_g, transforming from a brittle, glassy state to rubbery state attributed to increased segmental mobility of the polymers. Modification in the T_g of the nanoparticle formulation (155°C) as compared to 125°C observed for alginate the primary polymer employed for the formulation of nanoparticles, resulted from the interaction of alginate with the copolymers, pectin and

PVA, as well as inter- and intramolecular crosslinking of alginate with Ca^{2+}. An increase in the T_g indicated a decline in the mobility of the polymer chains upon nanoparticle formulation, serving to support the slow release of AZT from the nanoparticles as observed in Section 4.4.7.1 above (Takka, 2003). Noteworthy is the large variation between the Tm obsevered for the optimised nanoparticle formulation of 240°C and that of the primary polymer alginate (280°C). The altered thermal behaviour observed influences the physicomechanical behaviour of the prepared nanoparticle and mutlipolymeric scaffold formulations as previously demonstrated by FTIR analysis and textural profiling conducted in Sections 4.4.1 and 4.4.4 respetively. Figure 4.11.2b and 4.11.2c elucidated no changes in thermal events occurring during the dispersion of AZT-loaded nanoparticles within the mulitpolymeric scaffold. As no energy was expended during the dispersion process, this was expected.

PCL, ECL and multipolymeric scaffold formulations were not analysed due to constraints posed by the equipment (the minimum temperature obtained by the Mettler Toledo DSC1 is -30°C).

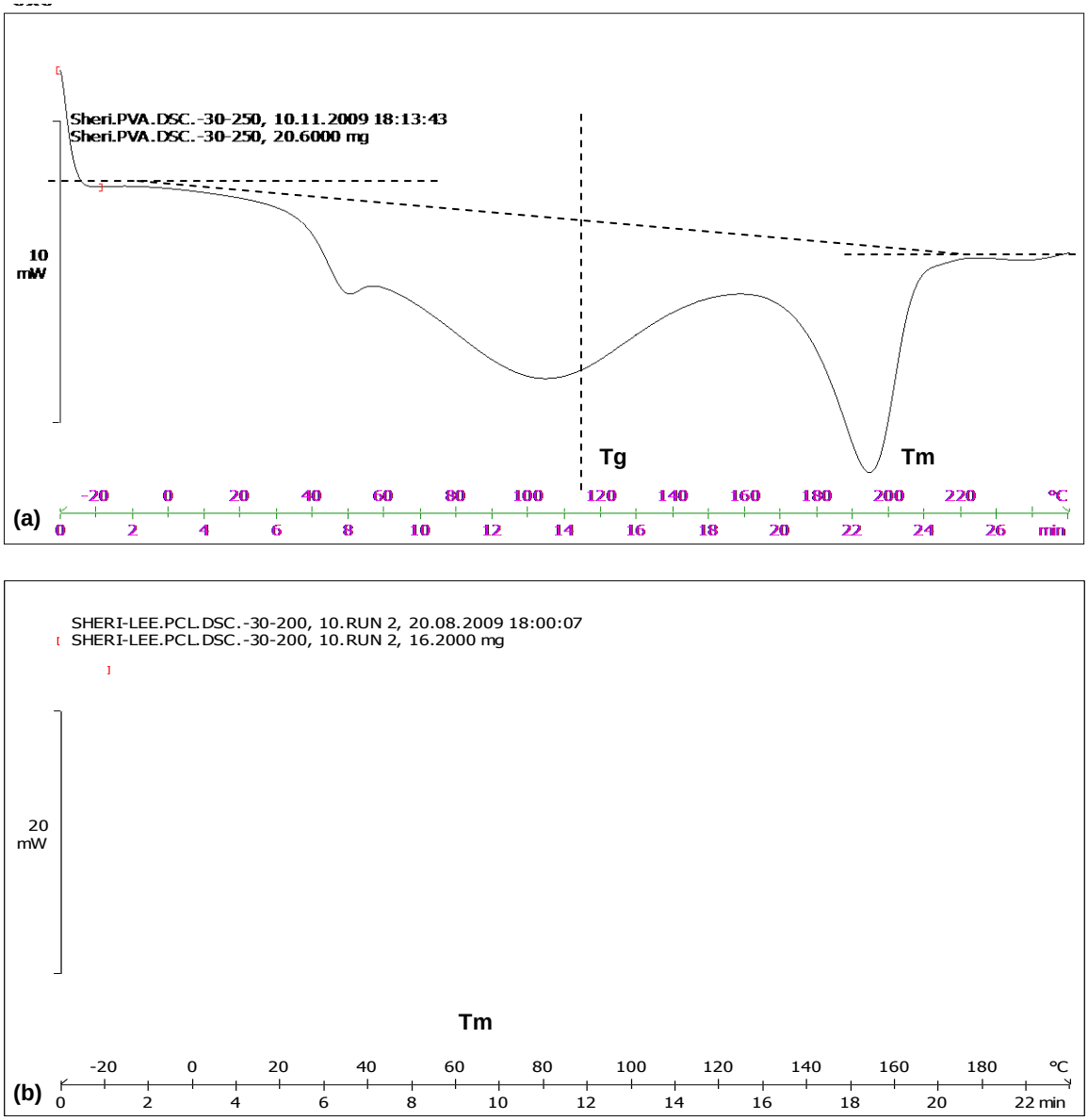

Figure 4.11.1: *DSC thermograms obtained for (a) PVA and (b) PCL indicating the Tg and Tm obtained.*

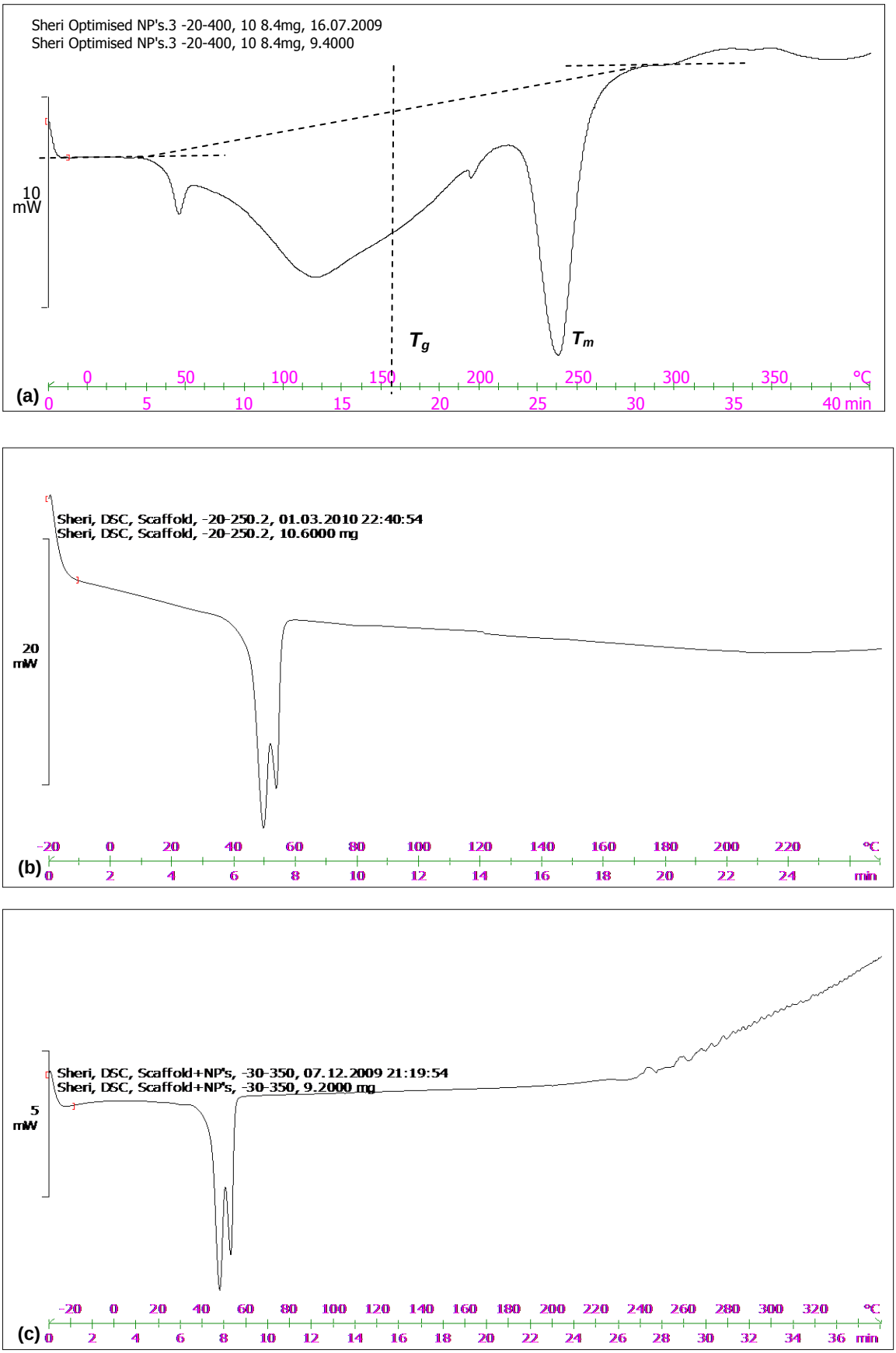

Figure 4.11.2: *DSC thermograms of (a) optimised nanoparticle formulations (b) optimised multipolymeric scaffolds and (c) nano-enabled drug delivery device.*

4.4.10.3 Matrix Erosion exhibited by the multipolymeric scaffold formulation

The optimised polymeric scaffold exhibited an average matrix erosion of 28% (SD<0.001) 30 days post exposure to PBS pH 7.4. ECL and PCL are semi-crystalline aliphatic polyester, containing both crystalline and amorphous regions. ECL and PCL degrades by hydrolytic cleavage of the ester bonds (Rezwan *et al*,. 2006; Chang and Lee, 2009), occurring primarily in the amorphous regions on the polymers as the crystalline regions of PCL are more chemically stable (Tarvainen *et al.*, 2002; Sinha *et al.*, 2004; Luong-Van *et al.*, 2006; Rezwan *et al.*, 2006; Uto *et al.*, 2008; Abbah *et al.*, 2009). CAP displays low solubility in water and is insoluble and unionised in acidic environments. CAP contains 35% phthalyl and 24% acetyl groups, the hydrolysis of which yields the insoluble cellulose ester (Bechard *et al.*, 1995). Erosion of the multipolymeric scaffold is slow as a result.

A 12.285%$^{w}/_{v}$ CAP solution was used to prepare the optimised scaffold formulation. As CAP was added to the formulation due to its ability to serve as an internal plasticiser to the crystalline ECL and PCL, adequate binding of the polymer solutions occurred (Berchard *et al.*, 1995). A 2%$^{w}/_{v}$ $CaCl_2$ solution was used to crosslinked the polymers (CT=88.1896minutes). A less porous scaffold was thus formed with low erosion due to decreased water permeation into the optimised multipolymeric formulation.

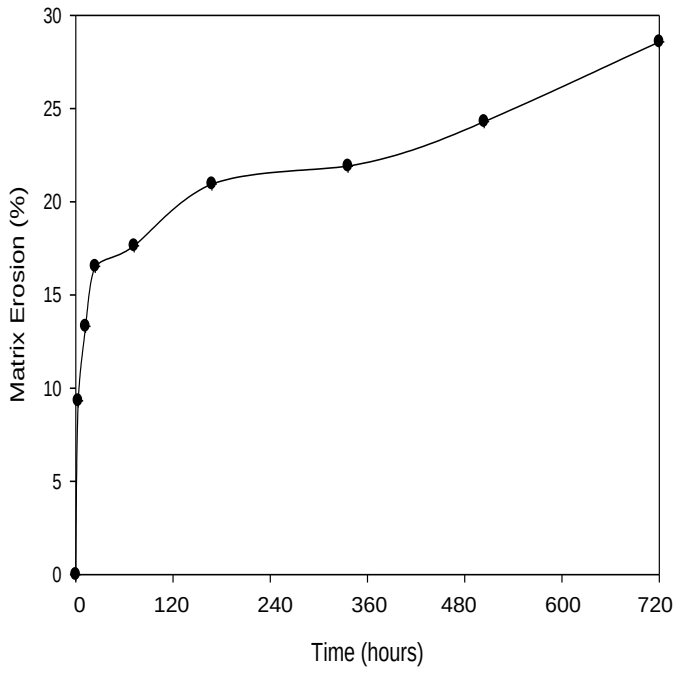

Figure 4.12: *Matrix erosion of the multipolymeric scaffolds in PBS pH 7.4 over 30 days (n=3, SD<0.001).*

4.4.10.4 Drug release of the optimised nanoparticle and scaffold formulations

The optimised nanoparticle formulation displayed an average drug release of 28.56% (SD<0.0005) 30 days post exposure to PBS and an MDT of 46.046 (SD<0.0005). A burst release of 18.10% was observed within 24hours due to adsorbed AZT on the surface of the particles. Ca^{2+} interaction with the COO^- groups on the guluronic acid residues yielded a tightly packed polymer matrix, with low water permeability. An insoluble gel was the result. Interaction of Ca^{2+} ions with the mannuronic acid residue also occurs, however this does not yield a stable compound. Nanoparticle swelling therefore occurs primarily as a result of Ca^{2+} leaching out of the mannuronic acid units, with resultant AZT release. As binding of Ca^{2+} to the guluronic acid units yield a stable compound, Ca^{2+} diffusion occurs only after prolonged exposure to PBS, with extensive swelling of the crosslinked matrix and ultimate degradation occurring (Bajpai *et al.*, 2004; Moebus *et al.*, 2009). High $CaCl_2$ concentrations were utilised for the preparation of the nanoparticles, with a tightly packed stable matrix resulting, as per zeta size analysis. Drug release, proposed to occur due to Ca^{2+} diffusion out of the mannuronic acid units, was therefore slow.

Dispersion of AZT-loaded nanoparticles within a multipolymeric scaffold served to reduce drug release to 17.35% and the MDT to 12.570, 30days post exposure to PBS. This is significantly lower than that of the nanoparticle formulation alone. Nanoparticles are entrapped within the pores of the multipolymeric scaffold. Nanoparticles are released with scaffold erosion, resulting in the retarded release of AZT when dispersed within the multipolymeric scaffold. However drug release was higher than expected. As polymeric scaffolds exhibited a low matrix erosion of 28% (SD<0.001) 30days post exposure to PBS pH 7.4, release can be attributed to diffusion of the hydrophilic AZT out of the nanoparticles still entrapped within the polymer matrix.

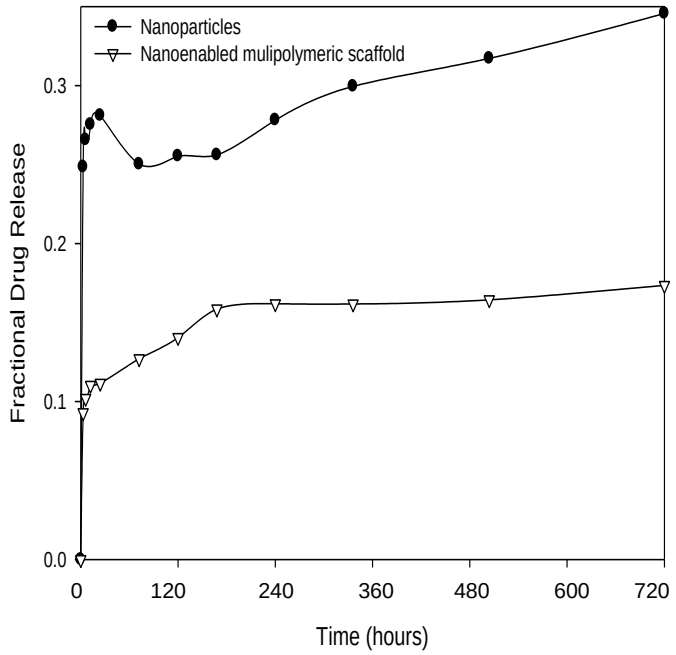

Figure 4.13: *Drug release from the nanoparticle formulation and the nanoenabled multipolymeric scaffold illustrating a decrease in AZT release upon dispersion within the scaffold (n=3, SD<0.0005).*

4.5 Concluding Remarks

The CNS is one of the principle reservoirs for the harbouring and replication of the HI virus. The resultant complications which ensue are debilitating and potentially fatal in nature, requiring therapeutically significant drug concentrations in the brain to manage the condition (Rao *et al.*, 2008). Nanotechnology offers significant promise for the improvement of quality of life of ADC sufferers through the development of novel controlled release drug delivery systems capable of achieving therapeutic levels of ARVs in the brain over a period of months to years (Yang *et al.*, 2008). Nanotherapeutic agents are capable of enhancing drug entry into the CNS due to its small size and larger surface area, as well as sustaining the retention of these drugs over prolonged periods. This is critical for the control of viral replication and to decrease drug resistance. Nanocarriers have therefore received much attention in recent years for the management of neurological disorders (Rao *et al.*, 2008) and have therefore been employed in the preparation of the multipolymeric implants.

AZT-loaded nanoparticles dispersed within a multipolymeric PCL/ECL/CAP scaffold displayed satisfactory drug release behaviour. High drug loading, suitable size and stability was observed with the nanoparticles prepared, with a further enhancement in formulation stability observed for the optimised formulation. Robust multipolymeric scaffolds were prepared which presented with low matrix erosion attributed to the use of semi-crystalline

polymers recognized for their slow degradation *in vivo*, which served to retard AZT release. The prepared nano-enabled multipolymeric drug delivery system has demonstrated suitability for application as a brain implant in the management of ADC. *In vivo* studies in an animal model follows in Chapter 5 serving to prove safety and compatibility of the NMDDD for human application as there is no standard currently available by which to compare the product being developed (Ginski *et al.*, 1999; Costa *et al.*, 2003).

CHAPTER 5

In vivo evaluation of an implantable polymeric configuration for application in AIDS dementia complex

5.1. Introduction

Since the introduction of highly active antiretroviral therapy (HAART) in 1995, the morbidity and mortality associated with Human Immunodeficiency Virus (HIV)/Acquired Immunodeficiency Syndrome (AIDS) has been dramatically reduced. However, millions of lives are still lost each year (Schneider *et al.,* 2005; Lewis *et al.,* 2007; das Neves *et al.,* 2009). The blood brain barrier (BBB) is compromised during infection with HIV, providing a means by which infected cells can enter into the brain. The brain forms a sanctuary for the HIV. An increased influx of viral cell into central nervous system (CNS) acts to form a viral reservoir for the replication of the virus, impermeable to antiretroviral therapy (ARV) therapy due to the restrictions posed by the BBB and blood-cerebrospinal fluid (CSF)-interface. An increase in neuropathologies, including neurocognitive impairment and ADC observed with HIV patients therefore results (Antinori *et al.*, 2007; Toborek *et al.,* 2005; Wang *et al.*, 2008; Valcour *et al.,* 2010).

The BBB and blood-CSF interface regulates the access of substances into the brain, thereby shielding it from harmful substances (Varatharajan and Thomas, 2009; Georgieva *et al.,* 2010) as illustrated in Figure 5.1. Many more ARV's have been found to cross the BBB and blood-CSF-interface as described in Table 5.1. However, of these drugs, zidovudine (AZT) remains the drug of choice for the treatment and management of neurological conditions associated with HIV infection of the CNS. AZT, a polar molecule, displays the best CNS penetration to date in the NRTI class of ARVs (Sawchuk and Yang, 1999; Narishetty and Panchagnula, 2004; Agarwal *et al.,* 2010). PI's are capable of traversing the BBB, however glycoprotein (P-gp), an ATP-dependent efflux pump, limits the accumulation of therapeutically significant concentrations of these drugs in the CNS. The CNS adverse effects, such as hallucinogenic dreams, associated with the use of efavirenz, an non-nucleoside reverse transcriptase inhibitor (NNRTI), limits its use due to the high concentrations required for the management of AIDS dementian complex (ADC) (Varatharajan and Thomas, 2009).

Table 5.1: *CNS-penetrating effectiveness (CPE) rank of AVR's as proposed by Letendre et al. (2008). This is based on the physicochemical characteristics of the drugs (adapted from Varatharajan and Thomas, 2009).*

High	Intermerdiate	Low
Zidovudine	Stavudine	Tenofovir
Abacavir	Lamivudine	Didanosine
Delavirdine	Emtricitabine	Zalcitabine
Nevirapine	Efavirenz	Nelfinavir
	Amprenavir	Ritonavir
	Fosamprenavir	Saquinavir
	Atazanavir	Enfuvirtide
	Indinavir	

Figure 5.1 presents the major pathways of penetration of drugs through the BBB into brain tissue. These pathways are frequently manipulated by pharmaceutical scientists for the formulation and development of new neurotherapeutic agents.

A number of approaches have been investigated and utilised for the delivery of therapeutic agents into the CNS as listed below:

- **Hyperosmolar BBB opening:** transient disruption of the BBB by means of intra-arterial injection of a hyperosmolar solution (nonelectrolyte solutions such as glucose, sucrose, aribinose, mannitol and urea is often used), usually into the carotid artery. This induces the widening of the tight junctions by the osmotic shrinkage of the capillary endothelial cells with resultant increased permeability of the BBB to drug molecules. Limitations include oedema, encephalitis and possible toxicity due to lack of selectivity of the substances entering the brain. Seizures have been reported in approximately 20% of patients receiving this therapy. Partial vascular distribution within the brain is achieved and targeting drug delivery remains a challenge (Prokai *et al.*, 2000; Kaya *et al.,* 2004; Fiandaca *et al.*, 2008; Bennewitz and Saltzman, 2009).
- **Ligand-specific transport systems:** brain capillaries contain carrier-mediated transport systems for the transport of endogenous molecules into the CNS. Ligands, including monoclonal antibodies and modified proteins, are therefore incorporated into drug delivery systems to mimic these endogenous substances to enhance drug uptake into the CNS. Protection against premature drug degradation in biological fluids is offered by the ligand-nanoparticulate complex. Limitations include competitive inhibition of the drug delivery system with the natural compounds (Misra *et al.*, 2003; Reis *et al.*, 2006; Benewitz and Saltzman, 2009).

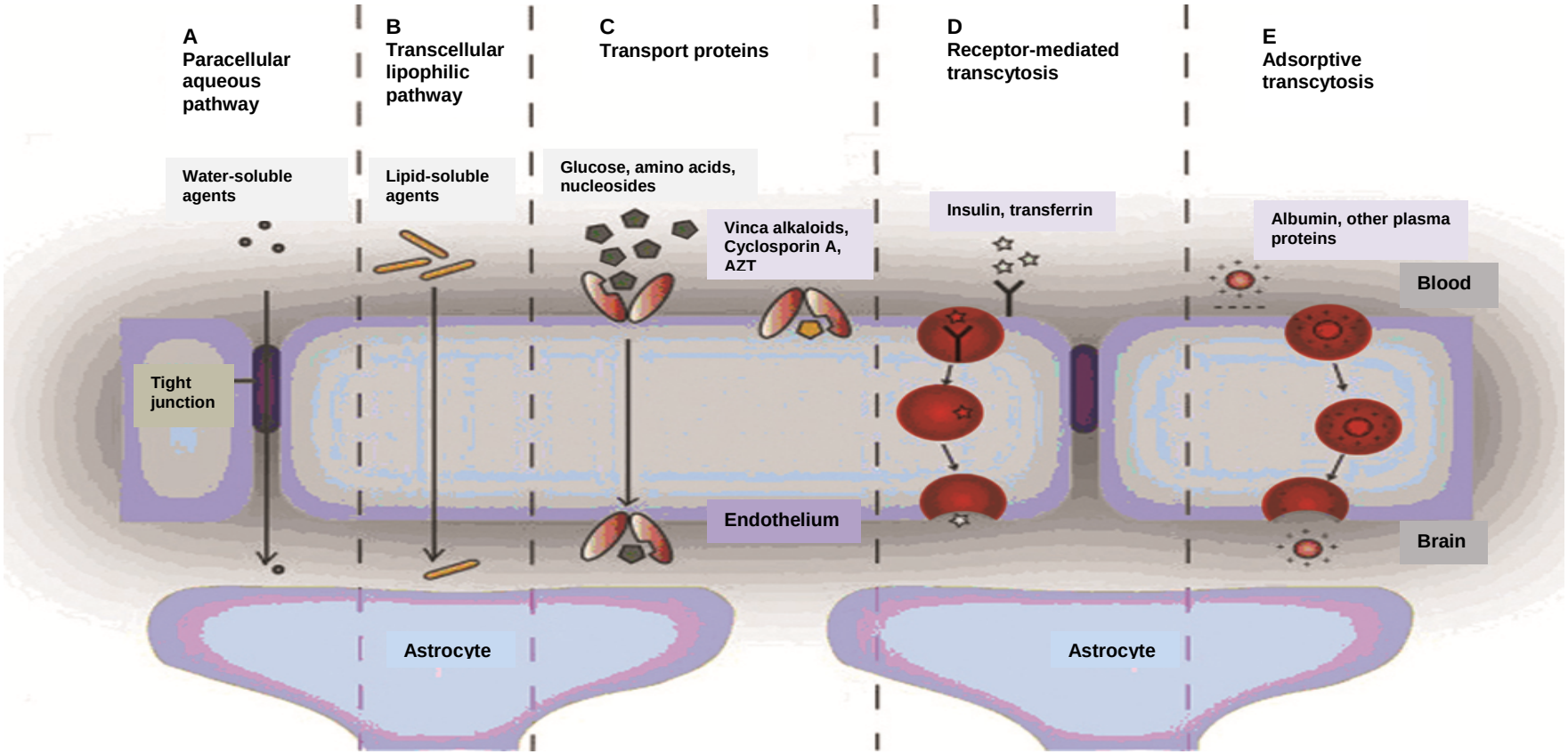

Figure 5.1*: Brain capillary endothelial cells and astrocytes present in the BBB regulate the passage of molecules into the brain. There are several pathways present which facilitates the entry and accumulation of drug molecules into the brain. Pathway A facilitates the entry of hydrophilic agents into the brain via tight junctions present between the endothelial cells, whereas pathway B facilitates the entry of hydrophobic molecules which can readily traverse the BBB by penetrating the phospholipid membrane. Transport proteins present on the surface of the BBB, pathway C, aids the entry of peptide and nucleoside drug molecules such as AZT, as well as amino acids, monosaccharides and organic cations. Receptors present on the surface of the BBB, pathway D, facilitates drug entry via transcytosis and pathway E aids the entry of positively charged drug molecules into the brain by means of adsorptive transcytosis (adapted from Bennewitz and Saltzman, 2009).*

- **Prodrugs:** a transient chemical modification of drug molecules by the attachment of the molecules to removable pharmacologically inactive compounds, with properties capable of protecting the active drug molecules from systemic degradation. This enables targeted delivery active drug molecules to the desired site of action. The prodrug is inactive, with the active parent compound liberated *in vivo* employing a single activating step, usually by means of enzymatic cleavage or hydrolysis. Additional molecules can be liberated with the drug molecules which can potentially increase lipophillicity of the drug molecules, thereby enhancing penetration into the CNS. Limitations include poor tissue retention and short biological activity due to non-specific tissue uptake and active efflux from the brain resulting from an increase in lipophillicity of the prodrug (Prokai *et al.*, 2000; Misra *et al.*, 2003; Benewitz and Saltzman, 2009; Brandt *et al.,* 2010; Semreen *et al.,* 2010).
- **Efflux pump inhibitors:** transient modification of BBB permeability is offered by the efflux pump inhibitors. Multi-drug resistance protein (MRP), Pgp and multi-specific organic anion transporter (MOAT), belonging to the ABC cassette family, are active efflus pumps present at the BBB which remove drug molecules from the brain, preventing distribution within the brain parenchyma. Inhibition of the activity of the efflux mechanism by coadministration of competitive or non-competitive inhibitors serves to enhance drug uptake into the CNS (Misra *et al.*, 2003; Bennewitz and Saltzman, 2009; Varatharajan and Thomas, 2009).
- **Intracerebroventricular/intrathecal administration:** direct administration of drug into the CSF or the lumbar region by means of outlet catheters connected to implantable reservoirs or pumps, with the implantable pumps the more favourable approach as it is capable of achieving continuous, elevated drug concentrations in the CSF. Systemic drug toxicity, drug opsonisation by serum protein and premature metabolism in the serum is diminished with this approach. Increased drug concentrations and half life ($t^1/_2$) in the CSF is achieved. Limitations to this approach include restricted penetration of drug into the brain parenchyma with localisation mainly at the ependymal cells lining the ventricles. The small pores size of the extracellular space reduces drug movement within the brain. CSF is recycled through the ventricular system every 4-5hours, with subsequent bulk flow into the systemic circulation. Intracerebroventricular administration is an invasive technique with the potential risk of infection and increased intracranial pressure occurring due to the injection of fluid into the brain (Wang and Sawchuk, 1995; Misra *et al.*, 2003; Bennewitz and Saltzman, 2009).
- **Convection enhanced delivery:** utilised to the enhance drug distribution throughout the brain parenchyma by means of gradual infusion of a drug solution using a

catheter into the interstitial space. Drug entry into the parenchyma occurs with diffusion resulting from an externally applied pressures source. Rapid transport of drug molecules occurs as compared to simply diffusion, with an extended distribution volume within the brain with high drug concentrations resulting at the desired site of action. Limitations include inefficient drug delivery occurring with back flow of drug solutions occurring due to the high pressures utilised for drug diffusion. Incorrect placement of the catheter within the brain can lead to brain tissue injury and the introduction of air bubbles into the CNS (Saito *et al.*, 2005; Bennewitz and Saltzman, 2009; White *et al.,* 2010).

- **Intracerebral administration:** involves direct drug delivery into the brain parenchyma by implantation or injection of drug. Direct targeting of the drug to the desired site of action is achieved with the drug delivery device having bypassed the BBB. Systemic toxicity is resultantly reduced. Utilisation of an implantable drug delivery device is favourable to injections as implants are capable of sustained drug release with longer drug exposure at the desired site of action. Limitations include sluggish diffusion and elimination mechanisms with a resultant drop in drug concentrations with increasing distance from the delivery site. Nondegradable implants require later removal of the device with the possibility of a foreign body response occurring due to the presence of a permanent fixture within the brain (Benewitz and Saltzman, 2009).

Folkman and Long first invented implantable polymeric drug carriers for controlled release with the implantation of digoxin-releasing silicone rubber devices into the myocardium of dogs in 1964 (Popovic and Brundin, 2006). Since then, numerous polymeric implantable systems have been developed and utilised for drug delivery applications (Popovic and Brundin, 2006; Bennewitz and Saltzman, 2009).

The implantation of a sterile biodegradable polymeric device into the brain would serve to reduce or eliminate the problems listed above associated with delivery of drug into the brain. A once-off implantation of the device is required with polymeric systems as the biodegradable nature of the device eliminates further surgical intervention for device removal. The use of nanoparticles as drug carriers ensures optimum dispersion of the drug throughout the brain as the small size of nanoparticles enables traversing of the extracellular spaces within the brain. Controlled drug delivery with subsequent device and nanoparticle erosion results, negating concerns associated with insufficient biodistribution of drug particles and systemic toxicity.

Numerous experiments have been conducted utilising brain implants, many of which used rats as the test specimen. Gamma-aminobutyric acid (GABA) was implanted into both hemispheres of the brain, near the substantia nigra, using a rat model, to observe epileptic activity in response to electric stimulation (Kokai *et al.*, 1994). Phenytoin, an antiepileptic drug, was implanted 1-2mm into the cortex of the brain, also using a rat model, after being encapsulated with a non-biodegradable controlled release polymer (Tamargo *et al.*, 2002). Álvarez and Ruarte (2003) implanted guide cannulae into the basolateral amygdala and the ventral hippocampus of adult male rats to assess the interaction of hippocampal glutamic acid-neurons with histamine-neurons in the basolateral amygdala to modulate memory and learning processes. Polymeric material, similar to that employed in the present study, was used in this experiment, with minimum deleterious effects experienced. Lagares *et al.* (1996) fixated β-amyloid and water implants into the hippocampus of Sprague-Dawley rats to assess the effects on psychomotor activity, psychomotor coordination and passive avoidance behavior, without significant harm being done to the animals. Tate *et al*. (1992) implanted brain grafts of β/A_4 amyloid into the suprachiasmatic nuclei of adult rats to examine the relationship between the neuropathology of Alzheimer's disease and circadian rhythm disruption. Little distress was experience by the animals during the conduction of this experiment due to the use of anaesthetizing and sedating agents, as well as other drug therapy, such as atropine to ensure the rats could breathe properly. Quester, Knifka and Schroder (2002) implanted polyester meshes into the fourth ventricle of Wistar rats to study host-tissue response to implants. Rats were anesthetized and provided with artificial respiration, with cardiovascular function being monitored using ECG and by monitoring of the blood pressure in the femoral artery. Rats were monitored daily by two separate researchers to assess for the development of possible neurological symptoms. This study was conducted to assess rat skull-brain specimens after implantation of the meshes, so as to optimize glycol methacrylate embedding into large specimens for reconstructive surgery. These are but a few of the experiments conducted on rats to assess the efficacy of implants into the CNS. The rat model is therefore a suitable model for which to conduct in vivo studies to analyse the safety and efficacy of the intended for the management of ADC.

5.2. Materials

Vials of Retrovir® (Glaxo Smith-Kline®, Gauteng, South Africa), commercially available AZT used for IV administration, was purchased from Milpark Pharmacy (Gauteng, South Africa). Ketamine/Xylazine (Bayer Veterinary department, Gauteng, South Africa), phenobarbitone (Bayer® Veterinary department, Gauteng, South Africa), caprofen (Pfizer® Veterinary medicine, Gauteng, South Africa), lignocaine (Bayer Veterinary department, Gauteng, South Africa) and Adrenaline-Fresenius (Intramed, South Africa) were obtained from the Central Animal Services (University of Witwatersrand, Gauteng, South Africa). Double deionised water was used for chromatographic analysis and was obtained from from a Milli-Q system, (Milli-Q, Millipore, Johannesburg). Analytical grade acetic acid and ammonium acetate were obtained from Sigma Aldrich (St. Louise, MO, USA) and methyl paraben was purchase from Merck (Merck (Pty) Ltd., Darmstadt, Germany). All other polymer and chemicals used were as per previous chapters. Healthy male Sprague Dawley rats, purchased from the Central Animal Services (CAS) (University of Witwatersrands, Johannesburg, South Africa) were used in this study.

5.3. Methods

5.3.1 Animal husbandry

75 male Sprague Dawley rats weighing 400-600g were used to carry out *in vivo* studies as per Figure 5.2. Rats were caged in groups of 2-3, depending on the size of the animals, and maintained on a 12hour light/12hour dark cycle. The rats had free access to food and water at all times. They were weighed weekly so as to indicate their general state of health and well being and to ascertain whether rats should be removed from the study as indicated by excessive weight loss. Furthermore, by following CAS protocol, any animal seen to enter into distress was removed from the study and appropriately treated.

All tests were performed with groups of 5 rats per sample set with a total of 50 rats used for the implantation procedure and 25 rats used for systemic administration of AZT as per Figure 5.2.

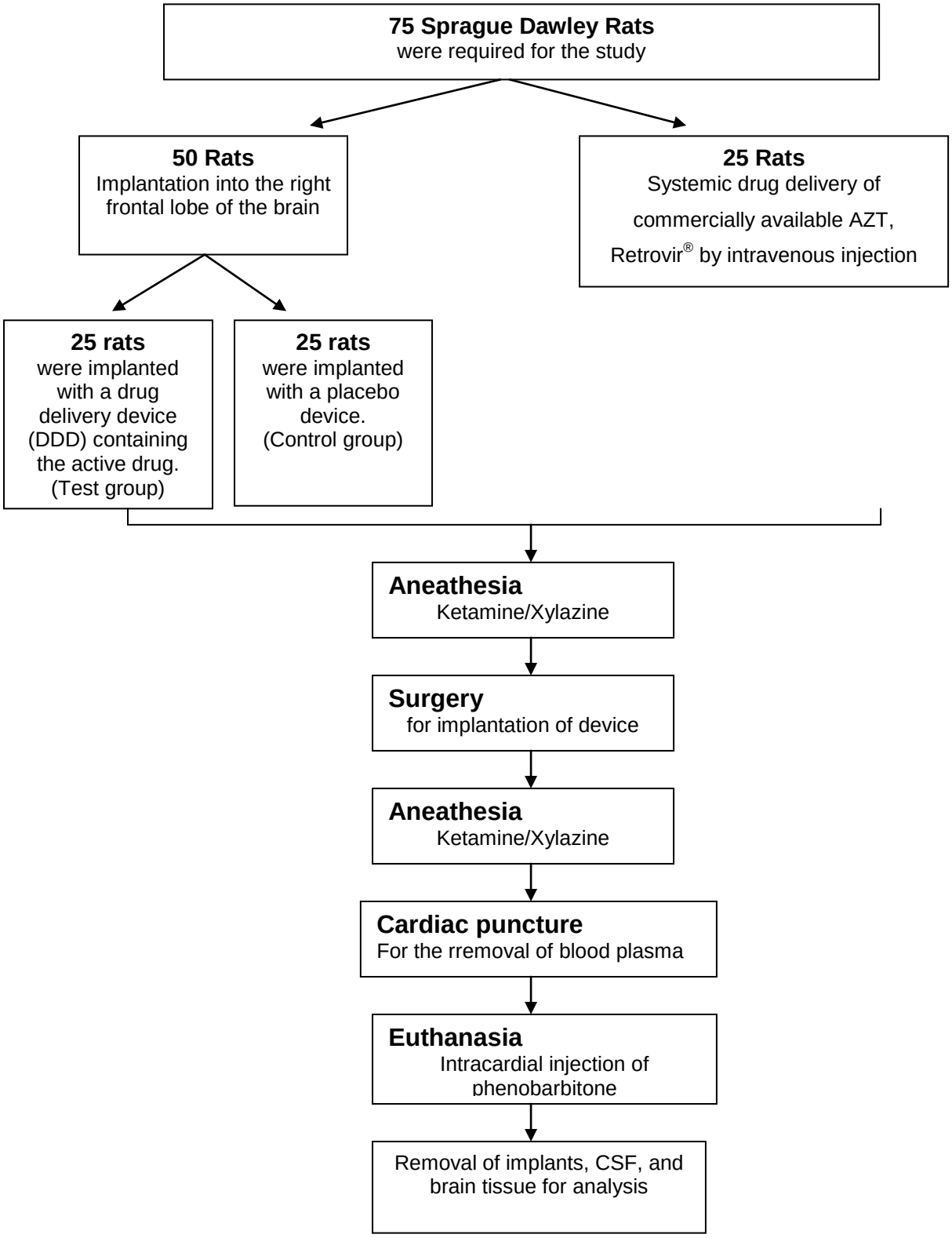

Figure 5.2: *A schematic diagram indicating the distribution of rats for in vivo studies. Systemic drug delivery and implantation of drug-free polymeric devices served as a control by which to compare the results obtained from the implantation of drug-loaded devices into the CNS. These tests therefore conformed to the tests performed with the drug-loaded devices.*

5.3.2 Rationale for use of sentient animals

In vivo studies allows for a clinical assessment of the drug delivery mechanisms in a realistic environment for the implantable device, allowing an *in vivo-in vitro* correlation (IVIVC) to be established, minimising the need for future *in vivo* studies on this device. As there is no implant currently on the market for the treatment of ADC, there is no standard by which to compare the product being developed. In addition, in vivo studies serves to correlate the results obtained from *in vitro* studies, allowing for a more accurate indication of the pharmacokinetic and the pharmacodynamic parameters of the implant.

5.3.3 *In vivo* administration of AZT and subsequent harvesting and treatment of samples

5.3.3.1 Intravenous administration of AZT

Intravenous (IV) administration of commercially available AZT (Retrovir®) was carried out on a test group of 25 rats. 0.75mg of AZT (1.5 mg/kg body weight) was injected into the tail vein of the rats, with samples being obtained at time intervals 3, 6, 12, 24 and 30 hours. IV administration of AZT served to assess drug distribution within the blood, CSF and brain after conventional systemic administration of AZT, serving as a standard by which the efficacy of the implanted device in the CNS over systemic drug delivery can be compared.

Rats were weighed prior to the study being conducted and the dose of Retrovir® administered was calculated for each rat. Rats were then placed into restraining boxes, the tail vein was wiped with alcohol to expose the vein and Retrovir® was injected into the tail vein using a 1mL syringe and a 26G needle.

5.3.3.2 Preparation and sterilisation of the NMDDD prior to implantation into the frontal lobe of the rat brain

The nano-enabled drug delivery device (NMDDD) was prepared using the method described in Section 4.4.9. The implant, measuring 0.000354cm^3 in volume was cylindrical in nature and was made to accommodate the small size of the rat brain, varying between 0.865 ± 0.026cm^3 to 1.165 ± 0.071cm^3 depending on the age of the rat. The implant was therefore prepared to be less than 20% of the volume of the rat brain.

Implants were sterilized using gamma radiation to eliminate the risk of infection due to impurities introduced into the NMDDD during formulation and handling of the NMDDD prior to implantation. Radiation of the NMDDD was carried out at Isotron South Africa (Kempton Park, Gauteng), radiated using a trial dose of 25kGy.

5.3.3.3 Implantation of PCL-ECL-CAP scaffolds into the frontal lobe of the rat brain

In vivo studies were conducted whereby placebo and drug-loaded devices were implanted into the brain parenchyma of male Sprague Dawley rats, to assess device erosion toxicity, as well as drug distribution within the blood, CSF and brain. The implant was implanted into the right frontal lobe of the brain using a technique analogous to that used for the insertion of an intra-cranial pressure monitor in the human subject.

Rats were intramuscularly injected with a ketamine (80mg/kg)/xylazine (40mg/kg) anaesthetic agent, after which their heads were shaved and prepared aseptically. A lignocaine/adrenaline solution was injected subcutaneously into the head, near the implantation site, to minimise post-surgical bleeding, as well as a subcutaneous injection of caprofen, an anti-inflammatory agent, into the neck for pain. Rats were then placed on a stereotaxic frame and taken into the sterile theatre. A para-midline scalp skin incision was made and the periosteum was reflected to expose the frontal lobe. A 3mm in diameter burr hole was drilled into the skull over the frontal lobe to expose the dura. The dura was perforated and the device inserted. The site of implantation was then sealed with sterile beeswax and the wound was sutured (Storm *et al.*, 2002), as observed in Figure 5.3.2 below).

Ringer's Lactate was administered to hydrate the rats post surgery. The rats were then administered an anaesthetic reversal agent and the wound was cleaned with antiseptic agent provided by CAS. Rats were housed individually for 24hours thereafter and monitored regularly to assess for abnormalities associated with motor activity and response.

Figure 5.3.1: *IV administration of Retrovir into the tail vein of Sprague Dawley rats.*

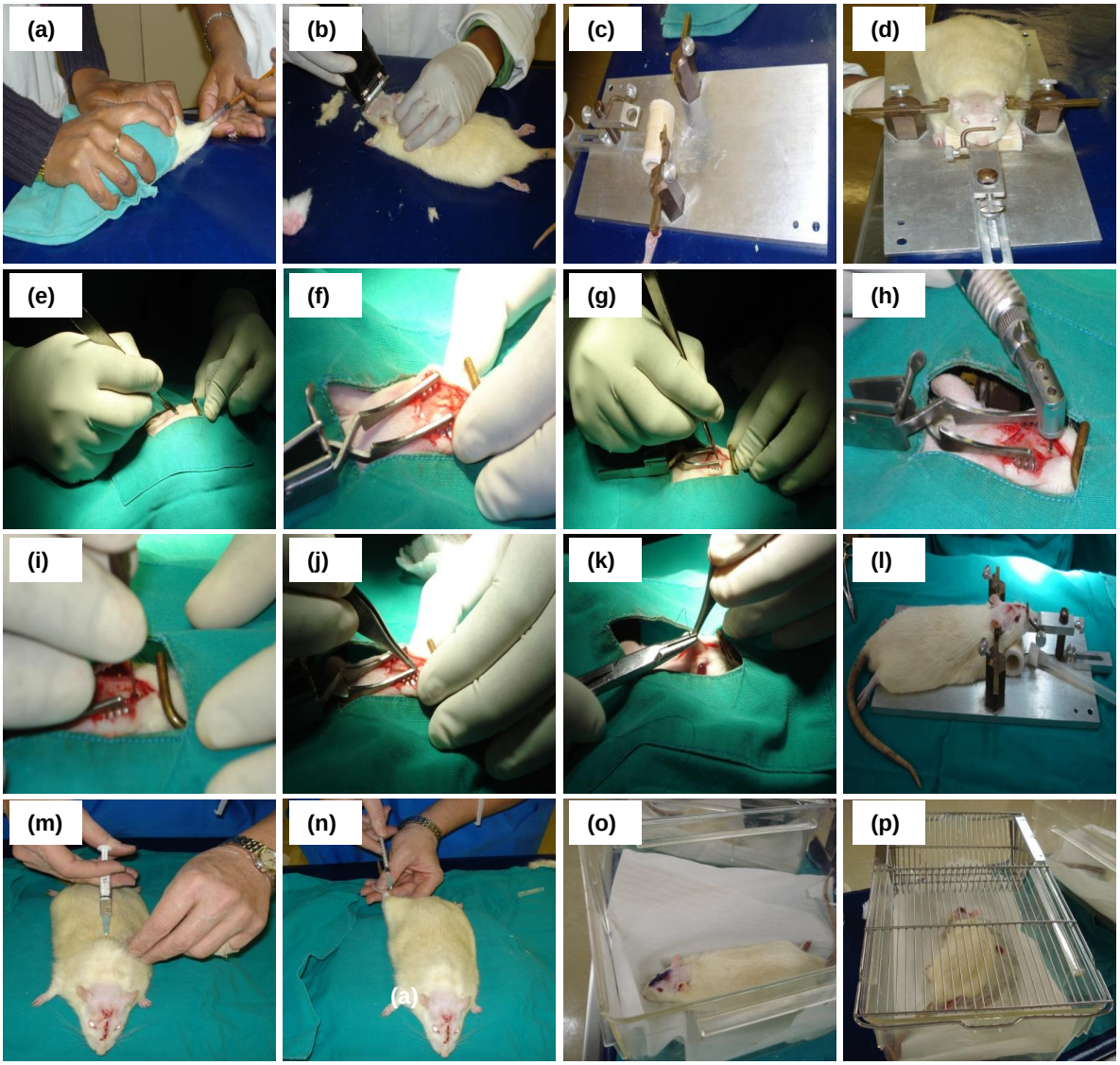

Figure 5.3.2: *Implantation of multipolymeric devices into the frontal lobe of the rat brain.*

5.3.3.4 Harvesting of blood, CSF and brain post implantation

CSF, blood plasma, and brain tissue were removed and analyzed to determine drug concentrations in these regions 3, 7, 14, 21, and 30 days post-implantation. Rats were anaesthetised with a ketamine/xylazine injection, a cardiac puncture was performed to harvest blood (5mL), placed into heparinised test tubes. Intracardial administration of phenobarbitone (200mg/kg) to euthanise the rats then followed. Rats were dissected at the neck to expose the cisterna magna from which CSF (approximately 100µL) was removed using polyethylene tubing, transferred into 2mL ependorfs and placed on ice. Polyethylene tubing was prepared 3 days prior to CSF harvesting, with a 25G needle inserted into one end of the tube and a 1mL syringe inserted into the other end. The tubing was then flushed with an alcohol/H_2O solution and then with double deionised water. Excess liquid was flushed out of the tube which was then placed into a formalin sterilisation drum for 3 days to ensure optimum sterility of the tubing.

Brain samples were obtained by dissection of the skull to reveal the brain which was removed and placed in a 10%$^{v}/_{v}$ formalin solution for later analysis as observed in Figure 5.4.

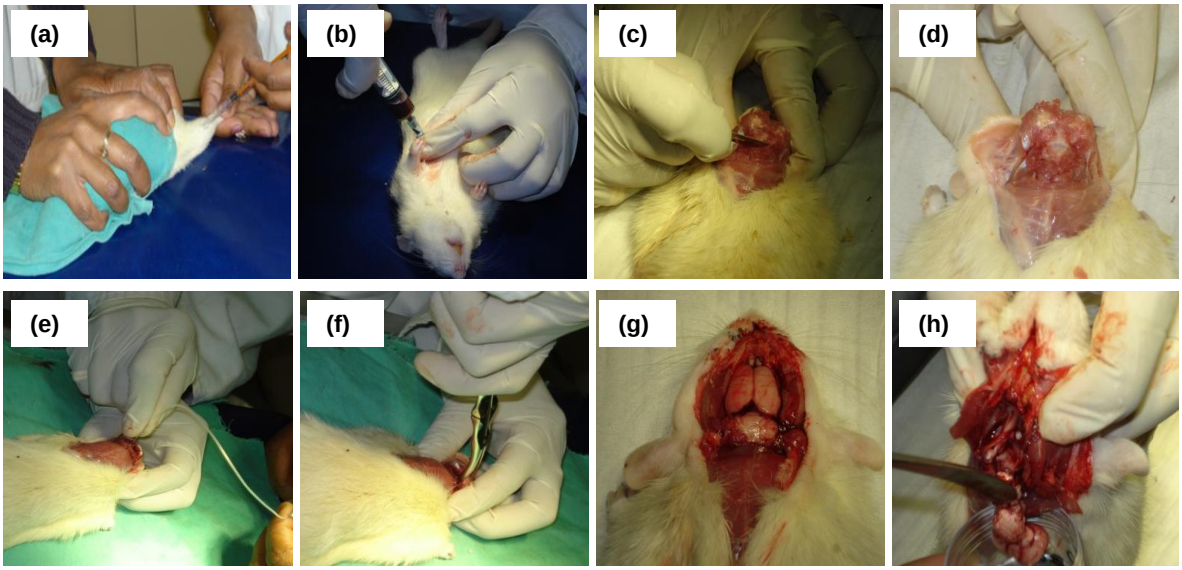

Figure 5.4: *Harvesting of blood, CSF and brain.*

5.3.3.5 Treatment of tissue samples post harvesting

Blood samples were centrifuged at 10 000rpm for 20minutes (Optima® LE-80K, Beckman, USA), to separate the plasma, which was removed and placed in polytops. Plasma samples were then refrigerated at -70°C for later analysis.

CSF samples were centrifuged at 10 000rpm for 10mins (Optima® LE-80K, Beckman, USA). The supernatant was removed and stores at -70°C for later analysis.

Brain samples were stored at room temperature in a 10%$^{v}/_{v}$ formalin solution.

5.3.4 Bioerosion of the multipolymeric device post implantation

Bioerosion was assessed at time intervals coinciding with the harvesting of brain tissue in rats. Multipolymeric implants were weighed prior to implantation and again post removal from the brain, with weight loss calculated as per Equation 3.2 in Chapter 3, Section 3.2.8. Microscopy of the implants employing a Olympus® Stereo Microscope (Model SZX-D2-200) fitted with an Olympus® SZX-TR30 camera (Tokyo, Japan) prior to implantation and post removal of the device was also conducted to ascertain swelling or deswelling behaviour of the device.

5.3.5 Ultraperformance Liquid Chromatographic (UPLC) Analysis of Biological Samples

5.3.5.1 Priming of instruments prior to analysis

All solutions and mobile phases were prepared in double deionised water with a restivity of 18.2MΩcm^{-1}, and filtered using a 0.22µm Cameo acetate membrane filter (Millipore Co., Bedford, Massachusetts), under a constant vacuum pressure.

The UPLC was primed using 50:50 strong acetonitrile/water wash (90/10$^{v}/_{v}$) and weak wash (10/90$^{v}/_{v}$) solutions set to prime for 2 cycles for 15minutes per cycle. This was performed to ensure removal of impurities from the system.

Mobile phases prepared consisted of 100%$^{v}/_{v}$ acetonitrile and a 0.2%$^{v}/_{v}$ formic acid solution prepared in water and was set to flow after the instrument was primed to equilibrate the system prior to analysis.

AZT is a polar acid/base compound with a pKa value of 9.68. Formic acid was employed for use in the mobile phase to decrease the pH of the mobile phase. This was done to ensure optimum elution of AZT and separation of the drug from the internal standard due to ionisation of the drug at pH 4.6 as per the Henderson-Hasselbalch Equation, 5.1.

$$pH = pKa + \log\frac{[A^{-}]}{[HA]} \qquad \textbf{(Equation 5.1)}$$

Where, pKa is the acid dissociation constant, [A^{-}] is the concentration of free acid in solution and [HA] is the concentration of conjugated base in solution.

5.3.5.2 Development of a UPLC method for AZT analysis

UPLC analyses were performed using a Waters® Acquity Ultra Performance LC system (Waters®, Milford, MA, USA), coupled with a PDA detector.

The UPLC column was equilibrated with an acetonitrile/formic acid (80/20$^{v}/_{v}$) mixture at a flow rate of 0.4mL/min. A 2.5µL sample was then injected into the column with the eluent monitored at a wavelength of 254µnm with a run time of 5.5minutes. An Aquity UPLC® BEH ShieldRP$_{18}$ column (Waters®, Milford, MA, USA), with a pore size of 1.7µm was utilised for AZT analysis. Methyl paraben (0.5mg/mL) was employed as the internal standard, (Suwanpidokkul *et al.*, 2004). Methyl paraben is a basic compound with a pKa of 8.47

(Brooks and Long, 2008; Foye *et al*., 2008; Ivanovic *et al*., 1995) which elutes using an acetonitrile/formic acid mobile phase; however methyl paraben retains on the column longer than AZT (4.3minutes) and was therefore chosen for use as an internal standard.

A calibration of AZT curve was generated in double deionised water which was used for the assessment of the efficiency of solid phase extraction.

5.3.5.3 Preparation of AZT standard solutions

A stock solution of AZT (15mg/mL) and methyl paraben (0.5mg/mL) were individually prepared in double deionised water. Standard solutions were prepared by dilution of the stock solutions and were employed for generating a calibration curve of AZT in double deionised water and for solid phase extraction. All solutions were filtered using a 0.22µm membrane filter and were refridgerated at 5°C. Stock solutions were replaced weekly and fresh standard solutions were prepared for each day of analysis.

Drug-free plasma was thawed and prepared by vortex mixing (Vortex-Genie 2, Scientific Industries, Inc, NY, USA) 2mL plasma with 2mL aqueous dispersion of AZT to obtain serial drug concentrations ranging between 0.0038-125µg/mL which was used to generate a calibration curve of AZT. CSF was treated similarly.

5.3.5.4 Solid phase extraction

Solid phase extraction (SPE) was employed for the separation of AZT from the constituent impurities present in plasma and CSF samples, with an increase in the purity obtained of the analyte (AZT). Interference of the constituent with the analyte decreases the accuracy of drug release obtained, necessitating removal. A standard Oasis® HLB SPE technique was employed for the extraction of AZT, where serial dilutions of methanol/water ($MeOH/H_2O$) solutions (5%-100%) were injected into Oasis® HLB cartridges attached to a Standard Lid (Waters®, Milford, MA, USA) and a Visiprep Vacuum Manifold (Waters®, Milford, MA, USA). The cartridge was conditioned with 1mL methanol and 1mL deionised water. A 1mL sample was then loaded onto the cardridge followed by elution of the analyte with serial dilutions (5%-100%) of 1mL $MeOH/H_2O$ with the impurities retained on the cartridge (refer to Figure 5.5). The elute was individually collected in test tubes, spiked with the methyl paraben internal standard, loaded into 2mL vials (Waters® LCMS certified clear, pre-slit PTFE/silicone Septa screw top vials, Waters®, Milford, MA, USA) and were analysed using UPLC.

SPE was also performed employing the standard Oasis® HLB acid/base SPE technique to assess optimum isolation of AZT. The method employed was similar to that explained

above, with an additional wash step added as described in Figure 5.5. MeOH/H_2O solutions were individually spiked with 2% acetic acid and 2% ammonium hydroxide, which were used to elute AZT.

5.3.6 Histomorphological characterisation of brain samples

The advantages of using synthetic polymers such as PCL and ECL for *in vivo* drug delivery include:

1. Predictable and reproducible mechanical and physical properties.
2. Control of the form and amount of impurities present in the materials.
3. Simple structures of the monomeric constituents and therefore lower risk of toxicity, immunogenicity and foreign body response (Rezwan *et al.*, 2006).

Rat brain samples were sent to Pretoria (IDEXX laboratories (Pty) Ltd.) for histomorphological analysis. Brain specimens were cross-sectioned at the anterior third of the brain, being the site of surgical implantation, and at the mid-brain and third section of the cerebellum. This was conducted to assess polymer tissue distribution within the brain and possible toxicity resulting at sites other than the frontal lobe. Tissue blocks were then prepared overnight in an automated histological tissue processor according to standard operating procedure (PTA-HISTO-SOP-27). This was followed by the preparation of wax blocks and histological sections cut at 6-7µm on a microtome. Slides were then prepared and stained with Haematoxylin and Eosin (H/E) stains in accordance with standard operating procedure (PTA-HISTO-SOP-49). Selected slides were stained with Luxol-fast-blue-Holmes (LFB-H) stains to evaluate myelin and neural tissue reaction.

Slides were then analysed under various magnifications using an Olympus® Stereo Microscope (Model SZX-D2-200) fitted with an Olympus® SZX-TR30 camera (Tokyo, Japan).

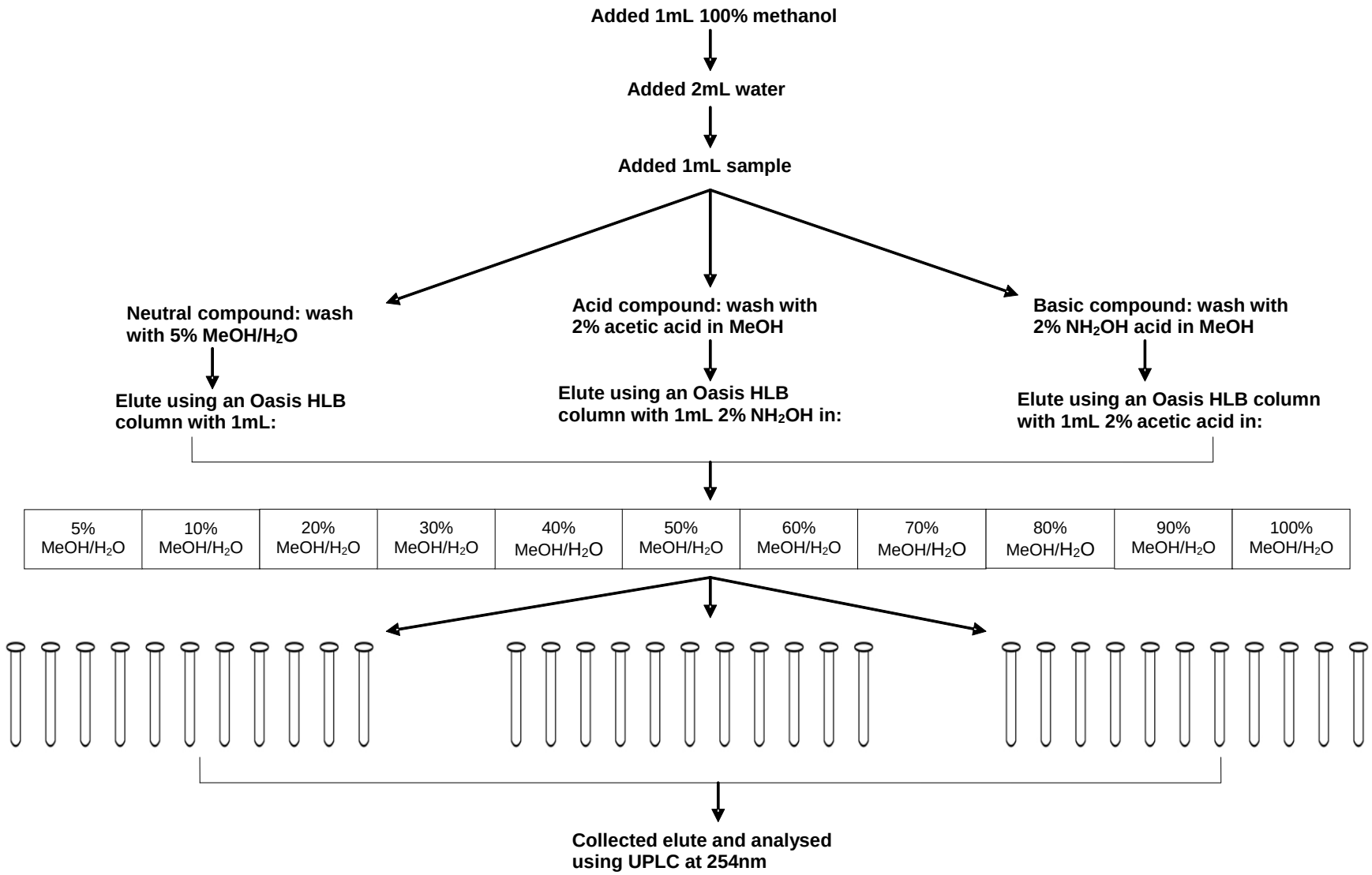

Figure 5.5: *Schematic representation of the generic SPE technique employed to increase purity of the analyte.*

5.4. Results and Discussion

5.4.1 Implantation of multipolymeric nanoenabled scaffolds

Following initial implantation self-limiting nose bleeds were observed. After investigation into this, it was found that nose bleeds was as a result of burr holes being drilled close to the sinuses in the head of the rats. As the nose bleeds did not persist and rats did not present with signs of distress post surgery, these rats were not removed from the study. Re-evaluation of the surgical procedure followed with intensive studies of the anatomy of the rat skull and sinus cavities ensued to ensure optimal implantation of subsequent devices.

Further implantation procedures were successfully undertaken. A stereotaxic frame (refer to Figure 32 (c) and (d)) was employed to ensure the head was positioned to curtail movement during drilling, ensuring minimal post-surgical bleeding. The use of an electric drill guaranteed a clean incision was made into the skull with minimal trauma to the brain.

Larger rats (400-600g) were employed in this study as implantation conducted previously with smaller rats presented with adverse effects resulting from surgery. Larger rats presented with larger brain volumes with ease of implantation transpiring.

Rats were observed for motor abnormalities and were stimulated as per CAS protocol to assess responsiveness. Animals were weighed daily to ensure excessive weight loss did not occur post-surgery. An insignificant decline in weight was observed post-surgery which was expected. Weight gain and normal activity was observed approximately 5-7days post-surgery indicating optimal healing occurring. Infection and severe bleeding at the wound site was absent serving to reinforce this.

Of the 75 rats used in this study, 1 rat died from pulmonary complications resulting from the use of anaesthetic. Post-mortem reports (Appendix C) revealed death occurred due to pulmonary distress resulting from the use of anaesthic drugs.

5.4.2 Bioerosion of the multipolymeric device post implantation

Bioerosion was calculated at 14.14% 30days post implantation. PCL is renowned for its slow *in vivo* degradation post implantation (Sinha *et al*, 2004; Luong-Van *et al*, 2006; Rezwan *et al.*, 2006), implants were therefore expected to exhibit slow erosion, with high molecular weight PCL reported to take 3years for complete removal from the body (Rezwan *et al*, 2006). Radiation of the multipolymeric scaffold prior to implantation served to further retard bioerosion of the device asUV and gamma radiation is frequently used to crosslink PCL and

ECL. Radiation therefore serves to reinforce the density of crosslinked NMDDD and hence retards bioerosion of the implant (Lee and Yang, 2002; Kweon *et al*., 2003; Abdel-Rehim *et al*., 2004)

CSF is reported to be produced at a rate of 25mL/hour with a turnover time of 3.7 times a days; erosion of the multipolymeric device within the brain is therefore lower than observed with *in vitro* studies (Citrin *et al.,* 1987; Saunders *et al.,* 2002). However, because of fragmentation of the implants during insertion and removal of the multipolymeric device into and out of the brains due to the size of the device, 20-15mm in length and 11-8mm in diameter, erosion of the device was higher than expected (refer to Figure 5.6).

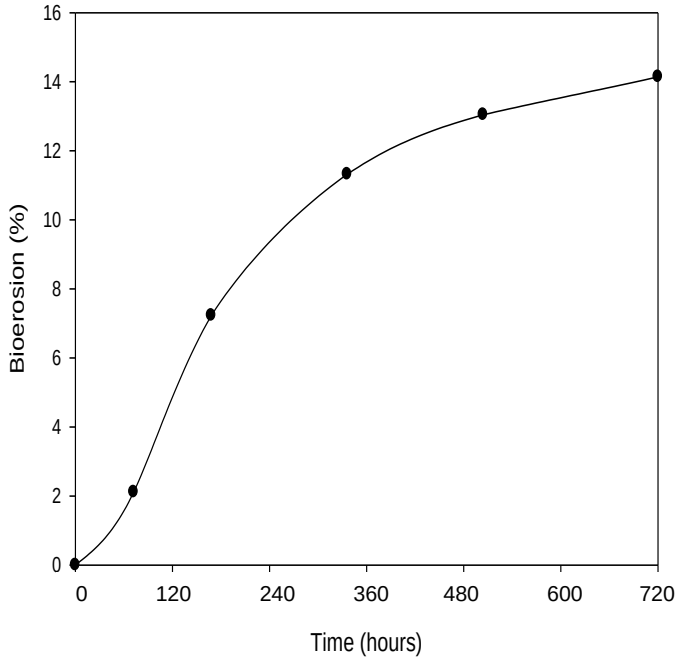

Figure 5.6.1: *Bioerosion profile of the multipolymeric scaffold post implantation into the rat brain (n=3, SD<0.002).*

SEM of the multipolymeric devices prior to implantation revealed a densely packed polymeric matrix with uniformly sized pores dispersed within. Nanoparticles can be observed dispersed within these pores as viewed in Figure 5.6.2b, ideal for sustained delivery of AZT as drug release will occur with matrix erosion and subsequent nanoparticle release from the scaffold matrix.

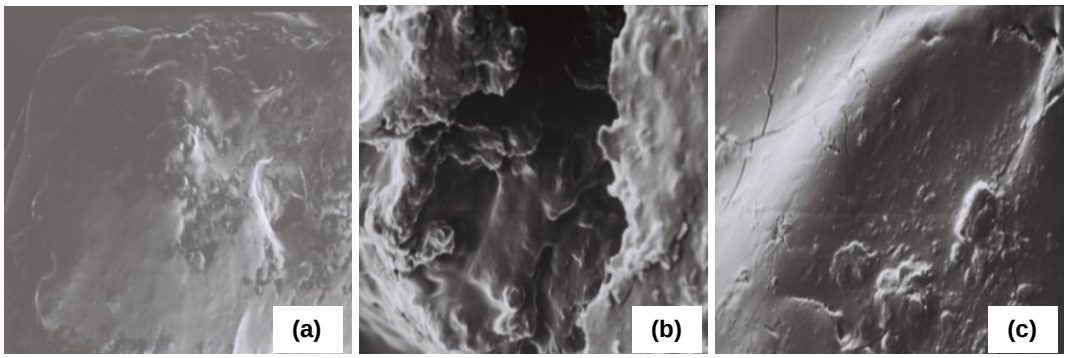

Figure 5.6.2: *SEM images of multipolymeric devices prior to implantation within the rat brain. (a) Pores were observed on the surface of the scaffolds, ideal for nanoparticle and subsequent AZT release following implantation into the brain. (b) Observation of scaffolds under higher magnification revealed a porous interior, with dispersed nanoparticles as seen in (c). Plasticity of the prepared device was maintained, revealed by the smooth inner and outer surfaces of the scaffold.*

As observed in Figure 5.6.3, the multipolymeric device maintains its shape 30days post implantation, with erosion of the device occurring over extended periods, indicating that the device will remain intact over the required period of treatment.

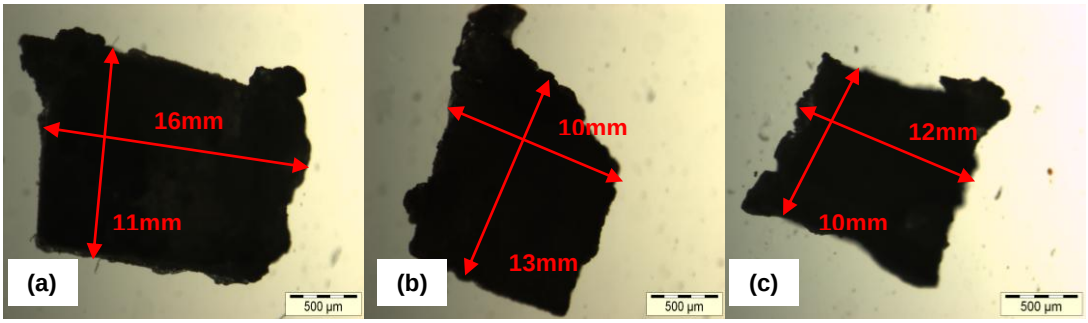

Figure 5.6.3: *Light microscopy of multipolymeric scaffolds (a) prior to implantation, (b) 14 days post implantation and (c) 30 days post implantation within the rat brain.*

5.4.3.1 UPLC method validation

Precision and accuracy of the method employed for AZT analysis was assessed by means of intra- and interday validation using 5 quality control samples of AZT in plasma in concentrations of 15ng/mL, 150ng/mL, 1.5µg/mL, 15µg/mL and 150µg/mL. Intraday validation consisted of multiple injections of samples over five consecutive days (n=5) and interday validation was determined by means of multiple sample injections over a 24 hour period (n=5). These samples were eluted using SPE and were injected into the UPLC to determine percentage extraction yield for the samples which was calculated by comparing the peak areas of analytes obtained from standard solutions at the same theoretical concentration. Precision and accuracy was expressed as the percentage coefficient of variance (CV) and percentage deviation of the mean concentration respectively (Lewis *et al*., 2006; Dubey *et al*., 2009).

5.4.3.2 AZT Calibration curve generated in water

Figure 5.7 presents with a calibration curve for AZT obtained at a wavelength of 254nm employing UPLC (Waters, Milford, MA, USA).

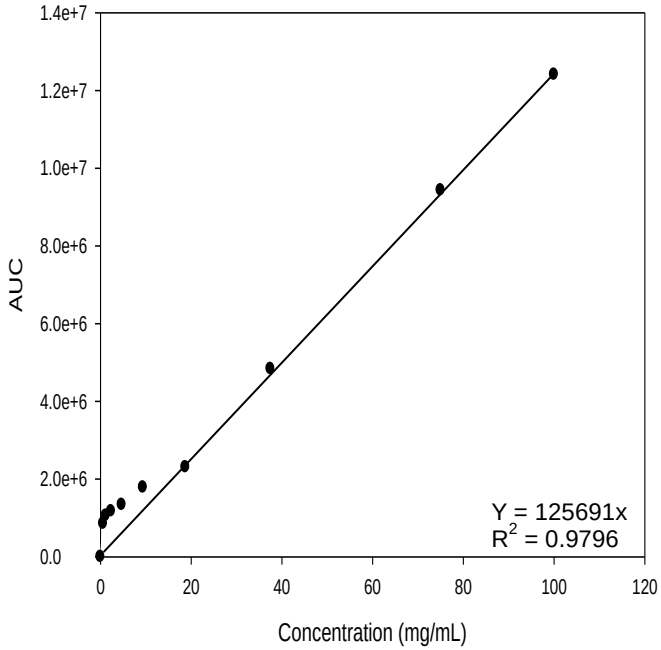

Figure 5.7: *AZT calibration curve at λ_{254nm} in double distilled water (n=3, SD<0.0005 in all cases).*

5.4.3.3 Solid phase extraction of AZT

SPE was performed using serial dilutions of MeOH/H_2O as well as with MeOH/H_2O spiked with 2% acetic acid (CH_3COOH) and 2% ammonium hydroxide (NH_4OH). This procedure was employed to obtain maximum isolation of AZT indicated by the peak height and extraction yield as observed in Table 5.2.

Extraction of AZT was optimum in MeOH/H_2O solutions, with the highest extraction yield (93.48%) obtained in 5% MeOH/H_2O. AZT is a hydrophilic compound (Thomas and Panchagnula 2003; Prakash *et al,* 2008). Extraction of the drug will therefore be more efficient in an aqueous solution. Extraction of AZT in plasma was found to be more efficient in 2.5% MeOH/H_2O solutions (92.13%), with 5% solutions demonstrating minimal isolation of the drug (3.40%).

Table 5.2: *SPE of AZT in double deionised water and plasma.*

SPE	UPLC AUC	Extraction yield (%)
Extraction in double deionised water		
5	2937333	93.48
10	2407674	76.62
15	207469	6.60
Acid	980823	31.21
Base	1148911	36.56
5% acid	53829	1.71
5% base	18213	0.58
10% acid	9283	0.30
10% base	10015	0.32
15% acid	19862	0.63
15% base	8446	0.27
Extraction in plasma		
2.5%	1736915	92.13
5%	64139	3.40
7.5%	7781	0.41

5.4.3.3 AZT calibration curves generated in plasma and CSF

Calibration curves of AZT in plasma and CSF, as illustrated in Figures 5.8a and b respectively, obtained at a wavelength of 254nm employing SPE methodology. Extraction of AZT was performed in a 2.5% methanol/water solution and analysed using UPLC.

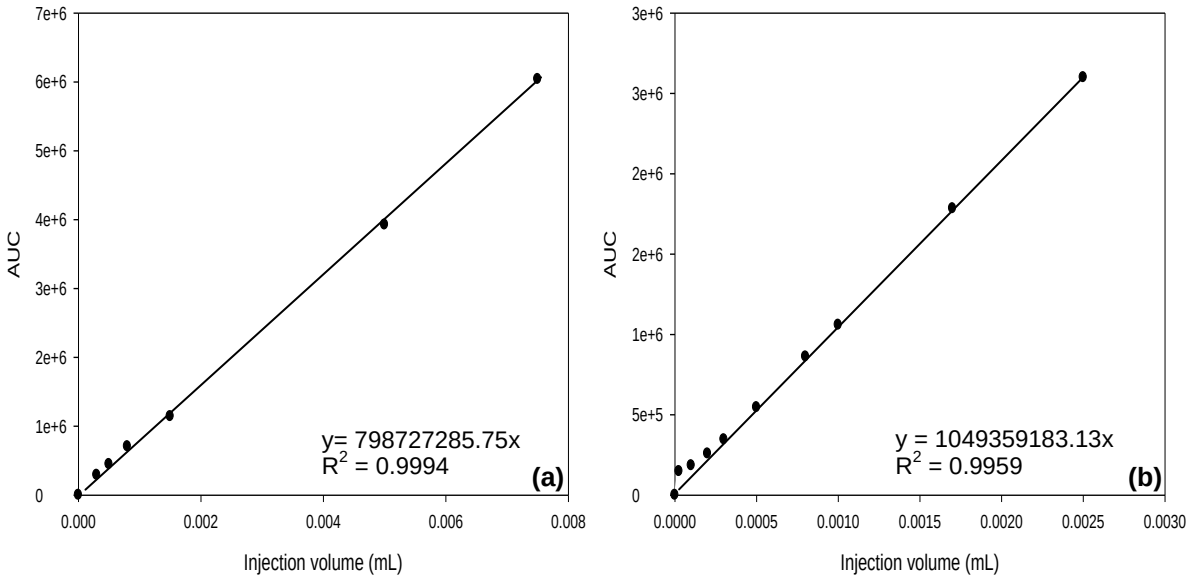

Figure 5.8: *AZT calibration curve at λ_{254nm} in (a) plasma and (b) cerebrospinal fluid (n=3, SD<0.0005 in all cases).*

5.4.3.4 Drug concentrations present in blood and CSF samples

A release of 11.601ng/mL and 9.180ng/mL (S.D<0.002) was obtained in plasma and CSF respectively 30hours post IV administration of Retrovir®. Drug concentrations within plasma were high due to systemic administration of drug, with peak plasma concentrations (31.923ng/mL) achieved within 3hours post administration. As AZT has been reported to reach peak plasma concentrations within 0.4-2hours post oral administration, this was expected (GlaxoSmithKline, Combivir package insert 2006; Quevedo and Brinon, 2009). AZT is significantly metabolised following systemic administration with only 60-70% of drug available in the plasma, attributed to hepatic first pass metabolism of the drug (McDermott *et al.*, 1992; Allan Macnab *et al.,* 1996; Carvalho *et al.,* 2010). This, added to the plasma half life of 1-1.5hour observed with AZT (Lotter *et al.*, 1991; McDermott *et al.*, 1992; GlaxoSmithKline, Combivir package insert 2006; Quevedo and Brinon, 2009), accounts for the decline in plasma drug concentrations with time (refer to Figure 5.9a). The low CSF concentrations attained can be attributed to metabolism of drug prior to reaching the brain as well as the limitations posed by the BBB to the entry of AZT into the brain (Giammano *et al*., 1999; Pardridge, 2005; Modi *et al*, 2009). Efflux of AZT out of the brain is also accountable for low CNS concentration of AZT achieved (Dykstra *et al.,* 1993; Brewster *et al.,* 1995; Varatharajan and Thomas, 2009; Bennewitz and Saltzmann, 2009).

Optimised scaffolds exhibited a release of 12.793ng/mL and 35.225ng/mL (S.D<0.002) in plasma and CSF respectively 30 days post implantation of the nanoenabled multipolymeric device. Plasma drug concentrations can be attributed to AZT elimination from the CNS and is therefore significantly lower than that of the CSF AZT concentrations. Drug concentrations within the plasma and CSF increased with time (refer to Figure 5.9b) consistent with device erosion and subsequent release of AZT from the nanoparticles, supporting sustained AZT release from the multipolymeric device. As nanoparticles are capable of sustained release of the entrapped AZT molecules, they are therefore capable of maintaining therapeutic levels of the drug within the brain, thus decreasing viral load (Rao *et al,* 2008).

Drug concentrations within the CNS obtained from the nanoenabled multipolymeric device was superior to that of the commercially available Retrovir® and will therefore offer superior management of ADC to Retrovir®. The use of nanoparticles to encapsulate AZT as well direct administration of AZT into the CNS is responsible for this. Nanoparticles were formulated with PVA which results in steric hindrance of the nanoparticle, serving to reduce nanoparticle adhesion to macrophage cells. As macrophage cells are responsible for foreign body removal from the brain, the targeting of AZT-loaded nanoparticles to target non-

macrophage brain cells results in prolonged drug release within the brain (Bennewitz and Saltzman, 2009), with a decreased occurenced of systemic toxicity experienced by patient as AZT concentrations within the systemic circulation is significantly reduced.

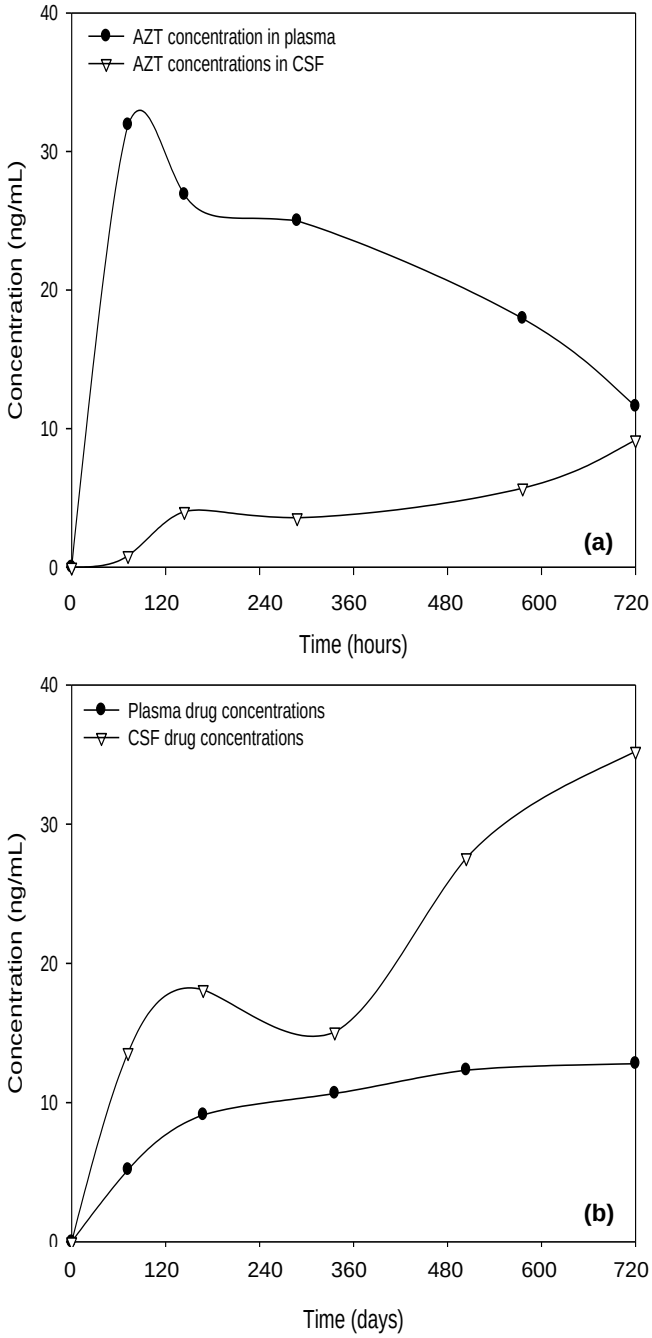

Figure 5.9: *In vivo AZT release in plasma and CSF following (a) IV administration of Retrovir® and (b) implantation of the optimised nanoenabled multipolymeric device (n=3, SD<0.002 in all cases).*

5.4.4 Histomorphological analysis

5.4.4.1 Brain specimens obtained from intravenous administration of Retrovir®

Histological evaluation revealed no neuropathology in brain specimens obtained from the IV administration of AZT (refer to Figure 5.10.1). LFB-H staining exposed no defects in the white and grey matter of the brain. As AZT is routinely used for the management of HIV in the brain, this was expected (Dykstra *et al.,* 1993; Brewster *et al.,* 1995; Giammano *et al*., 1999; Enting *et al.,* 2000; Mishra *et al.,* 2006).

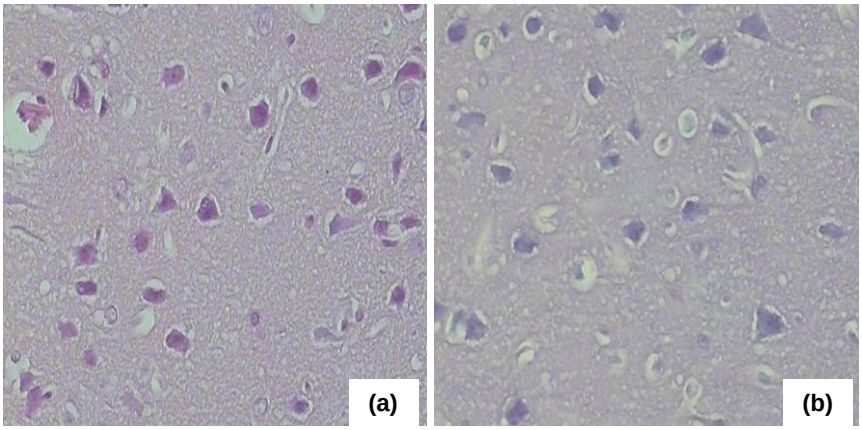

Figure 5.10.1: *Histomorphology of normal brain tissue as revealed on the histographs of rats injected with Retrovir® (a) using the H&E staining technique and (b) using the LFB –H stain.*

5.4.4.2 Brain specimens obtained from the implantation of placebo and AZT-loaded devices

Histomorphological assessment of placebo and AZT-loaded devices revealed no discrepancies occurring due to the presence of the drug as findings from both sets of histology slides were similar. The presence of inflammatory cells and cells involved in the immune cascade can be observed due to the procedure. However, an absence of any ischemic events, infection of the implantation site and hyperaemia resulted from device implantation as observed in Figure 5.10.2.

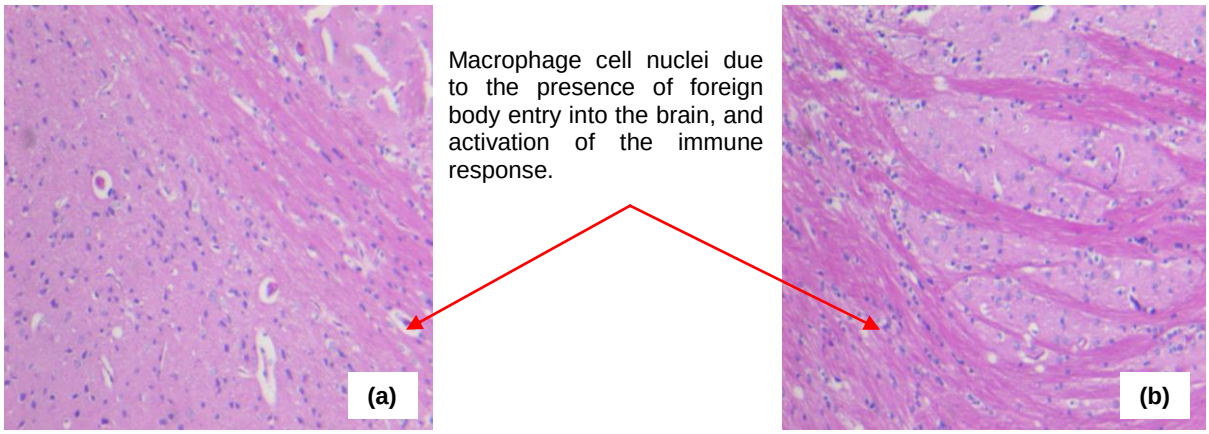

Figure 5.10.2: *Histographs of cerebral tissue following H&E staining (a) 3 days post implantation of the placebo device and (b) 21 days post implantation of the placebo device.*

Day 3: the anterior region of the cerebrum (site of implantation) was sectioned to assess neuroparenchyma responsive to the presence of the multipolymeric implant. Focal areas of encephalomalacia were identified with acute cerebral malacia and neutrophil infiltrates visible as seen in Figure 5.10.3b. The leptomeninges (consisting of the arachnoid mater and pia mater) adjacent to the area of malacia presented with moderate leptomeningitis with lymphocytic round cells predominating, in accordance with the presence of a foreign body in the brain. Minor destruction of the cortical grey matter was observed, with acute inflammation and necrotic material present. Mild dystrophic calcification and status spongiosis was found in the necrotic regions of the parenchyma. Haemorrhage and haemosiderin pigmentation was detected indicating post-surgical bleeding, as noted in Figure 5.10.3a. LFB-H stains revealed an absence of demylination in the neuroparenchyma.

Sections obtained away from the implantation site presented with normal morphology of the neuroparenchyma. Areas adjacent to the site of implantation presented with minimal macrophages and lymphocytic cells.

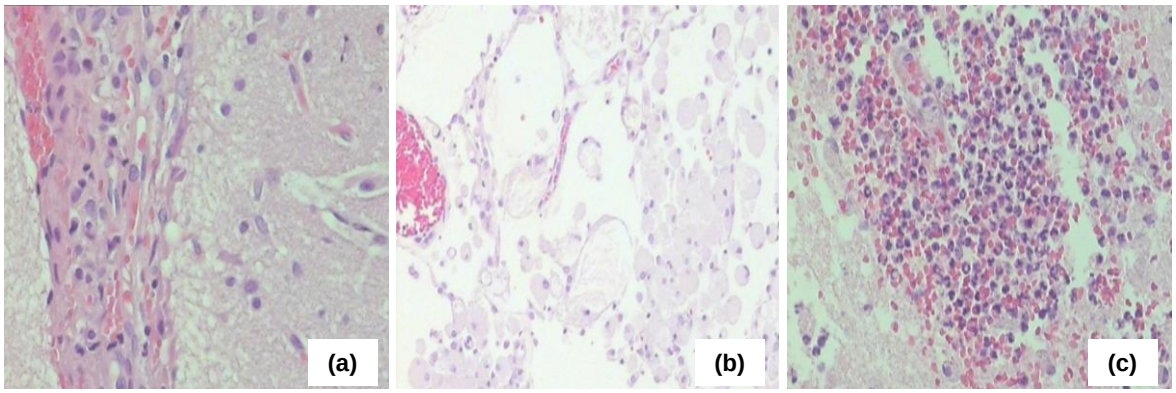

Figure 5.10.3: *Acute hyperaemia was observed on histographs (a) and (b), indicative of post surgical bleeding. (c) Neutrophil and macrophage infiltration was present, indicative of foreign body entry.*

Day 7: focal encephalomalacia with liquefactive necrosis was observed in the anterior cerebrum. Heterophils and macrophages originating from microglia cells with phagocytic material in the cytoplasm were prominent, as seen in Figure 5.10.3c. Foci of dystrophic calcification and minimal inflammation were found in the parenchyma and leptomeninges surrounding the site of implantation. Haemorrhage, haemosiderin pigments and fibrin was also present at the site of implantation.

LFB-H staining revealed focal areas of subacute encephalomalacia resulting from the implant, however demylination and axonal death was absent.

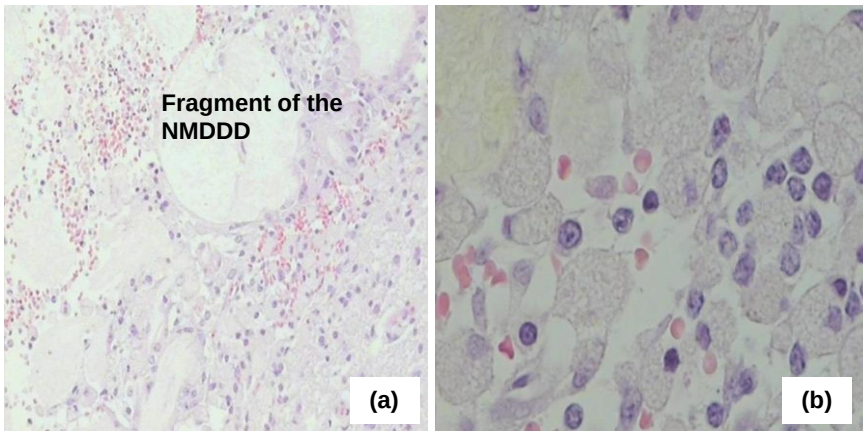

Figure 5.10.4: *(a) The multipolymeric implant was clearly observed on the histograph with macrophage and microglia cell infiltration at the site of implantation. (b) Glitter cell infiltration was also observed at the implantation site.*

Day 14: focal areas of liquefactive necrosis with moderate microglial phagocytic cells were present in the parenchyma. Multiple dystrophic calcified foci were found with necrotic tissue containing small fragments of the multipolymeric implant as seen in Figure 5.10.4a. Debris is

therefore still visible in the encephalomalacia. Minimal inflammation was detected in the neuroparenchyma and leptomeninges.

Findings from the LFB-H stain were as observed on day 7 above.

Day 21: a focal region of malacia with numerous microglial macrophages containing a granular cytoplasm due to phagocytosis of necrotic brain material was seen in the cerebral cortex. Few multinucleated cells with minimal inflammatory infiltrates were observed in the leptomeninges. Some microglial macrophages and necrotic proteinaceous eosinophilic material was visible at sites near the implant, attributed to fragments of the multipolymeric device present in the cerebrum, refer to Figure 5.10.5b.

Findings from the LFB-H stain were as observed on day 7 above.

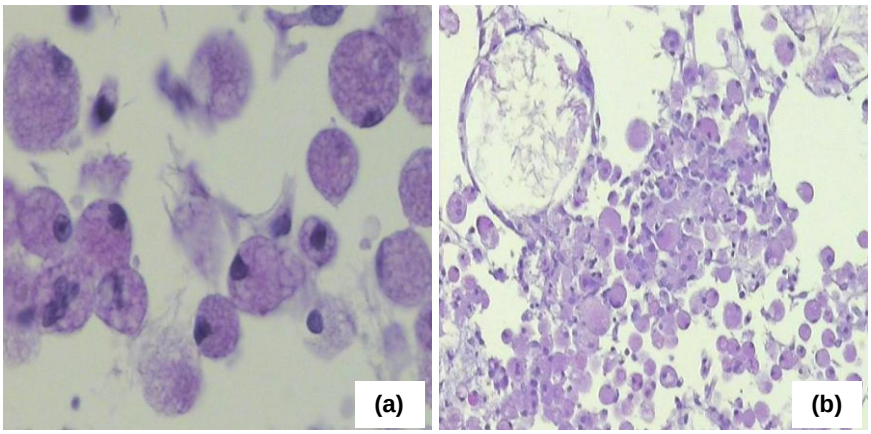

Figure 5.10.5: *LFH-B stains revealed (a) giltter cell infiltration attributed to the presence of necrotic tissue resulting from the erosion of the device. (b) Debri and subsequent phagocytosis due to device erosion was revealed with LFH-B staining.*

Day 30: sectioning of the anterior cerebrum revealed a focal area consistent with polymer tissue destruction indicating erosion of the device as observed in Figure 5.10.6. Macrophages, multinucleated cells and proteinaceous material were identified in this region. Microglial macrophages with some haemosiderin pigments within were observed in the cerebrum close to the site of implantation in the absence of inflammation. Leptomeninges appeared normal.

Findings from the LFB-H stain were as observed on day 7 above.

Histomorphological analysis supported biocompatibility of the multipolymeric device, negating later removal of the device post implantation.

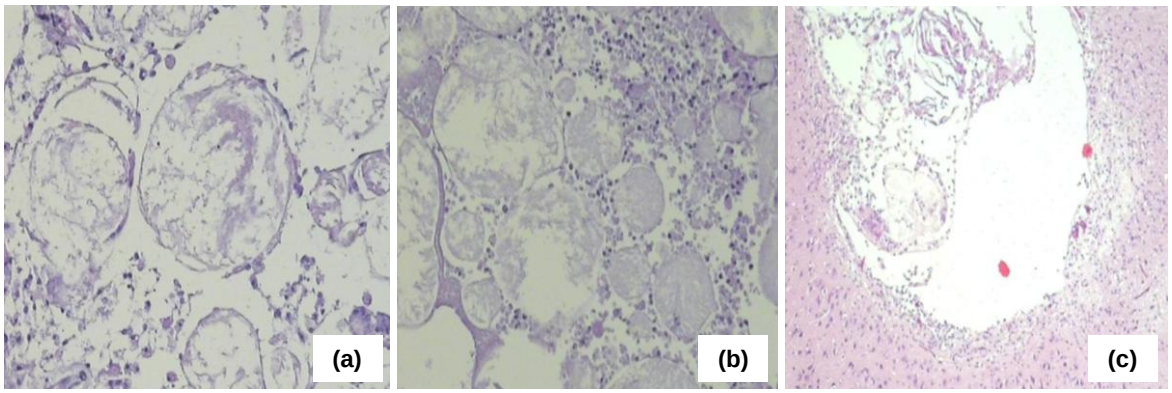

Figure 5.10.6: *Device erosion and subsequent phagocytosis of the foreign material was observed on micrographs (a) and (b). (c) Subsequent nerve tissue damage was noted.*

5.5 Concluding Remarks

In vivo studies were employed to correlate results obtained from performed *in vitro* studies, serving to ascertain device erosion and subsequent drug release within the brain. In vivo analysis also served to assess device safety and toxicity within the brain.

The surgical procedure employed for device implantation was successfully implemented, ascertained by the lack of morbidity exhibited by the animals post surgery. Recovery was quick and efficient with an absence of infection and motor adverse effects observed.

Bioerosion of the multipolymeric device was calculated to be 14.14% 30days post implantation. Slow erosion of the device with subsequent slow release of nanoparticles accounted for drug release from the nanoenabled multipolymeric device being superior to that of the commercially available Retrovir®, 35.225ng/mL (30days post implantation) as compared to 9.1796ng/mL (30hours post IV administration) as observed in CSF. This indicated suitability of the device for the management of ADC. Plasma drug concentrations obtained with the implantable device (12.793ng/mL 30days post implantation) were less than that obtained with the IV formulation (31.923ng/mL 3hours post IV administration), supporting distribution of AZT within the CNS, with drug concentrations in the plasma post implantation thought to be due to AZT elimination from the CNS.

Tissue distribution of AZT within brain tissue is minimal following systemic administration (Dystra *et al.,* 1993; Brewster *et al.,* 1995; Mandal and Tenjarla, 1996), incorporation of AZT within nanoparticles will allow for an increase in the distribution of the drug within the CNS due to the small size range of the nanoparticles prepared (68.04d.nm) and the negative potential of -10.61mV attained, allowing ease of entry into the brain tissue and interstitial fluid.

Histomorphological analysis revealed minimal inflammation at the site of implantation which decreased with time. Neural apoptosis was not present post surgery, revealed by LFB-H staining of brain tissue, supporting biocompatibility of the multipolymeric device. Leptomeningitis was seen at the site of implantation and the immune response was elicited, observed by the infiltration of machrophages and lymphocytes, due to the introduction of a foreign body within the CNS (Rocha and Tanchot, 2004). However, this too was observed to decrease with time. Histomorphology of brain samples obtained following IV administration of AZT presented with normal brain tissue with no inflammation or neural damage observed, supporting the safety of AZT for the treatment of HIV-1 infection of the CNS.

Active influx transporters are found on lymphocytes and $CD4^+$ T-cells and are thought to aid the entry of antiretrovirals, including AZT into the brain and into HIV-1 infected cells within the CNS (Varatharajan and Thomas, 2009). The use of nanoparticles to transport AZT into the CNS, with subsequent drug release as the nanoparticles erode, would serve to protect AZT from efflux out of the CNS by means of active efflux transporters. The implantation of a nanoenabled multipolymeric scaffold into the brain would serve as a drug reservoir within the CNS with the management of ADC significantly enhanced due to site-specific delivery therapeutically effective concentrations of AZT. Sustained drug release of AZT results with the use of biodegradable polymers exhibiting slow in vivo degradation (Popovic and Brundin, 2006).

Implantation of a nanoenabled multipolymeric PCL-ECL-CAP device within the CNS has proved to be successful within satisfactory distribution of AZT within CSF being obtained. In vivo studies in larger animal models, an example being monkeys, will provide greater insight into tissue distribution of AZT within the brain and will therefore be considered for later studies.

CHAPTER 6

Concluding Remarks

6.1 Challenges

Challenges faced during the study focused mainly on the preparation of the polymer scaffold. Carboxymethyl cellulose (NaCMC)-epsilon caprolactone (ECL)-poly ethylene oxide (PEO) scaffolds were first prepared by means of crosslinking the polymer solution with a calcium chloride-sodium thiosulphate-zinc chloride ($CaCl_2$-$Na_2S_2O_4$-ZnCl) salt solution. These scaffolds demonstrated a high degree of swelling, causing the polymer matrix to erode at a more rapid rate than polycaprolactone (PCL)-epsilon caprolactone (ECL)-cellulose acetate phlatate (CAP) scaffolds after exposure to PBS due to excess water intake. Further efforts are required to optimise crosslinking of these polymer solutions to ensure formulation of a device capable of drug release over extended periods.

A stable nanoparticle suspension was prepared however, further effort is required to enhance the stability (expressed as the zeta potential) of the colloidal system. As the nanoparticles are dispersed within a multipolymeric device which prevents agglomeration, zeta potential is of little importance. Optimisation of the formulation stability will enable administration of drug-loaded nanoparticle in the absence of a polymeric scaffold, further reducing the costs.

6.2 Recommendations

Future work will focus on applying the zidovudine (AZT)-loaded nano-enabled polymeric device to a human model. Further research is required to optimise the device for human application, ensuring the *in vitro* and *in vivo* results obtained during the study can be correlated to the human model.

In vivo studies using a rat model demonstrated safety and biocompatibility of the nano-enabled polymer device, as well as a successful implantation procedure. However, due to the size of the rat brain (approximately 0.865cm^2), adequate distribution of nanoparticle and AZT throughout the brain was difficult to establish. Adequate drug loading within a device, 0.000354cm^3 in volume, was challenging. A larger animal model, an example of which is a primate model, will provide more accurate data regarding drug release from the polymer

device and distribution of nanoparticles and AZT in the brain. This can then be more accurately correlated to the human model.

Distribution of AZT within the brain has not been explored in this study. This should be considered in future studies with AZT diffusion within the central nervous system (CNS) being the focus. Addition of biomarkers to the nanoparticle formulation, explored previously for stem cell and cancer research, will allow tracking of the nanoparticles throughout the brain by means of immunofluorescence (Suh *et al.,* 2009). It can then be determined whether nanoparticle distribution is localised to the brain or if it distributed systemically following implantation into the brain. Nanotechnology has the potential to trace and detect brain pathology, with enhanced specificity obtained by the ability of nanostructures to cross the BBB and to distribute within the brain tissue. This can be achieved by the coupling of the device with quantum dots, enabling imaging of the AIDS dementia complex (ADC) affected brain tissue and the progress made resulting from AZT therapy, as quantum dots exhibit a low photodegradation rate, enabling imaging over extended periods (Bailey *et al.*, 2004; Gommersall *et al.*, 2007).

ADC related cerebral injury is worsened by aging, increasing cognitive impairment experienced by patients, as both conditions reduce similar metabolites in the brain, the N-acetyl methyl group (NA), being of most significance (Chang *et al.*, 2004). Formulation of a combined AZT- anti-dementia drug implant can therefore be explored as it will prove beneficial in the treatment of ADC in geriatric patients. As ADC does not exist in isolation, a combination of other drugs applicable to HIV related CNS conditions, such as antibiotic, steroid and antifungal agents, can be coupled with AZT for the management of ADC as well as other HIV related neurological conditions. A combination of fast release and slow release nanoparticles can be considered for this.

As the device is intended for application in a multitude of neurodegenerative disorders, drug loading of various neurotherapeutics within the device will enable more efficient management of CNS conditions. As the development and implementation of new neurotherapeutics is limited by drug penetration into the CNS due to size and pharmacokinetic parameters, the use of nanoparticles bypasses this obstacle with potentially gorund breaking discoveries occurring by tailoring the size of therapeutic agents to the nanosize range (Gommersall *et al*., 2007; das Neves *et al*., 2009; Suh *et al.,* 2009).

6.3 Conclusions

The past year has heralded a significant increase in the research and development of novel drug delivery devices capable of controlled and sustained delivery of drug site specifically. However, poor pharmacokinetic parameters, drug solubility and the limitations posed by this, in vivo stability and toxicity have limited the advances made by drug formulation scientists. The era of nanotechnology promises to change this with the design and development of nanoenabled devices capable of overcoming the concerns and challenges previously encountered by scientists (Ravichandran, 2004). To date numerous advances have been made in the field of nanomedicine, with the potential to transform the practice of medicine. Drug delivery and diagnostics by means of in vivo imaging have been the current market leaders, focused mainly in the area of cancer therapy, with it being estimated that in the next five years, the market for nanoenabled drug delivery devices will reach $200 billion US dollars. The novelty offered by nanotechnology to existing products when formulated using nanosystems, coupled to patent extensions and higher profit margins obtained, this target will effortlessly be visualized (Ravichandran, 2004; Majuru and Oyewumi, 2009).

Research shows that one in 10 drugs currently on the market and 95% of potentially marketable therapeutic agents exhibits pharmacokinetic and biopharmaceutical issues due to poor solubility, with drug accessibility into the CNS limiting the development of neuropharmaceutical products (Koo *et al.*, 2005; Lemaire and Desrayaud, 2005; Majuru and Oyewumi, 2009). The BBB hinders the efficacy of the majority of pharmaceutical products developed and marketed for neurological disorders (Bodor and Buchwald 1999; Lemaire and Desrayaud 2005; das Neves *et al.,* 2009). A drug delivery device with predictable and stable pharmacokinetic and pharmacodynamic parameters therefore has potential for several applications, as was prepared in this study. The use of nanotechnology allows for the delivery of lipophilic drug molecules due to altered pharmacochemical parameters occurring with the preparation of the drug in the nano-size scale (das Neves *et al.*, 2009; Suh *et al.,* 2009). The device can be used to treat chronic diseases, such as Alzheimer's disease and other neurodegenerative conditions, as well as systemic HIV infection by means of implantation of the device at varying sites in the body.

Despite the invasive nature of the procedure involved in the administration of the nanoenabled multipolymeric implants into the brain, the device still has potential to transform the management of ADC due to the controlled and sustained delivery of AZT over months to a year. This will enable the administration of lower drug concentrations, less frequent dosing intervals and will minimise the incidence of adverse effects experienced, all serving to

enhance drug therapy (Prokai *et al.*, 2000). Once off implantation of the device in the absence of later removal makes the nanoenabled multipolymeric device preferable to non-biodegradable implants previously developed for the brain delivery of drug molecules (Pardridge 1995). Nanoparticles will also enable superior drug distribution within the CNS due to the small size of the particles, and therefore will facilitate efficient suppression of viral loads within the brain (Modi *et al.*, 2009; Muthu *et al.*, 2009; Suh *et al.*, 2009).

It has been reported that approximately 90% of HIV infected individuals will eventually develop CNS manifestation of the virus (Sakaie and Gonzalez, 1999). Dementia affects approximately 24 million people worldwide (Modi *et al.*, 2009). Adequate drug concentrations within the CNS are necessary to combat this. Drug delivery into the CNS as well as the development of new therapeutic agents capable of managing neurodegenerative conditions is currently impede by the limited penetration of drug into the brain (Lemaire and Desrayaud 2005). Nanotechnology, a rapidly expanding technology, can potentially surmount these barrier to CNS drug delivery, with the implementation of a multidisciplinary approach, consisting of pharmaceutical scientists, doctors and neuroscientists, required for advances in the field of nanoenabled CNS drug delivery to be achieved (Koo *et al.*, 2005; Modi *et al.*, 2009).

REFERENCES

1. Abbah S.A Lam C.X.L, Hutmacher D.W, Goh J.C.H and Wong H, Biological performance of a polycaprolactone-based scaffold used as fusion cage device in a large animal model of spinal reconstructive surgery, **(Biomaterials), 30,** (2009), pp. 5086-5093.
2. Abdel-Rehim H.A, Yoshii F and Kume T, Modification of polycaprolactone in the presense of polyfunctional monomers by irradiation and its biodegradability, **(Polymer Degradation and Stability), 85,** (2004), pp. 689-695.
3. Abdelwahed W, Degobert G and Fessi H, A pilot study of freeze drying of poly(epsilon-caprolactone) nanocapsules stabilized by poly(vinyl alcohol): Formulation and process optimisation, **(International Journal of Pharmaceutics), 309,** (2006), pp. 178-188.
4. Agarwal D, Chakravarty J, Chaube L, Rai M, Agrawal N.R, Sundar S, High incidence of zidovudine induced anaemia in HIV infected patients in eastern India, **(The Indian Journal of Medical Research),** (2010), pp. 386-389.
5. Ahmad S, Nanotechnology in Drug Delivery: Introduction and recent developments, **(The Internet Journal of Nanotechnology), 2,** (2007).
6. Ahmed A.E, Jacob S, Loh J.P, Samra J.K, Nokta M and Pollard R.B, Comparative disposition and whole-body autoradiographic distribution of [2-^{14}C]azidothymidine and [2-^{14}C]thymidine in mice, **(Journal of Pharmacology and Experimental Therapeutics), 257,** (1991), pp. 479–486.
7. Ajima K, Yudasaka M, Murakami T, Maigne A, Shiba K and Iijimat S, Carbon nanohorns as anticancer drug carriers, **(Molecular Pharmaceutics), 2,** (2005), pp. 475-480.
8. Akhtar L.N, Qin H, Muldowney M.T, Yanagisawa L.L, Kutsch O, Clements J.E, Benveniste E.N, Suppressor of cytokine signaling 3 inhibits antiviral IFN-{beta} signaling to enhance HIV-1 replication in macrophages, **(Journal of Immunology), 185,** 2010, pp. 2393-2404.
9. Alavijeh M.S, Chishty M, Qaiser M.Z and Palmer A.M, Drug Metabolism and Pharmacokinetics, the Blood-Brain Barrier, and Central Nervous System Drug Discovery, **(The Journal of the American Society for Experimental NeuroTherapeutics), 2,** (2005), pp. 554-571.
10. Allan Macnab K, Gill M.J, Sutherland L.R, Murphy A and Brant R, Zidovudine absorption and small intestine function in HIV seropositive patients, **(Journal of Antimicrobial Chemotherapy, 37,** (1996), pp. 825-829.

11. Altekar M, Homon C.A, Kashem M.A, Mason S.W, Nelson R.M, Patnude L.A, Yingling J and Taylor P.B, Assay optimisation: A statistical design of experiments approach, **(Journal of the Association for Laboratory Automation), 11,** (2006), pp. 33-41.
12. Ananworanich J, Introduction to antiretroviral therapy, (Search Regional HIV/AIDS Training), 2007.
13. Anderson P.L, Rower J.E, Zidovudine and lamivudine for HIV infection, **(Clinical Medicine Reviews in Therapeutics),** (2010), Article in Press.
14. Annadurai G and Sheeja R.Y, Use of Box-Behnken design of experiments for the absorption of verofix red using biopolymer, **(Bioprocess and Biosystems Engineering), 18,** (1998), pp. 468-466.
15. Antinori A, Arendt G, Becker JT, Brew BJ, Byrd DA, Cherner M, Clifford DB, Cinque P, Epstein LG, Goodkin K, Gisslen M, Grant I, Heaton RK, Joseph J, Marder K, Marra CM, McArthur JC, Nunn M, Price Rw, Pulliam L, Robertson KR, Sacktor N, Valcour V, Wojna VE, Updated research nosology for HIV-associated neurocognitive disorders, **(Neurology), 69,** (2007), pp. 1789-1799.
16. Aulton ME, Cole G, Hogan J, Pharmaceutical Coating Technology, Taylor and Francis, London, Brighton, Basingstoke, Abingdon, UK. 1995.
17. Aungst B.J, P-glycoprotein, secretory transport, and other barriers to the oral delivery of anti-HIV drugs, **(Advanced Drug Delivery Reviews), 39,** (1999), pp. 105-116.
18. AVERT Averting HIV and AIDS, **www.avert.org/aids-drugs-table.htm,** (accessed on 21/06/2010).
19. Avison M.J, Nath A and Berger J.R, Understanding pathogenesis and treatment of HIV dementia: A role for magnetic resonance, **(Trends in Neurosciences), 25,** (2002), pp. 468-473.
20. Badri M, Maartens G, Mandalia S, Bekker L, Penrod J.R, Platt R.W, Wood R and Beck E.J, Cost-Effectiveness of Highly Active Antiretroviral Therapy in South Africa, **(PLoS Medicine), 3,** (2006).
21. Bailey R.E, Smith A.M and Nie S, Quantum dots in biology and medicine, **(Physica E: Low-Dimensional Systems and Nanostructures), 25,** (2004), pp. 1-12.
22. Bajpai S.K and Sharma S, Investigation of swelling/degradation behaviour of alginate beads crosslinked with $Ca2^{+}$ and $Ba2^{+}$ ions, **(Reactive and Functional Polymers), 59,** (2004), pp. 129-140.
23. Ballou B, Lagerholm B, Ernst L, Bruchez M and Waggoner A, Noninvasive imaging of quantum dots in mice, **(Bioconjugate Chemistry), 15,** (2004), pp. 79-86.
24. Bawa R, Patents and nanomedicine, **(Nanomedicine), 2,** (2007), pp. 351-374.

25. Bean B, Antiviral therapy: Current concepts and practices, **(Clinical Microbiology Review), 5,** (1992), pp. 146-182.
26. Beblo S, Allmendinger J, Pfäffle R, Strehlau J, Schulz M, Wintergerst U, Schuster V, Kiess W, Merkenschlager A, Addison's disease and severe encephalopathy in an infant with HIV infection, **(Journal of Pediatriatric Endocrinology and Metabolism), 23,** (2010), pp. 297-302.
27. Bender A, Schafer V, Steffan A, Royer C, Kreuter J, Rubsamen-Waigmann H and von Briesen H.V, Inhibition of HIV in vitro by antiviral drug-targeting using nanoparticles, **(Respiratory Virology), 145,** (1994), pp. 215–220.
28. Bender A, von Briesen H, Kreuter J, Duncan I.B and Rubsamen-Waigmann H, Efficiency of nanoparticles as carrier system for antiviral agents in human immunodeficiency virus-infected human monocytes/macrophages in vitro, **(Antimicrobial Agents Chemotherapy), 40,** (1996), pp. 1467–1471.
29. Bennewitz MF and Saltzman WM, Nanotechnology for Delivery of Drugs to the Brain for Epilepsy, **(Nanotherapeutics: The Journal of the American Society for Experimental Neurotherapeutics), 6,** (2009), pp. 323-336.
30. Berchard S.R, Levy L and Clas S, Thermal, mechanical and functional properties of cellulose acetate phthalate (CAP) coating obtained from neutralised aqueous solutions, **(Internal Journal of Pharmaceutics), 114,** (1995), pp. 205-213.
31. Bezy V, Morin P, Couerbe P, Leleu G and Agrofoglio L, Simultaneous analysis of several antiretroviral nucleosides in rat-plasma by high-performance liquid chromatography with UV using acetic acid/hydroxylamine buffer. Test of this new volatile medium-pH for HPLC –ESI-MS/MS, **(Journal of Chromatography B), 821,** (2005), pp. 132-143.
32. Bina M, MedLine Neurology, http://massoudbina.com/neurodisorders/BrainAnatomy.php, (accessed on 24/07/2010).
33. Biswal D.R and Singh R.P, Characterisation of carboxymethyl cellulose and polyacrylamide graft copolymer, **(Carbohydrate Polymers), 57,** (2004), pp. 379-387.
34. Bodor N and Buchwald P, Recent advances in the brain targeting of neuropharmaceuticals by chemical delivery systems, **(Advanced Drug Delivery Reviews), 36,** (1999), pp. 229-254.
35. Bourges J.L Bloquel C, Thomas A, Froussart F, Bochot A, Azan F, Gurny R, Benezra D and Behar-Cohen F, Intraoccular implants for extended drug delivery: Therapeutic applications, **(Advanced Drug Delivery Reviews: Ocular Drug Delivery), 58,** (2006), pp. 1182-1202.

36. Bouwer M, AIDS Dementia Complex, **(Bulletin of Experimental Treatment for AIDS),** (1996).
37. Box G, Behnken D, Some new three level designs for thr study of quantitative variables, **(Technometrics), 2,** (1960), pp. 455-475.
38. Brandt C, Nozadze M, Heuchert N, Rattka M, Löscher W, Disease-modifying effects of phenobarbital and the NKCC1 inhibitor bumetanide in the pilocarpine model of temporal lobe epilepsy, **(Journal of Neuroscience), 30,** (2010), pp. 8602-8612.
39. Brewster M.E, Loftsson T, Amselem S, Friedman D, Yogev A, Anderson W.R, Helton D.O, Dinculescu A, Bodor N and Pop E, Formulation development for a zidovudine chemical delivery system:1. Parental dosage forms, **(International Journal of Pharmaceutics, 125,** (1995), pp. 17-30.
40. Brown S.D, Bartlett M.G and White C.A, Pharmacokinetics of intravenous acyclovir, zidovudine and acyclovir-zidovudine in pregnant rats, **(Antimicrobial Agents and Chemotherapy), 47,** (2003), pp. 991-996.
41. Brown J.A, Pack L.R, Fowler J.D, Suo Z, Pre-steady state kinetic analysis of the incorporation of anti-HIV nucleotide analogs catalyzed by human X- and Y-family DNA polymerases, **(Antimicrobial Agents and Chemotherapy),** (2010), Artcicle in Press.
42. Budka H, Neuropathology of Human Immunodeficiency Virus infection, **(Brain Pathology), 1,** (1991), pp.163-175.
43. Cai L and Li X, Stability and hope bifurcation in a delayed model for HIV infection of $CD4^+$ T cells, **(Chaos, Solitons and Fractals), 42,** (2009), pp. 1-11.
44. Cameron D.J, Shaver M.P, Aliphatic polyester polymer stars: synthesis, properties and applications in biomedicine and nanotechnology, **(Chemical Society Reviews),** 2010, Article in Press.
45. Carvalho F.C, Barbi M.S, Sarmento V.H.V, Chiavacci L.A, Netto F.M and Gremiao M.P.D, Surfactant systems for nasal zidovudine delivery: Structural, Rheological and mucoadhesive properties, **(Journal of Pharmacy and Pharmacology), 62,** (2010), pp. 430-439.
46. Chang L, Lee P.L, Yiannoutsos C.T, Ernst T, Marra C.M, Richards T, Kolson D, Schifitto G, Jarvik J.G, Miller E.N, Lenkinski R, Gonzalez G, Navia B.A, and HIV MRS Consortium, A Multicenter in vivo proton-MRS study of HIV-associated dementia and its relationship to age**, (NeuroImage), 23,** (2004), pp.1336-1347.
47. Chang K and Lee Y, Ring-opening polymerisation of Ɛ-caprolactone initiated by the antitumor agent doxifluridine, **(Acta Biomaterialia), 5,** (2009), pp. 1075-1081.
48. Cihlar T and Ray A.S, Nucleoside and nucleotide HIV reverse transcriptase inhibitors: 25 years after zidovudine, **(Antiviral Research, Twenty-five Years of**

Antiretroviral Drug Development: Progress and Prospects), 85, (2010), pp. 39-58.

49. Ciofani G, Raffa V, Pizzorusso T, Monciassi A and Dario P, Characterisation of an alginate-based drug delivery system for neurological application, **(Medical Engineering and Physics), 30, Issue 7,** (2008), pp. 848-855.
50. Clavel F and Hance A.J, HIV drug resistance, **(The New England Journal of Medicine), 350, No.10,** (2004), pp. 1023-1035.
51. Cook-Easterwood J, Middaugh L.D, Griffin W.C, Khan I, Tyor W.R, Highly active antiretroviral therapy of cognitive dysfunction and neuronal abnormalities in SCID mice with HIV encephalitis, **(Experimental Neurology), 205, Issue 2,** (2007), pp. 506-512.
52. Costa F.O, Sousa J.J.S ,Pais A.A.C.C and Formosinho S.J, Comparison of dissolution profiles of ibuprofen pellets, **(Journal of Controlled Release), 89, Issue 2,** (2003), pp. 199-212.
53. Crowley M.M, Zhang F, Koleng J.J and McGinity J.W, Stability of polyethylene oxide in matrix tablets prepared by hot-melt extrusion, **(Biomaterials), 23,** (2002), pp. 4241-4248.
54. Crowley M.M, Fredersdorf A, Schroeder B, Kucera S, Prodduturi S, Repka M.A, McGinity J.W, The influence of guaifenesin and ketoprofen on the properties of hot-melt extruded polyethylene oxide films, **(European Journal of Pharmaceutical Sciences), 22,** (2004), pp. 409-418.
55. Cysique L.A.J, Maruff P, Darby D and Brew B.J, The assessment of cognitive function in advanced HIV-1 infection and AIDS Dementia Complex using a new computerised cognitive test battery, **(Archives of Clinical Neuropsychology), 21,** (2006), pp. 185-194.
56. Dahan B, Levi S, Luccardini C, Rostaing P, Riveau B and Triller A, Diffusion dynamincs of glycine receptors revealed by single-quantum dot trackers, **(Science (New York)), 302,** (2003), pp. 442-445.
57. Dallas S, Read S.E, King S, Koren G and Bendayan R, Pharmacokinetic interaction between zidovudine and trimethoprim/sulphamethoxazole in HIV-1 infected children, **(The Canadian Journal of Infectious Disease), 11, Issue 5,** (2000), pp. 254-258.
58. Danesi R, Falcone A, Conte P.F and Del Tacca M, Pharmacokinetic optimisation of the treatment of cancer with high dose zidovudine, **(Journal of Clinical Pharmacokinetics), 34,** (1998), pp. 173-180.
59. das Neves J, Amiji M.M, Fernanda Bahia M and Sarmento B, Nanotechnology-based systems for the treatment and prevention of HIV/AIDS, **(Advanced Drug Delivery Reviews), Article in Presss,** (2009).

60. Dean JA, The Analytical Chemistry Handbook, New York, McGraw Hill Inc, (1995), pp.15.1-15.5.
61. Don T, Huang M, Chiu A, Kuo K, Chiu W and Chiu L, Preparation of thermo-responsive acrylic hydrogels useful for the application in transdermal drug delivery systems, **(Materials Chemistry and Physics), 107, Issue 2-3,** (2008), pp. 266-273.
62. Douglas K.L, Piccirillo C.A and Tabrizian M, Effects of alginate inclusion on the vector properties of chitosan-based nanoparticles, **(Journal of Controlled Release), 115, Issue 3,** (2006), pp. 354-361.
63. Du Toit L.C, Pillay V, Choonara Y, Pillay S and Harilall S, Patenting of nanoparticles in drug delivery: No small issue, **(Recent Patents on Drug Delivery and Formulations), 1, Number 2,** (2007), pp. 131-142.
64. Duarte A.R.C, Costa M.S, Simplício A.L, Cardoso M.M and Duarte C.M.M, Preparation of controlled release microspheres using supercritical fluid technology for delivery of anti-inflammatory drugs, **(International Journal of Pharmaceutics), 308,** (2006), pp. 168-174.
65. Dubey S.K, Tomar M.S, Patni A.K, Khuroo A, Reyar S and Monif T, Rapid, sensitive and validated ultra-performance liquid chromatography/mass spectrometric method for the determination of fenofibric acid and its application to human pharmacokinetic study, **(E-Journal of Chemistry), 7, Number 1,** (2010), pp. 25-36.
66. Dunge A, Sharda N, Singh B and Singh S, Validated specific HPLC method for determination of zidovudine during stability studies, **(Journal of Pharmaceutical and Biomedical Analysis), 37,** Issue 5, 2005), pp. 1109-1114.
67. Dykstra K.H, Arya A, Arriola D.M, Bungay P.M, Morrison P.F and Dedrick R.L, Microdialysis study of zidovudine (AZT) transport in rat brain, **(The Journal of Pharmacology and Experimental Therapeutics), 267, Number 3,** (1993), pp. 1227-1236.
68. Enting R.H, Foudraine N.A, Lange J.M.A, Jurriaans S, van der Poll T, Weverling G and Portegies P, Cerebrospinal fluid β2-microglobulin, monocyte chemotatic protein-1, and soluble tumor necrosis factor α-receptors before and after treatment with lamivudine plus zidovudine or stavudine, **(Journal of Neuroimmunology), 102,** (2000), pp. 216-221.
69. Epstein L.G et al. Expression of HIV in CSE of children with progressive encephalopathy, **(Annals of Neurology), 21,** 1987, pp. 397-401.
70. Feijen J, Grijpma D.W and Zhang Z, Poly(trimethylene carbonate) and monomethoxy poly(ethylene glycol)-*block*-poly(trimethylene carbonate) nanoparticles for the controlled release of dexamethasone, **(Journal of Controlled Release)**, (2005).

71. Fernandes S.P, Edwards T.M, Ng K.T and Robinson S.R, HIV-1 protein gp 120 rapidly impairs memory in chicks by interrupting the glutamate-glutamine cycle, **(Neurobiology of Learning and Memory),** (2006).
72. Fiandaca M.S, Forsayeth J.R, Dickinson P.J and Bankiewicz K.S, Image-guided convection-enhanced delivery platform in the treatment of neurological diseases, **(Neurotherapeutics), 5,** (2008), pp. 123-127.
73. Fischl M.A, Richman D.D, Grieco M.H, Gottlieb M.S, Volberding P.A, Laskin O.L, Leedom J.M, Groopman J.E, Mildvan D, Schooley R.T, Jackson G.G, Durack D.T and King D, The efficacy of azidothmidine (AZT) in the treatment of patients with AIDS and AIDS-related complex: a double-blind placebo controlled trial, **(New England Journal of Medicine), 317,** (1987), pp. 185-191.
74. Foudraine N.A, Hoetelmans R, Lange J, de Wolf F, van Benthem B, Maas J, Keet I and Portegies P, Cerebrospinal fluid HIV-1 RNA and drug concentrations after treatment with lamivudine plus zidovudine or stavudine, **(The Lancet), 351,** (1998), pp. 1547-1551.
75. Fowler M.G, Gable A.R, Lampe M.A, Etima M, Owor M, Perinatal HIV and Its Prevention: Progress Toward an HIV-free Generation, **(Clinics in Perinatology), 37,** (2010), pp. 699-719.
76. Fox E, Bungay P.M, Bacher J, McCully C.L, Dedrick R.L and Balis F.M, Zidovudine concentration in brain extracellular fluid measured by microdialysis: Steady-state and transient results in rhesus monkey, **(Pharmacology and Experimental Therapeutics), 301, Issue 3,** (2002), pp. 1003-1011.
77. Frumkin L, Promising Treatments for AIDS Dementia Complex: Highlights of Neurological Research from the VIII International Conference on AIDS, Amsterdam, July 19-24, 1992, **(Seattle Treatment Education Project: STEP Perspective), 4, Number 3,** (1992).
78. Gabuzda D, Nerve Cell “Suicide” in AIDS Dementia, **(The Harvard Mahoney Neuroscience Institute Letter on the Brain), 5, Number 1,** (1996).
79. Galinsky R.E, Hoesterey B.L and Andeerson B.D, Brain and cerebrospinal fluid uptake of zidovudine (AZT) in rats after intravenous injection, **(Life Sciences), 47,** (1990), pp. 781-788.
80. Gallo J.M, Delivery of anti-HIV nucleosides to the central nervous system, **(Advanced Drug Delivery Reviews), 14, Issues 2-3,** (1994), pp. 199-209.
81. Ganta S, Devalapally H, Shahiwala A and Ajima M, A review of stimuli-responsive nanocarriers for drug and gene delivery, **(Journal of Controlled Release), 126,** (2008), pp. 187-204.

82. Gardner E.R, Dahut W, and Figg W.D, Quantitative determination of total and unbound paclitaxel in human plasma following Abraxane treatment, **(Journal of Chromotography B), 862,** (2008), pp. 213-218.

83. Gelperina S.E, Khalansky A.S, Skidan I.N, Smirnova Z.S, Bobruskin A.I, Severin S.E, Turowski B, Zanella F.E and Kreuter J, Toxicological studies of doxorubicin bound to polysorbate 80-coated poly(butyl cyanoacrylate) nanoparticles in healthy rats and rats with intracranial glioblastoma, **(Toxicology Letters), 126,** (2006), pp. 131–141.

84. Georgieva J.V, Kalicharan D, Couraud P.O, Romero I.A, Weksler B, Hoekstra D, Zuhorn I.S, Surface Characteristics of Nanoparticles Determine Their Intracellular Fate in and Processing by Human Blood-Brain Barrier Endothelial Cells In Vitro, **(Molecular therapy : the journal of the American Society of Gene Therapy),** (2010), Article in Press.

85. Ghaderi S, Ramesh B, Seifalian A.M, Fluorescence nanoparticles "quantum dots" as drug delivery system and their toxicity: a review, **(Journal of Drug Targeting),** (2010), Article in Press.

86. Gillie J.K, Hochlowski J, Arbuckle-Keil G.A, Infrared-spectroscopy, **(Analytical Chemistry Fundamental Reviews), 72,** (2000), pp. 71-79.

87. Ginski M.J and Polli J.E, Prediction of dissolution-absorption relationships from a dissolution/CaCO-2 system, **(International Journal of Pharmaceutics), 177,** (1999), pp. 117-125.

88. Giunta B, Obregon D, Hou H, Zeng J, Sun N, Nikolic V, Ehrhart J, Shytle D, Fernandez F and Tan J, EGCG mitigates neurotoxicity mediated by HIV-1 proteins gp120 and Tat in the presence of IFN-γ: Role of JAK/STAT1 signalling and implications for HIV-associated dementia, **(Brain Research), 1123,** (2006), pp. 216-225.

89. Glavas Dodov M, Calis S, Crcarevska M.S, Geskovski Petrovska V and Goracinov K, Wheat germ agglutinin-conjugated chitosan-Ca-alginate Microparticles for local colon delivery of 5-Fu: Development and in vitro characterisation, **(International Journal of Pharmaceutics), 381, Issue 2,** (2009), pp. 166-175.

90. Gommersall L, Shergill I.S Ahmed H.U, Hayne D, Arya M, Patel H.R.H, Hashizume M and Gill I.S, Nanotechnology and its relevance to the Urologist, **(European Urology), 52,** (2007), pp. 368-375.

91. González-Scarano F and Martín-García J, The neuropathogenesis of AIDS, **(Nature Reviews, Immunology) 5,** (2005), pp. 69–81.

92. Guo J, Skinner G.W, Harcum W.W and Barnum P.E, Pharmaceutical applications of naturally occurring water-soluble polymers, **(Pharmaceutical Science and Technology Today), 1, Issue 6,** (1998), pp. 254-261.

93. Guttinger M, Fedele D, Koch P, Padrun S, Pralong WF, Brustle O and Boison D, Suppression of Kindled Seizures by Paracrine Adenosine Release from Stem-Cell Derived Brain Implants, **(Epilepsia 46), 8,** (2005), pp. 1162-1169.
94. Harris D, Hermann R, Bawa R, Cleveland J.T and O'Neill S, Stratergies for resolving patent disputes over nanoparticle drug delivery systems, **(Nanotechnology Law and Business), 1,** 2004, pp. 372-390.
95. Hartz A.M, Bauer B, Regulation of ABC transporters at the Blood-Brain Barrier: New targets for CNS therapy, **(Molecular Interventions), 10,** (2010), pp. 293-304.
96. Hawkins M.J, Soon-Shiong P, Desai N, Protein nanoparticles as drug carriers in clinical medicine, **(Advanced drug delivery reviews), 60,** (2008), pp. 876-885.
97. Hedaya M.A and Sawchuk R.J, Effects of probenecid on the renal and non-renal clearance of zidovudine and its distribution into cerebrospinal fluid in rabbit, **(Journal of Pharmaceutical Sciences), 78,** (1989), pp. 716-722.
98. Hennink W.E and van Nostrum C.F, Novel crosslinking methods to design hydrogels, **(Advanced Drug Delivery Reviews), 54,** (2002), pp. 13-36.
99. Hewitt R.G, Morse G.D, Lawrence W.D, Maliszewski S.M.L, Santora J, Bartos L, Bonnem E and Poiesz B, Pharmacokinetics and pharmacodynamics of granulocyte-macrophage colony-stimulating factor and zidovudine in patients with AIDS and sever AIDS-related complex, **(Antimicrobial Agents and Chemotherapy)37, Number 3,** (1993), pp. 512-522.
100. HIV Web Study, http://depts.washington.edu/hivaids/arvres/case3/discussion.html, (accessed on 14/09/2010).
101. Hood E, Nanotechnology: Looking as we leap, **(Environmental Health Perspective), 112, Issue 13,** (2004), pp. 740-749.
102. Hu K, Li J, Shen Y, Lu W, Gao X, Zhang Q and Jiang X, Lactoferrin-conjugated PEG-PLA nanoparticles with omproved brain delivery: In vitro and in vivo evaluation, **(Journal of Controlled Release), 134,** (2009), pp. 55-61.
103. Huang M, Li Sand Vert M, Synthesis and degradation of PLA–PCL–PLA triblock copolymer prepared by successive polymerization of ε-caprolactone and DL-lactide, **(Polymer), 45,** (2004), pp. 8675-8681.
104. Husseini G.A and Pitt W.G, Micelles and nanoparticles for ultrasonic drug and gene delivery, **(Advanced Drug Delivery Reviews), 60, Issue 10,** (2008), pp. 1137-1152.
105. Islam MT, Rodríguez-Hornedo N, Ciotti S and Ackermann C, Fourier Transform Infrared Spectroscopy for the Analysis of Neutralizer-Carbomer and Surfactant-Carbomer Interactions in Aqueous, Hydroalcoholic, and Anhydrous Gel Formulations, **(AAPS Journal), 6,** (2004).

106. Ives N.J, Gazzard B.G and Easterbrook P.J, The Changing Pattern of ADIS-defining Illnesses with the Introduction of Highly Active Antiretroviral Therapy (HAART) in a London Clinic, **(Journal of Infection), 42,** (2001), pp.134-139.

107. Jeong J, Lee J and Cho K, Effects of crystalline microstructure on drug release behaviour of poly(Ɛ-caprolactone) microspheres, **(Journal of Controlled Release), 92, Issue 3,** (2003), pp. 249-258.

108. Juang R.H and Storey D.E, Quantitative determintation of the extent of neutralisation of carboxylic acid functionality in carbopol(R)974P NF by diffuse reflectance fourier transform infrared spectroscopy using Kubelka-Munk function, **(Pharmaceutical Research), 15,** (1998), pp. 1714-1720.

109. Jølck R.I, Feldborg L.N, Andersen S, Moghimi S.M, Andresen T.L, Engineering liposomes and nanoparticles for biological targeting, **(Advances in Biochemical Engineering and Biotechnology),** 2010, Article in Press.

110. Kanmogne G.D, Kuate C.T, Cysique L.A, Fonsah J.Y, Eta S, Doh R, Njamnshi D.M, Nchindap E, Franklin D.R, Ellis R.J, McCutchan J.A, Binam F, Mbanya D, Heaton R.K, Njamnshi A.K, HIV-associated neurocognitive disorders in sub-Saharan Africa: a pilot study in Cameroon, **(BMC Neurology), 10,** (2010), pp. 60.

111. Kato S, Itoh K, Yaoi T, Tozawa T, Yoshikawa Y, Yasui H, Kanamura N, Hoshino A, Manabe N, Yamamoto K, Fushiki S, Organ distribution of quantum dots after intraperitoneal administration, with special reference to area-specific distribution in the brain, **(Nanotechnology), 21,** (2010), pp. 335103.

112. Kaya M, Gulturk S, Elmas I, Kalayci R, Arican N, Kocyildiz Z.C, Kucuk M, Yorulmaz H, Sivas A, The effects of magnesium sulfate on blood-brain barrier disruption caused by intracarotid injection of hyperosmolar mannitol in rats, **(Life Sciences), 76,** (2004), pp. 201-212.

113. Kidane A and Bhatt P.P, Recent advances in small molecule drug delivery, **(Current Opinions in Chemical Biology), 9,** (2005), pp. 347-351.

114. Kim D.M, Tien R, Byrum C, Krishnan K.R.R, Imaging in Acquired Immunodeficiency Syndrome Dementia Complex (AIDS Dementia Complex): A review, **(Progress in Neuro-Psychopharmacology & Biological Psychiatry), 20,** (1996), pp. 349-370.

115. Kimura T, Okuno A, Miyazaki K, Furuzono T, Ohya Y, Ouchi T, Mutsuo S, Yoshizawa H, Kitamura Y, Fujisato T and Kishida A, Novel PVA–DNA nanoparticles prepared by ultra high pressure technology for gene delivery, **(Materials Science and Engineering:C), 24,** 2004, pp. 797-801.

116. Kiragga A.N, Castelnuovo B, Nakanjako D, Manabe Y.C, Baseline severe anaemia should not preclude use of zidovudine in antiretroviral-eligible patients in resource-limited settings, **(Journal of the International AIDS Society), 13,** (2010), pp. 42.

117. Kokai M, Aebischer P and Elmer E, Seizure suppression in kindling epilepsy by intracerebral implants of GABA- but not noradrenaline-releasing polymer matrices, (**Experimental Brain Research), 100,** (1994), pp. 385-394.
118. Koo O.M, Rubinstein I and Onyuksel H, Role of nanotechnology in targeted drug delivery and imaging: A concise review, **(Nanomedicine: Nanotechnology, Biology and Medicine), 1,** (2005), pp. 193-212.
119. Kratz F, Albumin as a drug carrier: Design of prodrugs, drug conjugates and nanoparticles, **(Journal of Controlled Release), 132,** (2008), pp. 171-183.
120. Kuo Y and Chen H, Effect of nanoparticulate polybutylcyanoacrylate and methylmethacrylate–sulfopropylmethacrylate on the permeability of zidovudine and lamivudine across the *in vitro* blood–brain barrier, **(International Journal of Pharmaceutics),** (2006).
121. Kweon H, Yoo M.K, Park I.K, Kim T.H, Lee H.C, Lee H, Oh J, Akaike T and Cho C, A novel degradable polycaprolactone networks for tissue engineering, **(Biomaterials), 24,** (2003), pp. 801-808.
122. Lawrence???
123. Lee J, Kim J.S and Lee H.G, γ-Oryzanol-loaded calcium pectinate microparticles reinforced with chitosan: Optimization and release characteristics, **(Colloids and Surfaces B: Biointerfaces), 70,** (2009), pp. 213-217.
124. Lee R and Yang Y, Synthesis of novel pseudo amino acid/functional Ɛ-caprolactone polyesters and photo-cross-linked networks, **(Polymers), 34,** (2002), pp. 252-2002.
125. Lemaire M and Desrayaud S, The priorities/needs of the pharmaceutical industry in drug delivery to the brain, **(International Congress Series: Drug Transporters and the Diseased Brain), 1277,** (2005), pp. 32-46.
126. Lewis S.R, White C.A and Bartlett M.G, Simultaneous determination of abacavir and zidovudine from rat tissues using HPLC with ultraviolet detection, **(Journal of Chromatography B), 850, Issues 1-2,** (2007), pp. 45-52.
127. Li P, Dai Y, Zhang J, Wang A and Wei Q, Chitosan-Alginate nanoparticles as a novel drug delivery system for nifedipine, **(International Journal of Biomedical Science), 4,** 2008, pp. 221-228.
128. Li T, Shi X, Du Y, Tang Y, Quaternized chitosan/alginate nanoparticles for protein delivery, **(Journal of Biomedical Materials Research Part A),** 2007, pp. 383-390.
129. Lin L.N, Liu Q, Song L, Liu F.F, Sha J.X, Recent advances in nanotechnology based drug delivery to the brain, **Cytotechnology,** (2010), Article in Press.
130. Link D, AIDS Dementia Complex, ***(*The Gay Men's Health Crisis Newsletter of Experimental Therapies), 6, Number 2,** (1992).
131. Link D, AIDS Dementia Complex, **(Treatment Issues), 6, Number 2,** (1992), pp. 4-9.

132. Liu J and Williams R.O, III, Properties of heat-humidity cured cellulose acetate phthalate free films, **(European Journal of Pharmaceutical Sciences), 17,** (2002), pp. 31-41.

133. Liu L.S, Fishman M.L, Hicks K.B and Kende M, Interaction of various pectin formulations with porcine colonic tissues**, (Biomaterials), 26,** (2005), pp. 5907-5916.

134. Liu P, Zhai M, Li J, Peng J and Wu J, Radiation preparation and swelling behaviour of sodium carboxymethyl cellulose hydrogels, **(Radiation Physics and Chemistry), 63,** 2002, pp. 525-528.

135. Liu Z, Jiao Y, Wang Y, Zhou C and Zhang Z, Polysaccharides-based nanoparticles as drug delivery systems, **(Advanced Drug Delivery Reviews), 60,** (2008), pp. 1650-1662.

136. Lobenberg R, Araujo L and Kreuter J, Body Body distribution of azidothymidine bound to nanoparticles after oral administration, **(European Journal of Pharmaceutics and Biopharmaceutics), 44,** (1997), pp. 127–132.

137. Lockman P.R, Oyewumi M.O, koziara J.M. Roder K.E, Mumper R.J and Allen D.D, Brian uptake of thiamine-coated nanoparticles, **(Journal of Controlled Release), 93,** (2003), pp. 271-282.

138. Lotterer E, ruhnke M, Trautmann M, Beyer R and Bauer F.E, Decreased and variable systemic availability od zidovudine in patients with AIDS if administered with a meal, **(European Journal of Clinical Pharmacology), 40,** (1991), pp. 305-308.

139. Luong-Van E, Grondahl L, Ngiap Chua K, Leong K.W, Nurcombe V and Cool S.M, Controlled release of heparin from poly(***ε***-caprolactone) electrospun fibers, **(Biomaterials), 27,** (2006), pp. 2042-2050.

140. Maggi L, Segale L, Torre M.L, Ochoa Machiste E and Conte U, Dissolution behaviour of hydrophilic matrix tablets containing two different polyethylene oxides (PEOs) for the controlled release of a water-soluble drug. Dimensionality study, **(Biomaterials), 23,** (2002), pp. 1113-1119.

141. Majuru S and Oyewumi M.O, Nanotechnology in drug development and life cycle management, (Biotechnology: Pharmaceutical Aspects), Springer , New York, USA, (2009).

142. Mandal T.K and Tenjarla S, Preparation of biodegradable microcapsules of zidovudine using solvent evaporation: Effect of the modification of aqueous phase, **(International Journal of Pharmaceutics), 137,** (1996), pp. 187-197.

143. Martín-García J, Cao W, Varela-Rohena A, Plassmeyer M.L and González-Scarano F, HIV-1 tropism for the central nervous system: Brain derived envelope glycoproteins with lower CD4 dependence and reduced sensitivity to a fusion inhibitor, **(Virology), 346,** (2006), pp. 169-179.

144. McDermott J, Kennedy J, Roderick B, Pegler E and Thomas M.G, Pharmacokinetics of zidovudine plus probenecid, **(The Journal of Infectious Diseases), 166,** (1992), pp.687-688.
145. McKelvy ML, Britt TR, Davis BL, Gillie JK, Graves FB, and Lentz LA, Infrared Spectroscopy, **(Analytical Chemistry), 70,** (1998), pp. 119-178.
146. McKenzie J.L, Waid M.C, Shi R and Webster T.J, Decreased functions of astrocytes on carbon nanofiber materials, **(Biomaterials), 25, Issue 7-8,** (2004), pp. 1309-1317.
147. MedscapeCME, cme.medscape.com/viewarticle/418820, (accessed on 21/06/2010).
148. Melton S.T, Kirkwood, C.K and Ghaemi S.N, Pharmacotherapy of HIV dementia, **(Ann. Pharmacotherapy), 31,** (1997), pp. 457-473.
149. Misra A, Ganesh S, Shahiwala A and Shah S.P, Drug delivery to the central nervous system: A review, **(Journal of Pharmacological and Pharmaceutical Science), 6, Issue 2,** (2003), pp. 252-273.
150. Modi G, Pillay V, Choonara Y.E, Ndesendo V.M.K, du Toit L.C and Naidoo D, Nanotechnological application for the treatment of neurodegenerative disorders, **(Progress in Neurobiology), Article in Press,** (2009).
151. Moebus K, Siepmann J and Bodmeier R, Alginate-poloxamer Microparticles for controlled drug delivery to mucosal tissue, **(European Journal of Pharmaceutics and Biopharmaceutics), 72, Issue 1,** (2009), pp. 42-53.
152. Moore K, Raasch R.H, Brouwer K, Opheim K, Cheeseman S.H, Eyster E, Lemon S.M and van der Horst C.M, Pharmacokinetics and Bioavailability of Zidovudine and Its Glucuronidated Metabolite in Patients with Human Immunodeficiency Virus Infection and Hepatic Disease (AIDS Clinical Trial Group Protocol 062), **(Antimicrobial Agents and Chemotherapy), 39, Number 12,** (1995), pp. 2732-2737.
153. Murray C.B, Kagan C.R, Bawendi M.G, Synthesis and characterisation of monodisperse nanocrystals and close-packed nanocrystal assemblies, **(Annual Review of Materials Research), 30, Issue 1,** (2000), pp. 545-610.
154. Muthu M.S, Rawat M.K, Mishra R and Singh S, PLGA nanoparticle formulations of risperidone: Preparation and neuropharmacological evaluation, **(Nanomedicine: Nanotechnology, Biology and Medicine), 5,** (2009), pp. 323-333.
155. Narishetty STK and Panchagnula R, Transdermal delivery of zidovudine: effects of terpenes and their mechanism of action, **(Journal of Controlled Release), 95,** (2004), pp. 367-379.
156. NATAP National AIDS treatment advocacy project, http://www.natap.org/2003/march/031703_2.htm, (accessed on 21/06/2010).

157. National Department of Health, National Antiretroviral Treatment Guidelines, South Africa, 2004.
158. Neto C.G.T Dantas T.N.C, Fonseca J.L.C and Pereira M.R, Permeability studies in chitosan membranes. Effects of crosslinking and poly(ethylene oxide) addition, **(Carbohydrate Research), 340,** (2005), pp. 2630-2636.
159. Oh S.Y, Jeong S.Y, Park T.G and Lee J.H, Enhanced transdermal delivery of AZT (Zidovudine) using iontophoresis and penetration enhancer, **(Journal of Controlled Release), 51,** 1998, pp. 161-168.
160. Orsega S, Treatment of adult HIV infection: Antiretroviral update and overview, **(The Journal for Nursing Practitioners), 3, Issue 9,** (2007), pp. 612-624.
161. OyaGen Inc., http://www.oyageninc.com/drugs**,** (accessed on 14/092010).
162. Pardridge W.M, Vector-mediated peptide drug delivery to the brain, **(Advanced Drug Delivery Reviews), 15,** (1995), pp. 109-146.
163. Pardridge W.M, The blood-brain barrier: Bottleneck in brain drug development, **(NeuroTherapeutics), 2, Issue 1,** (2005), pp. 3-14.
164. Park J.H, Lee S, Kim J, Park K, Kim K and Kwon I.C, Polymeric nanomedicine for cancer chemotherapy, **(Progress in Polymer Science),** (2007).
165. Park K, Nanotechnology: What it can do for drug delivery, **(Journal of Controlled Release), 120, Issue 1-2,** (2007), pp. 1-3.
166. Parolis L.A.S, van der Merwe R, Groenmeyer G.V and Harris P.J, The influence of metal cations on the behaviour of carboxymethyl cellulose as a talc depressant, **(Colloids and Surfaces A: Physicochemical and Engineering Aspects), 317, Issue 1-3,** (2008), pp. 109-115.
167. Parris G.E, How did the ancestral HIV-1 group M retrovirus get to Leopoldville from southeastern Cameroon, **(Medical Hypotheses), 69,** (2007), pp. 1098-1101.
168. Patarca R, Singh R.P, Durfee T, Freeman G, Blattner F.R and Cantor H, Definition of T-cell specific DNA-binding factors that ineract with a 3'-silencer in the $CD4^+$ T-cell gene Rpt-1, **(Gene), 85,** (1989), pp. 461-469.
169. Pemberton L.A and Brew B.J, Cerebrospinal fluid S-100β and its relationship with AIDS dementia complex, **(Journal of Clinical Virology), 22,** (2001), pp. 249-253.
170. Penedo F.J, Gonzalez J.S, Dahn J.R, Antoni M, Malow R, Costa P and Schneiderman N, Personality, quality of life and HAART adherence among men and women living with HIV/AIDS, **(Journal of Psychosomatic Research), 54,** (2003), pp. 271-278.
171. Perry S.W, Barbieri J, Tong N, Polesskaya O, Pudasaini S, Stout A, Lu R, Kiebala M, Maggirwar S.B, Gelbard H.A, Human immunodeficiency virus-1 Tat activates calpain proteases via the ryanodine receptor to enhance surface dopamine transporter levels

and increase transporter-specific uptake and Vmax, **(The Journal of Neuroscience), 30,** (2010), pp. 14153-64.

172. Pialoux G, Fournier S, Moulignier A, Poveda J.D, Clavel F and Dupont B, Central nervous system as a sanctuary for HIV-1 infection despite treatment with zidovudine, lamivudine and indinavire, **(AIDS), 11,** (1997), pp. 1302-1303.
173. Pillay V and Fassihi R, In vitro release modulation from crosslinked pellets for site-specific drug delivery to the gastrointestinal tract: I. Comparison of pH-responsive drug release and associated kinetics, **(Journal of Controlled Release), 59,** (1999), pp. 229-242.
174. Pippi F, A novel approach to HIV therapy: Highly active antiretroviral therapy and autologous haematopoietic cell transplantation, **(Medical hypotheses),** (2007).
175. Pirzada Y, Khuder S and Donabedian H, Predicting AIDS-related events using CD4 percentage or CD4 absolute counts, **(AIDS Research and Therapy), 3,** (2006).
176. Pison U, Welte T, Giersig M and Groneberg D.A, Nanomedicine for respiratory diseases, **(European Journal of Pharmacology), 533,** (2006), pp. 341-350.
177. Popovic N and Brundin P, Therapeutic potential of controlled drug delivery systems in neurodegenerative diseases, **(International Journal of Pharmaceutics),** (2006).
178. Portegies P Enting, R.H, de Jong M.D, Danner S.A, Reiss P, Goudsmit J, Lange J, AIDS dementia complex and didanosine, **(The Lancet), 344,** (1994).
179. Portegies P, de Gans J, Lange J, Derix M, Speelman H, Bakker M, Danner S and Goudsmit J, Declining incidence of AIDS dementia complex after introduction of zidovudine treatment, **(British Medical Journal), 299,** (1989), pp. 819-821.
180. Prakash K, Narayana Raju P, Shanta Kumari K and Lakshmi Narasu M, Solubility and Dissolution Rate Determination of Different Antiretroviral Drugs in Different pH Media Using UV Visible Spectrophotometer, **(E-Journal of Chemistry), 5,** (2008), pp. 1159-1164.
181. Price R.W, AIDS Dementia Complex, **(HIV InSite Knowledge Base Chapter)**, (1998).
182. Prokai L, Prokai-Tatrai K and Bodor N, Targeting drugs to the brain by redox chemical delivery systems, **(Medical Research Reviews), 20,** (2000), pp. 367-416.
183. Pungor E, A Pratical Guide to Instrumental Analysis, Boca Raton, Florida, (1995), pp. 181-191.
184. Pushpamalar V, Langford S.J, Ahmad M and Lim Y.Y, Optimisation of reaction conditions for preparing carboxymethyl cellulose from sago waste, **(Carbohydrate Polymers), 64,** 2006, pp. 312-318.
185. Puthanakit T, Aurpibul L, Oberdorfer P, Akarathum N, Kanjananit S, Wannarit P, Sirisanthana T,[1] and Sirisanthana V, Hospitalization and mortality among HIV-

infected children after receiving highly active antiretroviral therapy, **(Clinical Infectious Diseases), 44,** (2007), pp. 599–604.

186. Rahman MF, Wang J, Patterson TA, Saini UT, Robinson BL, Newport GD, Murdock RC, Schlager JJ, Hussain SM and Ali SF, Expression of genes related to oxidative stress in the mouse brain after exposure to silver-25 nanoparticles, **(Toxicology Letters), 187,** (2009), pp. 15-21.
187. Rajaonarivony M, Vauthier C, Couarraze G, Puisieux F, Couvreur P, Development of a new drug carrier made from alginate, **(Journal of Pharmaceutical Science), 82,** 1993, pp 912-917.
188. Ramachandran G, Hemanthkuma A.K, Kumaraswami V and Swaminathan S, A simple and rapid liquid chromatography method for simultaneous determination of zidovudine and nevirapine in plasma, **(Journal of Chromatography B),** (2006).
189. Ramautarsing R and Ananworanich J, Generic and low dose antiretroviral therapy in adults and children: implication for scaling up treatment in resource limited settings, **(AIDS Research and Therapy), 7**, (2010).
190. Ramirez S.H, Fan S, Dykstra H, Reichenbach N, Del Valle L, Potula R, Phipps R.P, Maggirwar S.B, Persidsky Y, Dyad of CD40/CD40 ligand fosters neuroinflammation at the blood-brain barrier and is regulated via JNK signaling: implications for HIV-1 encephalitis, **(The Journal of Neuroscience), 30,** (2010), pp. 9454-9464.
191. Rao K.S, Reddy M.K, Horning J.L and Labhasetwar V, TAT-conjugated nanoparticles for the CNS delivery of anti-HIV drugs, **(Biomaterials), 29,** (2008), pp. 4429-4438.
192. Raub T.J, Kuentzel S.L and Sawada G.A, Permeability of bovine brain microvessel endothelial cells in vitro: barrier tightening by a factor released from astroglioma cells, **(Experimental Cell Research), 199,** (1992), pp. 330–340.
193. Ravichandran R, Nanotechnology-based drug delivery systems, **(NanoBioTechnology),** (2009), Article in Press.
194. Reis C.P, Neufeld R.J, Ribeiro A.J and Veiga F, Nanoencapsulation II. Biomedical applications and current status of peptide and protein nanoparticulate delivery systems, (**Nanomedicine: Nanotechnology, Biology and Medicine), 2,** (2006), pp. 53-65.
195. Reshmi G, Kumar P.M and Malathi M, Preparation, characterisation and dielectric studies on carbonyl iron/cellulose acetate hydrogen phthalate core/shell nanoparticles for drug delivery applications, **(International Journal of Pharmaceutics), 365,** (2009), pp. 131-135.
196. Rezwan K, Chen Q.Z, Blaker J.J and Boccaccini A.R, Biodegradable and bioactive porous polymer/inorganic composite scaffolds for bone tissue engineering, **(Biomaterials), 27, Issue 18**, (2006), pp. 3413-3431.

197. Rocha B and Tanchot C, Towards a cellular definition od CD8 T-cell memory: The role of CD4+ T-cells helps in CD8+ T-cell response, **(Current Opinions in Immunology), 16, Issue 3,** (2004), pp. 259-263.

198. Rokhade A.P, Agnihotri S.A, Patil S.A, Mallikarjuna N.N, Kulkarni P.V and Aminabhavi T.M, Semi-interpenetrating polymer network microspheres of gelatin and sodium carboxymethyl cellulose for controlled release of ketorolac tromethamine, **(Carbohydrate Polymers), 65, Issue 3,** (2006), pp. 243-252.

199. Roney C, Kulkarni P, Arora V, Antich P, Bonte F, Wu A, Mallikarjuana N.N, Manohar S, Liang H, Kulkarni A.R, Sung H, Sairam M and Aminabhavi T.M, Targeted nanoparticles for drug delivery through the blood–brain barrier for Alzheimer's disease, **(Journal of Controlled Release), 108,** (2005), pp.193-214.

200. Roonasi P and Holmgren A, An ATR-FTIR study of sulphate sorption on magnetite; rate of adsorption, surface speciation, and effect of calcium ions, **(Journal of Colloidal and Interface Science), 333,** (2009), pp. 27-32.

201. Roumeliotis, 2006, In-Pharma Technologists.com, www.in-pharmatechnologist.com/Materials-Formulation/Abbott-ordains-Elan-to-marry-Tricor-and-Crestor Ahmed 2007, (accessed on 21/06/2010)

202. Routy J.P, Blanc A.P, Rodriguez E, Escoffier M, Joliot Y, Kiegel P, Viallet F and Chardon H, Intrathecal zidovudine for AIDS dementia, **(The Lancet), 336,** (1990), pp. 248.

203. Ruseckaite R.A and Jimenez A, Thermal degradation of mixtures of polycaprolactone with cellulose derivatives, **(Polymer Degradation and Stability), 81,** (2003), pp. 353-358.

204. Sacktor N, The Epidemiology of Human Immunodeficiency Virus-Associated Neurological Disease in the Era of Highly Active Antiretroviral Therapy, **(Journal of Neurovirology), 8,** (2002), pp. 115-121.

205. Sahoo S and Labhasetwar V, Nanotech approaches to drug delivery and imaging, **(Drug Delivery Today), 8,** (2003), pp. 1112-1120.

206. Saito R, Krauze M.T, Bringas J.R, Noble C, McKnight T.R, Jackson P, Wendland M.F, Mamot C, Drummond D.C, Kirpotin D.B, Hong K, Berger M.S, Park J.W and Bankiewicz K.S, Gadolinium-loaded liposomes allow for real-time magnetic resonance imaging of convection-enhanced delivery in the primate brain, **(Experimental Neurology), 196,** (2005), pp. 381-389.

207. Sakaie K.E and Gonzalez R.G, Imaging of NeuroAIDS, **(NeuroAIDS), 2,** (1999).

208. Saksena N.K, Jozwiak R and Wang B, Molecular and biological mechanisms in the development of AIDS dementia complex (ADC), **(Bulletin de l'Institut Pasteur, 96,** (1998), pp. 171-187.

209. Samikkannu T, Rao K.V, Gandhi N, Saxena S.K, Nair M.P, Human immunodeficiency virus type 1 clade B and C Tat differentially induce indoleamine 2,3-dioxygenase and serotonin in immature dendritic cells: Implications for neuroAIDS, **(Journal of Neurovirology),** (2010).
210. Sanli O, Ay N and Isiklan N, Release characteristics of diclofenac sodium from poly(vinyl alcohol)/sodium alginate and poly(vinyl alcohol)-grafted-poly(acrylamide)/sodium alginate beads, **(European Journal of Pharmaceutics and Biopharmaceutics), 65,** (2009), pp. 204-214.
211. Sarmento B, Ferreira D, Veioa F and Ribeiro A, Characterisation of insulin-loaded alginate nanoparticles produced by ionotropic pre-gelation through DSC and FTIR studies, **(Carbohydrate Polymers), 66,** (2006), pp. 1-7.
212. Sarmento B, Ferreira D.C, Jorgensen L and van de Weert M, Probing insulin's secondary structure after entrapment into alginate/chitosan nanoparticles, **(European Journal of Pharmaceutics and Biopharmaceutics), 65,** (2007), pp. 10-17.
213. Sawchuk R.J and Yang Z, Investigation of distribution, transport and uptake of anti-HIV drugs to the central nervous system, **(Advanced Drug Delivery Reviews: Delivery of Anti-HIV Drugs), 39,** 1999, pp. 5-31.
214. Schutzer S.E, Berger J.R and Brunner M, Identification of potential markers in HIV-associated dementia, **(Journal of Neuroimmunology), 157,** (2004), pp. 120-125.
215. Semreen M.H, El-Shorbagi A.N, Al-Tel T.H, Alsalahat I.M, Targeting gamma-Aminobutyric Acid (GABA) Carriers to the Brain: Potential Relevance as Antiepileptic Pro-Drugs, **(Medicinal Chemistry), 6,** (2010), pp. 144-149.
216. Sendil D, Maszczynska Bonney I, Carr D.B, Lipkowski A.W, Wise D.L and Hasirci V, Antinociceptive effects of hydromorphone, bupivacaine and biphalin released from PLGA polymer after intrathecal implantation in rats, **(Biomaterials), 24,** (2003), pp. 1969-1976.
217. Silva G.A, Nanotechnology applications and approaches for neuroregeneration and drug delivery to the central nervous system, **(Annals of the New York Academy of Science), 1199,** (2010), pp. 221-30.
218. Singh B, Dahiya M, Saharan V and Ahujan N, Optimising drug delivery systems using systematic "Design of Experiments" Part II: Retrospect and prospects, **(Critical Reviews in Therapeutic Drug Carrier Systems), 22,** (2005), pp. 215-294.
219. Singh R and Lillard J.W, Nanoparticle-based targeted drug delivery, **(Experimental and Molecular Pathology), Article in Press,** (2009).

220. Sinha V.R, Bansal K, Kaushik R, Kumria R and Trehan A, Poly-Ɛ-caprolactone microspheres and nanospheres: An overview, **(International Journal of Pharmaceutics), 278,** (2004), pp. 1-23.
221. Skoog DA, Holler FJ and Nieman T, Principles of Instrumental Analysis, Fifth Edition, New York, (1998), pp. 905-908.
222. Smit T.K, Brew B.J, Tourtellotte W, Morgello S, Gelman B.B and Saksena N.K, Independent evolution of Human Immunodeficiency Virus (HIV) drug resistance mutations in diverse areas of the brain in HIV-infected patients, with and without dementia, on antiretroviral treatment, **(Journal of Virology), 78,** (2004), pp. 10133-10148.
223. Song Y, Lee J and Lee H.G, α-Tocopherol-loaded Ca-pectinate microcapsules: Optimization, *in vitro* release, and bioavailability, **(Colloids and Surfaces B: Biointerfaces),** (2009).
224. Sriamornsak P, Thirawong N, Weerapol Y, Nunthanid J and Sungthongjeen S, Swelling and erosion of pectin matrix tablets and their impact on drug release behaviour, **(European Journal of Pharmaceutics and Biopharmaceutics), 67, Issue 1,** (2007), pp. 211-219.
225. Statistics South Africa, Causes of death in South Africa 1997-2001: Advance release of recorded causes of death, (2002).
226. Subbiah R, Veerapandian M, Yun K.S, Nanoparticles: Functionalization and multifunctional applications in biomedical sciences, **(Current Medicinal Chemistry),** (2010), Article in Press.
227. Sudhamani S.R, Prasad M.S and Udaya Sankar K, DSC and FTIR studies on gellan and polyvinyl alcohol (PVA) blend films, **(Food Hydrocolloids), 17, Issue 3,** (2003), pp. 245-250.
228. Suh WH, Suslick KS, Stucky GD, and Suh Y, Nanotechnology, nanotoxicology, and neuroscience, **(Progress in Neurobiology), 87,** (2009), pp. 133-170.
229. Suwanpidokkul N, Thongnopnua P and Umprayn K, Transdermal Delivery of Zidovudine (AZT): The Effects of Vehicles, Enhancers, and Polymer Membranes on Permeation Across Pig Skin, **(APPS PharmSciTech), 5, Issue 3, Article 48,** (2004).
230. Suzuki E, High-resolution scanning electron microscopy of immunogold-labelled cells by the use of thin plasma coating of osmium, **(Journal of Microscopy), 208, Issue 3,** (2002), pp. 153-157.
231. Taha M.O, Nasser W, Ardakani A and Al Khatib H.S, Sodium lauryl sulfate impedes drug release from zinc-crosslinked alginate beads: Switching from enteric coating release into biphasic profiles, **(International Journal of Pharmaceutics), 350,** (2008), pp. 291-300.

232. Takka S, Propranolol hydrochloride–anionic polymer binding interaction, **(Il Farmaco), 58,** (2003), pp. 1051-1056.
233. Tamargo RJ, Rossell LA, Kossoff EH, Tyler BM, Ewend MG and Aryanpur JJ, The intracerebral administration of phenytoin using controlled-release polymers reduces experimental seizures in rats, **(Epilepsy Research), 48,** (2002), pp. 145-155.
234. Tarvainen T, Karjalainen T, Malin M, Peräkorri K, Tuominen J, Seppälä J and Järvinen K, Drug release profiles from and degradation of a novel biodegradable polymer 2,2-bis(2-oxazoline) linked poly(ε-caprolactone), **(European Journal of Pharmaceutical Science), 16,** (2002), pp. 323-331.
235. The Project on Emerging Nanotechnologies, www.nanotechproject.org/inventories/medicine/apps, (accessed on 21/06/2010).
236. Thorne RG and Nicholson C, In vivo diffusion analysis with quantum dots and dextrans predicts the width of brain extracellular space, (Proceedings of the National Academy of Science of the United States of America), **103,** (2006), pp. 5567-5572.
237. Thomas N.S and Panchagnula R, Transdermal delivery of zidovudine: effect of vehicles on permeation across rat skin and their mechanism of action, **(European Journal of Pharmaceutical Sciences), 18, Issue 1,** (2003), pp. 71-79.
238. Thomas S.A and Segal M.B, Saturation kinetics, specificity and NBMPR sensitivity of thymidine entry into the central nervous system, **(Brain Research), 760,** (1997), pp. 59-67.
239. Thompson P.M, Dutton R.A, Hayashi K.M, Toga A.W, Lopez O.L, Aizenstein H.J, and Becker J.T, Thinning of the cerebral cortex visualised in HIV/AIDS reflects CD4 T lymphocyte decline, **(PNAS: Early Edition),** (2005).
240. Tilloy S, Monnaert V, Fenart L, Bricout H, Cecchelli R and Monflier E, Methylated β-cyclodextrin as P-gp modulators for deliverance of doxorubicin across an in vitro model of blood-brain barrier, **(Bioorganic and Medicinal Chemistry Letters 6),** (2006), pp. 2154-2157.
241. UNAIDS, AIDS Epidemic Update: December 2006, **(WHO library cataloguing),** (2006).
242. Uslu B, Özkan S.A, Determintion of lamivudine and zidovudine in binary mixtures using first derivative spectrophotometric, first derivatives of the ratio-spectra and high-performance liquid chromatography-UV methods, **(Analytica Chimica Acta), 466, Issue 1,** (2002), pp. 175-185.
243. Uto k, Yamamoto K, Hirase S and Aoyagi T, Temperature-responsive crosslinked poly(Ɛ-caprolactone) membrane that functions near body temperature, **(Journal of Controlled Release), 110,** (2009), pp. 408-413.

244. Valcour V.G, Shikuma C.M, Watters M.R, Sacktor N.C, Cognitive Impairment in older HIV-1 seropositive individuals: prevelance and potential mechanisms, **(AIDS), 18,** (2004), pp. 79-86.

245. Valcour V.G, Shiramizu B.T, Shikuma C.M, HIV DNA in circulating monocytes as a mechanism to dementia and other HIV complications, **(Journal of Leukocyte Biology), 87,** (2010), pp. 621-626.

246. Varatharajan L and Thomas SA, The transport of anti-HIV drugs across the blood-CNS interfaces: Summary of current knowledge and recommendations for further research, **(Antiviral Research),** (2009).

247. Vergoni A.V, Tosi G, Tacchi R, Vandelli M.A, Bertolini A and Costantino L, Nanoparticles as drug delivery agents specific for CNS: In vivo distribution, **(Nanomedicine: Nanotechnology, Biology and Medicine), Article in Press,** (2009).

248. Vinogradov S.V, Poluektova L.Y, Makarov E, Gerson T, Senanayake M.T, Nano-NRTIs: efficient inhibitors of HIV type-1 in macrophages with a reduced mitochondrial toxicity**, (*A*ntiviral Chemistry and Chemotherapy), 21,** (2010), pp. 1-14.

249. Vitiello B, Vitkovic L, The link between infections and psychiatric diseases, **(Medscape Psychiatry & Mental Health eJournal), 2,** (1997).

250. Wang Y, Sawchuk R.J, Zidovudine transport in the rabbit brain during intravenous and intracerebroventricular infusion, **(Journal of Pharmaceutical Science), 84,** (1995), pp. 871-876.

251. Wang C, Huang L, Hou L, Jiang L, Yan Z, Wang Y and Chen Z, Antitumor effects of polysorbate-80 coated gemcitabine polybutylcyanoacrylate nanoparticles in vitro and its pharmacodynamics in vivo on C6 glioma cells of a brain tumor model, **(Brain Research), 1261,** (2009), pp. 91-99.

252. Wang Y, Shyam N, Ting J.H, Akay C, Lindl K.A, Jordan-Sciutto K.L, E2F1 localizes predominantly to neuronal cytoplasm and fails to induce expression of its transcriptional targets in human immunodeficiency virus-induced neuronal damage*,* ***(*Neuroscience Letters), 479,*** (2010), pp. 97-101.

253. Warnke D, Barreto J and Temesgen Z, Antiretroviral drugs, **(The Journal of Clinical Pharmacology), 47,** (2007), pp. 1570-1579.

254. White E, Woolley M, Bienemann A, Johnson D.E, Wyatt M, Murray G, Taylor H, Gill S.S, A robust MRI-compatible system to facilitate highly accurate stereotactic administration of therapeutic agents to targets within the brain of a large animal model, **(Journal of Neuroscience Methods),** (2010), Article in Press.

255. Wong S.L, Van Belle K and Sawchuk R.J, Distributional transport kinetics of zidovudine between plasma and brain extracellular fluid/cerebrospinal fluid in the

rabbit: investigation of the inhibitory effect of probenecid utilizing microdialysis, **(Journal of Pharmacological Experimental Therapy) 264,** (1993), pp. 899–909.

256. World Health Organisation, Basic information on AIDS, **(HIV/AIDS Reference Library for Nurses), 1,** (1993).
257. Worley J and Price R, Management of neurological complications of HIV-1 infection and AIDS, **(The Medical Management of AIDS), 3, (**1992).
258. Wu Y, Zhao Y, Tang M, Zhang-Nunes S.X, McArthur J.C, AIDS Dementia Complex in China, **(Journal of Clinical Neuroscience), 14,** (2007), pp. 8-11.
259. Xiong H, Zeng Y.C, Lewis T, Zheng J, Persidsky Y and Gendelman H.E, HIV-1 infected mononuclear phagocyte secretory products affect neuronal physiology leading to cellular demise: Relevance for HIV-1-associated dementia, **(Journal of Neurovirology), 6,** (2000), pp. 14-23.
260. Yang W, Peters J.I and Williams R.O III, Inhaled nanoparticles-A current review, **(International Journal of Pharmaceutics), 356,** (2008), pp. 239-247.
261. Yeboah I.E.A, HIV/AIDS and the construction of Sub-Saharan Africa: Heuristic lessons from the social sciences for policy **(Social Sciences and Medicine), 64, Issue5,** (2007), pp. 1128-1150.
262. Yiannoutsos C.T, Ernst T, Chang L, Lee P.L, Richards T, Marra C.M, Meyerhoff D.J, Jarvik J.G, Kolson D, Schifitto G, Ellis R.J, Swindells S, Simpson D.M, Miller E.N, Gonzalez R.G and Navia B.A, Regional patterns of brain metabolites in AIDS dementia complex, **(NeuroImage), 23,** (2004), pp. 928-935.
263. Yuan N, Lin, Ho M, Wang, D, Lai J and Hsieh H, Effects of the cooling mode on the structure and strength of porous scaffolds made of chitosan, alginate, and carboxymethyl cellulose by the freeze-gelation method, **(Carbohydrate Polymers), 78,** 2009, pp. 349-356
264. Yuen S, Choi S, Phillips DL and Ma Z, Raman and FTIR spectroscopic studies of carboxymethylated non-starch polysaccharides, **(Food Chemistry), 114,** (2008), pp. 1091-1098.
265. Zactiti E.M and Kieckbusch T.G, Potassium sorbate permeability in biodegradable alginate films: Effects of the antimicrobial agent concentration and crosslinking degree, **(Journal of Food Engineering), 77,** (2006), pp. 46-467.
266. Zahoor A, Sharma S and Khuller G.K, Inhalable alginate nanoparticles as antitubercular drug carriers against experimental tuberculosis, **(International Journal of Antimicrobial Agents), 26,** (2005), pp. 298-303.
267. Zahoor A, Pandey R, Sharma S, Khuller G.K, Pharmacokinetics and pharmacodynamic behaviour of antitubercular drugs encapsulated in alginate

nanoparticles at two doses, **(International Journal of Antimicrobial Agents), 27,** (2006), pp. 409-416.

268. Zhang N, Liu D, Cancer chemotherapy with lipid-based nanocarriers, **(*C*ritical Reviews in Therapeutic Drug Carrier Systems),** 27, (2010), pp. 371-417.

269. Zweers M.L.T, Engbers G.H.M, Grijpma D.W and Feijen J, In vitro degradation of nanoparticles prepared from polymers based on DL-lactide, glycolide and poly(ethylene oxide), **(Journal of Controlled Release), 100,** (2004), pp. 347-356.

APPENDICES

Appendix A: Protocol

Appendix B: Ethics Approval Certificate

Appendix C: Post Mortem Report

Appendix D: Abstracts Submitted